# The Role of Plasma Membrane Calcium Pump during Pancreatic Cancer

A thesis submitted to The University of Manchester for the degree of
Doctor of Philosophy
in the Faculty of Biology, Medicine and Health

**2019**

**PISHYAPORN SRITANGOS**

**School of Medical Sciences/ Division of Cancer Sciences**

# Table of Contents

## Chapter 2 – General Methods and Optimizations ..................................................51

## Chapter 3 – PMCA4 is important for cell migration and apoptotic resistance of MIAPaCa-2 pancreatic cancer cell line

## Chapter 4 –Plasma Membrane Calcium ATPase 4 (PMCA4) functional activity is dependent on Cav-1 expression in MIAPaCa-2 pancreatic cancer cell line

# List of Figures

**Chapter 1**

**Chapter 2**

**Chapter 3**

## Chapter 4

## Chapter 5

## Chapter 6

# List of Tables

## Chapter 2

## Chapter 5

# List of Abbreviations

$\Delta\Psi m$ = mitochondrial membrane potential
2-DG = 2-deoxyglucose
3PO = 3-(3-pyridinyl)-1-(4-pyridinyl)-2-propen-1-one
$\alpha KG$ = $\alpha$-ketoglutarate
A = adenine
AA = antimycin A
ADP = adenosine diphosphate
ALD = aldolase
ALDOA = aldolase A
AM = antimycin
ANOVA = analysis of variance
ATA = aurintricarboxylic acid
ATCC = American Type Culture Collection
ATP = adenosine triphosphate
$ATP_{global}$ = global cellular ATP
$ATP_{PM}$ = hypothetical previledged ATP localised to the sub-plasma membrane domain
ATP2B4 = gene encoding PMCA4 protein
AU = absorbance unit
AUC = area under curve
Bcl-2 = B-cell lymphoma 2
BFP = blue fluorescence protein
BirA = Bifunctional ligase/repressor BirA
BirA* = mutant promiscuous biotin ligase derived from *E Coli.*
BRCA2 = BRCA2 DNA repair associated
BrPy = bromopyruvate
$^oC$ = degrees Celsius
C= cytosine
$Ca^{2+}$ = calcium
$[Ca^{2+}]_i$ = intracellular calcium
$CaCl_2$ = calcium chloride
CaM = calmodulin
CaMKII = $Ca^{2+}$/CaM-dependent protein kinase II
cAMP = cyclic adenosine monophosphate
CASK = $Ca^{2+}$/calmodulin-dependent serine kinase
CAV1 = caveolin-1, referring to mRNA/gene
Cav-1 = caveolin-1, referring to protein
CBD = $Ca^{2+}$ binding domain
CCCP = carbonyl cyanide m-chlorophenyl hydrazone
CDK = cyclin-dependent kinase
CDK2NA = cyclin dependent kinase inhibitor 2A/p16
CE = carboxyeosin
$CO_2$ = carbondioxide
COQ6 = Coenzyme Q6, monooxygenase
CPA = cyclopiazonic acid
CSD = conserved scaffolding domain
DHAP = dihydroxyacetone phosphate
DhF1 = DharmaFect1 transfection reagent
DMEM = Dulbecco's modified Eagle's medium
DMSO = dimethyl sulfoxide
DNA = deoxyribonucleic acid
DPBS = Dulbecco's phosphate buffer saline
DTT = dithiothreitol
$EC_{50}$ = effective concentration of treatment which elicits 50% response
ECAR = extracellular acidification rate
ECL = enhanced chemiluminescence reagent
ECM = extracellular matrix
EDH = Esps 15 homology domain EDH
EDTA = ethylenediaminetetraacetic acid

EGFR = endothelial growth factor receptor
EGTA = ethylene glycol-bis(β-aminoethyl ether)-N,N,N',N'-tetraacetic acid
ENO = enolase
eNOS = endothelial nitric oxide synthase
ER = endoplasmic reticulum
ERK = extracellular signal-regulated kinase
ETC = electron transport chain
EtOH = ethanol
F1,6BP = fructo-1,6-bisphosphate
F-2,6BP = fructose-2,6-bisphosphate
FACs =fluorescence-activated cell sorting
FBS = fetal bovine serum
FCCP =carbonyl cyanide-p-trifluoromethoxyphenylhydrazone
FGFR = fibroblast growth factor receptor
FRET = Förste/Fluorescence Resonance Energy Transfer
(g) = gas phase
G = guanine
G6P = glucose-6-phosphate
GAPs = GTPase-activating proteins
GAPDH = glyceraldehyde 3-phosphate dehydrogenase
GEs = glycolytic enzymes
GEF = guanine nucleotide exchange factors
GFP = green fluorescence protein
Glu, E = glutamate
GLUT = glucose transporter
glycoATP = glycolysis-derived ATP
glycoPER = glycolysis-derived proton efflux rate
GPCR = G-protein coupled receptor
GPI = glucose-6-phosphate isomerase
GTPase = guanosine-5-triphosphatase
HEPES = 4-(2-hydroxyethyl)-1-piperazineethanesulfonic acid
HIF1-α = hypoxia inducing factor-1α
HK = hexokinase
HPDE = human pancreatic ductal epithelial cell line
hPKM2 = endogenous human PKM2 protein
HPNE = human pancreatic nestin-expressing cells
hPSC = human pancreatic stellate cells
HPSS = HEPES-buffered physiological saline solution
HRP = horse raddish peroxidase
h = hour
IAA = iodoacetate
$IC_{50}$ = half maximal inhibitory concentration
IGFR= insulin-like growth factor receptor
IP3R = inositol 1,4,5-trisphosphate receptor
IPA = Ingenuity Pathway Analysis
ISCD = inter-subunit contact domain
JMJD5 = Jumonji C domain containing dioxygenase
KCl = potassium chloride
KCNH4 = voltage-gated potassium channel subfamily H member 4
Kd = dissociation constant
LDH = lactate dehydrogenase
LDHA = lactate dehydrogenase A
LGCC = ligand-gated $Ca^{2+}$ channels
Lys, K = lysine
MAGUKs = membrane-associated guanylate kinases
MaxΔ$[Ca^{2+}]i$ = maximum change in intracellular calcium
MβC = methyl-β-cyclodextrin
MBS = 2-(N-Morpholino) ethanesulfonic acid-buffered saline
MCT= monocarboxylate transporter
MCU = mitochondrial $Ca^{2+}$ uniporter

MgCl$_2$ = magnesium chloride
MIC = metabolic inhibitor cocktails
min = minute
Mit C = mitomycin C
mitoATP = mitochondrial-derived ATP
ml = millilitre
MLCK = myosin light chain kinase
mM = millimolar
MMPs = matrix metalloproteases
MNCX = mitochondrial Na$^+$/Ca$^{2+}$ exchanger
MPTP = mitochondrial permeability transition pore
MRPL23 = mitochondrial ribosomal protein L23, isoform CRA_a
msec = milliseconds
NaCl = sodium chloride
NaPY = sodium pyruvate
NCX = Na$^+$/Ca$^{2+}$ exchanger
nAChRs = acetylcholine-gated nicotinic acetylcholine receptors
NIF = near-infared
nm = nanometer
nM = nano molar
NMDA = glutamate-gated N-methyl D-glutamate receptors
nNOS = neuronal nitric oxide synthase
O-GlcNAculated = glycolysation of O-linked β-*N*-acetylglucosamine
OCR = oxygen consumption rate
OD = optical density
OFP = orange fluorescence protein
OM = oligomycin
OXPHOS = oxidative phosphorylation
PanIN = pancreatic intraepithelial neoplasia
P/O = theoretical number of ATP synthesized per oxygen atom
PBS = phosphate buffer saline
PC = pyruvate carboxylase
PDAC = pancreatic ductal adenocarcinoma
PDH = pyruvate dehydrogenase
PEP = phosphoenolpyruvate
PER = proton efflux rate
PES = polyethersulfone
PFK = phosphofrutokinase
PFK-1 = phosphofrutokinase-1
PFKFB3 = 6-phosphofructo-2-kinase/fructose-2,6-biphosphatase 3/ phosphofructokinase-2
PGK = phosphoglycerate kinase
PGM = phosphoglycerate mutase
PHGDH = phosphoglycerate dehydrogenase
PK = pyruvate kinase
PKA = phosphokinase A
PKC = phosphokinase C
PKL = pyruvate kinase liver isoform
PKM1 = pyruvate kinase muscle isoform 1
PKM2 = pyruvate kinase muscle isoform 2
PKR = pyruvate kinase erythrocyte isoform
PLA = proximity ligation assay
PM = plasma membrane
PM-GEs = plasma membrane associated glycolytic enzymes
PMCA = plasma membrane calcium ATPase, referring to protein
PMCA4-GCaMP = PMCA4 attached with fusion green fluorescence protein and calmodulin-binding domain and M13 myosin light chain kinase
PPP = pentose phosphate pathway
PTMs = post-translational modifications
PtdIns(4,5)P2 = phosphatidylinositol 4,5-bisphosphate
qPCR = quantitative polymerase chain reaction

$R_1$ = first calcium clearance phase
$R_2$ = second calcium clearance phase
RASSF1 = Ras-associated factor 1
rcf = relative centrifugal force
Ref = references
rpm = rotation per minutes
$R_{max}$ = maximum ratio
$\Delta R_{max}$ = change with respect to maximum ratio
$R_{min}$ = minimum ratio
RIPA = radioimmunoprecipitation assay
RNA = ribonucleic acid
ROR1 = receptor tyrosine kinase-like orphan receptor 1
ROS = reactive oxygen species
Rot = rotenone
Rot/AA = rotenone/antimycin A mixture
$R_t$ = Ratio at relative time
RT = room temperature
RTKs = receptor tyrosine kinases
RYR = ryanodine receptor
SAICAR = succinylaminoimidazolecarboxamide ribose-5′-phosphate
SDS = sodium dodecyl sulphate
SDS-PAGE = sodium dodecyl sulphate-polyacrylamide gel electrophoresis
sec = seconds
SE = standard error
SEM = standard error of means
Ser, S = serine
SERCA = sarco/endoplasmic reticulum $Ca^{2+}$ ATPase
shRNA = short hairpin RNA
siCav-1 = siRNA targeting CAV1 mRNA, generating Cav-1 expression knockdown
siNT = non-targeting siRNA
siPMCA1 = siRNA targeting ATP2B1 mRNA, generating PMCA1 expression knockdown
siPMCA2 = siRNA targeting ATP2B2 mRNA, generating PMCA2 expression knockdown
siPMCA3 = siRNA targeting ATP2B3 mRNA, generating PMCA3 expression knockdown
siPMCA4 = siRNA targeting ATP2B4 mRNA, generating PMCA4 expression knockdown
siRNA = small/short interfering RNA
SMAD4 = SMAD family member 4
SOCE = store-operated calcium entry
SPCA = secretory pathway $Ca^{2+}$ ATPase
SR = sarcoplasmic reticulum
SRB = sulforhodamine β
STIM = stromal interaction molecule
T = thymine
TBS = Tris buffer solution
TBST = Tris buffer solution with added Tween
TCA = tricarboxylic acid cycle
TGCA-PAAD = the cancer genomic atlas - pancreatic adenocarcinoma cohort
TGFR = tumour growth factor receptor
TGFβR=TGF-β receptor
Thr, T = threonine
TP53 = P53 tumour suppressor
TPI = triosephosphate isomerase
TRP = transient receptor potential channel
Tyr, Y = tyrosine
μl = micro litre
μM = micro molar
VDCC = voltage dependent calcium channels
VEGF = vascular endothelial growth factor
WST-8 = water-soluble tetrazolium dye-8/ cell count kit-8
WT = wild-type

**TOTAL WORD COUNT:** 73,361

# Abstract

**ABSTRACT OF THESIS** entitled **The role of plasma calcium membrane pump during pancreatic cancer** submitted by **Pishyaporn Sritangos** to **The University of Manchester**

for the degree of **PhD Pharmacology**

**September 2019**

Pancreatic ductal adenocarcinoma (PDAC) is a commonly diagnosed malignancy with one of the poorest patient survival prognoses that has barely improved over the past three decades, prompting the need to find novel therapeutic target and treatment strategies. Ongoing efforts have identified metabolic reprogramming and remodelling of $Ca^{2+}$ signalling machinery as vulnerable targets which could be exploited therapeutically in multiple cancers, including PDAC. Evidence suggests that plasma membrane $Ca^{2+}$ ATPases (PMCAs), shown to be the primary $Ca^{2+}$ efflux machinery in PDAC, is functionally driven by glycolytic ATP to prevent cytotoxic $Ca^{2+}$ overload in PDAC cells, which exhibit a highly glycolytic phenotype. It was hypothesized that plasma membrane (PM) associated glycolytic enzymes (GEs) are functionally coupled to ATP-consuming pumps, including the PMCAs. Glycolytic ATP fuels the pumps while the consumption of ATP prevents metabolite-induce inhibition of GEs, driving the glycolytic flux. Therefore, understanding the role of PMCAs in PDAC, its functional coupling with glycolytic ATP, and identification of putative PM-GEs binding protein responsible for this functional coupling, might provide a novel strategy for the therapeutic targeting of PDAC. The current thesis highlights the relevance of PMCA4 overexpression in patient-derived PDAC tumours and survival prognosis through datamining and also identifies MIAPaCa-2 cell line as a glycolysis-reliant PDAC model which predominantly overexpresses PMCA4 at both protein and mRNA level, representing the characteristics of patient-derived PDAC tumour. Knocking down PMCA4 expression using siRNA led to inhibited $Ca^{2+}$ clearance, elevated resting intracellular $Ca^{2+}$ ($[Ca^{2+}]_i$), inhibited cell migration and enhanced apoptotic cell death under $Ca^{2+}$ stress; collectively suggesting that PMCA4 plays a critical role in $Ca^{2+}$ homeostasis and contributes towards cancer phenotypes in PDAC. As PM-GEs and PMCA4 are reported to co-localise with caveolin-1 (Cav-1) enriched PM subdomains which may facilitate their functional coupling, PMCA and GEs co-localization with Cav-1 in MIAPaCa-2 cells was verified by sucrose gradient ultracentrifugation. Disruption of this Cav-1-enriched compartment, by cholesterol depletion, led to inhibited PMCA-mediated $Ca^{2+}$ clearance which occurred independently of global ATP-depletion. This suggests that compartmental ATP may be important for fuelling PMCA activity. Although selective siRNA knockdown of Cav-1 resulted in modestly impaired PMCA activity which had no consequential effect on resting $[Ca^{2+}]_i$, nonetheless, this work provides the first evidence to suggest that Cav-1 expression could modulate PMCA4 activity in PDAC cells. Interestingly, neither PMCA4 nor Cav-1 siRNA knockdown had effect on basal metabolic phenotype as assessed by Agilent Seahorse XFe96 Mito stress and glycolytic stress tests. Lastly, we performed proximity-labelling bio-identification of pyruvate kinase M2 (PKM2), a key oncogenic GE, fused to a mutant biotin ligase BirA* and identified voltage-gated $K^+$ channel subfamily H member 4 (KCNH4) as a novel putative PM-GEs binding protein potentially responsible for coupling glycolytic ATP to PMCA activity. However, further validation and experiments are required to determine whether these PM-GEs could be therapeutically targeted to inhibit oncogenic PMCA4 activity in PDAC.

## Declaration

No portion of the work referred to in the thesis has been submitted in support of an application for another degree or qualification of this or any other university or other institute of learning.

## Copyright Statement

# Acknowledgements

# Chapter 1 - Introductions

## 1.1    Pancreatic ductal adenocarcinoma

Pancreatic cancer is ranked the 11th most commonly diagnosed cancer in the United Kingdom (UK) [1] but is ranked the 6th leading cause of cancer-related death in 2016 [1]. According to the UK Office for National Statistics report (2017), pancreatic cancer had the lowest 5-year survival rate of all cancers of 6.4% in male and 7.5% in females between 2012-2016 [2]. The main risk factors associated with pancreatic cancer are old age, smoking, alcohol, obesity, chronic pancreatitis [3], and diabetes [4]. These factors potentiate the risk of inflammation, oxidative stress, DNA damage and signalling dysfunctions which can potentially initiate a malignant transformation of the pancreas [5].

There are two types of pancreatic carcinoma, deriving from either endocrine (hormone secretion cells) or exocrine (digestive enzyme production cells) origins. Although pancreatic exocrine cells are comprised of both ductal and acini cells, pancreatic ductal adenocarcinoma (PDAC) accounts for 95 % of pancreatic neoplasm cases [1,6]. PDAC is a malignancy derived from the ductal tissue of the pancreatic exocrine cell. However, pancreatic endocrine cells, e.g. the acini cells, can also de-differentiate to acquire ductal-like characteristics upon malignant transformation [7]. As pancreatic cancer is often asymptomatic in the early stages of diseases [8] and approximately 80% of the patients are diagnosed at advanced stage III (invasive) and IV (metastasis), making the tumour unresectable [6,9]. This late-stage diagnosis contributed to poor disease prognosis and survival outcomes [8].

Pathophysiology of PDAC includes several decades of asymptomatic progression from the early development of lesions, primarily the pancreatic intraepithelial neoplasias (PanINs), to malignant PDAC (Figure 1.1). PanINs are asymptomatic lesions, less than 0.5 cm in size, of the pancreatic duct and are classified into 3 stages based on the level of morphological abnormality. Activation of oncogenic KRAS [10] and ERBB2 (Erb-B2 receptor tyrosine kinase 2; HER-2/Neu) mutation are often acquired at the earlier stages of PanINs [11]. Moreover, telomere shortening is observed at the earliest stages PanIN in more than 90% of the lesion, facilitating chromosomal instability and mutations [12]. Progression of PanINs then involves aberrant growth due to the inactivation of multiple tumour suppressor genes including CDKN2A (cyclin dependent kinase inhibitor 2A/p16), TP53 (p53), SMAD4 (SMAD family member 4), and BRCA2 (BRCA2 DNA repair associated).

Malignant PDAC possesses characteristic cancer hallmarks, which includes: sustained proliferative signalling, insensitivity to growth suppressors, immunosuppression, replicative immortality, inflammation, mutation, angiogenesis, metabolic reprogramming, invasion and metastasis [13] (Figure 1.2). PDAC is characterised by distinct stromal hypertrophy (desmoplasia), hypovascularization [14], genomic instabilities [15] and metabolism alterations [16,17]. Stromal desmoplasia is a common pathological feature of pancreatic carcinoma and may comprise up to 80% of the PDAC tumour mass [18]. As the fibrotic stromal hypertrophy reduces vascularization, this is responsible for the inherent hypoxic tumour microenvironment, limitation of nutrients, as well as protecting the tumour from anti-cancer therapies [18,19].

Clinical treatment of pancreatic cancer varies depending on disease stage and usually includes surgical resection of the tumour via pancreaticoduodenectomy (Whipple procedure), which involves the removal of the pancreatic head with or without partial removal of stomach and duodenum [20]. Combinations of radiotherapy and chemotherapy are commonly used as adjuvant therapies in pre- and post-surgical resection in an attempt to reduce tumour recurrence, although generally ineffective [21]. The currently used first-line chemotherapy for the treatment of PDAC often includes gemcitabine, FOLFIRINOX (a combination of oxaliplatin, irinotecan, leucovorin and 5-fluorouracil), S-1 (Tegafur, gimeracil, oteracil), and a combination of gemcitabine with Nab-paclitaxel [22,23]. Current conventional treatments have minimally improved the survival of pancreatic cancer patients over the past three decades [1,8]. Therefore, further understanding of PDAC is required to provide better insights into better targeting and treatment of PDAC.
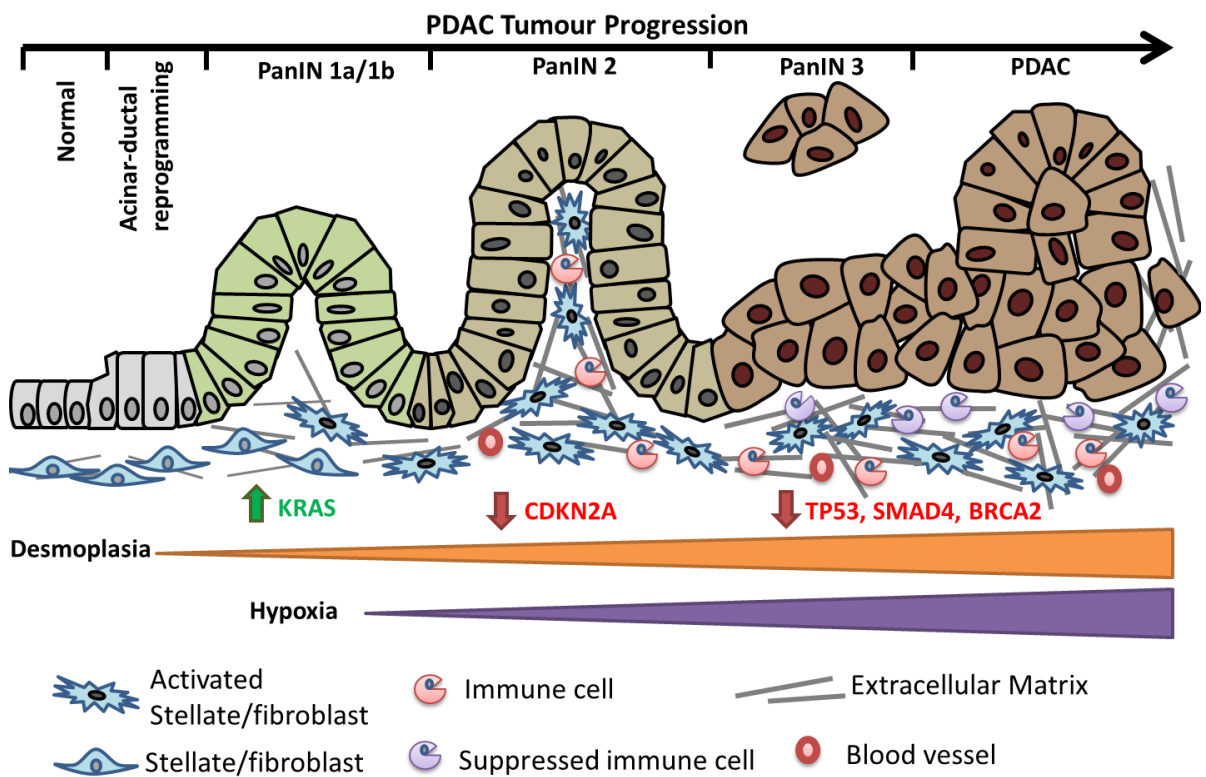


**Figure 1.1 – Progression of PDAC from multiple stages of precursor pancreatic lesions and the hallmarks of cancer.** Abbreviation – PDAC: pancreatic ductal adenocarcinoma, PanIN: pancreatic intraepithelial neoplasia, K-RAS: KRAS, CDK2NA: cyclin dependent kinase inhibitor 2A/p16, TP53: P53 tumour suppressor, BRCA2: BRCA2 DNA repair associated. The green arrow indicates gene upregulation and the red arrow indicates gene downregulation. Orange and purple triangles depict the degree of desmoplasia and hypoxia, respectively. Figure modified from Perera, R.M. and Bardeesy, N. (2015) [10]
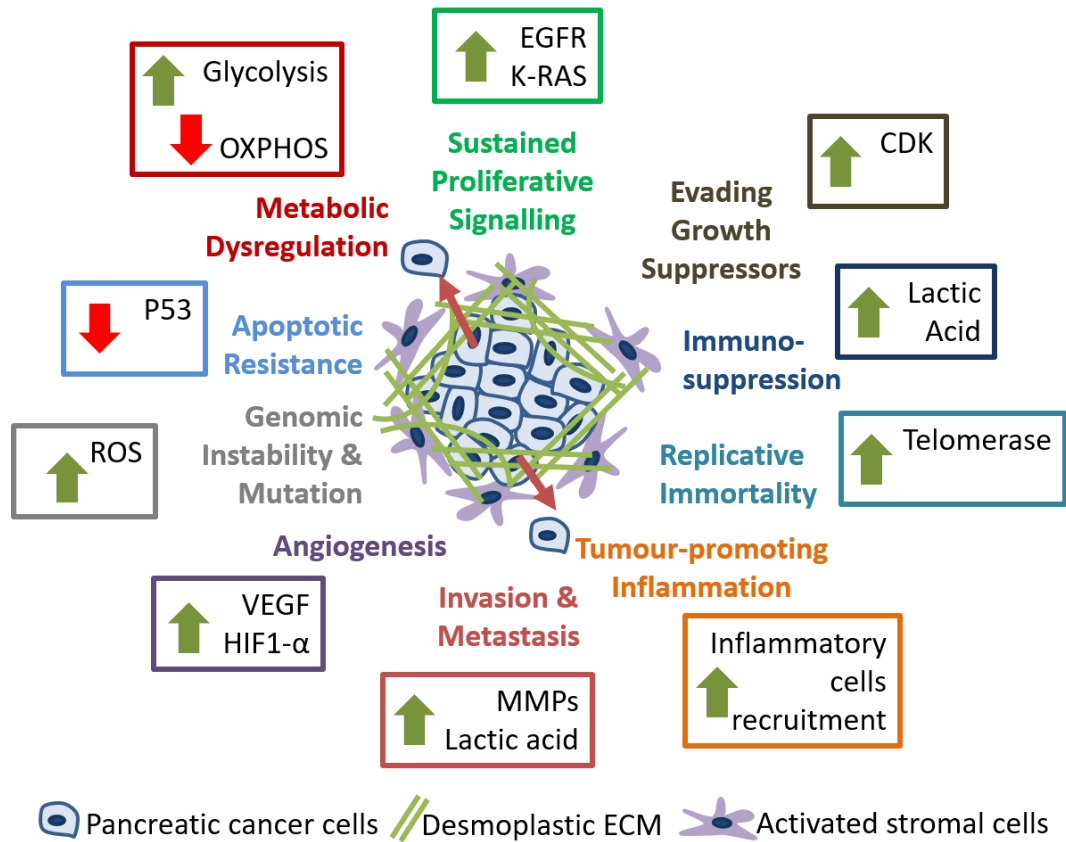
**Figure 1.2 – Hallmarks of pancreatic cancer.** Key cancer hallmarks and examples of these characteristics in pancreatic cancer. Abbreviation – CDK: cyclin-dependent kinase, EGFR: endothelial growth factor receptor, HIF1-α: hypoxia inducing factor-1α, K-RAS: KRAS GTPase, MMPs: matrix metalloproteases, OXPHOS: oxidative phosphorylation, P53: TP 53 tumour suppressor, ROS: reactive oxygen species, VEGF: vascular endothelial growth factor, ECM: extracellular matrix. Figure modified from Hanahan, D. *et al.* (2011) [13]

## 1.2 Cancer metabolism in PDAC

### 1.2.1 Cell metabolism – Glycolysis and Oxidative Phosphorylation

Adenosine triphosphate (ATP) is considered the primary universal energy unit in cells. ATP is essential to maintain homeostatic housekeeping processes essential for cell survival, from cell proliferation until programmed apoptotic cell death. Aside from matching sufficient ATP supply to the cellular ATP demand, a constant level of ATP ranging between 1-10 mM is normally maintained despite fluctuations of ATP demand [24]. ATP is mainly generated from the glucose metabolism through two key metabolic pathways, cytosolic glycolysis and mitochondrial oxidative phosphorylation (OXPHOS), depending on the oxygen availability.

Under aerobic condition (normoxia), glucose imported into eukaryotic cells undergo glycolysis in the cytosol to preferentially metabolize glucose into pyruvate, generating a net of 2 ATP molecules per 1 glucose molecule. The resulting pyruvate is converted into acetyl coenzyme A (acetyl CoA) and enters the tricarboxylic acid cycle (TCA cycle/Krebs cycle) inside the mitochondrial matrix, generating NADH and $FADH_2$. NADH and FADH2 drive the electron transport chain (ETC) complex I-IV to transport protons ($H^+$) against the concentration gradient from the mitochondrial matrix into the inner membrane, using oxygen as the final electron acceptor. The movement of $H^+$ down the concentration gradient is used by the ATP synthase/Complex V to phosphorylate ADP and produce ATP. This coupling process of ATP synthesis to the consumption of oxygen is known as OXPHOS which yields up to a net of 36 ATP molecules per molecule of glucose. Mitochondrial-mediated OXPHOS is, therefore, more energetically favourable and proficient in yielding more ATP molecule per glucose than glycolysis [25,26]. (Figure 1.3)

In poorly oxygenated conditions (hypoxia), however, the lack of electron acceptor led to inefficient ETC function and insufficient generation of $H^+$ gradient to drive the ATP synthase. Therefore, to maintain ATP production under hypoxia, cells undergo anaerobic/fermentation glycolysis. Glycolysis-derived pyruvate is converted by lactate dehydrogenase (LDH) to yield lactate and a net of 2 ATP molecule per glucose molecule without consumption of oxygen [25,26]. Although the ATP yield is much less than OXPHOS, anaerobic glycolysis produces ATP at a faster rate at the expense of higher glucose consumption [27,28].

Although normal cell preferentially uses glycolytic pyruvate to drive the TCA cycle for mitochondrial OXPHOS, some normal cells, particularly activated immune cells and fast proliferating cells (e.g. vascular endothelial during angiogenesis), preferentially utilizes glycolysis under normoxia [29]. Recent findings suggest that aerobic glycolysis is likely a characteristic of cell proliferation and is required for macromolecule biosynthesis [29,30]. Similarly, cancer cells generally exhibit metabolic preference towards aerobic glycolysis (the Warburg effect) to accumulate biosynthetic intermediates to fuel malignant growth.
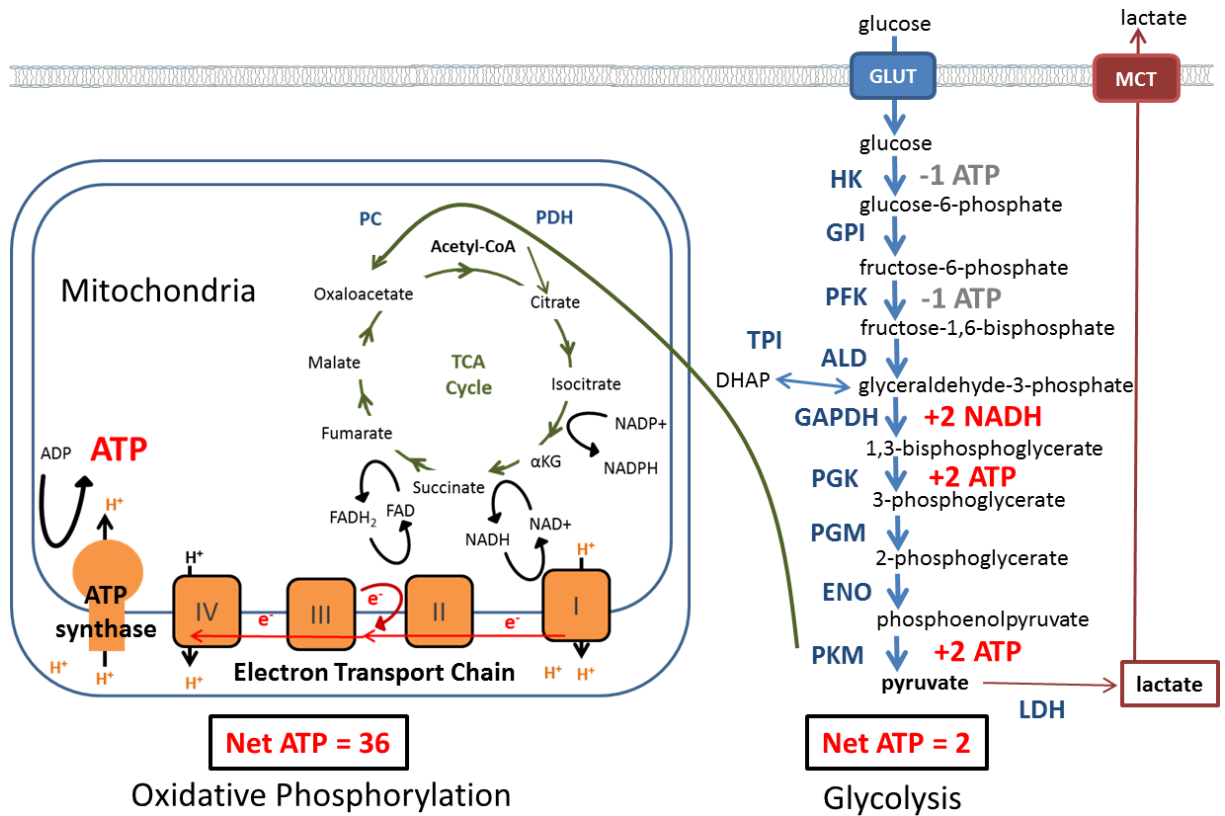
**Figure 1.3 – Metabolic ATP synthesis via Oxidative Phosphorylation and Glycolysis**. Glycolytic steps are labelled in blue, TCA cycle is labelled in green, and the electron transport chain is shown as orange. Abbreviation – GLUT: glucose transporter, MCT: monocarboxylate transporter, ADP: adenosine diphosphate, ATP: adenosine triphosphate, HK: hexokinase, GPI: glucose-6-phosphate isomerase, PFK: phosphofructokinase, ALD: aldolase, TPI: triosephosphate isomerase, DHAP: dihydroxyacetone phosphate, GAPDH: glyceraldehyde 3-phosphate dehydrogenase, PGK: phosphoglycerate kinase, PGM: phosphoglycerate mutase, ENO: enolase, PK: pyruvate kinase LDH: lactate dehydrogenase, PC: pyruvate carboxylase, PDH: pyruvate dehydrogenase, TCA: tricarboxylic acid cycle, αKG: α-ketoglutarate. Figure modified from Vander Heiden, M.G *et al.* (2009) [26] and DeBerardinis, R.J *et al* (2016) [31].

## 1.2.2  The Warburg effect – a shift towards aerobic glycolysis

To accommodate malignant growth and survival, most PDAC tumours exhibited metabolic reprogramming in preference of aerobic glycolysis – a phenomenon known as the Warburg effect and a well-recognized cancer hallmark [13]. The Warburg effect is a phenomenon observed by Otto Warburg in 1924 that, in comparison to normal cells, cancer cells showed a preference for anaerobic glycolysis and had enhanced lactic acid production even under normoxic conditions [26,32]. Warburg hypothesized that mitochondrial impairment led to an oncogenic shift towards aerobic glycolysis. However, the mitochondria in multiple cancers had been later shown to be functionally intact and contributed to ATP synthesis as well as oncogenic progression (e.g. biosynthesis of anabolic intermediates) [26,33]. In the presence of both oxygen and functional mitochondria, it seems counterintuitive that cancer cells would prefer aerobic glycolysis (2 ATP molecule per molecule of glucose) over the more energetically efficient OXPHOS (up to 36 ATP molecule per molecule of glucose). However, the Warburg effect offers cancer cells numerous oncogenic advantages which outweigh the cellular bioenergetic requirement, including:

pro-proliferative accumulation of biosynthetic metabolites, lactic acid-mediated malignant invasion and immunosuppression, as well as the production of anti-oxidative NADH to maintain redox homeostasis and reducing oxidative stress [13,34]. Metabolic intermediates of anaerobic glycolysis are also essential for anabolic biosynthesis. These metabolites can enter the pentose phosphate pathway (PPP) and/or truncated tricarboxylic acid (TCA) cycle to yield amino acids, nucleic acids and lipids [13,34]. (Figure 1.4)

Unlike Warburg's initial hypothesis, mitochondrial impairment is not solely responsible for metabolic reprogramming towards glycolysis. The current understanding of the Warburg phenomenon is that both intrinsic (e.g. oncogenes) and extrinsic (e.g. hypoxia) factors drive oncogenic metabolic reprogramming towards a highly glycolytic phenotype [35–37], enhancing glycolytic flux. A recent study in immortalized baby mouse kidney cells (iBMK cell line), by Tanner, LB *et al.* (2018), suggests that the Warburg effect is driven by the Ras oncogene and the glycolysis flux is substantially controlled at four key steps: glucose uptake (GLUT), hexokinase (HK) metabolism of glucose to glucose-6-phosphate, phosphofructokinase (PFK) conversion of fructose-6-phosphate to fructose-1,6-bisphosphate, and lactate export (MCT) [38]. Although controversial, PKM2 is suggested to function as a rate-limiting glycolytic enzyme due to its sensitivity to allosteric regulation [39,40] while conflicting findings suggest that PKM2 is not a rate-limiting step of glycolysis due to its high catalytic capacity in comparison to HK and PFK as well as its lack of effect on glycolytic flux upon overexpression [38,41].

Upregulation of glycolytic machinery, particularly rate-limiting glycolytic enzymes (GEs), are commonly observed in multiple cancers. The overexpression of embryonic pyruvate kinase isoform PKM2 is a common characteristic of the malignant glycolytic shift [42]. PKM2, like PKM1, is the rate-limiting GE involved in the conversion of phosphoenolpyruvate to pyruvate, yielding ATP. However, PKM2 can dynamically switch between an active tetrameric form to a low-activity dimeric form, suggested to create glycolytic bottle-neck to promote the accumulation of upstream anabolite metabolites at the expense of ATP production [43,44]. Conversely, oncogenic glycolytic flux is maintained by upregulation of hexokinase (HK) and phosphofructokinase-1 (PFK-1). These GEs act as glycolytic flux-limiting enzymes and consume ATP to produce glucose-6-phosphate (G6P) and F1,6BP glycolytic intermediates, respectively. F1,6BP, in particular, is known to allosterically promote tetramerization of PKM2 [45]. However, both HK and PFK-1 activity are negatively regulated by glycolytic metabolites. For instance, HK is allosterically inhibited by G6P [46] whereas PFK-1 is inhibited by high concentrations of glycolytic metabolites, including ATP (>2 mM), phosphoenolpyruvate, glyceraldehyde-3-phosphate and citrate (0.2-0.3 mM) as well as low pH [45,47–49]. Cancer cells, thereby, enhance oncogenic PFK-1 activity by upregulating 6-phosphofructo 2-kinase/fructose-2,6-bisphosphatase 3 (PFKFB3) which produces fructo-2,6-bisphosphate (F2,6BP), an allosteric activator of PFK-1 [50].
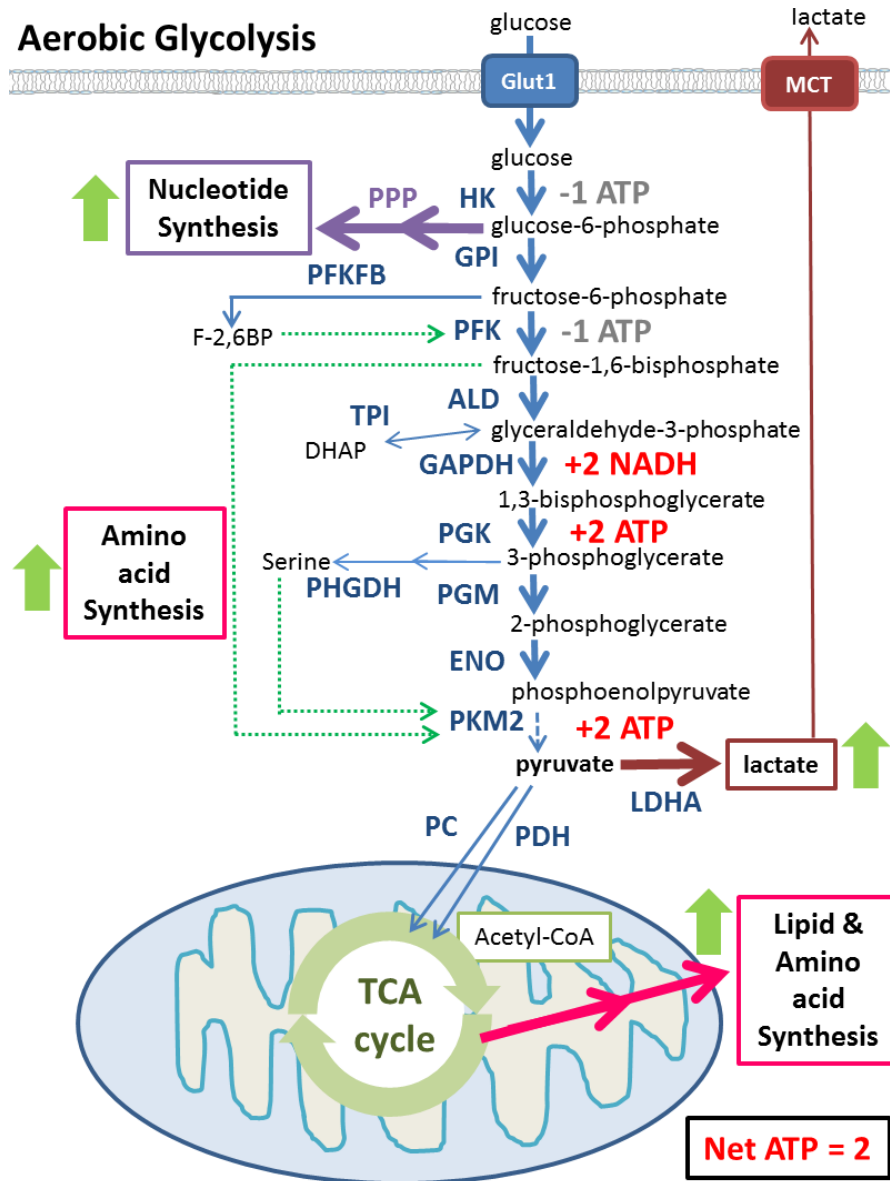
**Figure 1.4 – Aerobic glycolysis (Warburg effect).** A shift towards aerobic glycolysis is a key cancer hallmark which promotes anabolic synthesis of nucleotides, amino acids and lipids. Glycolytic enzymes are shown in blue while glycolytic intermediates/metabolites are shown in black. Blue arrow indicates the directional flow of glycolytic steps. ATP invested at the preparatory steps of glycolysis (grey text) and the ATP and NADH yields (red text) from the pay-off glycolytic steps are shown. Green dash arrow indicates allosteric activation of glycolytic enzymes by glycolytic metabolites. Abbreviation – GLUT: glucose transporter, MCT: monocarboxylate transporter, ADP: adenosine diphosphate, ATP: adenosine triphosphate, HK: hexokinase, GPI: glucose-6-phosphate isomerase, PFK: phosphofructokinase, ALD: aldolase, TPI: triosephosphate isomerase, DHAP: dihydroxyacetone phosphate, GAPDH: glyceraldehyde 3-phosphate dehydrogenase, PGK: phosphoglycerate kinase, PGM: phosphoglycerate mutase, ENO: enolase, PKM1/2: pyruvate kinase muscle isoform 1/2, LDHA: lactate dehydrogenase A, PC: pyruvate carboxylase, PDH: pyruvate dehydrogenase, TCA: tricarboxylic acid cycle, PPP: pentose phosphate pathway, F-2,6BP: fructose-2,6-bisphosphate, PFKFB: phosphofructokinase 2, PHGDH: phosphoglycerate dehydrogenase. Figure modified from Vander Heiden, M.G *et al.* (2009) [26] and Porporato, P.E. *et al* (2011) [51].

Besides GEs, enhanced glycolytic flux is also modulated by upregulation of glucose transporter (GLUT) and lactate transporter (monocarboxylate transporter; MCT). It is well established that "glucose addiction" is a characteristic of cells exhibiting the Warburg phenomenon [52]. It is reasoned that aerobic glycolysis yields less ATP; hence, a faster ATP production rate is achieved at the expense of higher glucose consumption [26]. Therefore, glucose transporters (GLUT) are often upregulated to enhance cellular glucose uptake and further fuel this "glucose addiction" and sustain the Warburg phenomena [36]. Conversely, the removal of lactate, the final production of glycolysis, by MCT is also an important glycolytic flux-controlling step [38]. Accumulation of lactate is associated with inhibition of LDH, cytosolic acidification, and inhibition of key GEs (e.g. PFK), which subsequently reduces the glycolytic flux [49,53]. Lactate, excreted from the cell by MCTs as lactic acid into the tumour microenvironment has been linked to tumour invasion [54] and immunosuppression [55]. Lactate may also be symbiotically taken up by the aerobic tumour-associated stromal cells and converted into pyruvate to further fuel the hypoxic cancer cells (lactate shuttling) [56].

### 1.2.3  Metabolic reprogramming in PDAC

In PDAC, metabolic reprogramming towards aerobic glycolytic has been associated with multiple factors, including intrinsic oncogenes signalling (e.g. KRAS [55]) and extrinsic hypoxic PDAC tumour microenvironment (e.g. HIF-1α). These factors drive the upregulation of multiple glycolytic machineries involved in importing glucose (e.g. GLUT1) into the cell, metabolizing glucose (e.g. PKM2, PFK-1) as well as eliminating lactate (MCT1) [56]. The following section broadly introduces key aberrant signalling, either due to the loss of tumour suppressor genes or activation of oncogenic genes, which contributes to the metabolic shift in malignant PDAC.

#### 1.2.3.1  Oncogenes activation in PDAC

**KRAS –** Considered as a PDAC tumour initiating factor, KRAS signalling has been correlated to aberrant growth, apoptotic resistance, immunosuppression, metastasis and metabolic reprogramming [57]. KRAS belongs to the RAS oncogene superfamily which encodes small guanosine-5-triphosphatase (GTPase) proteins known to regulate multiple cellular processes including cell growth, differentiation, adhesion, migration, and survival. As a GTPase, Ras hydrolyses GTP to GDP and acts as a binary switch by alternating between the active GTP-bound and the inactive GDP bound conformations [58]. These conformational changes alter the interaction interphase of Ras and its effector molecules, enabling specific Ras signalling upon GTP-binding and termination of signalling upon hydrolysis of GTP to GDP [59]. However, Ras possesses low GTPase activity and requires help from GTPase activating proteins (GAP) to enhance GTP hydrolysis to GDP. As Ras tightly associates to either GTP or GDP ($K_D$ ~10-100 pM), further assistance from guanine nucleotide exchange factors (GEF) is required to weaken GDP association in exchange for GTP, reactivating Ras [58].

Implicated in the early development of PanIN lesions [10] and PDAC tumour progression [57], KRAS mutation plays an important role in pro-survival pathways and is considered as a key driver of PDAC. Mutations resulting in constitutive activation has been observed in over 95% of PDAC tumours [60].

Typically associated with mutations at codon 12 of KRAS oncogene, aberrant KRAS activation often stems from reduced sensitivity to GAP-mediated termination of KRAS signalling, resulting in constitutively active KRAS [61]. Downstream signalling of KRAS includes the phosphoinositide 3-kinase (PI3K)/Akt/mTOR signalling, Raf/mitogen-activated protein kinase (MAPK) and nuclear factor kappa B (NFκB). Oncogenic KRAS expression has been associated with elevation of HIF1-α expression and PI3K/Akt signalling which promotes pro-anabolic metabolic reprogramming toward glycolysis [57,60]. Oncogenic KRAS activation has been associated with upregulation of key glycolytic machineries including PFK1, HK, ENO, GLUT1, LDHA [62].

**Hypoxia-inducible factor (HIF-1)** – Hypoxia is one of the key extrinsic factors which promote metabolic reprogramming towards glycolysis and glucose addiction in multiple cancers, including PDAC. Overexpression of HIF-1α in PDAC has been correlated to early stages of PanIN [63], hypoxic tumour regions, malignant tumour growth as well as poor PDAC patient prognosis [64–66].

HIF-1 is a hypoxic response protein which acts as a transcription factor for multiple target genes which regulates vascularization, promotes cell survival, proliferation and anaerobic metabolism [67]. HIF-1 is heterodimeric and is structurally comprised of a constitutively expressed β-subunit and an oxygen-dependent degradation domain-containing α-subunit (either HIF-1α, HIF-2α, or HIF-3α) [67,68]. Under normoxia, propyl hydroxylase mediates hydroxylation at the oxygen-degradation dependent domain of HIF α-subunits, leading to ubiquitination by von Hippel-landau tumour suppressor and subsequently targeted for proteasomal degradation [68]. On the contrary, HIF α-subunits are stabilized under hypoxic conditions, enabling the α-subunits to translocate into the nucleus to dimerize with HIF β-subunit to initiate transcription of hypoxia-response genes associated with anaerobic/fermentation (e.g. GLUT, PKM2, MCT, HK, LDH) [68–70]. As PDAC tumours are typically hypoxic, the overexpression of HIF-1α plays an important role in PDAC survival, metabolic reprogramming, and malignant progression [71]. HIF-1 transcriptional activation regulates the expression of glycolytic machineries including key glycolytic enzymes and glycolytic flux-controllers: glucose transporter (GLUT), hexokinases (HKs), MCT4 [69,70], lactate dehydrogenase (LDH) [72], PFKFB3, PFK [73], and PKM2 [74]. HIF-1 also dampens mitochondria functional capacity by inhibiting mitochondrial biogenesis [75], further promoting the shift from OXPHOS to fermentation glycolysis.

### 1.2.3.2   Inactivation of tumour suppressor genes in PDAC

**p53 tumour suppressor protein –** The inactivation of p53 tumour suppressor activity has been linked to metabolic reprogramming to fermentation glycolysis in PDAC [76]. p53 protein, encoded from the TP53 gene, is a strictly regulated tumour suppressor transcriptional activator which dictates cell survival or cell death in response to cellular stress (e.g. metabolic stress, hypoxia, and oncogenic stimuli) and DNA damage [77]. The activation of p53 is strictly controlled at both expression level (MDM2) and transcriptional activity level (MDMX). Under normal conditions, p53 protein is repressed at low levels by MDM2, an E3 ubiquitin protein ligase, which targets p53 for proteasomal degradation. In conjunction with MDM2, MDMX protein acts as a transcription repressor of p53 by suppressing the transcriptional activation domain [78]. Cellular stress signalling, resulting in post-translation modification of p53 (e.g. phosphorylation, acetylation) or sequestration/degradation of MDM2 and MDMX, leads to the disruption

of p53-MDM2/MDMX repressors interaction and subsequent stabilization of the p53 transcriptional activator [79]. Depending on the severity of the stress signal, p53 can either promote pro-survival responses in cells with reparable damage or mediates triggering apoptotic cell death or cellular senescence to prevent the propagation of severely damaged or malignantly transformed cells [80]. Structurally, p53 contains tetramerization domain, DNA binding domain, and transcriptional activation domains. Tetrameric p53, comprised of two dimeric p53 at the tetramerization domain, is required for DNA binding. The DNA-binding domain is critical for sequence-specific binding to p53 response elements which mediate tumour suppressor functions. Therefore, oncogenic inactivation mutations of p53 are often associated with either structural misfolding or missense mutations of this critical DNA-binding domain which prevents p53 from binding to its response elements [80,81].

In the context of metabolism, tumour suppressor p53 both directly and indirectly represses glycolysis through the downregulation and/or inhibition of key glucose machineries [76] while concomitantly promotes mitochondrial respiration. It is known that p53 negatively regulates glycolysis by downregulating GLUT1 and GLUT4 expressions [82], promoting degradation of phosphoglycerate mutase (PGM) downstream glycolytic enzyme [83], and enhancing the transcription of TIGAR (TP53-induced glycolysis and apoptosis regulator) [84]. TIGAR negatively regulate glycolytic flux by dephosphorylating F2,6BP, a potent allosteric activator of PFK-1 [76]. Furthermore, p53 signalling also exerts inhibitory effects on the glucose-6-phosphate dehydrogenase (G6PD), a rate-limiting enzyme involved in the first step of the pentose phosphate pathway, limiting glucose use for anabolic biosynthesis [85]. In conjunction with glycolysis repression, p53 promotes mitochondrial oxidative phosphorylation through transcriptional activation of SCO2 (synthesis of cytochrome C oxidase assembly protein 2), a gene requires for the assembly of mitochondrial complex IV, enhancing to the activity of the electron transport chain [86].

In PDAC, inactivation mutation of p53 tumour suppressor protein frequently occurs in advance PanIN 3 [87] and is found in 70 % of PDAC cases [88]. Missense mutation of p53, commonly found in PDAC, can give rise to a mutational gain of function (GOF mutp53) which can stimulate the Warburg effect [89]. GOF mutp53 has been shown to promote glycolysis and lactate secretion by stabilizing cytosolic GAPDH localization in PDAC cells [90]. Evidence suggests that p53 mutation leads to the paraoxonase 2-mediated stimulation of GLUT-1 activity in PDAC [91], promoting glycolysis and subsequently enhances the sensitivity PDAC to LDHA inhibitor [76]. The inactivation mutation of p53, therefore, plays a contributing role to the upregulation of glycolytic machineries and contributes towards the Warburg effect in PDAC [92].

**Cyclin dependent kinase inhibitor 2A (CDKN2A/p16/p16[INK4A]/MTS1)** – Inactivation of CDKN2A tumour suppressor gene increases with the advancement of PanIN stage [93] and has been observed in ~80 % of PDAC cases [94,95]. The CDKN2A gene encodes p16 (also known as p16[INK4A] or MTS1), an inhibitor of cyclin dependent kinase 4, which acts as a key regulator of the G1/S phase cell cycle progression [88,95]. Therefore, loss or inactivation of this CDKN2A critical tumour suppressor gene has been correlated to uncontrolled cell cycle progression and malignant growth [96].

Functional inactivation of CDKN2A occurs by intragenic mutation, homozygous deletion, and aberrant methylation silencing of p16 promoter [95]. Studies in mouse models suggest that concomitant aberrant KRAS activation and p16 inactivation are key oncogenic drivers of PDAC pathogenesis which drive the metabolic reprogramming during oncogenic PDAC progression [97,98]. Both p16 inactivation and KRAS activation have been suggested to upregulate NADPH oxidase 4 (NOX4) and stimulate the production of $NAD^+$, an important glycolytic cofactor essential for promoting the Warburg effect in PDAC [98].

**SMAD4** – Approximately 50% of PDAC has shown the loss of SMAD4 gene, encoding signalling proteins downstream of signalling pathways which include transforming growth factor-β (TGF-β)/activin and bone morphogenic protein signalling pathways [99,100]. SMAD4 tumour suppressor gene encodes a Smad4 transcription factor which mediates signal transduction downstream of the transforming growth factor (TGF)-β signalling pathway [99]. In PDAC, SMAD4 inactivation has been associated with the inhibition of TGF-β-mediated tumour suppressor functions [101].

SMAD4 is a co-mediator which either forms homomeric or heteromeric complexes with TGF-β receptor-activated Smad2 and Smad3 proteins to mediate TGF-β signalling [102]. Smad4 transcriptionally activates Smad-binding element to elicit its TGF-β-associated tumour suppressor function which includes cell cycle arrest at G1 and triggering apoptotic cell death. Functional TGF-β signalling potently inhibits PDAC by reducing vascular endothelial growth factor while enhancing angiogenesis inhibitor thrombospondin-1 [101,103]. Although limited evidence suggests that Smad4 directly contributes towards metabolic reprogramming in PDAC, Basso, D *et al* (2017) reported that the exosomes derived from PDAC lacking SMAD4 expression have been linked to overexpression of glycolytic enzymes, increase glucose consumption and lactic acid production in peripheral blood mononuclear cells [104]. Furthermore, it has been suggested that TGF-β drives metabolic reprogramming towards glycolysis in breast cancer-associated fibroblast [105]. Therefore, SMAD4 potentially contributes to the Warburg phenomenon in PDAC.

## 1.3  Functional coupling between glycolysis and Ca²⁺ signalling

Correlations between hypoxic tumour microenvironment and glycolytic shift are critical for PDAC survival and its malignant progression [106–108]. As previously described in the previous sections (1.2.2 The Warburg effect – a shift towards aerobic glycolysis and 1.2.3 Metabolic reprogramming in PDAC), PDAC typically acquires metabolic reprogramming in preference of glycolysis (Warburg phenomenon) to fuel malignant survival and growth. Warburg phenomenon primarily manifests by upregulation of glycolytic machinery, enabling high glycolytic flux to facilitate ATP production rate at the expense of lower ATP yield (compared to OXPHOS) and enhanced glucose consumption.

Glycolytic flux in cancer is often enhanced by the upregulation of PFKFB3 which subsequently promotes the production fructo-2,6-bisphosphate (F2,6BP), an allosteric activator of PFK-1 [109]. In turn, PFK-1 produces fructo-1,6-bisphosphate (F1,6BP), an allosteric activator of PKM2 [110]. However, although upregulation of glycolytic machinery can enhance glycolytic flux, the activity of key rate-limiting glycolytic enzymes, particularly PKM2 and PFK-1, are still allosterically inhibited by glycolytic

metabolites, particularly high ATP/ADP ratio (>2 mM ATP) [48,51]; thereby, hindering glycolytic flux. To maintain high glycolytic flux, cancer cells overcome allosteric inhibition through multiple means by: upregulation of glycolytic activators (F2,6BP, ADP) [109], mutational insensitivity to allosteric inhibitors [110,111], and consumption of glycolytic metabolites (ATP consuming processes).

A key ATP-consuming process essential for driving cell survival is $Ca^{2+}$ homeostasis. $Ca^{2+}$ is a versatile signalling molecule required for cellular homeostasis (further discussed in section 1.4 Regulation of $Ca^{2+}$ signalling). To maintain intracellular $Ca^{2+}$ concentration ($[Ca^{2+}]_i$), multiple $Ca^{2+}$ regulatory requires ATP to move $Ca^{2+}$ against its concentration gradient.

The relationship between cellular metabolism and $Ca^{2+}$ signalling has been continuously investigated for the past few decades. Evidence suggests that both plasma membrane $Ca^{2+}$ ATPase isoform 4 [112,113] and key GEs are expressed in close proximity to caveolin-1 (CAV-1) enriched caveolae [114]. Evidence in erythrocyte suggests that GEs is associated with the cytosolic side of the plasma membrane [115]. Furthermore, Raikar, L.S. *et al.* (2006) reported that, in vascular smooth muscle cells, PFKs, aldolases and potentially other glycolytic enzymes can interact with CAV-1 to enable compartmentalised metabolism [116]. Since PDAC shows overexpression of CAV-1 [117] as well as PMCA4 [118], glycolytic enzymes may exist in association with, or in close proximity to, the ATP-consuming PMCA, within the CAV-1 enriched caveolae.

It is well established that the function of PMCA-mediated $Ca^{2+}$ efflux is dependent on ATP availability [106]. Remodelling of $Ca^{2+}$ signalling, particularly elevated cytosolic $Ca^{2+}$, has been shown to impair mitochondrial OXPHOS by inhibiting $Ca^{2+}$-sensitive dehydrogenases of the Kreb's cycle [119] and facilitate the glycolytic shift in metabolism [120]. Glycolytic ATP has also been shown to be essential for PMCA activity in PDAC. James, A.D *et al.* (2013) have reported that glycolytic inhibition causes extreme ATP-depletion, compromises PMCA activity, subsequently induces $Ca^{2+}$ overload and cell death in MIAPaCa-2 and PANC-1 PDAC cell lines [121]. Consistent with the previous study, Epstein, T *et al.* (2014) suggested that a glycolytic metabolon is required to spontaneously supply ATP to the PMCAs while oxidative phosphorylation (OXPHOS) is responsible for stably supplying energy for macromolecule synthesis and nucleus [122].

Indeed, our previous findings by James, A.D *et al* (2015) suggests that glycolysis ATP, not mitochondrial ATP, fuels the plasma membrane $Ca^{2+}$ ATPases (PMCAs) mediated $Ca^{2+}$ efflux pump, leading to cytotoxic $Ca^{2+}$ overload and PDAC cell death [121,123]. Therefore, a better understanding of the relationship between glycolytic metabolism and $Ca^{2+}$ homeostasis may provide novel therapeutic targets for the improvement of pancreatic cancer clinical treatment.

# 1.4 Ca²⁺ signalling and its remodelling in cancer

Besides metabolic rewiring towards glycolysis, remodelling of $Ca^{2+}$ signalling is often associated with multiple cancers [124]. This is because $Ca^{2+}$ signalling universally regulates most aspects of cellular processes [125,126] from cell proliferation, cell cycle progression [127], differentiation [128], cellular motility [129], secretion [130], metabolic regulation [131], to apoptosis signalling [132]. Therefore, it is not surprising that alterations of $Ca^{2+}$ signalling and homeostasis have been associated, either directly or indirectly, with multiple cancer hallmarks [124].

The following section will briefly describe the importance of $Ca^{2+}$ signalling, the remodelling of $Ca^{2+}$ signalling machinery involved in the elevation of $[Ca^{2+}]_i$, the reduction of $[Ca^{2+}]_i$, and a brief summary of $Ca^{2+}$ signal remodelling in PDAC.

## 1.4.1 Ca²⁺ – a versatile signalling molecule

$Ca^{2+}$ is one of the most versatile and ubiquitous signalling molecules utilized by all cells. This is because $Ca^{2+}$ can act as first and secondary messengers to modulate crucial biological processes [125,126] mentioned above. These diverse cellular processes are regulated by $Ca^{2+}$ signalling, achieved through organized shaping of intracellular $Ca^{2+}$ concentrations ($[Ca^{2+}]_i$) into different spatiotemporal patterns which form spatially restricted spikes/sparks, global elevations, oscillations, and waves [125,133]. Depending on its spatiotemporal properties, which includes signal localisation, duration, frequency amplitude, $Ca^{2+}$ signals can modulate diverse and even opposing downstream responses [126]. For instance, $Ca^{2+}$ can elicit diametrically opposing responses in the regulation of Ras signalling, a key oncogenic driver of PDAC. Elevated $[Ca^{2+}]_i$ levels has been linked to $Ca^{2+}$/calmodulin-induce activation KRAS [134]. In contrast, $Ca^{2+}$ signals can also inhibit Ras via the activation of GTPase-activating proteins (GAPs) [135].

As different $Ca^{2+}$ signals can differentially influence multiple cellular processes, it is critical for cells to sense subtle spatiotemporal changes in $[Ca^{2+}]_i$. Therefore, it is essential for cells to maintain a low resting $[Ca^{2+}]_i$ (~100 nM) in order to efficiently propagate and respond to $Ca^{2+}$ signals. Regulation of $Ca^{2+}$ homeostasis and signalling are dependent on $Ca^{2+}$ signalling machinery which includes diverse classes of $Ca^{2+}$ ATPases, transporters, channels and binding proteins which are responsible for either elevating or reducing cytosolic $[Ca^{2+}]$ [125,126]. (Figure 1.5)
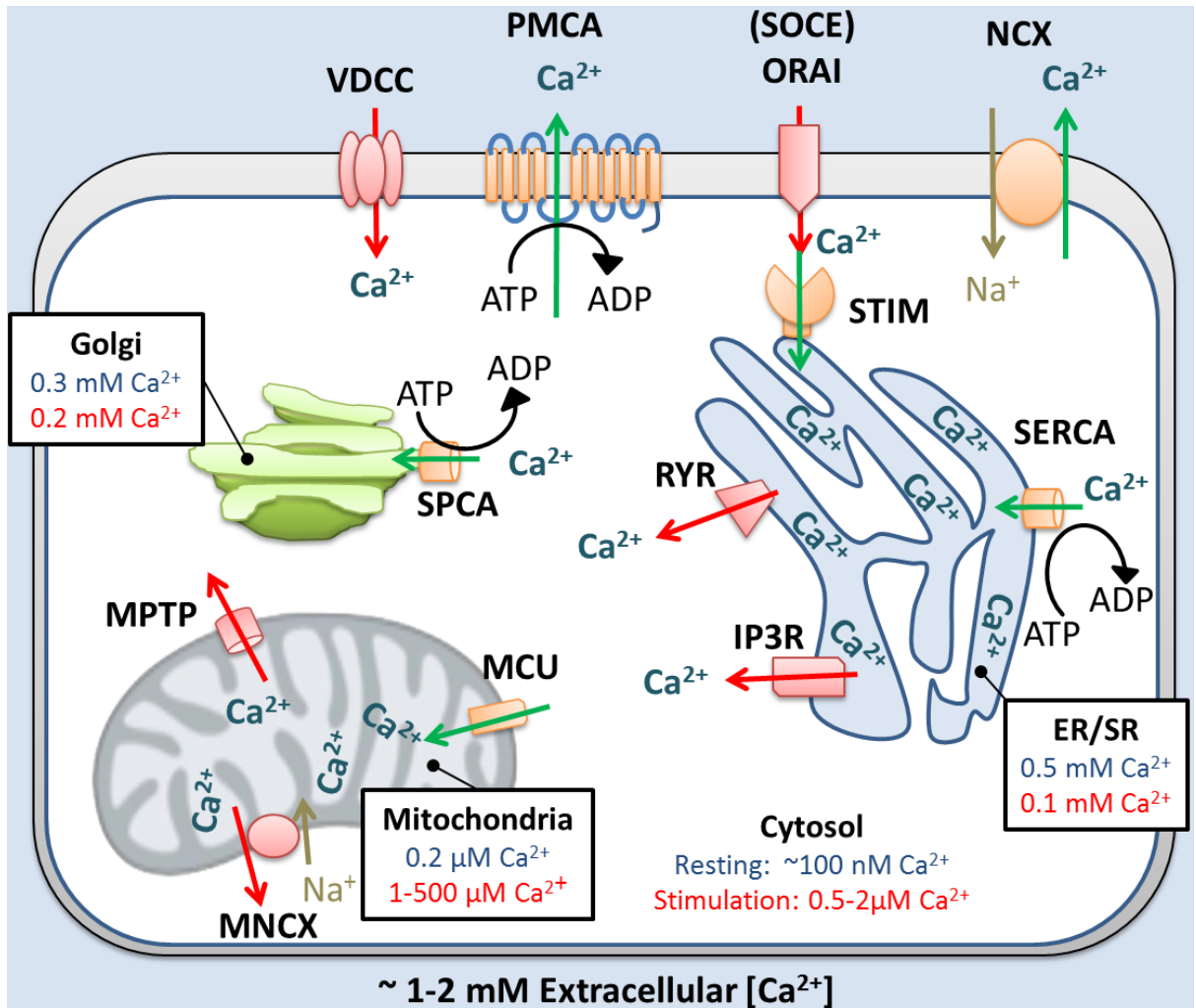
**Figure 1.5 – Cellular Ca$^{2+}$ regulation.** The cell illustrated typifies a non-contractile cell. Intracellular [Ca$^{2+}$] during resting (blue text) and stimulation vary depending on cellular compartments and their contribution towards the regulation of intracellular Ca$^{2+}$ ([Ca$^{2+}$]$_i$). Elevation of [Ca$^{2+}$]$_i$ is achieved by two key mechanisms: i) concentration-gradient driven Ca$^{2+}$ entry via SOCE and VDCC, and ii) release of Ca$^{2+}$ from intracellular Ca$^{2+}$ storages (e.g. ER/SR, Golgi Apparatus and Mitochondria). Reduction of [Ca$^{2+}$]$_i$ is similarly achieved by: i) Ca$^{2+}$ efflux into the extracellular environment (e.g. PMCA, NCX), and ii) uptake of free cytosolic Ca$^{2+}$ into intracellular Ca$^{2+}$ storages. Directional movement of [Ca$^{2+}$]$_i$ into (red arrow) or out of (green arrow) the cytosol indicate Ca$^{2+}$ elevation and reduction mechanisms, respectively. Abbreviations – VDCC: voltage-dependent Ca$^{2+}$ channel, PMCAs: plasma membrane Ca$^{2+}$ ATPase, ATP: adenosine triphosphate, ADP: adenosine diphosphate, SOCE: stores-operated Ca$^{2+}$ entry, TRP: transient receptor potential channel, STIM: stromal interaction molecule, NCX: Na$^+$/Ca$^{2+}$ exchanger, SPCA: secretory pathway Ca$^{2+}$ ATPase, ER: endoplasmic reticulum, SR: sarcoplasmic reticulum, SERCA: sarco/endoplasmic reticulum Ca$^{2+}$ ATPase, RYR: ryanodine receptor, IP3R: inositol 1,4,5-trisphosphate receptor, MCU: mitochondrial Ca$^{2+}$ uniporter, MPTP: mitochondrial permeability transition pore, MNCX: mitochondrial Na$^+$/Ca$^{2+}$ exchanger. Figure modified from Clapham, D.E (2007) [125] and Laude, A.J *et al* (2009) [136].

### 1.4.1.1 Elevation of [Ca$^{2+}$]$_i$

Propagation of Ca$^{2+}$ signalling involves the controlled elevation of intracellular Ca$^{2+}$. This influx of cytosolic Ca$^{2+}$ is achieved through two key mechanisms: i) extracellular Ca$^{2+}$ entry and ii) Ca$^{2+}$ release from intracellular Ca$^{2+}$ storages.

Extracellular Ca$^{2+}$ concentrations are over 10,000 fold higher than the [Ca$^{2+}$]$_i$ (~100 nM), ranging between 1-2 mM Ca$^{2+}$ [125]. This creates a concentration gradient which is essential to facilitate extracellular Ca$^{2+}$ influx into the cytosolic compartment, raising the resting [Ca$^{2+}$]$_i$ from 100 nM to 500-1000 nM during Ca$^{2+}$ signalling [125]. Extracellular Ca$^{2+}$ enter the cells through multiple ion permeable channels located on the plasma membrane which include voltage-dependent Ca$^{2+}$ channels (VDCCs), transient receptor potential (TRP) channels, ligand-gated Ca$^{2+}$ channels (LGCC), and store-operated Ca$^{2+}$ entry (SOCE) channels. VDCCs, classified into subtypes L, N, P/Q, R and T, are commonly found in excitatory cells (e.g. neurons, secretory cells, skeletal muscles and, cardiomyocytes) and are activated by changes in membrane potential, in response to action potentials and depolarizing signals [137]. Conversely, TRP channels are a large family of cation channels, comprising of TRPA, TRPC, TRPM, TRPML, TRPP and TRPV subfamily. TRP channels are mostly Ca$^{2+}$ permeable non-selective cation channels which exhibit varying selectivity for Ca$^{2+}$ and are heterogeneously activated by ligands (e.g. Ca$^{2+}$, menthol, calmodulin, capsaicin), chemical (e.g. pH, redox status and ATP depletion), temperature or mechanical stimuli. Hence, enabling the TRP channels to function as important "cellular sensor" [138]. LGCC are Ca$^{2+}$-selective ionotropic receptors which includes glutamate-gated N-methyl D-glutamate (NMDA) receptors, ATP-gated P2X receptors, and acetylcholine-gated nicotinic acetylcholine receptors (nAChRs) [139]. SOCE is the major Ca$^{2+}$ elevation pathway required to maintain intracellular Ca$^{2+}$ storages in non-excitable cells (e.g. epithelial cells) [140]. These intracellular Ca$^{2+}$ stores include endo/sarcoplasmic reticulum (ER/SR) and Golgi apparatus. Low luminal ER/SR Ca$^{2+}$ concentration triggers SOCE by the activation of stromal interaction molecule (STIM) and the opening of ORAI Ca$^{2+}$ release-activated Ca$^{2+}$ modulator (Orai), enabling Ca$^{2+}$ influx which refills the ER/SR intracellular Ca$^{2+}$ stores. [141].

The second mechanism which contributes towards the elevation of [Ca$^{2+}$]$_i$ is Ca$^{2+}$ release from intracellular storages, primarily the ER/SR. Intracellular Ca$^{2+}$ release is regulated by ER/SR-localised ryanodine receptors (RyRs) and inositol 1,4,5-trisphosphate (IP$_3$)-gated Ca$^{2+}$ receptors (IP3Rs). While IP$_3$Rs also require IP$_3$ for its activation, the opening of both RyRs and IP$_3$Rs are triggered by Ca$^{2+}$. This Ca$^{2+}$ induced Ca$^{2+}$ release (CICR) mechanism is important for amplifying and propagating Ca$^{2+}$ signals [142,143].

### 1.4.1.2 Reduction of [Ca$^{2+}$]$_i$

Propagation and termination of Ca$^{2+}$ signals require a tightly coordinated reduction of [Ca$^{2+}$]$_i$ to prevent unwarranted cellular responses, including Ca$^{2+}$-dependent apoptosis and necrosis [144,145]. Ca$^{2+}$ clearance is achieved through two key mechanisms: i) efflux of cytosolic Ca$^{2+}$ into extracellular space, and ii) Ca$^{2+}$ uptake into intracellular Ca$^{2+}$ storages.

Ca$^{2+}$ efflux mechanisms, localised at the plasma membrane, primarily include the ATP-driven plasma membrane Ca$^{2+}$ ATPase (PMCA) and Na$^+$/Ca$^{2+}$ exchanger (NCX). These transporters play a

critical homeostatic role in maintaining low resting $[Ca^{2+}]_i$ (~100 nM) by removing $Ca^{2+}$ from the cytosol, against its concentration gradient (~10,000 fold difference), into the extracellular space (1-2 mM $Ca^{2+}$) [125]. The PMCAs utilizes ATP to drive the efflux of one $Ca^{2+}$ ion per ATP. PMCA functions as a low capacity($K_{cat}$ ~100 $Ca^{2+}$ ions/sec) [146] but high $Ca^{2+}$ affinity (Kd ~100-200 nM) efflux pathway, responsible for the fine-tuning $[Ca^{2+}]_i$ and maintaining low resting $[Ca^{2+}]_i$ (further discussed in section 1.5 Plasma membrane Calcium ATPases). Conversely, NCX couples the efflux of one $Ca^{2+}$ ion to the uptake of three $Na^+$ ions and serves as a low affinity (Km ~10–20 µM) but high capacity transporter ($K_{cat}$~ 2500 $Ca^{2+}$ ions/sec), enabling rapid removal of $[Ca^{2+}]_i$ [147,148].

Following $Ca^{2+}$ release from intracellular storage compartments, $Ca^{2+}$ uptake is an indispensable mechanism required to replenish these intracellular $Ca^{2+}$ stores. $Ca^{2+}$ uptake machineries primarily include the sarco/endoplasmic reticulum (SERCA), Golgi apparatus/secretory pathway $Ca^{2+}$ ATPases (SPCA) and the mitochondrial $Ca^{2+}$ uniporter (MCU). SERCA, similar to PMCAs, are P-type ATPase which consumes ATP to drive the transport of two $Ca^{2+}$ ions from the cytosol into the ER/SR and Golgi apparatus lumen. Following $IP_3R$ and RyRs-mediated $Ca^{2+}$ release, SERCA functions to concurrently restores low resting $[Ca^{2+}]_i$ (~100 nM) while replenishing the ER/SR luminal $Ca^{2+}$ stores (~100-500 µM) [149]. Under basal conditions, passive $Ca^{2+}$ leaks from the ER/SR lumen through RyRs and SERCA [150] is recovered by SERCA at the expense of ATP [151,152]. SPCA pumps are P-type ATPases which utilizes ATP hydrolysis to drive the transport of one $Ca^{2+}$ or $Mn^{2+}$ ion, from the cytosol into Golgi apparatus lumen [153]. SPCAs is suggested to function as a housekeeping protein and contributes towards the maintenance of low resting $[Ca^{2+}]_i$ [154] and the shaping of $Ca^{2+}$ signalling [155] in keratinocytes [156].

The mitochondrial uniporter also serves as an important $Ca^{2+}$ uptake mechanism. Following increases in cytosolic $Ca^{2+}$, rapid and transient elevation of mitochondrial $Ca^{2+}$ concentration is observed [157]. Although $Ca^{2+}$ uptake into mitochondrial intermembrane space is driven by negative membrane potential, $Ca^{2+}$ uptake into the mitochondrial matrix requires the activation of MCU and accessory proteins, including mitochondrial $Ca^{2+}$ uptake 1/2 (MICU1 and MICU2) and essential MCU regulator (EMRE). As MCU has a low affinity for $Ca^{2+}$ and a high activation threshold (Kd ~50 µM), MCU activation requires coupled tethering between the mitochondria and the ER. $Ca^{2+}$ release from the ER/SR intracellular storages by the RyRs and $IP_3Rs$ at the mitochondria/ER/SR junctions generates a high $Ca^{2+}$ microdomain which sufficiently meets the threshold of the MCU [158–160]. In addition, MCU mediated $Ca^{2+}$ uptake also modulate mitochondrial metabolism [136] by $Ca^{2+}$-mediated allosteric activation of TCA cycle dehydrogenases [161] and enhancing the activity of ETC [162].

## 1.4.2  Remodelling of $Ca^{2+}$ signalling modulates cancer hallmarks

As previously mentioned, $Ca^{2+}$ is a versatile signalling molecule which regulates numerous cellular processes and functions, from cell proliferation until cell death [125,126]. Therefore, remodelling of $Ca^{2+}$ signalling can lead to the propagation of unwarranted $Ca^{2+}$ signals and aberrant cellular responses which facilitates malignant tumour progression. Typically, the remodelling of $Ca^{2+}$ signalling is the consequence of alterations of various $Ca^{2+}$ regulatory proteins, collectively referred to as the $Ca^{2+}$ signalling machinery. Alterations of $Ca^{2+}$ signalling machineries often manifest as altered levels of expressions, the abnormal

gain of $Ca^{2+}$ regulatory proteins and/or isoforms not normally native to the healthy tissues, and altered functional activity due to mutations, post-translation modifications as well as dysregulated downstream responses [124]. This remodelling of $Ca^{2+}$ signalling has been associated, either directly or indirectly, with multiple cancer hallmarks [124] which include: sustained proliferative signalling, replication immortality, insensitivity to growth suppression signals, apoptosis resistance, enhanced invasion, metastasis and angiogenesis, as well as dysregulation of cellular energetics [13].

**Sustained proliferation** – $Ca^{2+}$ is an important modulator of various signalling pathways and transcription factors which regulates cell proliferation throughout all phases of the cell cycle [127]. $Ca^{2+}$ signalling differentially modulates direct effectors of $Ca^{2+}$ such as CaM, $Ca^{2+}$/CaM-dependent protein kinase II (CaMKII), calcineurin and PKC, which in turn, activates transcription factors regulating cell cycle progression [127]. These $Ca^{2+}$-dependent transcription factors includes the immediate early genes (FOS, JUN and MYC) required during G1 phase, retinoblastoma (RB1) during G1/S phase [163], cAMP-responsive element binding protein (CREB) [164], nuclear factor of activated T cells (NFAT), NFκB [165], cyclin and cyclin-dependent kinase D/E [127], as well as Ras-ERK signalling pathways [166]. In cancer, aberrant cell proliferation has been associated with extensive remodelling of $Ca^{2+}$ signalling machinery which contributes towards elevation of cytosolic [$Ca^{2+}$] via $Ca^{2+}$ influx (e.g. TRP channels [167,168] , T-type VDCCs [169], PMCAs [170]) or intracellular $Ca^{2+}$ release (e.g. $IP_3Rs$ [171], RyRs [172], SERCAs [173], SPCAs [174]), or sustained refilling of ER/SR stores (e.g. STIM/ORAI [171]) [175]. These remodelling results in sustained activation of $Ca^{2+}$-dependent transcription factors, enhancing cell cycle progression [127,175]. For instance, the overexpression of TRP channels in multiple cancers, including TRPV6 [167] and TRPM7 [168] in PDAC [167], is linked with enhanced $Ca^{2+}$ influx which promotes downstream activation of NFAT, enhancing cell proliferation [175,176]. Moreover, C-MYC, an oncogenic driver of PDAC, is suggested to be upregulated by constitutively activated $Ca^{2+}$-dependent calcineurin-mediated NFAT signalling which subsequently enhances G1/S phase transition and anchorage-independent cell growth [177].

**Apoptotic resistance** – Apoptosis, or programmed cell death, is a fundamental mechanism necessary for the regulation of normal cell turnover and for preventing the proliferation of severely damaged and/or aberrantly transformed cells. Apoptosis is primarily regulated by are B-cell lymphoma 2 (Bcl-2) family proteins, comprised of anti-apoptotic regulators (e.g. Bcl-2 and Bcl-xL) and pro-apoptotic mediators (e.g. Bad, Bax and Bak) [178]. Proapoptotic stimuli can trigger $Ca^{2+}$-dependent calcineurin-mediated dephosphorylation of Bad, allowing it to inhibit Bcl-2/Bcl-xL, promoting apoptosis [179]. Alternatively, $Ca^{2+}$-dependent activation of proteolytic calpains has been shown to cleave anti-apoptotic Bcl-2 family proteins (e.g. Bcl-2, Bcl-xL) [180] as well as caspases (e.g. caspase 12) [181,182].

$Ca^{2+}$-dependent apoptotic cell death is associated with sustained global elevation of [$Ca^{2+}$]$_i$ or cytosolic $Ca^{2+}$ overload, mediated by substantial $Ca^{2+}$ influx and/or persistent $Ca^{2+}$-release from the ER intracellular stores release [183], which triggers ER-stress and mitochondrial apoptotic pathways [184]. Therefore, cancer cells can avoid apoptotic $Ca^{2+}$ overload by reducing $Ca^{2+}$ influx into the cytosol, promoting $Ca^{2+}$ efflux into the extracellular space, and adapting to sustained SR/ER depletion-related stress [175,185,186]. Typically, this reduced cytosolic $Ca^{2+}$ influx and enhanced cancer cells against

$Ca^{2+}$ overload in response to pro-apoptotic stimuli, preventing downstream activation of cytosolic and mitochondrial apoptotic signalling pathways[175]. Similarly, cancer adaptations to decreased SR/ER luminal $[Ca^{2+}]$ impairs ER-stress mediated apoptotic response [175,185,186]. Indeed, prostate cancer cells downregulate SOCE components, including ORAI1 [187] and STIM1 [188], reducing $Ca^{2+}$ influx into SR/ER intracellular stores, consequentially limiting $Ca^{2+}$ release from these store into the cytosol. Conversely, the overexpression of PMCA2 in breast cancer is reported to lower $[Ca^{2+}]_i$ levels, preventing calpain activation and apoptosis [189]. Similarly, aggressive androgen-independent prostate cancer exhibit adaptations to low luminal ER by downregulating calreticulin, an ER luminal $Ca^{2+}$ binding protein which functions as a proapoptotic factor in absence of $Ca^{2+}$, inducing ER adaptions which reduce the expression of SERCA2b mediated $Ca^{2+}$ uptake into the ER [190].

**Enhanced cell migration and invasion** – Cell migration is an important process necessary during wound healing, immune response as well as cancer metastasis [129,191]. $Ca^{2+}$ signalling coordinates the dynamic assembly and disassembly of actin-myosin contractile machinery and focal adhesion complexes which drives cell protrusion, adhesion to the extracellular matrix (ECM) and retraction processes during migration [129,191]. An essential $Ca^{2+}$ gradient is maintained during migration, where cytosolic $Ca^{2+}$ kept low at the migration front and high towards the back of the cell [129,192]. This low $Ca^{2+}$ levels at the migration front are achieved by enriched distribution of PMCA at the migration front [193], enabling $IP_3R$ and TRP to efficiently mediate localised $Ca^{2+}$ pulses and flickers [192,194]. These transient $Ca^{2+}$ signals activate $Ca^{2+}$-dependent assembly of focal adhesion complexes at the migration front [192,194] while activating myosin light chain kinase (MLCK) [195] to induce actin-myosin contraction [192] responsible for rear retraction [194]. High $Ca^{2+}$ towards the back of the migrating cell facilitates rear retraction and detachment from the ECM [129,191] via $Ca^{2+}$-dependent calpain disassembly of focal adhesion complexes [196]. Remodelling of $Ca^{2+}$ signalling typically facilitates metastasis and invasion by enhancing actin-myosin contractions, promoting focal adhesion disassembly and degradation of the ECM [194]. For example, the overexpression of TRPM7 is associated with increased myosin tension In breast cancer whereas the overexpression of TRPV2 in prostate cancer is reported to enhance malignant invasion by matrix metalloprotease-induced ECM degradation [197]. In PDAC, the overexpression of TRP channels, particularly TRPC1 [198], TRPM7 [199], TRPM8 [198] and TRPV6 [167] has been correlated to enhanced migration. TRPM7, associated with membrane stretch responses at the migration front [192], has been implicated in facilitating m-calpain-mediated peripheral adhesion complex turnover [200] and exhibits enhanced activity under low $Mg^{2+}$-ATP level during hypoxia [201]. The overexpression of TRPM7 has been correlated with PDAC tumour progression and poor prognostic outcome [199].

## 1.5    Plasma membrane calcium ATPases

As previously described (1.4 $Ca^{2+}$ signalling and its remodelling in cancer), multiple cancers exhibit remodelling of calcium signalling machinery, including PDAC [202]. In PDAC, specifically, the overexpression [118] and activities of PMCAs have been associated with resistance to $Ca^{2+}$ overload-mediated cell death in PDAC [121,123,203].

Besides NCX, PMCAs is another pathway responsible for extruding $Ca^{2+}$ across the plasma membrane, removing $Ca^{2+}$ from the cell. PMCAs are the major ATP-consuming $Ca^{2+}$ efflux machinery required for fine-tuning cytosolic $[Ca^{2+}]_i$ signalling and homeostasis in eukaryotic cells [204]. In comparison to SERCA which transport two $Ca^{2+}$ ions per ATP hydrolysed [205], the PMCAs are considered as a low capacity $Ca^{2+}$ efflux pathway as they could only couple efflux of a $Ca^{2+}$ ion to the uptake of 1-2 $H^+$ ions per ATP hydrolysed [206,207]. However, uncoupling of this $Ca^{2+}$ efflux to $H^+$ uptake can occur under extracellular alkalinisation (pH 8.5), enabling the PMCAs to mediate $Ca^{2+}$ efflux independent of $H^+$ uptake [208]. Therefore, PMCAs are vulnerable to pH changes and the pump activity is inhibited under high extracellular pH [209] and intracellular acidification [210].

Although the PMCAs are considered as a low capacity $Ca^{2+}$ efflux pathway, these pumps possess high $Ca^{2+}$ binding affinity (Kd 200 nM) [206,211] and the lowest activation threshold in comparison to other $Ca^{2+}$ transporters including the SERCA, NCX, and MCU [212]. The PMCA, therefore, play an important role in fine-tuning $Ca^{2+}$ signalling and resting $[Ca^{2+}]_i$ at physiological concentrations of ~ 100 nM [125,206]. PMCA mediates $Ca^{2+}$ efflux by ATP-driven conformational changes, from phosphorylated E1 to E2 states, altering its $Ca^{2+}$ binding affinity [206,213,214]. Through these conformational changes, the $Ca^{2+}$ binding affinity of PMCA changes from high (E1) to low affinity (E2), at the cytosolic and the extracellular side, respectively. As a member of the P-type ATPase family, the PMCA characteristically exhibit auto-phosphorylation of a conserved aspartate residue, forming a high-energy covalent intermediate state (E2) during its reaction cycle [206,214]. This phosphorylated-E2 conformation transfers the bound-$Ca^{2+}$ towards the extracellular side and reduces $Ca^{2+}$ binding affinity of the pump, thereby facilitating $Ca^{2+}$ release. After the release of $Ca^{2+}$ from the pump, the phosphorylated-E2 intermediate is then cleaved and the pump returns to E1 state [206,213].

PMCAs are independently encoded by 4 different genes (ATP2B1-4). Four isoforms of PMCA1-4 proteins and approximately 20 spliced variants of these isoforms have been reported. The affinity and stimulation response of these PMCA isoforms varies. PMCA1 is a critical housekeeping $Ca^{2+}$ efflux pump which is ubiquitously expressed in all cells. PMCA2 and PMCA3 are 'rapid response pumps' which are selectively expressed in excitatory cells of the nerves, brain and skeletal muscles. PMCA4 are also extensively expressed in the heart, sperm tail, endothelial cells, including the pancreas. In contrast to PMCA1, PMCA4 is not critical for the maintenance of $Ca^{2+}$ homeostasis [215].

Structurally, PMCAs are 10 transmembrane proteins which feature a variable N-terminus sequence, two intracellular loop domains and a long C-terminus tail (Figure 1.6). The N-terminus, particularly first ~80-90 amino acids, has a low sequence homology amongst PMCA isoforms. Despite the variation in sequence, the N-terminus is suggested to provide a binding site for 14-3-3ε protein, a conserved adaptor

protein, which negatively regulates the activity of PMCA isoforms 1,3 and 4 [216,217]. PMCAs also possess two intracellular loop regions – a transducer region and a catalytic region. The first intracellular loop is a transducer domain (A-domain) located between transmembrane domain 2-3. This domain is activated by acidic phospholipids and auto-inhibited by the calmodulin binding domain (CBD) [218]. The catalytic domain of the PMCA is located on the second intracellular loop region between transmembrane domain 4-5. This region contains ATP binding domain (N-domain) and a conserved aspartate phosphorylation site (P-domain) required for E2 conformational transition as well as an autoinhibition CBD [219]. The long C-terminus tail contains the primary CaM CBD (site-C) which binds with the first and second intracellular loop to exert an autoinhibitory effect on unstimulated PMCA ($K_d$ ≥10 µM $Ca^{2+}$) and would, therefore, be inactive under physiological $[Ca^{2+}]_i$ of ~100 nM. This autoinhibition is reversed when calmodulin (CaM), a key activator of the PMCA, binds to the CBD, shifting the $Ca^{2+}$ affinity from ≥10 µM down to 200 nM [206,211]. The C-terminus also serves as an interaction site for kinases (e.g. phosphokinase A/C) and caspases (e.g. caspase-3) [220]. Isoform b of PMCAs also contains PDZ binding domain on the C-terminus which enables to the PMCA to interact with other signal transducing proteins e.g. nNOS [221]. The activity of PMCA is known to be further modulated by phospholipids, particularly acidic phospholipid (e.g. phosphoinositide 4,5-bisphosphate; PIP2) is also a major activator of PMCA and is thought to account for ~50% of the activity of PMCA at restPIP2), binding at the CBD which enhances $Ca^{2+}$ binding to (Kd ~100 nM) [222,223]. Moreover, the activity of PMCAs is primarily regulated at the transcriptional level, while the functional activity of the pump is modulated by post-transcriptional modification and subcellular localization of pump [224,225].

The localization of PMCAs has been associated with lipid rafts and caveolae, high lipid density invagination sites on the plasma membrane. El-Yazbi, A.F. *et al.* (2008) reported that the full-length PMCA4b is localised in the caveolae, associated with Cav-1, whereas the truncated PMCA4a is found in lipid rafts [113]. Differences in localization and post-translational modification of these PMCA4 variants result in different functionality, for instance, while PMCA4a is a faster response pump, PMCA4b has slower basal activity and activation rate [226]. In addition, PMCAs have been proposed to possess their own glycolytic ATP supply [203,227]. Therefore, this localisation of both PMCAs [113,228] and GEs at the caveolae [116,229] may also play an important role in the assembly of glycolytic machinery required to provide a privileged supply to the PMCAs [203].

As PMCA plays an important role in shaping $Ca^{2+}$ signalling which regulates multiple cellular homeostasis processes (as previously described in 1.4 Regulation of $Ca^{2+}$ signalling), it is not surprising that alterations of PMCA expression have been suggested to play a role in cancer [170,220,230]. Remodelling of PMCAs expression has been associated with dysfunctional proliferative response and apoptotic resistance, promoting malignant cell growth and survival [170,203]. Indeed, remodelling of PMCA expressions has been observed in multiple cancers [124,231–233], including PDAC [118]. Multiple studies suggested that overexpression of PMCA increases apoptotic resistance associated with $Ca^{2+}$ overload [219]. For instance, PMCA2 has been reported to be overexpressed in breast cancer [231] while PMCA4 has been reported to decrease upon de-differentiation and has been associated with increased proliferative signalling in colon cancer [233].

**A.** Unstimulated PMCA at resting $Ca^{2+}$

**B.** *Activated PMCA during elevated $Ca^{2+}$*
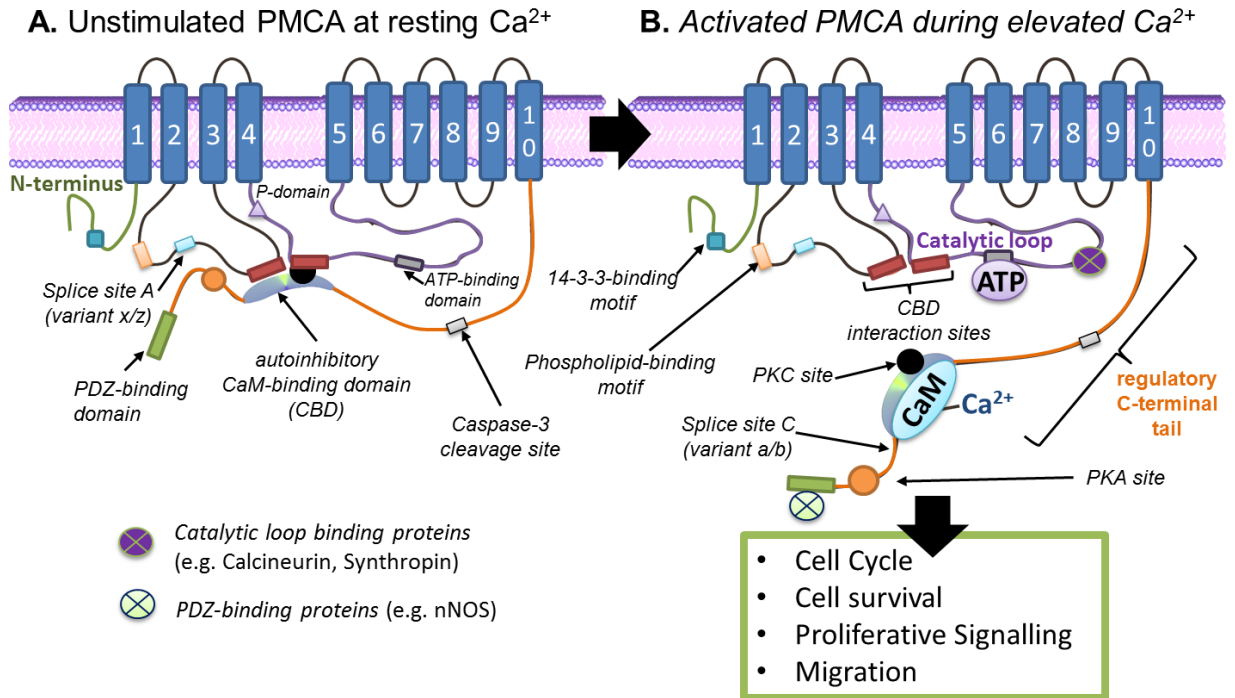
**Figure 1.6 – The structure of PMCA.** Structurally, PMCA is a 10-transmembrane protein which possesses large intracellular loops between transmembrane 2-3 (Site A, x/z splicing domain) and 4-5 (P-domain/catalytic loop). The N-terminus (green coloured tail) acts as a binding site for 14-3-3 protein. The C-terminus (orange coloured tail) of PMCAs could be splice form different variants. PMCA4, in particular, is known to possess three splice variants at the C-terminus. E.g. PMCA4a variant is truncated at splice site C whereas PMCA4b possesses PDZ-binding domain, enabling PMCA4b to act as a signal transduction hub. PMCA is suggested to modulate cell cycle, survival, proliferation and migration. Abbreviations: PMCA: plasma membrane $Ca^{2+}$ ATPase, CBD: $Ca^{2+}$ binding domain, CaM: calmodulin, PKC: phosphokinase C, PKA: phosphokinase A, nNOS: neuronal nitric oxide synthase, ATP: adenosine triphosphate. Figure modified from Bruce, J.I.E (2018) [203] and Strehler, E.E (2013) [234].

## 1.5.1   Plasma membrane calcium ATPase isoform 4 (PMCA4)

PMCA4 protein, encoded by the gene ATP2B4, is a member of the 10-transmembrane PMCA family. Although ubiquitously expressed in both excitatory and non-excitatory tissues (e.g. sperm, skeletal muscles, erythrocytes, etc.), knocking out PMCA4 is not embryonic lethal but notably resulted in male mice infertility [235]. Unlike the critical housekeeping role of PMCA1, PMCA4 is considered to possess a low basal activity and different splice variants of PMCA4 are suggested to play tissue-specific roles. PMCA4 splice variants are generated depending on the splicing at either the A-domain (PMCA4x/z) or the C-terminus (PMCA4a/b/d) [234] (Figure 1.6). These different combinations of splice variants led to structural variations that contribute to different PMCA4 functions and activity. Splice variations at the C-terminus of PMCA4a and PMCA4b result in altered basal autoinhibition, CaM-activation and dissociation rate. Caride, A.J *et al* (2007) demonstrated that PMCA4a has a truncated C-terminus which exhibits a fast CaM activation and dissociation rate by ~10-fold in comparison to PMCA4b which possesses a longer C-terminus [236]. In addition, increasing concentrations of $Ca^{2+}$ between 0.2 - 2 µM decreases the inactivation of PMCA4b (CaM dissociation) by ~30-fold whereas PMCA4a is less sensitive to the same $Ca^{2+}$ concentrations (~2-fold decrease) [236]. Due to its fast activation and inactivation rate, PMCA4a exhibits higher basal activity than PMCA4b [236] and function as a fast

response pump [220]. In contrast, PMCA4b is considered a slow response pump in comparison to other PMCA isoforms and variants [220].

The C-terminus of PMCA4b also contains a PDZ-binding domain which enables PMCA4b to interact with cytoskeletal, scaffolding and signalling molecules including nNOS [237], $Ca^{2+}$/calmodulin-dependent serine kinase (CASK) [238] and other membrane-associated guanylate kinases (MAGUKs) [206,214]. In addition to the PDZ-domain, other signalling molecules also interacts with PMCA4b, including tumour suppressor Ras-associated factor 1 (RASSF1) [239] and calcineurin [240], and truncated renalase RP-220 [241]. PMCA4, therefore, plays a diverse role in modulating signal transduction and has been suggested to participate in the vascular tone regulation via nNOS inhibition [242,243], G1 cell cycle progression [244], corneal epithelial cell migration during wound healing [245] and regulation of angiogenesis by calcineurin/NFAT modulation [246]. In addition, PMCA4 is suggested to play a role in cell migration as the expression of the pump is shown to be selectively enriched at the migration front of endothelial cells [193].

Remodelling of PMCA4 expression has been observed in multiple cancers, including PDAC [118]. Indeed, the alterations of PMCA4 expression has been associated proliferation [231,247], migration [246,248], and apoptosis resistance [249]. However, depending on the type of cancer, the role of PMCA4 is shown to mediate opposing roles. For instance, the expression of PMCA4 is suggested to play a role in proliferation and apoptotic resistance in breast cancer [231,247,249], however, its overexpression in colon cancer lead to decrease cell proliferation [233]. In the context of PDAC, Nakamura, T. et al. (2004) reported a 5-fold ATP2B4 (PMCA4) mRNA overexpression in PDAC tumours compared to normal pancreatic tissue [118], suggesting that PMCA4 may potentially play a role in PDAC malignancy.

## 1.6 Caveolae – a potential intersection between PMCA and glycolytic enzymes?

### 1.6.1 Caveolae

Caveolae are specialised lipid-enriched domains which manifest as 60-100 nm cave-like invaginations of the surface plasma membrane [250,251]. It is suggested that the caveolae facilitate spatial clustering of signalling components, thereby, facilitating signal transduction associated with the regulation of lipid homeostasis, $Ca^{2+}$ signalling, metabolism, mechanoprotection and endocytosis [251–254]. The loss of caveolae has been shown to influence plasma membrane lipid composition (e.g. cholesterol) [255], reduced endocytosis [256], inhibited lipid synthesis [257], altered mitochondrial respiration [258,259], cell migration [260], and impaired PMCA-mediated $Ca^{2+}$ clearance [113].

The following section briefly discusses the caveolae structure and function, the role of caveolin, as well as its potential relevance in the functional coupling between key GEs and PMCA (1.6.2 PMCA localisation in the caveolae and potential coupling to glycolytic enzyme)

### 1.6.1.1  Caveolae structural composition

The two key components of the caveolae are: structural proteins and phospholipids [251]. Key caveolae proteins are comprised of two main classes: 1) core structural proteins and 2) accessory proteins [251]. Core structural proteins are indispensable proteins required for caveolae formation. Formation of the caveolae bulb-like structure is dependent on the presence of cholesterol-binding caveolin-1 and 3 (Cav-1 and Cav-3) [250,251]. Conversely, the neck of the caveolae requires the presence of pacsin-2 and 3/syndapin II [261]. The stability of the caveolae curvature is modulated by lipid-binding cavin1 while the Esps 15 homology domain (EDH) isoforms 1, 2, and 4, modulates the stability of the caveolae neck [262]. Key accessory proteins, such as caveolin-2 (Cav-2), cavin2,3,4 as well as receptor tyrosine kinase-like orphan receptor 1 (ROR1) [263] are required to further modulate the shape, functional activity and stability of the caveolae [251,253].

As lipid-binding caveolins and cavins are core caveolae structural proteins, it is not surprising that lipids serve as a major structural component of the caveolae. Caveolins selectively binds to cholesterol, phosphatidylserine, phosphatidylinositol 4,5-bisphosphate (PtdIns(4,5)P2) [251] and sphingolipids [250]. Similarly, cavins are known to bind to phosphatidylserine and PtdIns(4,5)P2 [251]. The lipid composition of the caveolar compartment, therefore, is highly enriched in cholesterol, phospholipids, sphingolipids [250,251] and saturated fatty acids [264]. Although the enrichment of these lipids similarly occurs in "lipid rafts" [250], another distinctive lipid-enriched domain of the plasma membrane; the co-localisation of these lipids with caveolins is a characteristic used to distinguish caveolae from lipid rafts [265].

### 1.6.1.2  Functional role of the caveolae

Besides critical caveolar structural proteins and lipids, multiple signalling components also localise within the caveolae. The caveolae are suggested to act as a signalling platform by spatially clustering various signalling machineries, including modulators (e.g. cAMP, adenylyl cyclase), receptors (e.g. G-protein coupled receptors, tyrosine kinase receptors) and ion channels (e.g. Orai1, TRPC, PMCA) [266,267]. Therefore, depending on what residential signalling machineries are present within the compartment, the caveolae can play diverse roles in the regulation of these signalling pathways. The caveolae have been functionally associated with endocytosis, lipid homeostasis, $Ca^{2+}$ signalling, and metabolism [251–254].

**Signal transduction** – Various signalling receptors and effector molecules have been reported to reside within the caveolae, including TGF-β receptor (TGFβR), receptor tyrosine kinases (RTKs, e.g. VEGF, insulin receptor), G-protein coupled receptors (GPCRs e.g. adrenoceptor, muscarinic receptor), endothelial nitric oxide synthase (eNOS) [268,269]. The caveolae are suggested to compartmentally regulate and negatively modulate signal transductions by either inhibitory caveolin-binding or endocytosis. For instance, Cav-3 is suggested to bind to adenylyl cyclase, inhibiting its activation of β1-adrenoceptor in cardiomyocytes [270]. Indeed, Agarwa, SR. *et al* (2011) has reported that cholesterol depletion-mediated caveolae, releasing adenylyl cyclase from Cav-3, leads to altered sensitivity of β1-adrenoceptor activation of L-type $Ca^{2+}$ channels in rat cardiomyocytes [271], suggesting that the caveolae play an important role in compartmentalising β1-adrenoceptor to a local domain [269].

**Endocytosis** – Caveolae-mediated endocytosis has also been suggested to modulate signal transduction by internalization of signalling components (e.g. insulin receptor), cellular uptake of specific ligands (e.g. albumin) as well as caveolae turnover. For example, it has been shown in rat adipocytes that insulin promotes caveolae-mediated internalization of the insulin receptor [272] while Cav-1 knockout mice demonstrated insulin resistance [273]. Although caveolae are relative stable sub-domain structures where only 1% of formed caveolae undergo endocytosis [274], multiple ligands have been associated with caveolae-mediated endocytosis (e.g. albumin, folic acid, phosphatases) [275]. Findings in PDAC model suggest that caveolae-mediated endocytosis is important in albumin uptake [276], required to provide amino acids required for biosynthesis to fuel malignant growth [277].

**Lipid homeostasis** – Consistent findings demonstrate that Cav-1 and cavin-1 knockout mice exhibit a loss of caveolae in non-muscular tissues, small adipocyte due to lipodystrophy, and dysfunctional insulin response [273,278]. These observations suggest that caveolae play a role in the regulation of lipid homeostasis. As previously described (1.6.1.1 Caveolae structural composition), caveolins and cavins are lipid-binding proteins which been implicated in membrane lipid-trafficking to the plasma membrane, thereby, regulating lipid homeostasis [279] and signal transduction efficiency [280]. Indeed, the plasma membrane cholesterol content is altered depending on Cav-1 expression as its overexpression leads to enhance cholesterol contents [255] while Cav-1 knockdown shows reduced cholesterol content [281].

**Caveolae and metabolism –** The caveolae provide a clustering platform for multiple signalling machineries associated with glucose metabolism, such as insulin receptor, GLUT4 [282], glycolytic enzymes (PFK and ALD) [116,229]. Lloyd, PG and Hardin, CD (2001) have shown that methyl-β-cyclodextrin-mediated caveolae disruption leads to decrease lactate and glucose production in pig vascular smooth muscle cells [283]. Therefore, it has been suggested that the caveolae play a role in organising glucose metabolism and caveolae disruption results in disorganization of these glycolytic components, consequently reducing the glycolytic efficiency [283]. The same authors also reasoned that that caveolae-localised glycolysis components may provide privilege ATP for ATP-consuming processes at the plasma membrane e.g. ATPases and migration [283].

**Caveolae and $Ca^{2+}$ signalling** – Multiple $Ca^{2+}$ modulators (e.g. PMCAs, $IP_3R$, NCX, RyR2, TRPC, VDCC) and effectors (e.g. eNOS, PKC, PLC, CaM) reside within the caveolae, suggesting the caveolae serves as a microdomain for $Ca^{2+}$ signalling [228]. The caveolae have been widely suggested to facilitate the assembly and coupling of $Ca^{2+}$ signalling components. For instance, the caveolae are suggested to be required for the assembly/coupling of TRPC1 and $IP_3R$, enabling SOCE in human submandibular cells [284,285]. In addition, $Ca^{2+}$ signalling can be directly modulated by the caveolae, specifically by inhibitory Cav-3 binding to CaMII, preventing CaMII-mediated activation of VDCC in cardiomyocytes [286].

### 1.6.2 Caveolin

Caveolins (Cav) are oligomeric cholesterol-binding integral membrane proteins which are crucial for the formation of caveolae [251]. Caveolin possesses four domains: i) C-terminus, ii) intramembrane domain, iii) conserved scaffolding domain (CSD) and iv) N-terminus. A study by Ariotti, N *et al.* (2015) showed that the CSD region is important for signalling protein interaction and is critical for caveolae

assembly [287]. It is predicted that Cav likely assumed a hairpin conformation in the plasma membrane with both the N- and C-terminus facing the cytoplasm [251,287]. Cav often undergoes palmitoylation at the C-terminus to facilitate compartmental trafficking to the lipid-rich domains of the plasma membrane [288].

The caveolin family is comprised of three caveolin genes (CAV): CAV-1, CAV-2 and CAV-3. Caveolin-1 protein (Cav-1) is predominantly expressed in non-muscle cells whereas Cav-3 is exclusively expressed in muscle cells. While Cav-1 and Cav-3 are essential core components of the caveolae, Cav-2 requires the presence of either Cav-1 or Cav-3 to be chaperoned to the plasma membrane. Although the absence of Cav-2 does not affect caveolae assembly, Cav-2 is considered as a key accessory protein which facilitates caveolae formation and modulates the shape of caveolae.

Although the current opinions regarding the potential interaction of Cav-1 with other proteins at the CSD remains controversial [289,290], Cav-1 has been suggested to potentially interact with various signal transduction proteins (e.g. insulin receptor, protein kinase C, eNOS) [291–293], mitochondrial proteins (AFG3L2 subunit of the matrix-oriented AAA mitochondrial protease) [258], and key canonical glycolytic enzymes (PFK and ALD) [116,229]. Cav-1 knockdown models have been shown to impair mitochondrial respiration due to reduced $NAD^+$/NADH ratio[294], and dysfunction of electron transport chain complexes [258,294]. Similarly, Cav-1 knockdown in colorectal cancer cells has been shown to reduce glycolysis flux primarily by reduced GLUT3-transcription, reducing glucose uptake and lactate production while overexpression of Cav-1 leads to higher glycolytic flux [295].

## 1.6.3 PMCA localisation in the caveolae and potential coupling to glycolytic enzyme

Compartmentalization and association/coupling of glycolytic enzymes with the plasma membrane have been reported in multiple cell models, particularly erythrocytes [296] and vascular smooth muscles [116]. Erythrocytes are known to exhibit glycolytic enzyme coupling to the plasma membrane. Since they lack the mitochondria, erythrocytes are entirely dependent on glycolysis which essentially represents an extreme model of the Warburg effect. Since the major consumption of ATP by ion pumps and signalling occur at the membrane, that localization of ATP metabolon near the membrane where ATP consumers are located is potentially plausible. Campanella, M.E et al. (2005) and Chu, H. et al. (2013) showed that multiple glycolytic enzymes are capable of forming organized complexes in close association with the plasma membrane, to generate ATP pool in close proximity to ATP-consuming PMCA as well as $Na^+$/$K^+$ ATPases [297,298]. Moreover, Hardin, CD and colleagues (1992) has reported that $^{45}Ca^{2+}$ uptake into plasma membrane vesicular fraction containing $Ca^{2+}$/ $Mg^{2+}$ ATPases, derived from pig stomach vascular smooth muscle, can be driven by the presence of glycolytic substrates and cofactors in absence of exogenous ATP [227]. This further suggests that PMCA potentially possesses its own glycolytic ATP supply. As both PMCA [228] and GEs have been reported to reside within the caveolae [116,229], the caveolae may provide a platform for this functional coupling between PMCA and GEs.

Caveolae are specialized membrane compartment suggested to play a role in organizing signal transduction of multiple signalling pathways, including glycolysis. PFK1, a key glycolytic enzyme, has

been reported to be associate and co-localise within the same proximity as CAV-1 and CAV-3 at the caveolae [299,300]. Overexpression of CAV-1 has been shown to redirect PFK towards the plasma membrane to enhance glycolysis [116]. The upregulation of caveolae and CAV-1 have also been correlated with pancreatic cancer progression [301]. Besides fuelling the PMCA to maintain $Ca^{2+}$ homeostasis, the coupling of glycolytic enzymes to the plasma membrane may also potentially promote glycolysis. For instance, PFK-1 is inhibited by ATP (>2 mM), producing a negative feedback mechanism. Therefore, it is entirely feasible that the localization of PMCA, which is a major ATP consumer, will rapidly reduce [ATP] within the vicinity to PFK-1, thereby enhances the function of PFK-1 and thus drives glycolytic flux. Conversely, increased expression of PMCA may also facilitate ATP consumption to enhance glycolytic flux and production of anabolic precursor to fuel cancer cell growth. This suggests that GEs and PMCA potentially exhibits a functionally symbiotic relation and a better understanding of this relationship may provide insights on the strategy to therapeutically target PDAC.

Pancreatic cancer, due to its characteristic tumour hypovascularization, is associated with the hypoxic tumour microenvironment, resulting in metabolic stress which favours glycolytic-dependent metabolism [106,302]. A large proportion of pancreatic cancer patients also suffer from hyperglycaemia and diabetes [303], which may be a factor which facilitates the malignant shift to glycolytic-dependent metabolism. Since PDAC generally possesses K-Ras and p53 mutations, glycolysis is enhanced, and apoptosis is impaired [302]. Despite their apoptotic resistance, cancerous cells still require sufficient ATP to maintain PMCA-mediate $Ca^{2+}$ efflux to prevent cytosolic $Ca^{2+}$ overload and cell death [106,203]. Recent findings from our lab group, James, A.D et al. (2013) and (2015), have provided insights on the potential functional relationship between glycolytic ATP and PMCA in pancreatic cancer [121,123]. Our preceding data strongly suggest that PMCA is likely the main $Ca^{2+}$ efflux mechanism in PDAC cells and glycolysis inhibitors are capable of disrupting PMCA-mediated $Ca^{2+}$ clearance [17,121,123]. These complex relationships between PMCA localisation in the caveolae, cellular metabolism and the role of PMCA4 in PDAC are currently unclear.

## 1.7 PKM2 – an oncogenic glycolytic enzyme

Pyruvate kinase (PK) is an important canonical glycolytic enzyme responsible for catalysing phosphoenolpyruvate (PEP) to glycolytic ATP and pyruvate production in the final glycolytic step. PK has four tissue-selective isoforms: PKL (liver, kidney and erythrocytes), PKR (erythrocytes), PKM1 (muscles, brain and other tissues) and PKM2 (embryonic and various adult tissues). These four PK isozymes are encoded by two distinct genes: i) PKLR and ii) PKM which encodes for PKL/R and PKM1/2 splice variants, respectively. The current section will focus on the well-studied oncogenic protein – PKM2.

One of the alterations in the malignant tumour is the acquisition of embryonic pyruvate kinase isoform, PKM2. Normally absent in most adult tissue, PKM2 is limitedly expressed in adult adipocytes and is highly expressed in malignant tumours [42], including PDAC [304]. A single PKM2 monomer is 58 kDa and is comprised of three types of functional domains: A, B and C. The region between A and B forms the catalytic active site. The C domain contains the inter-subunit contact domain (ISCD), the

F1,6BP allosteric activator binding site as well as the nuclear localization sequence. Alternately spliced from the same 12-exons PKM gene, the mutually exclusive presence of either exon 9 or exon 10 in the mature PKM mRNA dictates the translation of PKM1 and PKM2, respectively. Exon 9 and 10 differ by 22 amino acids which encode ISCD of PKM. Unlike PKM1 which only exists as an active tetramer, PKM2 dynamically switches between the inactive dimeric to the active tetrameric conformation upon allosteric activation by F1,6BP. The dimeric PKM2 is formed by two PKM2 monomers interacting at their A domain while the tetrameric PKM2 is formed by the interactions of two dimers at the ISCD region.

Different PKM2 oligomeric state is known to possess different kinetic properties. Tetrameric PKM2 has a higher affinity for the PEP substrate and has higher catalytic activity. In contrast, dimeric PKM2 has a lower PEP binding affinity and low catalytic activity. In cancer, dimeric PKM2 provides an advantageous glycolytic 'bottle-neck' by accumulating upstream glycolytic metabolites which are precursors required for anabolic synthesis while avoiding lactate production [45]. The formation of different PKM2 oligomeric states is modulated by multiple factors, including allosteric activation (e.g. F1,6BP), activation of oncogene/aberrant signalling (e.g. PI3K/Akt, C-Myc) post-translational modification. This regulation of dimeric:tetrameric PKM2 ratio is crucial to determine the glycolytic flux as well as the anabolic synthesis required for malignant growth.

### 1.7.1 Regulation of PKM2 oligomeric states

**Allosteric Activation** – Multiple metabolic intermediates have been reported to modulate the oligomeric state of PKM2. Two key metabolic intermediates, F1,6BP and serine, are independent allosteric activators which promote the assembly of the enzymatically active tetrameric PKM2. F1,6BP, a glycolytic intermediate produced by PFK, is a known allosteric activator of PKM2. F1,6BP binds to the PKM2 allosteric binding site to convert the inactive dimeric to a stabilized and active tetrameric form [305]. Conversely, serine is reported to bind to an uncharacterized binding pocket of the PKM2 and allosterically activates PKM2 activity at a completely different site from F1,6BP [232]. Deprivation of F1,6BP and serine has been shown to inhibit the enzymatic activity of PKM2, likely by dissociation of the tetrameric conformation into dimer subunits [232,305]. (Figure 1.7)

**Figure 1.7 – The dynamics of PKM2 during the Warburg Effect.** Dimer/monomer PKM2 formation is induced by tyrosine kinase-mediated post-translational modification (phosphorylation, acetylation, oxidation) and oncoproteins (red text). Tetrameric PKM2 formation is induced by glycolytic metabolites e.g. F1,6BP, serine and SAICAR (green text). Abbreviations: F1,6BP: fructose-1,6 bisphosphate, PEP: phosphoenolpyruvate, GLUT1: glucose transporter 1, PK: pyruvate kinase, TCA cycle: tricarboxylic acid cycle, ATP: adenosine triphosphate, ADP: adenosine diphosphate, PKM1/2: pyruvate kinase muscle isoform 1/2, EGFR: epidermal growth factor receptor, IGFR: insulin-like growth factor receptor, FGFR: fibroblast growth factor receptor, ERK: extracellular signal-regulated kinase, LDHA: lactate dehydrogenase A, SAICAR: succinylaminoimidazolecarboxamide ribose-5′-phosphate, ROS: reactive oxygen species. Figure modified from Prakasam, G. *et al* (2018) [306].

**Oncogenic signalling** – Activation of multiple receptor tyrosine kinases (RTKs), including RAS/Raf/MEK/ERK/MAPK signalling pathways, is capable of modulating tumour metabolism in multiple ways. For instance, RTK-mediates phosphorylation of PKM2 and allosterically promotes dimeric PKM2 formation, leading to catalytic inactivation. This consequentially produces a glycolytic bottleneck at the terminal end of glycolysis and accumulation of anabolic intermediates [40,42]. Moreover, some oncogenic proteins directly interact and regulate PKM2 enzymatic activity [306]. For instance, the Jumonji C domain-containing dioxygenase (JMJD5) and human papillomavirus encoded E7 oncoprotein have been shown to inhibit tetrameric PKM2 association, promoting the inactive dimeric PKM2 formation [306–308].

**Post-translational modifications –** PKM2 uniquely possesses multiple conserved sites which are post-translationally modified by various oncogenic signalling proteins to enhance metabolic reprogramming towards aerobic glycolysis. Post-translational modifications (PTMs) of PKM2 regulates the functional activity of PKM2 and often result in inhibition of the PK activity or the dissociation of active tetrameric

43

PKM2 into its inactive dimeric state. Key PTMs which modulates the oligomeric states of PKM2 includes phosphorylation, acetylation, glycosylation and oxidation. Oncogenic tyrosine kinases, including JAK2 [309] and FGFR1[310] associated with PDAC, phosphorylate PKM2 at tyrosine residue 105 (Y105). This phosphorylation at Y105 sterically hinders F1,6BP-mediated allosteric activation, prevents tetrameric formation, and consequently inhibits PKM2 activity [311]. Similar to phosphorylation at the Y105, acetylation of PKM2 at lysine residue 433 (K433) disrupts the binding of F1,6BP and promotes the dimeric form of PKM2 as well as nuclear translocation [312]. Glycosylation of O-linked β-*N*-acetylglucosamine (O-GlcNAculated) at the threonine residue 405 (T405) and serine residue 406 (S406) has been shown to inhibit PK activity by dissociation of the tetrameric form thereby promoting the dimeric PKM2 conformation [313]. Besides oncogenic proteins, PKM2 is reported to be post-translationally modified by oxidation associated with hypoxia/oxidative stress. Oxidative PTM by reactive oxygen species (ROS) at the PKM2 cysteine residue 358 (C358) led to the destabilization of the active tetrameric PKM2 into the inactive dimeric state [314].

## 1.7.2 Non-canonical role of PKM2

Besides its canonical glycolytic role, PKM2 uniquely mediates multiple 'moon-lighting' functions which include protein kinase activity, transcription activation, redox regulation and angiogenesis [306,315]. The oligomeric state of PKM2 determines the moon-lighting function of PKM2. The tetrameric PKM2 demonstrates pyruvate kinase activity whereas the dimeric PKM2 is associated with nuclear localization and protein kinase activity [316]. A study by Yang, W. *et al.* (2013) suggested that monomeric PKM2 also had non-canonical roles as a histone kinase. Translocation of monomeric PKM2 is shown to promote the expression of C-Myc proto-oncogene and cyclin D1, subsequently enhancing cell cycle progression and malignant growth [317].

## 1.8 Summary

Pancreatic cancer, particularly PDAC, is a commonly diagnosed cancer with poor survival prognosis and limited treatment successes. PDAC tumours typically exhibit hypovascularization and fibrotic stromal hypertrophy, making the tumour phenotypically hypoxic, which in part, drives the malignant metabolic reprogramming towards glycolysis. PDAC exhibit aberrant overexpression of PKM2, a key mediator of the Warburg effect, which provides an advantageous accumulation of anabolic metabolites required for malignant growth. However, this Warburg shift is acquired at the expense of lower yield of ATP (2 ATP molecule per molecule of glucose compared to OXPHOS which yields up to 36 ATP molecule per molecule of glucose) and a higher rate of glucose consumption. Therefore, high glycolytic flux must be maintained to produce sufficient ATP to maintain cellular homeostasis processes, particularly $Ca^{2+}$ homeostasis, to prevent $Ca^{2+}$ overload-associated cell death. Previous studies by James, AD *et al* (2013, 2015) suggest that glycolytic ATP, not mitochondrial-derived ATP, is required to fuel PMCA-mediated $Ca^{2+}$ efflux in PDAC cells. Interestingly, remodelling of $Ca^{2+}$ signalling machinery manifesting in PDAC also includes the overexpression of PMCA4. Unlike the PMCA1 housekeeping role, PMCA4 is suggested to play a specialised role in modulating migration and apoptosis resistance in various cancer. Moreover, both PMCA4 and key glycolytic enzymes (e.g. PFK-1) have been found in the caveolae – a specialised compartmental "signalling hub" located on the plasma membrane. This compartmentalisation is hypothesized to provide a symbiotic coupling of ATP-producing glycolytic enzymes to fuel PMCA activity to maintain $Ca^{2+}$ homoeostasis. Conversely, the PMCA consumption of ATP prevents metabolite-mediated inhibition of glycolytic enzymes (e.g. >2 mM ATP can inhibit PFK-1 and PKM2), thereby, drives the glycolytic flux. As PDAC demonstrates upregulation of PMCA4, Cav-1 and PKM2, understanding the regulatory relationship between cellular metabolism and calcium signalling may provide crucial insight to selectively target PDAC.

## 1.8.1 Overarching Hypothesis

The remodelling of $Ca^{2+}$ signalling machinery in PDAC includes PMCA4 overexpression, which in other cancers, has been associated with apoptosis resistance and enhanced cell migration. Previous findings from the Bruce lab, particularly by James, AD *et al* (2013, 2015), have shown that glycolytic ATP is crucial for maintaining PMCA activity and the regulation of low resting $[Ca^{2+}]_i$, vital for PDAC cell survival [121,123]. Moreover, evidence suggests that PMCAs and membrane-associated GEs may reside in close proximity, potentially within the caveolae, potentially coupled in a symbiotic relationship where ATP-generating GEs could fuel PMCA activity while ATP-consuming PMCAs drive glycolytic flux by preventing ATP-mediated inhibition of key GEs, particularly PFK-1 and PKM2 (Figure 1.8). The disruption of this potential coupling between the plasma membrane GEs and PMCA may hypothetically reduce glycolytic flux, the Warburg phenotype and cut off the glycolytic ATP to the PMCA, inducing $Ca^{2+}$ overload and selective cell death in glycolytic ATP-reliant cancer cells. Therefore, understanding the role of PMCAs in PDAC, its potential functional coupling with ATP-providing glycolytic enzymes, and identification of putative GE plasma membrane-binding protein responsible for this close physical coupling, are of paramount importance and might provide a novel therapeutic strategy for selectively targeting PDAC cells.
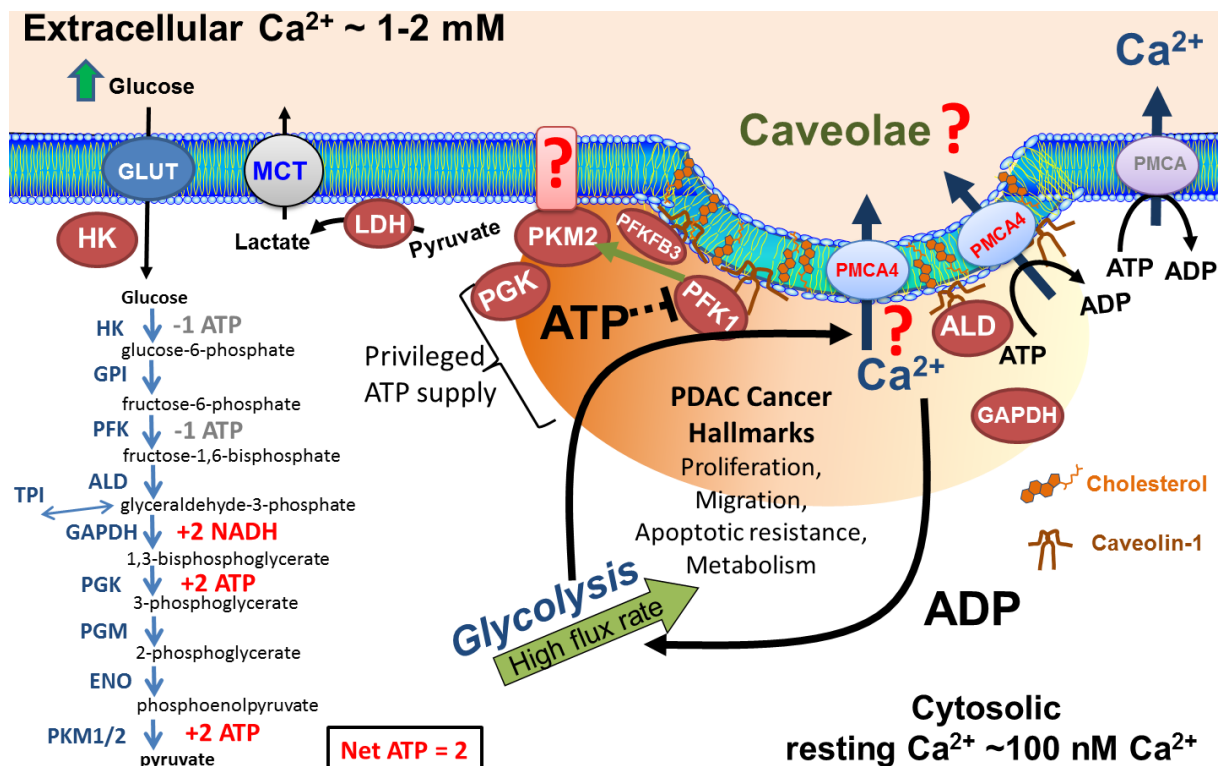


**Figure 1.8 – Hypothetical functional relationship between PMCA4 and membrane-associated glycolytic enzymes.** PDAC exhibiting the Warburg phenomenon is reliant on enhanced glycolytic flux to produce ATP. However, high ATP production is limited by PFK1 being allosterically inhibited by high ATP concentration. Evidence suggests that elevated expression of PMCA4 and membrane-associated glycolytic enzymes (PFK1, PFKFB3, and PKM2) are co-localised at the caveolae in PDAC. The localisation of key glycolytic enzymes near the ATP-consuming PMCA4 may prevent the ATP-induced negative feedback inhibition, enhancing glycolytic metabolism and fuelling cancer hallmarks. The red question mark indicates the key experimental objectives: 1) the role of PMCA4 in PDAC cancer hallmarks, 2) the functional relationship of caveolae, specifically caveolin-1, on PMCA4 activity, and 3) identification of putative GE (specifically PKM2)-plasma membrane binding protein.

### 1.8.2 Experimental objectives and specific aims

The following thesis examined three independent but interrelated topics of research. The key theme of the following thesis revolves around the role of PMCA4 on pancreatic cancer hallmarks, the functional importance of PMCA4 co-localization with GEs, particularly oncogenic PKM2, and the possible role of Cav-1 in facilitating compartmental clustering and functional coupling between GEs and PMCAs at the plasma membrane. In addition, we have used an unbiased approach to identify all putative GE-plasma membrane-binding proteins, specifically focusing on the most important ATP-generating and glycolytic flux regulating PKM2. Three manuscript style results chapter, each addressing three different main objectives and specific aims, are presented in this thesis. Each results chapter will contain its own introduction, methods, results and discussion chapter as follow:

## Results Chapter 1

**Objective** – To investigate the role of PMCA4 on different cancer hallmarks in PDAC cancer cell line.

**Specific aims**:

    i.    **To examine the clinical correlation between the expression of different PMCA isoforms and PDAC patient survival –** Achieved using data mining of publicly available databases

    ii.    **To examine the expression of different PMCA isoforms in different pancreatic cell lines and identify an *in vitro* PDAC model which reflects the clinical overexpression of PMCA4 –** Achieved using western immunoblotting and qPCR

    iii.    **To examine the functional (Ca$^{2+}$ efflux) contributions of PMCA4 in PDAC cells –** Achieved using in situ global Ca$^{2+}$ clearance and Ca$^{2+}$ overload assays in control vs siRNA-mediated PMCA4 knockdown cells

    iv.    **To examine the role of PMCA4 on PDAC hallmarks – cell metabolism, cell viability, proliferation and cell migration –** Achieved using siRNA knockdown of PMCA4

## Results Chapter 2

**Objective** – To investigate the role of Cav-1 in PDAC and its potential functional relationship with PMCA4

**Specific aims**:

    i)    **To examine the clinical correlation between PDAC patient survival and the expression of Cav-1 and its co-expression with PMCA4 –** Achieved using data mining of publicly available databases

    ii)    **To examine the effect of caveolae disruption using methyl-β-cyclodextrin on PMCA activity, Ca$^{2+}$ overload, cell viability and intracellular ATP levels –** Achieved using methyl-β-cyclodextrin sucrose gradient ultracentrifugation and Western immunoblotting.

Cell viability is assessed using sulforhodamine β assay. Intracellular ATP levels are assessed by ATP-luciferase and GO-ATeam transfected cells.

iii) **To investigate the effects Cav-1 knockdown on PMCA4 functional activity (Ca$^{2+}$ efflux) and metabolism in PDAC cells –** Achieved using in situ global Ca$^{2+}$ clearance and Ca$^{2+}$ overload assays in comparison to siRNA knockdowns of Cav-1. Cell metabolism was assessed using Seahorse XFe96 Analyzer (Mito Stress test, glucose stress test, ATP production rate test)

# Results Chapter 3

**Objective** – To screen for the putative plasma membrane PKM2-binding proteins in PDAC cancer cells

**Specific aims**:

i) **To examine the clinical correlation between the expression of PKM2 and PDAC patient survival –** Achieved by data mining from publicly available databases

ii) **To establish stable PDAC cell line (MIAPaCa-2) required for proximity-ligation bio-identification screening of PKM2 binding protein –** Cells stably transfected with proximity-ligation BirA* (E. Coli derived) protein fused to either PKM2-wild type, PKM2-mutant, and non-targeting Venus fluorophore bait. The expression of bait-BirA* is verified by FAC sorting, Western blot and immunofluorescence.

iii) **To investigate the effects of PKM2 binding protein in MIAPaCa-2 PDAC cells stably expressing PKM2 -BirA* in comparison to non-targeting Venus-BirA* –** Achieved by quantitative LC-MS/MS and publicly available protein-protein interaction databases

iv) **To screen and compare protein-protein interactions between PKM2 -BirA*, PKM2-mutant-BirA*, and Venus-BirA* –** Achieved by qualitative LC-MS/MS and publicly available protein-protein interaction databases

## 1.9 Journal/Alternative format thesis

The following thesis is presented in the Journal Format in accordance with the Presentation of Theses Policy (April 2019) of the University of Manchester. The three results chapters have been presented in the style of journal manuscripts to facilitate future manuscript submission processes. Aspects of the results chapters presented in this thesis have been reformatted into the same style to ensure continuity and coherency as a single body of work. To provide a continuous overview, this thesis provides an "Introductions" chapter and a "Concluding Discussion and Future Works" chapter to further ensure that this thesis is a single cohesive body of work.

Listed below are the title of the results chapters, author names, and the contributions of each author are indicated below as follow:

o **Chapter 2 – Results 1**

**Title:** PMCA4 is important for cell migration and apoptotic resistance of MIAPaCa-2 pancreatic cancer cell line

**Authors:** Pishyaporn Sritangos, Andrew D. James, Ahlam Sultan, Daniel A. Richardson, Jason I.E. Bruce

**Author contributions:** All the experiments presented in this study were designed, conducted, analysed and written by myself with supervision from Dr Jason Bruce. Preliminary experiments used as the based concept of this study were performed by Dr Andrew James. Ahlam Sultan and Daniel Richardson provided assistance in experimental preparations.

o **Chapter 3 – Results 2**

**Title:** Plasma Membrane Calcium ATPase 4 (PMCA4) functional activity is dependent on Cav-1 expression in pancreatic ductal adenocarcinoma cell

**Authors:** Pishyaporn Sritangos, Andrew D. James, Daniel A. Richardson, Eduardo Pena Alarcon, Ahlam Sultan, Jason I.E. Bruce.

**Author contributions:** The majority of experiments presented in this study were designed, conducted, analysed and written by myself with supervision from Dr Jason Bruce. Sucrose gradient ultracentrifugation and Western immunoblot of sucrose fractions were performed by Dr Andrew James. Daniel Richardson, Eduardo Pena Alarcon and Ahlam Sultan provided assistance in experimental preparations.

## Chapter 4 – Results 3

**Title:** Bio-identification of PKM2 interaction in MIAPaCa-2 pancreatic ductal adenocarcinoma Cells

**Authors:** Pishyaporn Sritangos, Andrew D. James and Jason I.E. Bruce

**Author contributions:** All the experiments presented in this study were conducted, analysed and written by myself with supervision from Dr Jason Bruce. Preliminary studies (cell surface biotinylation and plasmid validation) and the design of bait-BirA* plasmid were done by Dr Andrew James and Dr Jason Bruce. Generation of cell lines stably expressing bait-BirA* was performed by myself and Dr Andrew James.

# Chapter 2 – General Methods and Optimizations

## 2.1 Materials and methods

**2.1.1    Cell culture –** MIAPaCa-2 cell line was purchased from American Type Culture Collection (ATCC). Cells were cultured in 25 mM glucose Dulbecco's modified Eagle medium (DMEM; #D5796) supplemented with 10% fetal bovine serum (FBS; heat-inactivated FBS, #F9665) and 1% Penicillin/Streptomycin (#P0781), at $37^0$C, 5% $CO_2$ (g). Cells were subcultured at 80-90% confluence by washing with Dulbecco's phosphate buffer saline (DPBS; #D8537) then trypsinised for 3 minutes with 0.25% Trypsin-EDTA (#T4174). Cell suspensions were centrifuged at 93 rcf (relative centrifugal force) for 4 minutes at room temperature (RT) (U-32R centrifuge, BOECO Germany) then cell pellets were re-suspended in DMEM and transferred to either T-25 or T-75 flask (Corning®). Cells were passage 20 times or up to passage 30 after revival then discarded. Mycoplasma contamination was monitored using DAPI/Hoechst 33342 staining or PCR.

**2.1.2    Chemicals and reagents –** All chemicals and solvents were purchased from Sigma-Aldrich unless otherwise specified.

**2.1.3    Cell surface biotinylation –** Cell surface biotinylation assay was used to isolate plasma-membrane protein and any associated proteins. MIAPaCa-2 cells seeded to 95% confluence were rinsed twice with ice-cold phosphate buffered saline (PBS). The extracellular glycosylated transmembrane proteins were labelled with Sulfo-NHS-SS-Biotin. Cells were lysed and cell lysates were separated by centrifugation at 10000 rcf. A NeutrAvidin Agarose column (Thermo Fisher Scientific), pre-calibrated at room temperature (RT) on an end-over-end rotating mixer, was used to bind the biotinylated sample and separate the non-biotinylated fractions by centrifugation. Bounded biotinylated proteins were eluted with 1x SDS-PAGE sample buffer containing 50 mM dithiothreitol (DTT) then analysed by Western immunoblot. [114]

**2.1.4    Sucrose gradient ultracentrifugation –** The following method to separate proteins based on the density of the caveolin-rich fractions [318]. MIAPaCa-2 cells were homogenized in 400 μl 0.5 M $Na_2CO_3$ (pH 11) using an Omni blade homogenizer and sonication. Homogenate volume was adjusted to 450 μl with 0.5 M $Na_2CO_3$ buffer then mixed with 80% sucrose in MBS (2-(N-Morpholino) ethanesulfonic acid-buffered saline). Discontinuous sucrose gradient was produced by layering 700 μl of 35% sucrose then adding 625 μl of 5% sucrose on top. Samples were separated by centrifugation in a TLS55 rotor (Beckman TL100 centrifuge), at 131440 rcf for 16 h at 4°C. From discontinuous sucrose gradient, 12 fractions of 175 μl samples were precipitated with 175 μl 10% trichloroacetic acid (TCA) for 30 minutes on ice. Precipitants were separated by centrifugation at 5654 rcf for 5 min. Precipitated pellets were re-suspended in 2% SDS, 1M Tris pH 8.8 and 5 x Laemmli buffer then denatured at $90^0$C for 5 min. Cell lysates were stored at $-20^0$ C until used for Western blot analysis.[114]

**2.1.5    Western immunoblot**

**Protein lysate preparation –** Cells were harvested using radioimmunoprecipitation assay (RIPA) buffer (50 mM Tris Base, 40 mM sodium pyrophosphate, 100 mM sodium fluoride, 150 mM sodium chloride, 1% Triton-X, 0.5 M EDTA and EGTA and 0.1 mM sodium orthovanadate, pH 7.4) supplemented with

cOmplete, EDTA-free protease inhibitor cocktail (#11873580001) and PhosSTOP™ phosphatase Inhibitor (#4906837001). Cell lysates were sonicated on ice (amplitude 7-8, at 5 seconds interval, 5 times using Soniprep 150 Ultrasonic disintegrator, MSE), incubated on ice for 30 minutes, and then centrifuged at 17136 rcf (PRISMR centrifuge, Lab International Inc.) at 4°C, for 25 minutes. Lysate supernatant was collected and stored at -80°C until used.

**Bradford assay protein quantification –** The protein content of each protein lysates prepared were quantified by Bradford assay (Protein assay dye reagent, #500-0006, Bio-Rad), using a clear 96 well plate (Corning®) and a colourimetric plate reader (Synergy HT, BioTEK). Freshly prepared bovine serum albumin (BSA, #5217, Tocris) protein standards (10 µl of 0, 0.5, 1, 2, 3, 4, 5 mg BSA/ml dH$_2$O) and 10 µl of freshly diluted lysate samples (of 1:10-1:30 dilutions) were used for protein content quantification. Bradford reagent diluted according to manufacturer's instruction (1:5 in dH$_2$O) were added (200 µl/well) into the wells containing standards and samples. After 5 minutes of incubation at RT, optical density was measured at 595 nm absorbance. Protein standard concentrations are linearly correlated ($R^2 > 0.95$) between optical density measured at (595 nm), enabling the calculation of protein contents in the samples using a linear regression formula: $\mathbf{y = a + b}x$, where $\mathbf{y}$ = optical density at 595 nm, $\mathbf{a}$ = intersection, $\mathbf{b}$ = slope and $x$ = protein concentration (mg/ml). Blank values (BSA 0 mg/ml) were subtracted to eliminate background noise.

**Gel electrophoresis and Western immunoblot detection** – Equal concentrations of protein samples (ranging between 2-10 µg depending on the proteins probed) adjusted to equal volumes using RIPA buffer, were denatured in Laemmli sample buffer (Bio-Rad) at 95°C, for 5 minutes. Ladder protein standard (Broad range, # P7712, New England BioLabs Inc.) and denatured sample lysates were loaded at equal volumes into SDS-PAGE gels (4-12% NuPAGE® Bis-Tris gel, Invitrogen, Thermo Fisher Scientific). Using mini gel tank electrophoresis chamber, NuPAGE® MOPS SDS Running Buffer (#NP0001, Thermo Fisher Scientific), and electrophoresis power supply (160 Volts constant, 80-100 minutes, E831 electrophoresis power supply, Consort bvba) were used to resolve protein lysates by size. Resolved proteins were transferred onto nitrocellulose membranes (0.45 µm nitrocellulose, Amersham) using TransBlot® Turbo transfer buffer (#10026938, Bio-Rad) and transfer system (1.3 Amps constant, up to 25 V, 15 minutes; Bio-Rad). Nitrocellulose membranes were blocked in 5% BSA for 1 h at RT before blotted with primary antibody overnight at 4°C. PMCA4 (clone JA9, #MA1-914), pan PMCA (clone 5F10, #MA3-914), PMCA1 (#PA1-914), PMCA2 (#PA1-915), and PMCA3 (#PA1-916) primary antibodies were purchased from Thermo Fisher Scientific. Cav-1 (#3267), PKM2 (#4053) PFKP (#8164), PFKFB3 (#13123) and β-Actin (#3700) primary antibodies were purchased from Cell Signaling Technology. After primary antibodies incubation, membranes were washed with 0.1% Tween Tris buffer solution (TBST) then incubated with matching anti-Rabbit (#7074, Cell Signaling Technology) or anti-mouse (#7076 Cell Signaling Technology) horseradish peroxidase (HRP)-linked secondary antibodies for 1-2 hour at RT. After rinsing with TBST, the membranes were treated with enhanced chemiluminescence reagent (ECL; Clarity™ Western ECL substrate, Bio-Rad) at RT, and protein signals were quantitated using ChemiDoc XRS+ (Bio-Rad). Membranes were then later exposed to x-ray films (CL-XPosure, #34090, Thermo Fisher Scientific/ Amersham Hyperfilm, #28906837, GE Healthcare Life

Sciences) then developed. Relative protein contents in each protein bands were quantified based on band density, using Image Lab™ (version 5.0, Bio-Rad). Quantified proteins were normalised to housekeeping protein, primarily β-Actin, to account for gel loading errors.

**2.1.6    Sulforhodamine B (SRB) protein quantification assay –** Based on the protocol published by Vichai, V. and Kirtikara, K. (2006), SRB assay quantitates total cellular protein of cells adhering to the culture surface, where cell adherence is considered as criteria of cell viability [319]. Cells were seeded at 5,000 cells per well, in 50 µl volume, in 96-well plates. At least 4 replicates were performed per treatment condition. Blank wells, containing only media and no cells, were available for background subtraction. Cells were allowed to attach for 24 h prior to addition of 50 µl treatment media. After designated treatment time, cells were fixed with 100 µl chilled 10% trichloroacetic acid (TCA; #T6399) for 1 hr, at $4^0$C. Fixed cells were gently rinsed under tap water and allowed to dry. Cells were stained with 100 µl 0.0057% SRB (#S1402) for 30 min, at RT, then rinsed in 1% acetic acid to remove excess dye and dried. 200 µl of 10 mM Tris base, pH 10.5 was added to each well to re-dissolve the dye. To facilitate dye resuspension, the Tris-added plate was placed on the shaker at 100 rpm for 5 minutes at RT. The protein content in each well was quantitated with a microplate reader (Synergy HT, BioTEK) at 540 nm absorbance. Blank values were subtracted to eliminate background noise.

**2.1.7    Cell count kit-8 (WST-8) viability assay –** WST-8 assay quantifies the extracellular reductive environment of the cells, where the reductive capability of cells is considered as criteria of cell viability. Cells were seeded at 5,000 cells per well, in 100 µl volume, in 96-well plates. At least 4 replicates were performed per treatment condition. Cells were allowed to attach for 24 h prior to treatment. Blank wells containing media with no cells seeded were available for background subtraction. The multichannel pipette was used to add 10 µl treatment media to both seeded and blank wells. After the designated treatment time, 10 µl of WST-8 reagent (Cell count kit-8, Dojindo) was added to each well. The WST-8 added plates were incubated at $37^0$C, 5% $CO_2$ (g), for 2 h then cell viability was quantified with a microplate reader (Synergy HT, BioTEK) at 450 nm absorbance. Treatment matching blanks were subtracted to eliminate background noise.

**2.1.8    ATP-luciferase ATP quantification and cell viability assay –** The ATP-luciferase assay employs the addition of luciferin substrate and firefly-luciferase enzyme into cell lysate, using cellular ATP to produce luminescence. ATP levels can be used to investigate cell metabolism and cell viability, where maintenance of ATP is considered as the criteria for cell viability. Cells were seeded at 5,000 cells per well, in 50 µl volume, into white-wall flat-bottom 96-well plates. At least 4 replicates were performed per treatment condition. Blank wells containing media with no cells seeded were available for background subtraction. Cells were allowed to attach for 24 h before the addition of 50 µl treatment media. After the designated treatment period, cells were lysed with 50 µl of lysis buffer for 10 min, at RT, followed by addition of 100 µl AMR+ (ViaLight® Plus kit, Lonza) for 2 min, at RT. Luminescence derived from ATP was measured by a microplate reader (Synergy HT, BioTEK) at 595 nm. Treatment matching blanks were subtracted to eliminate background noise.

### 2.1.9 Live-cell fluorescence microscopy

**Seeding cells on glass coverslip –** Circular glass coverslips (16 mm; VWR) were sterilized with 70% absolute ethanol (EtOH) and placed into each well of a non-culture-coated 6-well plate and left to dry in the Biosafety Cabinet (Class II, Safefast Classic 212; Faster s.r.l). MIAPaCa-2 cells grown to 80% confluence were trypsinised and cell pellets were re-suspended in 6 ml of DMEM media. DMEM media and 100 µl of cell resuspension were added to each well containing sterilized coverslip. Cells were allowed to attach to the coverslips for at least 24 h before usage.

**Fura-2 ratiometric calcium indicator –** Fura-2 is a ratiometric $Ca^{2+}$ whereby binding of free $Ca^{2+}$ to the dye shifts its peak excitation from 380 nm ($Ca^{2+}$ free dye) to 340 nm ($Ca^{2+}$ bound dye). A stock of 0.5 mM fura-2 (AM, acetoxymethyl; #0103, TEFLabs) was made using 1:1 ratio of DMSO:pluronic acid. Cells were loaded with 4 µM fura-2 (AM) in 1x HEPES-buffered physiological saline solution (HPSS; 10 mM HEPES, 4.7 mM KCl, 0.56 mM $MgCl_2$, 138 mM NaCl, 1.28 mM $CaCl_2$, 5.5 mM Glucose, pH 7.4) at RT for 40 minutes. Then, dye-free HPSS was used to equilibrate de-esterified fura-2 dye loaded cells for 20 minutes, at RT. Dye-loaded cells were mounted to form the base of a perfusion chamber attached with a gravity-fed perfusion system (Harvard apparatus). Fluorescent images were acquired using a monochromator illumination system (Cairn Research) and charge-coupled device-based camera. Cells were excited at 340 and 380 nm (50 msec exposure) and the emitted light (510 nm) was separated using a 400 nm dichroic with 505LP filter. Background-subtracted images were collected at 5 second intervals on a Nikon TE2000 inverted microscope fitted with x40 oil immersion objective, 1.3 numerical aperture. The light was detected by CoolSNAP HQ interline progressive-scan CCD (Roper Scientific Photometrics). Images were acquired and analysed by MetaFluor software (Molecular Devices). Intracellular $Ca^{2+}$ ($[Ca^{2+}]_i$) was measured as fura-2 340/380 nm fluorescence ratio. [108]

**Fluo-4 calcium indicator –** A stock of 5 mM fluo-4 (AM) dye (#F14201, Molecular probe/Thermo Fisher Scientific) was made with 1:1 ratio of DMSO:pluronic acid. Cells seeded on to glass coverslips were incubated with 5 µM fluo-4 dye in HPSS for 30 minutes at RT. De-esterified fluo-4 dyes were allowed to equilibrate in dye-free HPSS for 10 minutes, at RT. Dye-loaded cells were mounted onto the perfusion chamber attached with gravity-fed perfusion system. Fluorescent images were acquired with a monochromator illumination system and cells were excited at 494 nm (50 msec exposure). Background-subtracted images acquired at 506 nm emission were collected at 5 second intervals on a Nikon TE2000 fitted inverted microscope (x40 oil immersion objective, 1.3 numerical aperture). The light was detected by CoolSNAP HQ interline progressive-scan CCD camera and image were acquired and analysed with MetaFluor software. $[Ca^{2+}]_i$ was obtained from 494 nm fluorescence signal.

**2.1.11 Fura-2 calcium concentration calibration –** As fura-2 340/380 nm fluorescence ratio represents the Ca$^{2+}$ bound dye/Ca$^{2+}$ free dye status, this relative fura-2 ratios ratio is proportional to [Ca$^{2+}$]. The equation established by Grynkiewicz *et al* (1985) could be used to calculated [Ca$^{2+}$] from fura-2 ratio [320] as follows:

$$[Ca^{2+}]_i = K_d \times \left( \frac{R - R_{min}}{R_{max} - R} \right) \times \left( \frac{Sf_{380}}{Sb_{380}} \right)$$

Following this equation, [Ca$^{2+}$]$_i$ represents intracellular Ca$^{2+}$ concentration and $K_d$ represents the cytosolic Ca$^{2+}$ binding affinity of fura-2 (225 nM, as determined by Grynkiewicz *et al* (1985)). In order to translate this 340/380 nm fluorescence ratio (R) into meaningful intracellular Ca$^{2+}$ concentrations ([Ca$^{2+}$]$_i$), the minimum ratio ($R_{min}$) and maximum ratio ($R_{max}$) as well as the raw fluorescence 380 nm signal of the fura-2 in the absence (Sf$_{380}$; Ca$^{2+}$ free dye state) and the presence of Ca$^{2+}$ (Sb$_{380}$; Ca$^{2+}$ bound dye state) must be determined.

Using 4 µM fura-2 loaded MIAPaCa-2 cells, these calibrations were performed firstly by perfusion with Ca$^{2+}$ free HPSS (supplemented with 1 mM EGTA). Once a stable basal fura-2 ratio has been established, the perfusion was stopped and 10 µM ionomycin (#BP25271, Fisher Scientific) was added to the static bath for 2 minutes. As an ionophore, ionomycin was employed to facilitate the depletion of intracellular Ca$^{2+}$ stores [321]. Afterwards, further perfusion with Ca$^{2+}$ free HPSS with 1 mM EGTA was continued to facilitate cellular Ca$^{2+}$ removal until a stable $R_{min}$ was reached. Later perfusion with 20 mM Ca$^{2+}$ HPSS was done to yield the $R_{max}$. Using Grynkiewicz *et al* (1985) equation, the [Ca$^{2+}$]$_i$ of each individual cells could be calculated, converted into log[Ca$^{2+}$]$_i$ and plotted against fura-2 ratio to establish a concentration curve (Figure 2.1). Through multiple independent calibrations experiments, a robust calibration curve was generated from 30-50 individual MIAPaCa-2 cells, enabling the extrapolation of this calibration for other fura-2 experiments done in MIAPaCa-2 cells. It should be noted, however, that fura-2 detection limit is reported to be 1 nM [322] and its saturation is reported to occur at 1 µM Ca$^{2+}$ [323]. Therefore, any calculated [Ca$^{2+}$]$_i$ value that fell out of this narrow 1-1000 nM range may not be an accurate estimation.
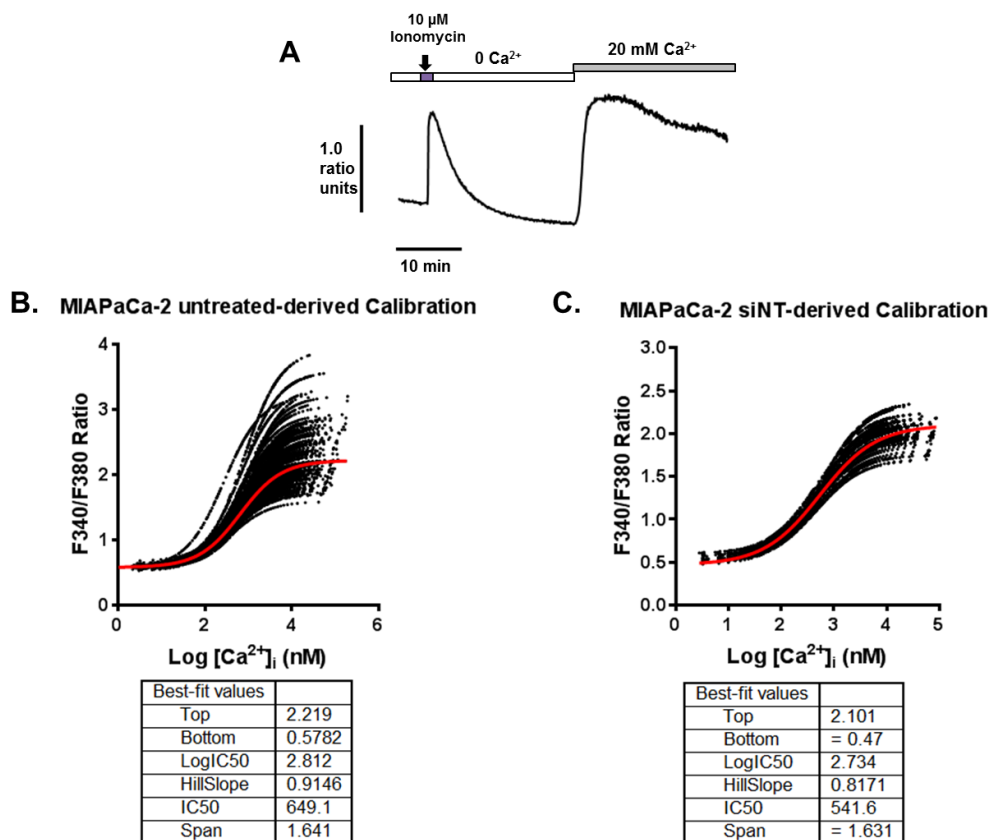
**Figure 2.1 – Fura-2 Ca²⁺ calibration curve. A,** Representative trace of Ca²⁺ calibration curve. White bar represents 0 Ca²⁺ HPSS perfusion whereas the grey bar represents 20 mM Ca²⁺ HPSS perfusion. The purple bar represents the treatment of 10 µM ionomycin under static bath condition. **B,** Ca²⁺ calibration derived from 50 individual untreated MIAPaCa-2 cells and **C,** calibration curved obtained from 30 individual siNT treated (48-72 h) MIAPaCa-2 cells. Black dotted lines represent data derived from individual cells. The red line represents a sigmoidal best-fit data. The key values in the table represent the averaged best-fit data: Top: $R_{max}$; Bottom: $R_{min}$; IC50: Kd.

**2.1.12  Calcium overload assay –** Cells were perfused with HPSS for at least 200 sec until the 340/380 nm fluorescence ratio stabilizes. Treated HPSS was either perfused or manually added into the perfusion chamber then treatment incubation was done under static bath condition. Non-treated HPSS was perfused into the chamber for 15 minutes to remove the remaining treatment from the chamber. Afterwards, 100 µM ATP was added to assess Ca²⁺ signalling response and cell viability. The following equation was used to calculate concentration of intracellular Ca²⁺ ($[Ca^{2+}]i$): $[Ca^{2=}]$ (nM) = Kd (nM) * ((Ratio - bottom)/(top - Ratio)) [324]. $[Ca^{2+}]i$ values calculated in this report were attained from the following two independent Ca²⁺ calibration equation (obtained from figure 2.1) as follow:

A.  *Untreated MIAPaCa-2 cells:* $[Ca^{2+}]_i$ nM = 649.1 nM * ((Ratio – 0.5782)/(2.219 - Ratio))

B.  *MIAPaCa-2 cells treated with siNT:* $[Ca^{2+}]_i$ nM = 541.6 nM * ((Ratio – 0.47)/(2.101 - Ratio)).

$[Ca^{2+}]i$ was quantified by the area under the curve (AUC) and maximum change in $[Ca^{2+}]i$ ($Max\Delta[Ca^{2+}]i$) during treatment and washing period. Response to ATP was defined as $\Delta[Ca^{2+}]i > 100$ nM in response to 100 µM ATP. Data are shown as % of cells responding to ATP.[108]

**2.1.13 Calcium clearance assay –** PMCA activity was measured by *in situ* $Ca^{2+}$ clearance assay [325]. MIAPaCa-2 cells were perfused with HPSS in the absence of external $Ca^{2+}$ with 1 mM of EGTA, a divalent cation chelator [326], and 30 µM of cyclopiazonic acid (CPA; # 1235, Tocris). CPA was used to inhibit sarcoendoplasmic reticulum calcium ATPase (SERCA) and prevent $Ca^{2+}$ uptake into the ER stores [327], enabling passive $Ca^{2+}$ leak from the ER. This induced a transient increase in cytosolic $[Ca^{2+}]_i$ and PMCA activity was assumed to restore the baseline $[Ca^{2+}]_i$ [114]. Subsequent perfusion with 20 mM $Ca^{2+}$ HPSS supplemented with CPA (20 mM $Ca^{2+}$ HPSS) induced a rapid $[Ca^{2+}]_i$ increase due to store-operated $Ca^{2+}$ entry (SOCE). After the $Ca^{2+}$ influx phase reached a maximum plateau, external $Ca^{2+}$ was again removed (1 mM EGTA and CPA HPSS buffer without $Ca^{2+}$; 0 $Ca^{2+}$ HPSS) to induce $Ca^{2+}$ clearance [44]. When the basal $[Ca^{2+}]_i$ recovered after the first influx/clearance phase, the perfusion was stopped to create a "static bath" and designated treatment was added. A static bath is beneficial when test reagents used are viscous (e.g. MβC) or very expensive and cannot be readily perfused (e.g. caloxin 1c2). After treatment incubation in a static bath, a second influx/clearance rate was induced and a paired comparison between the first non-treated clearance (R1) and the second treated clearance phase (R2) could be made to yield the relative clearance rate (R2/R1). To ensure that static bath condition had no effect on the second $Ca^{2+}$ clearance phase, cells were incubated in static condition with non-treated 0 $Ca^{2+}$ HPSS buffer for same duration as the treated cells, then a second clearance phase was induced (time-matched control). The $Ca^{2+}$ clearance rate could be measured by multiple methods such as fitting the clearance phase to either: i) a single exponential decay to yield the time constant (tau, τ) or ii) linear fit to yield % linear clearance rate [108,114,325]. The single exponential decay model can only be fitted to a clearance phase where the $[Ca^{2+}]_i$ baseline/asymptote is similar. In "unpaired" $Ca^{2+}$ clearance experiments (e.g. siRNA knockdown), where only a single clearance curve is generated, a single exponential decay fit was often used for $Ca^{2+}$ clearance analysis where the average time constant were compared between the treatment and controlled condition. However, in "paired" designed $Ca^{2+}$ clearance experiments, when treatments (e.g. carboxyoesin) severely inhibit the $Ca^{2+}$ clearance and induces a linear clearance phase where the basal $[Ca^{2+}]_i$ approaches a different asymptote, the single exponential decay fit cannot be used to assess the changes in $Ca^{2+}$ clearance rate. Linear regression was fitted over 60 sec on the first $Ca^{2+}$ efflux phase to yield the control $Ca^{2+}$ clearance rate (R1). The second $Ca^{2+}$ clearance rate over 60 seconds was calculated by fitting from the same fura-2 ratio values as the first clearance phase. It is important to linear-fit the first and second clearance phase from the same starting fura-2 ratio value to control for the possibilities that different $[Ca^{2+}]_i$ may influence the clearance rate [114,121]. The % linear clearance rate was calculated by normalizing the linear clearance R2/R1.
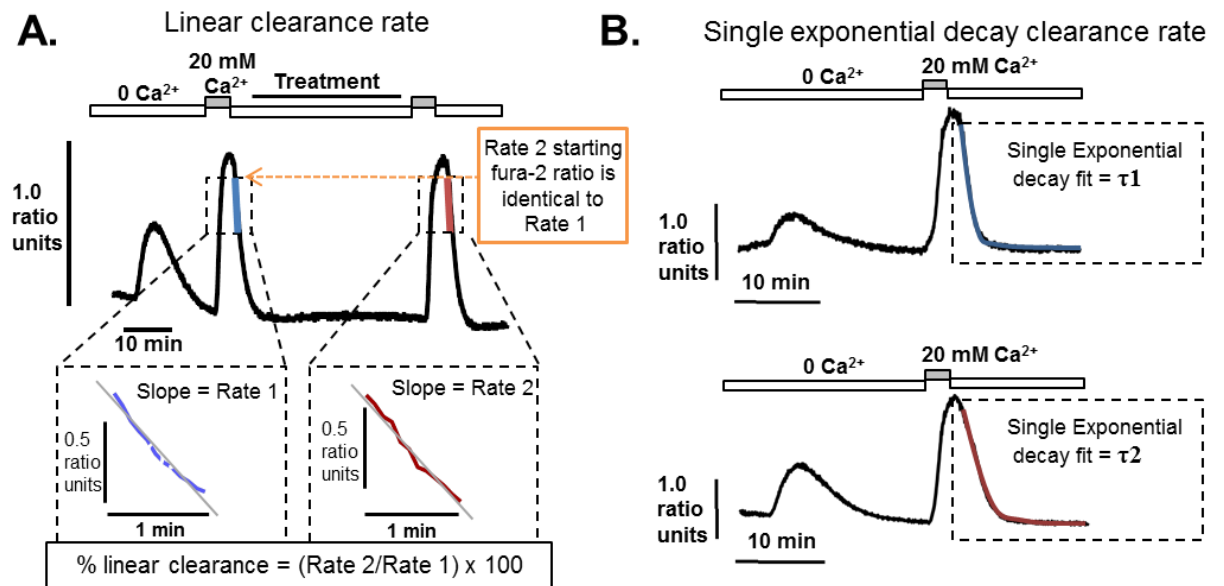
**Figure 2.2 –Ca$^{2+}$ clearance rate calculation methods. A,** Linear Ca$^{2+}$ clearance rate is calculated by obtaining the fastest clearance, from the first (Rate 1) and second (Rate 2) clearance phases during 60 sec duration. Then, these clearances are fitted to linear regression to obtain the clearance rate. It should be noted that Rate 2 starting fura-2 ratio for the linear rate calculation must be as similar, if not identical, to Rate 1. The % linear clearance rate comparison can then be done. This provides a paired-experimental design where the control (Rate 1) and treatment (Rate 2) can be compared within the same cell. **B,** Single exponential decay clearance fit was performed on siRNA treated cells which displayed less dramatic inhibition of PMCA activity. As siRNA knockdown process requires a period of 48-72 hr, a paired experimental design cannot be achieved. The clearance phase of siRNA treated cells was obtained and fitted to a single exponential decay curve. The $\tau$ obtained represents the clearance rate. White bar represents 0 Ca$^{2+}$ HPSS containing 30 µM while the grey bar represents 20 mM Ca$^{2+}$ HPSS containing 30 µM CPA. The blue line represents Rate 1 (control) and the red line represents Rate 2 (treated). Figure modified from James, A.D (2015) [114]**.**

**2.1.14  GO-ATeam ATP-FRET reporter assay –** GO-ATeam is a Förste resonance energy transfer (FRET)-based fluorescent ATP probe which employs green fluorescent protein (GFP) and orange fluorescent protein (OFP) as the FRET pair. In ATP-free conditions, the GFP and OFP FRET pairs are separated and green light at 510 nm is primarily emitted. In ATP-bound conditions, the FRET pair comes together and the GFP excites the OFP emitting an orange/red light at 560 nm.[328] GO-ATeam expressing cells were mounted in the perfusion chamber and perfused with HPSS at RT. The 470 nm excitation wavelength was separated from the emission peaks by a 505 nm dichroic with dual-band emission filter (59004m ER FITC/TRITC Dual emitter). The emitted fluorescence peak at 510 nm (ATP-free) and 565 nm (ATP-bound) was collected at 510 nm and above 560 nm using OptoSplit Image Splitter fitted with JC1 565 nm dichroic (Cairn Research), allowing two separate images to be projected onto the sensor. *In situ* ATP was quantified by the 565/510 nm fluorescence ratio (R). After perfusion with non-treated HPSS for at least 200 sec, the immediate fluorescence ratio was used as the maximum *in situ* ATP signal (Rmax). Treatment was added in HPSS and was either perfused or manually added into the perfusion chamber. After designated treatment time in static conditions, metabolic inhibitor cocktail (MIC; 2 mM iodoacetate, IAA; 500 µM bromopyruvate, BrPy; 10 µM oligomycin, OM; 2 µM antimycin) was added to demonstrate complete ATP depletion, yielding the minimum ATP signal (Rmin). Data were expressed as % ATP and were calculated by R$t$/$\Delta$Rmax, where R$t$ = average of 10 ratio values at 0, 5, 10, 20 and 30 minutes time points after treatment.[114]

**2.1.15 Immunofluorescence imaging –** MIAPaCa-2 cells were seeded at 20,000 cells onto sterile glass covers, into 12-well culture plates where each well contains pre-designated siRNA (25 nM of siNT, siPMCA4 or siCav-1) and 0.1% DharmaFect1 transfection reagent mixture. Cells were incubated in siRNA for at least 48 hours prior to further treatment for fixation.

**Immunofluorescence staining –** Cells grown on glass coverslips were fixed with 4% paraformaldehyde (PFA; #P6148) in HEPES buffer (15 mM HEPES, 135 mM NaCl, 5 mM KCl, 1.8 mM $CaCl_2$, 0.8 mM $MgCl_2$, pH 7.4) for 30 minutes, at RT. Fixed cells were rinsed with HEPES buffer then permeabilized with 0.1% saponin (#47036) in HEPES buffer for 3 minutes, at RT. As our experiment focuses on imaging plasma membrane-associated glycolytic enzymes, saponin was chosen to selectively permeabilize lipid enriched plasma membrane without permeabilizing the nucleus; hypothetically limiting immunofluorescence staining to the plasma membrane subdomains. Permeabilized cells were again rinsed with HEPES buffer then blocked with 1% BSA in HEPES buffer (at least 30 minutes, RT). Blocked coverslips were incubated with designated mixtures of primary antibody (1:400 of PMCA4, Cav-1, PKM2, anti-Myc, anti-biotin) overnight, at 4$^o$C. After primary antibody incubation, coverslips were rinsed then further incubated with corresponding mixtures of Alexa Fluor 488 (1:400) and 594 (1:400) secondary antibodies (Thermo Fisher Scientific) for 2 hours, at RT. Coverslips were further rinsed then incubated with 300 nM Hoechst 33342 (#3570, Invitrogen Thermo Fisher Scientific) in HEPES buffer for 10 minutes, at RT, to enable visualization of the nucleus. Stained cells were mounted onto glass slides with ProLong$^{TM}$ Gold antifade mountant (#P36934, Thermo Fisher Scientific). Mounted slides were dried overnight and kept in the dark until imaged.

**MitoTracker Red –** siRNA knocked down cells were treated with either 4 µM CCCP (#C2759) or 100 nM MitoTracker Red CMXRos (#M7512, Invitrogen$^{TM}$ Thermo Fisher Scientific) or 0.1% DMSO vehicle control for 10 minutes, at 37$^o$C, prior to fixation. Cells were fixed with 4% PFA for 15 minutes at RT, rinsed with HEPES buffer, then mounted on a glass slide using VectaShield containing DAPI (#H-1500, Vector Laboratories). Mounted slides were dried overnight and kept in the dark prior to imaging

**Immunofluorescence microscopy –** Images were obtained using a Zeiss Axioimager.D2 upright microscope using a 63x / 1.4 Plan Apochromat (Oil, DIC) objective and captured using a Coolsnap HQ2 camera (Photometrics) through Micromanager software v1.4.23. Specific band-pass filter sets for FITC and Texas red were used to prevent bleed-through from one channel to the next. Images were then processed and analysed using Fiji ImageJ (http://imagej.net/Fiji/Downloads).

**2.1.16 RT-qPCR –** RNA samples were isolated using TRIzol Plus mRNA purification kit (#12183555, Thermofisher Scientific) and samples were decontaminated with RQ-1 RNAse-free DNAase (#M6101, Promega). Reverse transcription was performed using Taqman reverse transcription reagent (#N8080234, Thermofisher Scientific). Pre-designed KiCqStart®SYBR® Green primers targeting human ATP2B4, ATP2B1, ATP2B2, ATP2B3, PKM, PFKFB3, CAV1 and 18S rRNA (Sigma-Aldrich) and POWER SYBR green master mix were used for qPCR. qPCR experiments were performed on a StepOnePlus qPCR machine (Fisher Scientific). The relative quantification of designated mRNA was achieved by S18 rRNA normalisation ($2^{-\Delta CT}$) then; if possible, further comparisons were made between siRNA knockdown conditions and siNT control ($2^{-\Delta\Delta CT}$).

| Oligo Name | Primer Pair ID | Tm (ºC) | Sequences (5'-3') |
|---|---|---|---|
| PMCA4a_Forward | Customized oligo | 66.3 | AAGGCGACAGAACATGGGTC |
| PMCA4a_Reverse | Customized oligo | 66.3 | ACCACTTTGATTGCCCATAGGA |
| PMCA4b_Forward | customized oligo | 65.4 | CCAGACTCAGATCAAAGTGGTCA |
| PMCA4b_Reverse | Customized oligo | 64.9 | TCGTGGCAACTCCTCCTCTA |
| ATP2B1_Forward | H_ATP2B1_1 | 54 | ATCCTCTTGTCTGTAGTGTG |
| ATP2B1_Reverse | H_ATP2B1_1 | 57.7 | TCACCATATTTCACTTGAGC |
| ATP2B2_Forward | H_ATP2B2_1 | 58.3 | GATAGTGATCGTGCAGTTTG |
| ATP2B2_Reverse | H_ATP2B2_1 | 59.7 | AATGAATATGCACCACATCC |
| ATP2B3_Forward | H_ATP2B3_1 | 56.2 | CACCCACTACAAAGAGATTC |
| ATP2B3_Reverse | H_ATP2B3_1 | 55.9 | GTAGTATTTTGGTGGTATAGGC |
| ATP2B4_Forward | H_ATP2B4_1 | 57.3 | AACTCTCAGACTGGAATCATC |
| ATP2B4_Reverse | H_ATP2B4_1 | 57.9 | ACCTTTCTTCTTTTTCTCCC |
| CAV1_Forward | H_CAV1_1 | 55.1 | CAGGGACATCTCTACACC |
| CAV1_Reverse | H_CAV1_1 | 57.6 | TCAAAGTCAATCTTGACCAC |
| PFKFB3_Forward | H_PFKFB3_1 | 58.4 | TGGAAGTTAAAATCTCCAGC |
| PFKFB3_Reverse | H_PFKFB3_1 | 56.4 | CATAGCAACTGATCCTCTTC |
| PKM2_Forward | H_PKM2_1 | 60.9 | ATGTTGATATGGTGTTTGCG |
| PKM2_Reverse | H_PKM2_1 | 60.4 | ATTTCATCAAACCTCCGAAC |
| S18rRNA_Forward | H_RN18S1_1 | 62.3 | ATCGGGGATTGCAATTATTC |
| S18rRNA _Reverse | H_RN18S1_1 | 59.6 | CTCACTAAACCATCCAATCG |

**Table 2.1 – Primer sequences targeting human designated gene.** Forward and reverse primer sequences are shown in a 5' prime to 3' prime order. Abbreviation: Tm = melting temperature; A = adenine; T = thymine; G = guanine; C= cytosine; H_prefix = derived from human

**2.1.17  Gap closure cell migration assay –** Gap closure assay, also known as area exclusion assay, is commonly used to assess cell migration on 2D growth surface. MIAPaCa-2 cells were seeded at 50,000 cells per chamber of a '2-chamber' Ibidi insert (#80209, Ibidi), pre-fitted into 12-well culture plates. At least 3 replicates were performed for each treatment condition. Seeded cells should show 95-100% confluence at 24 h after seeding. The Ibidi insert was removed and cells were gently rinsed with DPBS then immediately treated with 2 ml of treatment media. Mitomycin C (1 µg/ml, Mit C; #3258, Tocris) was added into all treatment conditions to prevent cell proliferation from confounding the cell migration results. Cell-free gaps were imaged at 1, 24, 48, 72, and 96 h intervals after treatment. Bright field images were acquired using an Olympus IX83 inverted microscope using a 4x / 0.13 LUC PlanFL N objective and captured using an Orca ER camera (Hamamatsu) using CellSens software (Olympus). Images were then transformed into binary images for gap comparison using Fiji ImageJ program. Data are expressed as the normalized area of the cell-free gap compared to the time-match gap area of the Mit C control.

**2.1.18  siRNA expression knockdown –** PMCA4 or Cav-1 protein expression was knocked down using 12.5-25 nM ON-TARGETplus SMARTpool siRNA targeting ATP2B4 mRNA (siPMCA4; L006118-00-0010) or CAV1 mRNA (siCav-1; L003467-00-0010). Non-targeting siRNA (siNT; D-001810-10-20) was used as a control. All knockdown conditions were performed using 0.1% DharmaFect1 transfection reagent (T-2001-03, Dharmacon). The individual target sequences of ON-TARGETplus SMARTpool siRNA used are listed as follow:

| Target Gene | ON-TARGETplus catalogue number | Target Sequence |
|---|---|---|
| ATP2B4 | J-006118-05 | UCAAAGCGUUCCAUAGUUC |
|  | J-006118-06 | GAACUGACCUGUAUCGCGG |
|  | J-006118-07 | CCUCUGAUCUCACGCACUA |
|  | J-006118-08 | UGACAAGGCUUCUAAGUUU |
| CAV1 | J-003467-06 | CUAAACACCUCAACGAUGA |
|  | J-003467-07 | GCAAAUACGUAGACUCGGA |
|  | J-003467-08 | GCAGUUGUACCAUGCAUUA |
|  | J-003467-09 | GCAUCAACUUGCAGAAAGA |
| Non-Targeting | D-001810-10-50 | UGGUUUACAUGUCGACUAA |
|  |  | UGGUUUACAUGUUGUGUGA |
|  |  | UGGUUUACAUGUUUUCUGA |
|  |  | UGGUUUACAUGUUUUCCUA |

**Table 2.2 – Gene targeting sequences of ON-TARGETplus SMARTpool siRNA purchased from Dharmacon.** Four individual siRNA targeting difference sequences of the same gene are shown.

siRNA knockdowns were performed according to manufacturer instructions. Only conditions that produced ≥70% expression knockdown in MIAPaCa-2 cells, usually requiring at least 48 hours of siRNA incubation, were used in the current study. RT-qPCR and Western immunoblot were used to confirm Cav-1 expression knockdown at the mRNA and protein level, respectively.

**2.1.19 Caspase 3/7 cleavage apoptosis assay –** MIAPaCa-2 cells were seeded at 2500 cells/well into a black wall, glass-bottom 96 well plates. Cells were incubated with either 0.1% DharmaFect1, 25 nM siPMCA4, or 25 nM siNT siRNA for 48 hr prior to treatment with various apoptotic inducing reagents. Staurosporine (STS; #J62837, Alfa Aesar™ Fisher Scientific), an inhibitor of kinase proteins, was used as a positive control to induce caspase3/7 cleavage. Treated cells were incubated with 5 μM of Caspase 3/7 green apoptosis reagent (#4440, IncuCyte) and 625 nM Nuclear-ID Red (#ENZ-52406, Enzo Life Sciences). Cells were imaged on the IncuCyte imaging system using 10x lens, on phase, red and green channel. Red and green signals were counted using the IncuCyte Zoom 2016 software (Incucyte). Data are presented as % Apoptosis [(green cell count/image ÷ red cell counts/image) x 100]

### 2.1.20 BirA* proximity Bio-Identification

### 2.1.20.1 Generating stably transfected BirA*-fusion cell lines

**Lentiviral plasmids** – Sequences of wild type mPKM2 (catalogue # 42512) and mPKM2-K433E (catalogue # 42514) as well as the -MycBirA*-blue fluorescence protein (BFP) containing lentiviral plasmid vector were obtained and purchased from Addgene (www.addgene.org). Venus-MycBirA*-BFP lentiviral plasmid was a kind gift from Dr Andrew Gilmore, University of Manchester.

**Plasmid amplification** – NEB® stable competent E. Coli containing lentiviral plasmids encoding either mPKM2-WT, mPKM2-K433E, or Venus fused to MycBirA* were grown in LB broth containing 100 μg/ml ampicillin at 37°C, on a shaker, overnight (14-16 hours). DNA plasmids were isolated using QIAGEN Plasmid Midi DNA Purification Kit according to Manufacturer's instructions.

**Lentiviral packaging** – A mixture of non-supplemented DMEM media (serum-free and penicillin/streptomycin free) containing 1x PEI, 4.5 μg PSpax2, 3 μg pMD2G and 6 μg of designated BirA* plasmid was prepared and incubated at room temperature for 30 minutes prior to usage. HEK 293T cells grown to 70% confluence were used for transfection. Culture media was replaced with fresh non-supplemented DMEM media then the cocktail containing the plasmid and lentiviral packaging was added. After overnight incubation, replace the media with DMEM containing 10 mM sodium butyrate for 8 hours then replace the media with normal supplemented DMEM (10% FBS). After a further 48 hours, media containing lentiviral were filtered using a 45 μm PES filter then transferred to a VIVASPIN® tube (Sartorius AG). Lentiviral was concentrated by ultracentrifugation (Beckman Coulter) at 30,000 rcf, 4°C, for 1 hour. Stocks of lentivirus were frozen at -80°C until required.

**Lentiviral transfection** – MIAPaCa-2 cells were seeded at 40% confluence into 6 well culture plates. Polybrene (1:2000 dilution) and 2 drops of harvested lentivirus concentrate were added per well. After 48 hours of lentiviral transfection, viral containing media was replaced with normal culture media. As the plasmid containing bait-MycBirA* also contained BFP, bait-BirA* and BFP were expressed on a 1:1 ratio. Cells were passaged normally over 2-3 weeks, checked for fluorescence expression under the microscope, then sorted for plasmid expression levels using fluorescence-activated cell sorting (FACs) for blue fluorescence protein.

### 2.1.20.2 Sample processing and enrichment

**BirA* labelling of proximal proteins** – MIAPaCa-2 cells stably expressing either mPKM2-WT, mPKM2-K433E or Venus fused to MycBirA* were grown to 70% confluence prior to usage. Cells were incubated with culture media containing 100 μM biotin for a period of 14-16 hours overnight. Cells were rinsed with Dulbecco's Phosphate-Buffered Saline (DPBS) twice then harvested with modified radioimmunoprecipitation assay (RIPA) buffer (150 mM NaCl, 50 mM Tris, 5mM EDTA, 5 mM EGTA, 1% Triton-X, 0.1% SDS, pH 7.6) supplemented with cOmplete\TM, EDTA-free protease inhibitor cocktail protease inhibitor cocktail and PhosSTOP™. Harvested cells were sonicated and incubated on ice for 30 minutes. Protein concentration was determined using Bradford assay.

**Streptavidin affinity purification** – Biotinylated proteins were enriched by adding 1 mg of each sample lysates were added to individual microtubes containing 100 μl of streptavidin agarose beads (Pierce™, #20349, Thermo Fisher Scientific). Samples were mixed using rotatory mixer overnight, at 4°C. Lysate portions unbound to the agarose beads were collected, labelled as "flow-through", and kept aside at -80°C until used. Streptavidin agarose beads were washed, and biotinylated proteins were eluted using 80 μl elution buffer then incubated at 95°C for 5 minutes. Collected samples were labelled as "biotinylated fraction", and then stored at -80°C until used.

### 2.1.20.3 Data processing and analysis

**Liquid chromatography-tandem mass spectrometry** – Equal volumes of each biotinylated fraction were loaded into 10 well, 10% Bolt Bis-Tris Plus gels (Thermo Fisher Scientific). Electrophoresis was performed at 200 V, 3 minutes, until the samples ran 0.5-0.8 cm into the gel top, without resolving the band. Gel top samples were then stained by InstantBlueTM gel stain then submitted for LC-MS/MS

processing by the University of Manchester Biological Mass Spectrometry facility, using Thermo Orbitrap Elite coupled with Thermo nanoRSLC system (Thermo Fisher Scientific).

**Bio-identification of interactions enrichment** – Mass spectrometry spectral analysis, determining protein identification and enrichment comparisons were performed by Dr Julian Selly (as a part of the data analysis service provided by The University of Manchester Biological Mass Spectrometry facility) using Ingenuity® Pathway Analysis (IPA; Qiagen). Focusing on statistically significantly enrichments, biotinylated proteins identified were categorized based on biological processes, localisation and function using *IPA* software (https://apps.ingenuity.com/ingsso/login) and *PANTHER – gene list analysis* (www.pantherdb.org) databases. Protein-protein interactions were broadly examined using *STRINGS: functional protein association network database* (https://string-db.org).

**2.1.21 Datamining –** Publicly available databases, including www.oncomine.org (ThermoFisher Scientific) and www.proteinatlas.org, version 18.1, were used to obtain Badea Pancreas (2008) gene chip microarray data and TGCA-PAAD Kaplan Meier survival data, respectively. All data used in this thesis were acquired between November 2018 - January 2019.

**2.1.22 Agilent Seahorse cell metabolism assays**

Agilent Seahorse XFe96 Extracellular Flux Analyzer is an instrument designed to simultaneously measure mitochondrial respiration and glycolysis based on oxygen consumption rate (OCR) and extracellular acidification rate (ECAR), respectively. Seahorse metabolic assays in this thesis were carried out by seeding MIAPaCa-2 cells (5,000 cells/well) into 96 well Seahorse cell culture plates. Cells were incubated for 48 hours in 25 nM of either siNT, siPMCA4 or siCav-1, containing 0.1% DharmaFECT1. Seahorse sensor cartridges were hydrated with 200 µl of PCR-grade sterile water (Invitrogen$^{TM}$ UltraPure$^{TM}$ DNase/RNase-free distilled water, #10977035, Fisher Scientific) per well overnight, in a non-$CO_2$ (g) humidifying incubator, at 37°C. Prior to loading the cartridges with designated treatments, sterile water was removed then replaced with Agilent Seahorse XF Calibrant (200 µl/well). Simultaneously, culture media in the Seahorse cell culture plate were exchanged for appropriately supplemented Seahorse media and cells were allowed to equilibrate for 1 h in a non-$CO_2$ (g) incubator, at 37°C. Depending on the type of assay performed, appropriate supplements were added into Agilent Seahorse media (Low phenol red DMEM, pH 7.4 media; # 103575-100, Agilent) and kit specific reagents were used for reagents loading. After loading test and kit reagents into appropriate ports, the sensor cartridge was further incubated at 37°C, in a non-$CO_2$ (g) humidifying incubator. After at least 1 h of incubation, the sensor cartridge was then loaded into the Agilent Seahorse XFe96 Extracellular Flux Analyzer to initiate the experimental run. It should be noted that the present work used acute injections of either 0.1% vehicle control or 30 µM CPA prior to the injections of designated kit reagents for all metabolic assays performed, with respect to the manufacturer's protocol. The pre-optimised carbonyl cyanide-p-trifluoromethoxy-phenylhydrazone (FCCP; #C2920) concentration for MIAPaCa-2 cells was 0.5 µM [114]. Any Seahorse data obtained were analysed using Wave analysis software (Agilent Technologies). Depending on the type of assay performed, the media, the test reagents, and programmed settings would vary according to the manufacturer's protocol as follow:

**Agilent Seahorse XF cell energy phenotype test (phenotype test)** – Designed to probe three key parameters of cell energy metabolism, the Seahorse phenotype test was used to assess the basal phenotype, stress phenotype and metabolic potential. The phenotype test performed in this work included a pre-injection with 30 µM CPA and a routine stressor mix injection (1 µM OM and 0.5 µM FCCP). Seahorse media used for this test were supplemented with 2 mM sodium pyruvate (NaPY; #103578-100), 4 mM L-glutamine (#103579-100), and 25 mM D-glucose (#103577-100) solutions purchased from Agilent.

**Agilent Seahorse XF cell Mito Stress test (Mito stress test)** – The Mito stress test is designed to measure mitochondrial function through the assessment of OCR in real-time. Similar to the phenotype test media, the base Seahorse media were supplemented with 2 mM NaPY, 4 mM L-glutamine, and 25 mM D-glucose purchased from Agilent. Acute injections of either vehicle control or 30 µM CPA were added prior to the injection of Mito Stress test reagents which includes the following sequence of injections: i) 1.5 µM OM (oligomycin; ATP synthase inhibitor), ii) 0.5 µM FCCP (proton gradient uncoupler), and iii) a mixture of 0.5 µM rotenone (Rot; complex I inhibitor; #R8875) and antimycin A (AA; complex III inhibitor; #A8674).

**Agilent Seahorse XF Glycolysis Stress test (glycolysis stress test)** – Designed to monitor cellular glycolytic functions based on the live changes in ECAR, the glycolysis stress test measures the basal glycolysis, glycolysis capacity, glycolytic reserve and the background non-glycolytic acidification. The media used for this glycolysis stress test were glucose free and were supplemented with 1 mM L-glutamine. Following the pre-injection with either 0.1% DMSO or 30 µM CPA, glycolysis stress test reagents were injected in the following order: i) 10 mM glucose (induces glycolysis; #G7021), ii) 1 µM OM (measures maximum glycolytic capacity), iii) 50 mM 2-deoxyglucose (2-DG; a competitive inhibitor of hexokinase and glycolysis; #11311867, Alfa Aesar™ Fisher Scientific).

**Agilent Real-time ATP Rate Assay (ATP production rate assay)** – Designed to monitor the dynamic changes in total ATP production rates in live cells, this metabolic assay utilizes two sequential stressor injections of 1.5 µM OM and 0.5 µM Rot/AA to calculate cellular ATP production rates. In response to these stressors, the dynamic changes of ECAR and OCR could be used to calculate glycolysis and mitochondrial ATP-production, respectively. Interestingly, these ATP rate stressor injections are the same as the stressors administered in Mito Stress tests. Therefore, as long as the buffer factor is known (e.g. buffer factor is 2.4 mmol/L/pH for Seahorse XF DMEM, pH 7.4 media) and glycolytic proton efflux rate (glycoPER) is available, existing Mito Stress test data could be used to calculate ATP production rates. Using Wave analysis software (Version 2.6.0; Agilent Technologies), the current work exported the existing Mito Stress test data using the "Glycolytic Rate Assay Reporter Generator", yielding the glycoPER parameter required for ATP rate calculations. Calculation of key ATP rate parameters included: mitochondrial ATP (mitoATP) production rate, glycolysis ATP (glycoATP) production rate, total ATP production rate, and XF ATP Rate Index. (Discussed in section 2.2.4)

**2.1.23  Statistical Analysis –** Prism 7 and Prism 8.2 software (GraphPad) were used for most graphing and statistical data analysis. All data with N≥3 independent experiments are presented as mean ± SEM (error bars). Normality of data was checked by the Shapiro-Wilk test. Statistical significance was

determined by unpaired t-test and Mann-Whitney test for comparing two groups with parametric and non-parametric distribution, respectively. For instance, the comparison of 3 or more groups with non-parametric distribution, One-way ANOVA Kruskal-Wallis test with Dunn's post-hoc test for multiple comparisons was used. For comparing the effects of 2 varying factors in 3 or more groups, two-way ANOVA with Bonferroni for multiple comparisons was used. For data with N≤2 independent experiments, data are represented as mean of replicates, and no statistical analysis was performed. Progenesis QI Nonlinear Dynamic software was used for quantitative LC-MS/MS small molecule discovery analysis (one-way ANOVA). Proteins identified by Quantitative LC-MS/MS are presented as the mean of 3 independent ± standard error of means (SEM; error bars). Qualitative LC-MS/MS data is indicative of the potential presence of the protein identified and therefore, no statistical analysis was performed (N=1). Statistical significance is defined as $p < 0.05$.

## 2.2 Methods Optimization

### 2.2.1 Comparing sulforhodamine B (SRB) and cell count kit-8 (WST-8) cell viability assay

Cell viability assays quantify 'living' potential of cells and can be flexibly used to quantify cell proliferation (cell growth over time) and/or cytotoxicity (cell death overtime). SRB is a colourimetric dye which binds to the cellular protein of fixed cells thus quantifies total cellular protein content of cells adherent to the bottom of multi-well culture plates. The nature of this assay utilizes cell adherence as a criterion of cell viability. SRB protocol requires a multistep fixation, rinsing and staining before the total protein could be measured. Therefore, any treatments which result in a cumulative loss of cell adhesion, independent of cytotoxicity, cannot be accurately assessed by SRB. Furthermore, mechanical agitations associated with rigorous washing steps may lead to the loss of less adherent cells, confounding the estimation of cell viability and cell proliferation. SRB assays also dismiss the viability of live non-adherent cells. Therefore, it was necessary to identify an alternative cell viability assay, capable of quantifying the cell viability of both adherent and non-adherent cells with better sensitivity and reliability than SRB.

Cell count kit-8, containing a tetrazolium salt variant (WST-8), assess cell viability based on the ability of the living cells to maintain a reducing environment. Whereas SRB is a multi-step assay, WST-8 is a single-step colourimetric assay which quantifies the extracellular 'reducing environment' of both adherent and non-adherent viable cells. WST-8 is non-toxic and is extracellularly reduced by live cells in the presence of cellular electron mediators, such as dehydrogenases, to yield an orange formazan product [329]. Hence, the reductive condition of viable cells is directly proportional to the formazan dye generated. Optimization of the WST-8 assay and comparing the assay sensitivity to SRB was determined. As multiple routine inhibitors used in our lab are coloured and may influence the colourimetric measurement of WST-8, multiple coloured drugs were also tested.

Optimization of WST-8 assay required identification of: i) cell seeding density, ii) WST-8 reagent incubation time, and iii) optimal range of detection. MIAPaCa-2 cells were seeded at 2500, 5000, 10000 cell per well in 96-well plates and allowed to attach for 24 h. Cells were treated with 10 µl of coloured treatments such as: BrPy (glycolytic inhibitor [330]; yellow), Oligomycin (mitochondrial OXPHOS inhibitor [331]; colourless), shikonin (PKM2 inhibitor [332]; dark red), ATA (PMCA4 selective inhibitor [333]; dark red/brown), and CCCP (mitochondrial OXPHOS uncoupler [334]; yellow-orange). After variable treatment periods (0-72 h), 10 µl of WST-8 was added to each well then incubated for 2 and 3 h before measurement of absorbance at 450 nm using a colourimetric plate reader. WST-8 measured plates were fixed and stained with SRB for further comparisons.

To identify the optimum condition for cell proliferation assay, the optimum seeding density and WST-8 incubation time which did not induce saturation was chosen from a 72 h growth curve. The optimal seeding density for WST-8 assay was identified as 2500-5000 cell per well and the optimal reagent incubation time which did not cause colourimetric saturation was 2 h (Figure 2.3Aii). Multiple coloured reagents routinely used within the lab were tested with WST-8 assay to investigate potential colourimetric interference. This was achieved by incubation of WST-8 reagent with cell-free blank wells containing only treatment media where colourimetric changes in these cell-free blank wells indicate potential

interaction of each treatment with the WST-8 reagent. Results showed elevated background signal in BrPy spiked blank wells, suggesting that WST-8 developed colour under acidic treatment condition (e.g. BrPy) (Figure 2.3Bii). SRB assay seemed to underestimate cell viability at 2 h after shikonin incubation compared to WST-8 (Figure 2.3B-C) where SRB showed 13.32±3.96% while WST-8 showed 85.5±6% cell viability compared to the non-treated control. Overall, WST-8 assay is a more sensitive method to assess cell proliferation compared to SRB. However, at 2 h after treatment, the SRB assay demonstrated a similar measurement of adherent cells between each treatment conditions while WST-8 showed elevated and varied measurement values (Figure 2.3Ai-ii). These inconsistencies in WST-8 reading were likely due to pipetting error. This suggests that although WST-8 is a single-step addition assay, technical errors can cause great variation in the measurement.

Overall, WST-8 assay can be used to perform both cell proliferation and cytotoxicity assays in semi/non-adherent cells without underestimating cell viability or overestimate cytotoxicity. However, it should be noted that WST-8 colourimetric development depends on extracellular 'reducing' environment within the treatment well. Hence, treatments which are coloured, acidic in pH, or behave as reducing agents may directly influence WST-8 colour development. To correct for any background alterations caused by drug and WST-8 interaction, blank wells spiked with treatments should always be performed to control for such interactions.
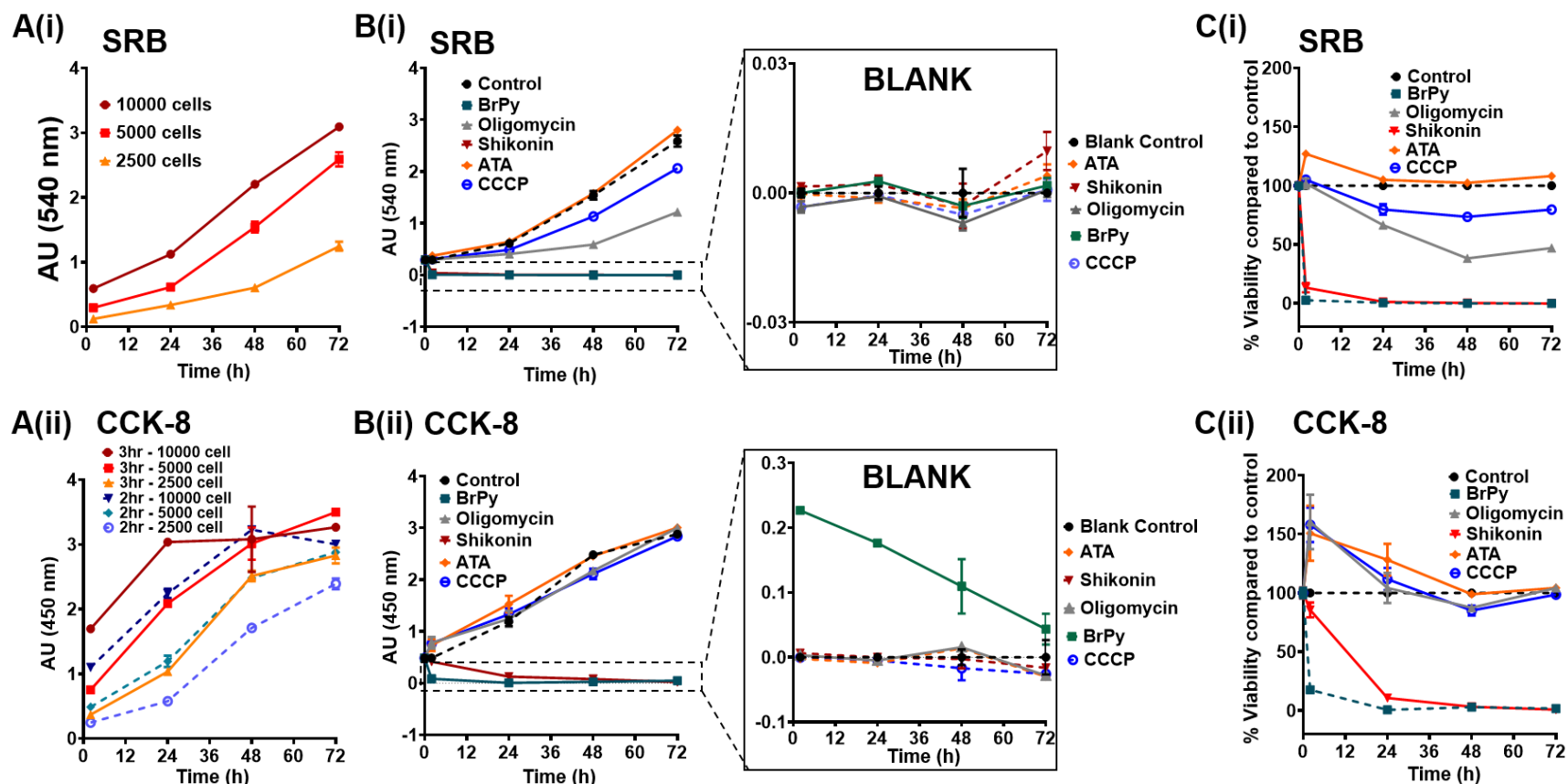
**Figure 2.3 – Optimization of Cell count kit-8 (WST-8) cell proliferation assay and parallel comparison with SRB assay.** MIAPaCa-2 cells cultured in 25 mM D-glucose DMEM media were seeded at 2500, 5000, 10000 cells per well in 96-well plates. Cell viability was assessed at 2, 24, 48, and 72 h after treatment. Various seeding density was compared between SRB **(Ai)** and WST-8 **(Aii)**. Optimal seeding density and WST-8 reagent incubation time were 5000 cell/well and 2 h, respectively. Potential colour interference by coloured drugs (500 μM BrPy, 10 μM Oligomycin, 5 μM Shikonin, 10 μM ATA, and 4 μM CCCP) was tested by spiking treatments into cell-free blank wells **(Bi-ii)**. Cells seeded at 5000 cells/well were treated with various coloured drugs and cell viability was assessed by SRB **(Bi)** and WST-8 assay **(Cii)**. Extended panels show enlarged cell viability of highly cytotoxic BrPy and Shikonin. Data are expressed as raw absorbance unit (AU) subtracted by matching blank treatment conditions. Data are expressed as % of cell viability compared to non-treated control **(Di-ii)**. Data is derived from N=1 independent experiment. Data are shown as mean ± SE of 4 replicates.

### 2.2.2    Optimization of gap closure cell migration assay

Gap closure usually involves the quantification of 2-D horizontal cell migration into a cell-free gap area over time. The following thesis utilizes Ibidi chamber inserts to generate a uniformed partition cell-free zone. Cells seeded into both sides of the partition would migrate and/or proliferate into the gap over time and closure of the cell-free gap can be quantified over time. Gap closure assay is preferable to the standard scratch assay as it minimizes mechanical injury and cellular stress at the migrating front. To determine the optimal gap closure protocol for MIAPaCa-2 cells, the optimization of seeding density was first established. Our preliminary data suggested that the seeding density of 50,000 cells per chamber partition was the optimum MIAPaCa-2 seeding density. For the migration front to be well defined, cells must be seeded to produce 95-100% confluence on both sides of the cell-free gap. Complete confluence and a well-distributed monolayer of MIAPaCa-2 cells were observed when cells were seeded at 50,000 cells per chamber partition. After identifying an optimal seeding density, the next step was to identify the period required for complete gap closure. Closure of cell-free gap was qualitatively identified when a negligible gap could be observed under 4x magnification. All seeding densities demonstrated apparent and/or complete gap closure at approximately 48 h after removal of Ibidi insert (Figure 2.4).

Gap closure assay is also influenced by three major factors: cell migration, cell proliferation and cell death. Hence, it is necessary to discern cell 'migration' from 'proliferation' without inducing 'cytotoxicity'. Mitomycin C (Mit C) is an anti-proliferative agent which acts by cross-linking DNA at the guanosine residues, preventing transcription and translation. We identified that 1µg/ml of Mit C could inhibit cell proliferation while negligibly affecting cell viability during the period required for complete gap closure (Figures 2.4B and 2.5). Based on qualitative observations, gap closure was delayed as the concentration of Mit C increased but high concentrations of Mit C (4-10 µg/ml) caused notable cell detachment (Figure 2.4B). WST-8 and SRB assays were used to ensure that the concentration of Mit C which delayed gap closure could effectively inhibit cell proliferation without inducing cytotoxicity (Figure 2.5). The result showed that 4-10 µg/ml Mit C reduced cell viability (cytotoxicity) while 0.5 µg/ml Mit C showed increased cell viability (proliferation) at 48 h. Therefore, these concentrations are not suitable for the gap closure assay. Concentrations between 1-2 µg/ml Mit C inhibited proliferation while negligibly affected cell viability (Figure 2.5).
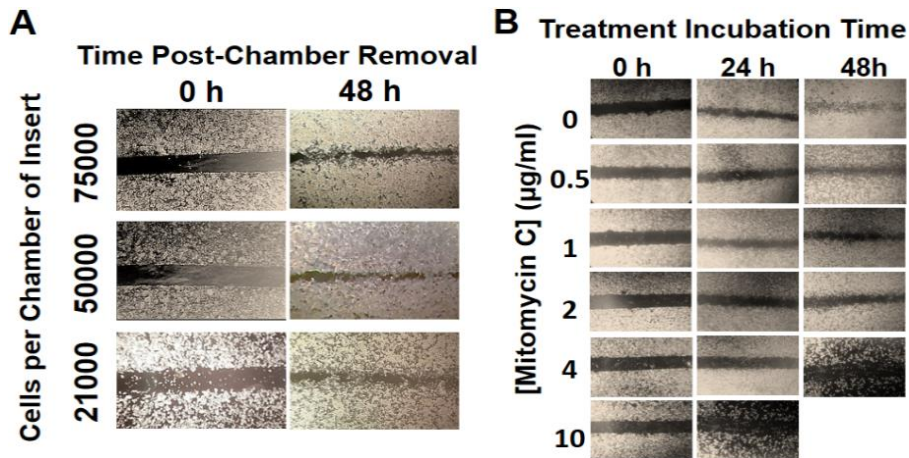
**Figure 2.4 – Identifying the optimal MIAPaCa-2 seeding density and concentration of mitomycin C for Ibidi gap closure assay.** MIAPaCa-2 cells were seeded in sterile Ibidi 2-chambers inserts fixed in 12-well culture plates. Cells were allowed to attach for 24 h before removal of Ibidi chamber to create a "cell-free" gap area. Cell debris was removed by gently washing with 500 µl DBPS. 2 ml of treatment media is then added to each well. **A,** Seeding densities of 21000, 50000 and 75000 cells per chamber side were examined. **B,** MIAPaCa-2 cells seeded at 50000 cell/chamber side were treated with 0, 0.5, 1, 2, 4, 10 µg/ml Mitomycin C. Qualitative observation of gaps after-treatment were made under 4x magnification. Complete gap closure is qualitatively identified when no cell-free gap area remained. Image of gaps could not be quantified as photographs were taken by Microsoft Lumia 640 LTE mobile phone over the microscope eyepiece. Representative images are derived from a single experimental run (N=1, 2 replicates per condition).
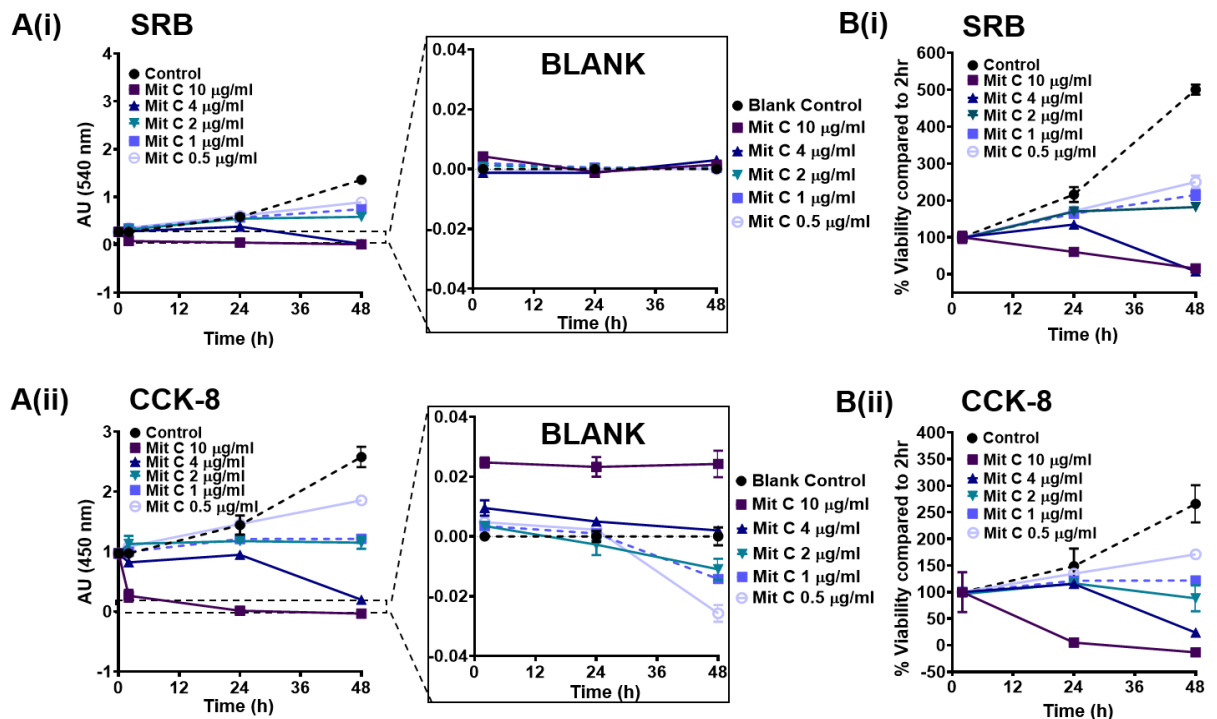


**Figure 2.5 – Validating effect of mitomycin C on MIAPaCa-2 cell viability and proliferation.** MIAPaCa-2 cells seeded at 5000 cells/well were allowed to attach for 24 h prior to treatment. Cells were treated with 0 (control), 0.5, 1, 2, 4, 10 µg/ml Mitomycin C. **A,** Cell viability was measured after 2hr incubation with WST-8 reagent **(A(ii))** then SRB assay was immediately performed on the same plate **(A(i))**. Extended panels show blank wells, spiked with treatment media but no seeded cells to demonstrate background values. Data expressed as raw absorbance unit (AU) are subtracted by matching blank treatment conditions. **B,** Cell viability is calculated from raw AU of WST-8 **(B(ii))** and SRB **(B(i))** experiments. Data are expressed as % cell viability with respect to the raw AU signal at 2 hr-after treatment. Data is derived from 1 independent experiment, with 4 replicates per treatment condition. Data are shown as mean ± SE of replicate.

### 2.2.3    siRNA expression knockdown, a necessary tool to study the role of PMCA4 and Cav-1

### 2.2.3.1    Selective PMCA4 inhibitors failed to inhibit PMCA activity in MIAPaCa-2 cells predominantly expressing PMCA4

As PMCA4 is reported to be overexpressed in PDAC tumours [118] and is shown to be the predominant PMCA isoform in MIAPaCa-2 PDAC cells (discussed in Chapter 3), we wanted to examine the role of PMCA4 in $Ca^{2+}$clearance and its contribution towards PDAC $Ca^{2+}$ homeostasis. To examine the effect of PMCA4 inhibition on PMCA activity, three PMCA inhibitors were used in this study: i) pan PMCA inhibitor (carboxyeosin, CE), ii) aurintricarboxylic acid (ATA) and, iii) caloxin 1c2. Used as a positive control to demonstrate total inhibition of PMCA activity, CE is a potent fluorescein analogue which non-selectively inhibits ATP binding site of all PMCA isoforms [234]. On the other hand, ATA is a small molecule selective inhibitor of PMCA4 demonstrated to potently inhibit PMCA4 activity at 1µM in HEK293 human embryonic kidney cells [333]. Since ATA is a small molecule inhibitor that has been shown to elicit multiple effects other than PMCA4 inhibition which may influence PMCA activity, it was necessary to cross-validate the result with an alternative PMCA4 inhibitor such as caloxin 1c2. Caloxin 1c2 is a peptide inhibitor which binds to the extracellular allosteric site of PMCA4 and has been shown to inhibit PMCA4 ATPase activity in leaky erythrocyte ghost models [335].

Time-match control experiments demonstrated consistent $[Ca^{2+}]_i$ clearance rate between the first and second clearance phase of 104±2.87 % relative clearance (R2/R1). CE decreased relative $Ca^{2+}$ clearance (21.7± 6.43 %, n=3) compared to non-treated control (104±2.87 %, n=7). Although inhibition of PMCA activity was expected, both ATA and caloxin 1c2 (concentrations up to 100 µM, reported to inhibit all PMCA isoforms [335]) had no effect on relative $[Ca^{2+}]_i$ clearance rate compared to non-treated control (Figure 2.6). The lack of caloxin 1c2 effect on $Ca^{2+}$ clearance may potentially be due to peptide degradation over time in static bath conditions, leading to a loss of potency. However, it is important to note that caloxin 1c2 possesses adenyl butyl (Bpa) amino acid residues which may crosslink to upon excitation at 340 nm [335]. Since fura-2 dye requires excitation at 340 nm (near the UV spectrum), cross-linking of peptides may potentially be responsible for the loss of peptide integrity and activity. Therefore, an alternative $Ca^{2+}$ detection dye with higher excitation wavelengths such as fluo-4 was used to test this hypothesis. Unfortunately, caloxin 1c2 still fails to elicit any inhibitory effect on PMCA activity in MIAPaCa-2 PDAC cells (Figure 2.7). Therefore, it was necessary to selectively knockdown PMCA4 expression in order to examine the importance of its function in MIAPaCa-2 PDAC cells (data presented in Chapter 3). Similarly, as MBC disruption of the caveolae results in rapid cytotoxicity, it was necessary to selectively disrupt the caveolae via Cav-1 selective knockdown in order to examine the importance of Cav-1 enrich caveolae on PMCA activity in PDAC cells (data presented in Chapter 4).
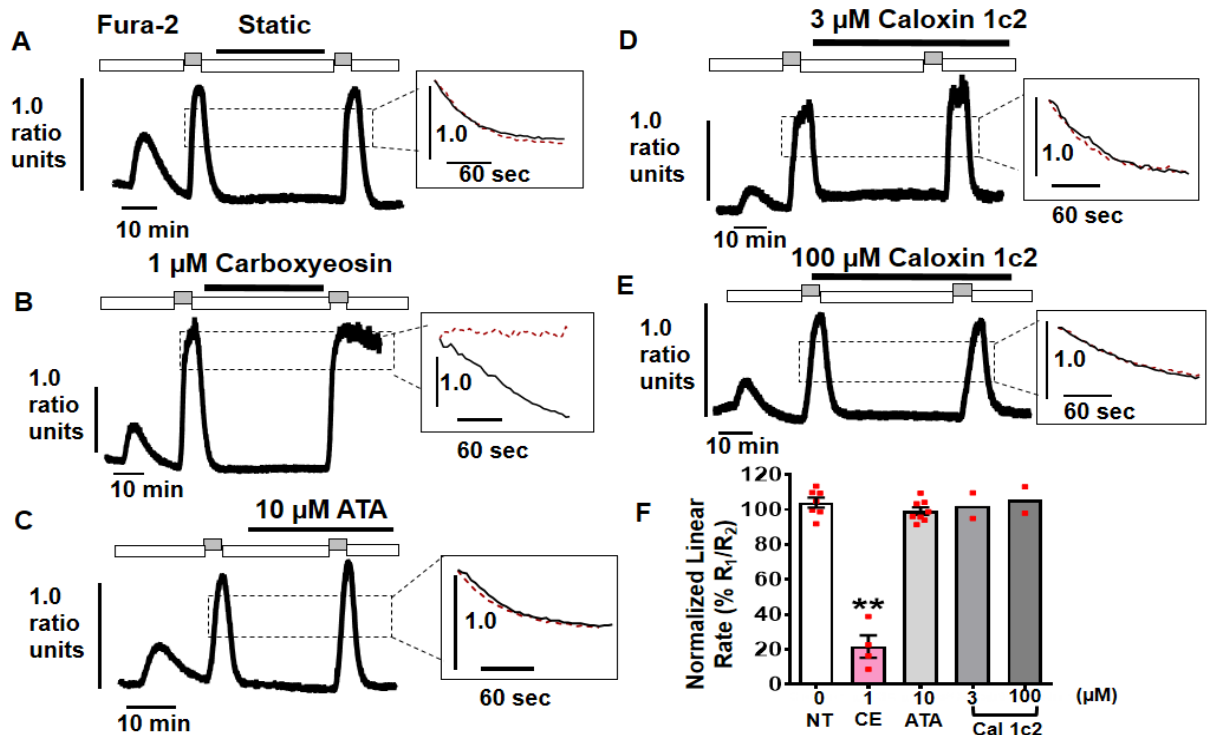
**Figure 2.6 – Effects of PMCA Inhibitors on *in situ* Ca²⁺ clearance.** PMCA-mediated $[Ca^{2+}]_i$ clearance is measured in MIAPaCa-2 cells loaded with fura-2 dye. Addition of 30 µM CPA to both 0 Ca²⁺ + 1 mM EGTA HPSS buffer (white box) or 20 mM Ca²⁺ HPSS buffer (grey box) to inhibit uptake of Ca²⁺ into intracellular storages. Release of $[Ca^{2+}]_i$ from intracellular storage was allowed before inducing the non-treated first Ca²⁺ clearance phase. Treatments were incubated in static condition for 30 min before inducing a second Ca²⁺ clearance phase. Representative traces show *in situ* $[Ca^{2+}]_i$ clearance of **A,** time-match control (NT; N=7), **B,** 1 µM carboxyeosin positive control (CE, N=3), **C,** 10 µM aurintricarboxylic acid (ATA, N=8), **D,** 3 µM caloxin 1c2 (Cal 1c2, N=2) and **E,** 100 µM Cal 1c2 (N=2) . Expanded box of each representative trace compares the clearance rate of the first (black trace) and second clearance phase (red dash trace). The effect of each inhibitor is quantified by normalizing the linear clearance rate over 60 sec during the second clearance (R2) to that of the first clearance rate (R1). **F,** Data of % relative clearance rate is expressed as the mean ± SEM where ≥ 3 independent experiments were performed. Where N≤3 independent experiments data are expressed as mean only. Each red dot on the graph represents the mean of a single independent experiment. Comparisons were made between treatment groups using the Kruskal-Wallis test with Dunn's post-hoc test for multiple comparisons.
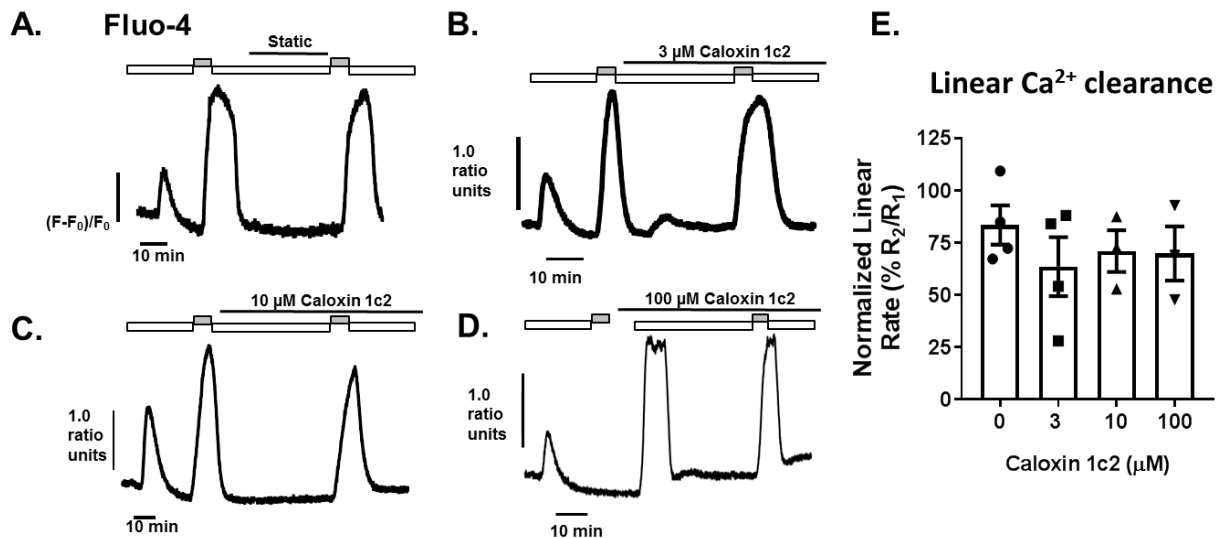
**Figure 2.7 – Effects of Caloxin 1c2 on *in situ* Ca²⁺ clearance measured using Fluo-4 Ca²⁺ indicator dye.** PMCA-mediated [Ca²⁺]ᵢ clearance is measured in MIAPaCa-2 cells loaded with fluo-4 dye. Addition of 30 µM CPA to both 0 Ca²⁺ + 1 mM EGTA HPSS buffer (white box) or 20 mM Ca²⁺ HPSS buffer (grey box) to inhibit uptake of Ca²⁺ into intracellular storages. Release of [Ca²⁺]ᵢ from intracellular storage was allowed before inducing the non-treated first Ca²⁺ clearance phase. Treatments were incubated in static condition for 30 min before inducing a second Ca²⁺ clearance phase. Representative traces show *in situ* [Ca²⁺]ᵢ clearance of **A,** non-treated control, **B,** 3 µM caloxin 1c2, **C,** 10 µM caloxin 1c2, and **D,** 100 µM caloxin 1c2. **E,** Average linear Ca²⁺ clearance of caloxin 1c2 treatments ranging from 0 -100 µM is shown. Dots indicate an average of individual experiment ran. (N≥3, data collected from at least 30 individual cells)

### 2.2.3.2 siRNA expression knockdown optimization

Since tested selective inhibitors of the PMCA4 (i.e. ATA and caloxin 1c2) did not inhibit PMCA activity in Ca²⁺ clearance assays performed and cholesterol depletion-induced disruption of caveolae disruption was not feasible due to its cytotoxicity, transient siRNA knockdown of PMCA4 and Cav-1 were performed. siRNA is typically 21 base pair long duplex RNA strands, comprised of the sense and antisense strands, designed to specifically targets its complementary mRNA for degradation. This sequence complementarity degradation is mediated by loading of the anti-sense siRNA to the RNA-induced silencing complex (RISC) which guides the RISC-mediated cleavage and degradation of the targeted gene [336,337]. As siRNA-mediated expression knockdown is usually transient (4-7 days depending on siRNA) [336], careful optimization of siRNA is required to ensure high transfection efficiency, knockdown efficacy and stability during the experimental duration.

As PMCA4 possess multiple variants forms, the current work utilizes ON-TARGETplus SMARTpooled siRNA (Dharmacon) which provides four individual siRNAs, targeting four independent sequences of the same gene thereby enhancing the knockdown efficacy. A pool of non-targeting siRNA (siNT) was also obtained as a negative control. Following the manufacturer's protocol, optimizations were performed to identify optimal transfection reagent concentration (DharmaFECT1, DhF1; Dharmacon) and the optimal siRNA concentration required to generate ≥70% expression knockdown of the following genes: ATP2B4 (siPMCA4), CAV1 (siCav-1), PKM (siPKM2), PFKFB3 (siPFKFB3), and ATP2B1 (siPMCA1).

Using cell viability assay, we tested the effect of three concentrations of DhF1 (0.1, 0.2, 0.3 %) on MIAPaCa-2 PDAC cells (Figure 2.8). Compared to the untreated control, we found that MIAPaCa-2 cells were relatively sensitive to lipid transfection reagent and that 0.3% and 0.2% DhF1 led to ≥ 20% loss of cell viability after 24 h and 96 h, respectively. As 0.1% DhF1 demonstrated relatively feasible cell viability (≤80% viable cells) between 24-96 hours, this concentration was further used for siRNA transfection. Using RT-qPCR, we showed that post-48 h treatment with 0.1% DhF and 25 nM of most siRNAs were sufficient to knockdown ≥70% expression of designated proteins in comparison to siNT control (Figure 2.9). In addition, we also showed that after siPMCA4 and siCav-1 expression knockdown, no statistical significant upregulation of proteins was observed. This was particularly crucial for siPMCA4 to ensure that no non-specific knockdown or unwarranted upregulation of other PMCA isoforms occurred as this could provide functional redundancy during PMCA activity assays. Although increases in PMCA3 and PMCA1 were observed, it should be noted that the mRNA expression present within MIAPaCa-2 (shown in Chapter 3) were relatively low and hence, qPCR data obtained were extremely variable.
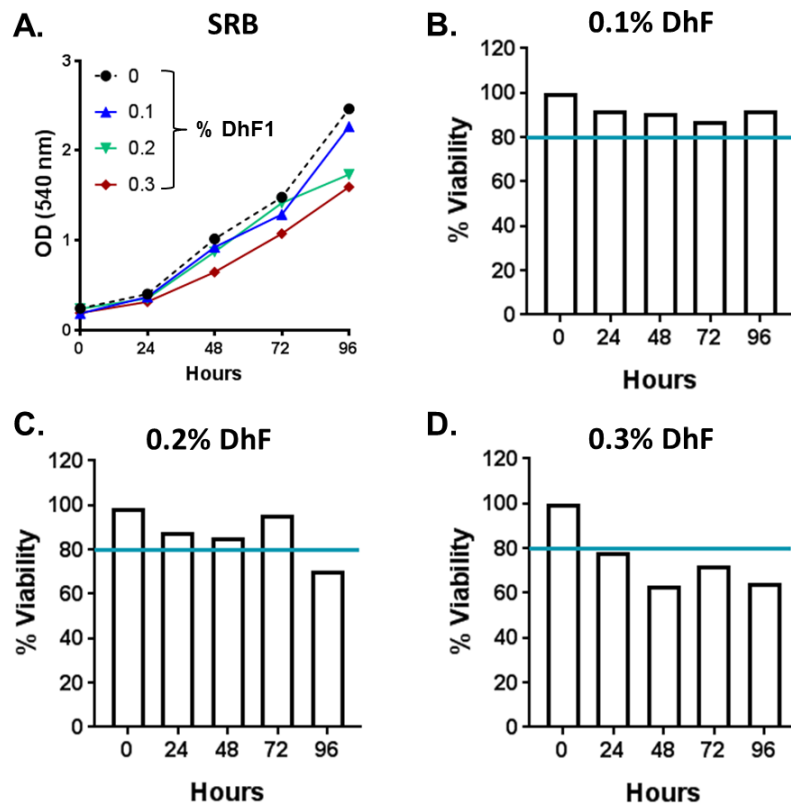


**Figure 2.8 – Identification of DharmaFect1 (DhF1) transfection reagent concentration which does not hinder MIAPaCa-2 cell viability and growth between 0-96 h duration.** MIAPaCa-2 were seeded at 5000 cells/well into 96 well cell culture plates containing 0, 0.1, 0.2 and 0.3 % DhF1 transfection reagent. At least 4 replicates were performed per treatment condition. A, Cell viability was examined using SRB assay based on the colourimetric optical density (OD) at 540 nm. Effect of 0.1% DhF1 (B), 0.2% DhF1 (C), and 0.3% DhF1 (D) are shown as % cell viability with respect to the time-matched untreated condition (0 % DhF1). The blue line marks 80% cell viability. This experiment was a preliminary experiment, comprising of 4 replicates per experimental condition. According to Dharmacon manufacturer's instructions, any treatment that decreases cell viability below 80% is deemed unsuitable for further transfection work.
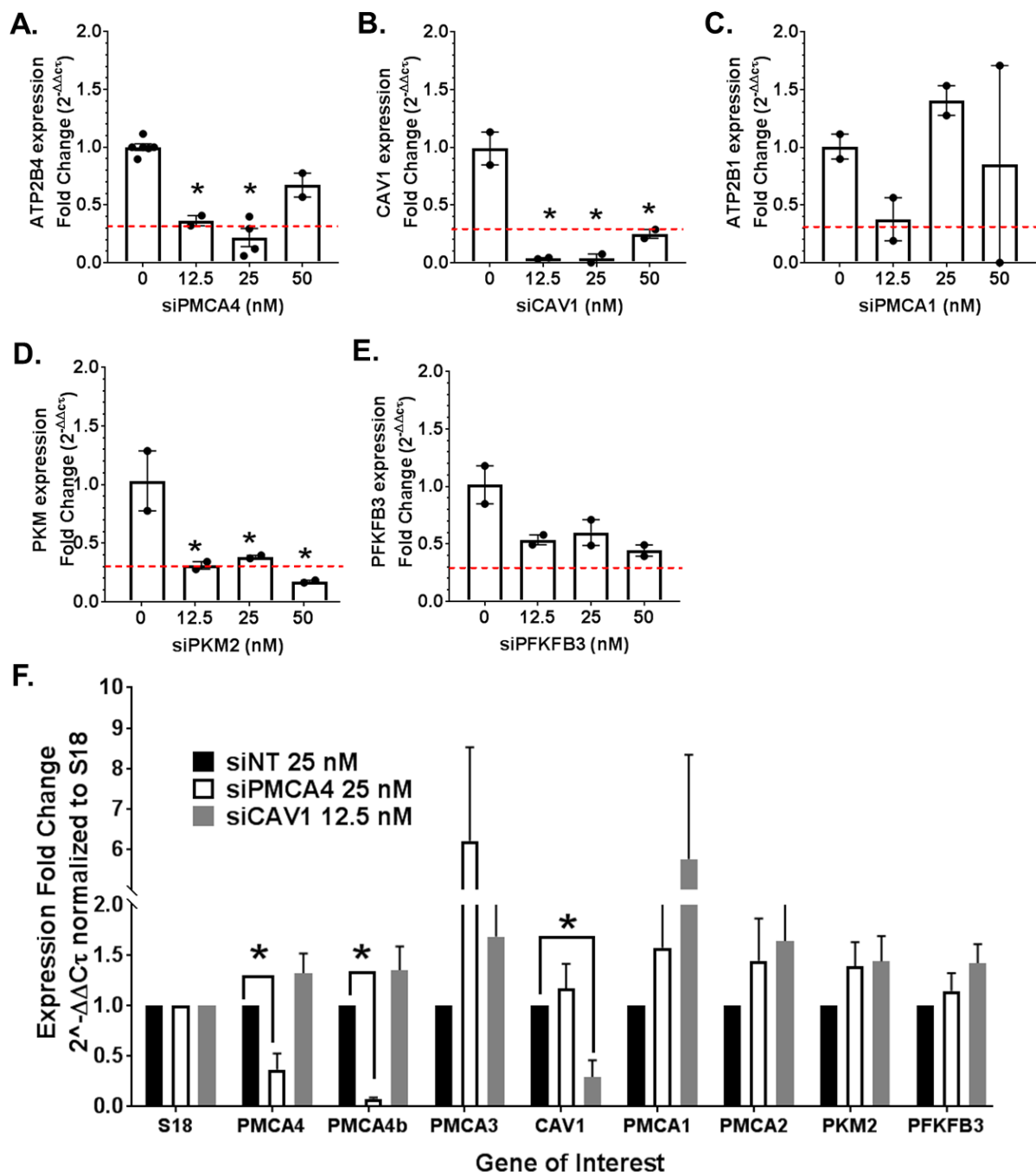
**Figure 2.9 – Identification of siRNA concentrations which provide 70% expression knockdown.** MIAPaCa-2 were seeded at 150,000 cells/well into 6 well cell culture plates containing 0.1 % DhF1 and varying concentrations (12.5, 25, 50 nM) of either: siPMCA4 (A), siCAV1 (B), siPMCA1 (C), siPKM2 (D), and siPFKFB3 (E). Post-48 hr of siRNA treatment, mRNA samples were harvested with Trizol and RT-qPCR was performed to determine the expression knockdown efficiency in comparison to the DhF1 control containing 0 siRNA (0). S18 rRNA was used as a loading control. The relative expression fold changes ($2^{-\Delta\Delta CT}$) were calculated by normalization to S18 rRNA then relative comparisons were made between siRNA knockdown conditions versus the siNT control. The red line indicates a 70% expression knockdown in comparison to the DhF1 control containing 0 siRNA (0). F, Multiple genes of interests were monitored for changes in expression 72 h post-siRNA treatment. siPMCA4 and siCAV1 were monitored in comparison to siNT control. Dots represent two independent experiments, each comprising of at least 4 replicates per treatment condition. One-Way ANOVA was used to determine statistical significance. * represents statistical significance where $p < 0.05$.

### 2.2.4 Analysis of ATP production rate from existing Mito Stress Test data

The recent availability of the Agilent Seahorse XF Real-Time ATP Rate Assay Kit has provided a new means to monitor the dynamic ATP production rates in live cells. Using two sequential injections of 1.5 µM OM and 0.5 µM Rot/AA, the assay relies on the changes in OCR and ECAR which could be used to calculate total ATP production rate, mitochondria ATP (mitoATP) production rate and glycolysis ATP (glycoATP) production rate [338]as follows:

| Parameter | Parameter Equations |
|---|---|
| mitoATP Production Rate | [(Last OCR rate measurement before first injection - Minimum OCR rate measurement after OM but before Rot/AA injection) x 2 x (P/O)] |
| glycoATP Production Rate | Last glycoPER measurement before the first injection |
| Total ATP Production Rate | (mitoATP Production Rate) + (glycoATP Production Rate) |
| XF ATP Rate Index | (mitoATP Production Rate) / (glycoATP Production Rate) |

**Table 2.3 – Parameters equations of Agilent Seahorse XF real-time ATP rate assay.** Abbreviations: ATP: adenosine triphosphate; mitoATP: mitochondrial respiration derived ATP; glycoATP: glycolysis derived ATP; OCR: oxygen consumption rate; ECAR: extracellular acidification rate; glycoPER: glycolysis derived proton efflux rate; P/O: theoretical number of ATP synthesized per oxygen atom; OM: oligomycin; Rot/AA: rotenone/antimycin A mixture. Table modified from Manufacturer's user guide [339].

After basal readings of OCR and ECAR, the addition of OM leads to the inhibition of ATP synthase, resulting in lower OCR. The changes in OCR in combination with the theoretical ratio of number of ADP phosphorylated to ATP per oxygen atom (P/O, suggested to be 2.75 [338]), enables the calculation of mitoATP production rate. On the other hand, the calculation of glycoATP production rate is obtained from the ECAR readings which are converted into proton efflux rate (PER) based on the Agilent Seahorse media buffer factor used (i.e. Buffer factor = 2.4 mmol/L/pH for Seahorse XF DMEM, pH 7.4) and the $CO_2$ contribution factor (CCF = 0.61 ± 0.13 for XFe96 and XF96 Analyzer [340]). Rot/AA mediated inhibition of complex I and III lead to complete inhibition of mitochondrial respiration, enabling the identification of mitochondrial-associated acidification.

As these parameters, required for ATP rate calculations, could also be obtained from Mito stress test data, we deemed that it was possible to calculate ATP production rate from existing Mito stress results. Firstly, Mito stress data must be exported as to yield the glycoPER readings required for ATP rate calculations. Using Wave analysis software (Version 2.6.0; Agilent Technologies), this is simply achieved by exporting the data set through a "Seahorse XF Glycolysis Rate Assay Report Generator". It should be noted that the buffer factor (e.g. assay media must be selected) must be known in order to generate PER and glycoPER calculations. Then, following the equations provided in Table 2.3 above, the key parameters of the ATP rate assays were calculated and obtained.

# Chapter 3 – PMCA4 is important for cell migration and apoptotic resistance of MIAPaCa-2 pancreatic cancer cell line

**Pishyaporn Sritangos[1], Andrew D. James[2], Ahlam Sultan[1], Daniel A. Richardson[1], Jason I.E Bruce[1]**

[1] Division of Cancer Sciences, School of Medical Sciences, Faculty of Biology, Medicine and Health, University of Manchester, Manchester, M13 9PT, United Kingdom

[2] Department of Biology, University of York, Heslington, York, YO10 5DD, United Kingdom

## 3.1  Abstract

The expression of plasma membrane calcium ATPase isoform 4 (PMCA4) is altered in multiple cancers and is reported to modulate key cancer hallmarks including cell migration, growth and apoptotic signalling. ATP2B4 mRNA, encoding PMCA4, is reported to be overexpressed in resected pancreatic ductal adenocarcinoma (PDAC) tumours and has been correlated to poor PDAC patient survival. The current study identified MIAPaCa-2 cells as a suitable cellular PDAC model which almost exclusively expresses PMCA4. Using siRNA, we showed that knocking down PMCA4 led to inhibited intracellular $Ca^{2+}$ ($[Ca^{2+}]_i$) clearance and subsequently resulted in elevated resting $[Ca^{2+}]_i$. Without affecting cell growth and viability, knocking down PMCA4 selectively decreased cell migration as well as sensitized cells to $Ca^{2+}$-stress inducer (cyclopiazonic acid; CPA) and classical apoptotic inducer (staurosporine). However, knockdown of PMCA4 in PDAC had no effect on glycolytic and mitochondrial parameters. Elevation in glycolytic ATP production rate and blunted changes in mitochondrial respiration parameters were observed under $Ca^{2+}$ stress. In conclusion, this study provides evidence that PMCA4 expression is mainly important for MIAPaCa-2 PDAC cell migration and apoptotic resistance. Therefore, understanding the role of PMCA4 may offer an attractive novel therapeutic target in PDAC.


**Keywords:** Plasma membrane $Ca^{2+}$ ATPases 4 (PMCA4), cell migration, apoptosis, cancer metabolism, pancreatic ductal adenocarcinoma

## 3.2 Introduction

Pancreatic cancer, particularly pancreatic ductal adenocarcinoma (PDAC), is a commonly diagnosed cancer with the lowest 5-year survival rate [1]. The early stages of pancreatic cancer are often asymptomatic resulting in advance stage diagnosis, involving high tumour metastatic burden [2]. Moreover, conventional chemotherapeutics, involving combinations of gemcitabine/nab-paclitaxel, have failed to improve the survival prospect of pancreatic cancer patients over the past three decades [3].

Dysregulation of calcium ($Ca^{2+}$) signalling has been reported to facilitate malignancies in multiple types of cancer, including PDAC [4]. Spatiotemporal shaping of $Ca^{2+}$ signalling is critical for regulating numerous physiological processes in all cells [5]. However, this can only be achieved if cytosolic $Ca^{2+}$ is maintained very low within cells. Pathological elevation of cytosolic $Ca^{2+}$, particularly irreversible increases in $[Ca^{2+}]_i$ ($Ca^{2+}$ overload), has been associated with apoptotic and necrotic cell death [6,7]. Overexpression of PMCAs, in particular, has been associated with resistance to $Ca^{2+}$ overload-mediated cell death in PDAC [8–10].

Plasma membrane $Ca^{2+}$ ATPases (PMCAs) are major ATP-consuming pumps which regulate $Ca^{2+}$ extrusion from the cells. There are four isoforms of PMCAs (PMCA1-4) encoded by four distinct genes (ATP2B1-4). PMCA1 is a ubiquitously expressed housekeeping $Ca^{2+}$ efflux pump. Conversely, PMCA2-3 isoforms are 'rapid response pumps' which are selectively expressed in excitatory cells (e.g. neurons). PMCA4, albeit ubiquitously expressed [11], has been shown to exhibit a more specific role as a signalling hub for proliferative signalling [12], NFkB nuclear translocation [13], TNF-induce cell death [14] and migration [15]. Many of these signalling pathways are important for the maintenance of cancer hallmarks [16]. Therefore, we hypothesized that PMCA4 may play be capable of modulating role in multiple PDAC hallmarks.

Characteristics of PDAC often includes high metastasis burden and metabolic shift toward glycolysis [2,17]. Our previous study in PDAC cells demonstrated that PMCAs are reliant on glycolytic ATP [9,10]. Evidence in red blood cells suggested that glycolytic enzymes reside in close proximity to fuel the plasma membrane ATPases [18]. Vice versa, as a population of key glycolytic enzymes such as phosphofructokinase [19] and pyruvate kinase are inhibited by high ATP concentrations [20], we suspect that ATP-consumption by PMCA may help to maintain glycolytic flux.

As PMCA4 regulates multiple processes associated with cancer hallmark, previous studies had specifically assessed the role of PMCA4 in MDA-MB-231 breast cancer cells [13] and HT-29 colon cancer cells [21]. Although ≥5-fold overexpression of PMCA4 mRNA has been detected in PDAC tumours compared to normal pancreatic ductal epithelial cells [22], limited studies have assessed the role of PMCA4 in PDAC.

The current study compares PMCA isoform expressions in pancreatic cell lines and identified MIAPaCa-2 as a PDAC cell line model which predominantly expresses PMCA4. We showed that siRNA knockdown of PMCA4 led to the inhibition of $Ca^{2+}$ efflux, cell migration and sensitizes cells to apoptosis in the presence of apoptotic inducer to stress inducers in MIAPaCa-2 PDAC cells. This work highlights

the importance of PMCA4 in multiple cancer hallmarks and provides insights into the potential benefits of clinically targeting PMCA4 in PDAC.

## 3.3  Materials and Methods

**Cell culture** – MIAPaCa-2 and PANC-1 were purchased from ATCC (Teddington, UK). Human pancreatic ductal epithelial cells (HPDE) and Human pancreatic stellate cells (hPSC) were a kind gift from Diane Simeone (University of Michigan) and David Yule (University of Rochester), respectively. MIA PaCa-2, PANC-1, and hPSC were cultured in DMEM media supplemented with 10% fetal bovine serum and 1% penicillin/streptomycin. HPDE were cultured in Keratinocyte-SFM media (Fisher Scientific, Loughborough, UK). All cells were cultured under 5% $CO_2$ (g), at $37^oC$. Mycoplasma contaminations were screened by DAPI staining or PCR.

**Chemicals and reagents** - All chemicals and solvents were purchased from Sigma-Aldrich (Gillingham, UK) unless otherwise specified.

**Data mining** - Badea Pancreas (2008) gene chip microarray data was obtained from www.oncomine.org, January 2019 (ThermoFisher Scientific, Waltham, MA). TGCA-PAAD Kaplan Meier survival data were obtained from www.proteinatlas.org, version 18.1, January 2019.

**siRNA knockdown of PMCA4 expression** – PMCA4 expression was knockdown using 25 nM ON-TARGETplus pool siRNA targeting ATP2B4 mRNA (siPMCA4). Scramble non-targeting/siRNA was used as a control. (Dharmacon, Colorado, USA) Transfection conditions that yielded ≥70% expression knockdown between 48-96 hours were used in the study. mRNA and protein expression knockdowns were confirmed by RT-qPCR and western immunoblot, respectively.

**RT-qPCR** – Pre-designed KiCqStart®SYBR® Green primers targeting ATP2B1-4 (PMCA1-4), ATP2B4b and 18S rRNA were purchased from Sigma-Aldrich (Haverhill, UK) and qPCR was performed using POWER SYBR green master mix. (Fisher Scientific, Loughborough, UK)

**Western immunoblotting** – Pan-PMCA, PMCA1, PMCA2, PMCA3, PMCA4, anti-rabbit and anti-mouse antibodies were purchased from Cell Signalling Technology (Massachusetts, USA). Protein bands were imaged and quantified using the ChemiDoc (Fisher Scientific, Loughborough, UK).

**Sulforhodamine B (SRB) cell viability assay** – Cells were fixed and stained according to the protocol by Vichai, V *et al.* (2006) [51]. Protein content was quantitated using Synergy HT microplate reader (BioTEK, Swindon, UK) at 540 nm absorbance.

**PMCA activity assay ($Ca^{2+}$ clearance)** – Cells seeded onto 16 mm circular glass coverslips were incubated with either siNT or siPMCA4 for 48 hours. Cells were loaded with 4 µM Fura-2 $Ca^{2+}$ dye (TEFLabs, Texas, USA) then perfused with $Ca^{2+}$-free HEPES-buffer physiological saline solution (HPPS) containing 1 mM EGTA and 30 µM CPA for 20 minutes. $Ca^{2+}$ clearance is observed by switching from 20 mM $Ca^{2+}$ HPPS to $Ca^{2+}$-free HPPS as previously described [9,10]. Fluorescent signals were acquired at 340/380 nm excitation and 50 ms exposure. Images were acquired using MetaFluor software

(Molecular Devices, California, USA). Relative $[Ca^{2+}]_i$ clearance was determined using a single exponential decay fit and results expressed as a time constant ($\tau$).

**$Ca^{2+}$ overload assay** – Fura2-loaded cells were perfused with HPPS until the 340/380 nm fluorescence ratio stabilizes. HPPS containing 30 µM CPA was perfused for 15 minutes then rinsed with CPA-free HPPS for another 15 minutes. All $[Ca^{2+}]_i$ calibrations were calculated using the following equation: $[Ca^{2+}]_i$ nM = 541.6 nM * ((Ratio – 0.47)/(2.101 - Ratio)). $[Ca^{2+}]_i$ was quantified by area under curve (AUC) as previously described [9,10].

**Caspase3/7 apoptosis assay** – siRNA treated cells were treated with apoptotic inducers (STS, OM, CPA, IAA). 5 µM of caspase 3/7 green apoptosis reagent (IncuCyte, Michigan, USA) and 625 nM Nuclear-ID Red (Enzo Life Sciences, Exeter, UK) were added 30 minutes prior to imaging. Cells were imaged on the IncuCyte, using 10x lens. Results were analysed using IncuCyte Zoom software and data are presented as % apoptosis [(green cell count/image ÷ red cell counts/image) x 100]

**Seahorse live-cell metabolic assays** – Cells seeded were incubated for 48 hours in either siNT or siPMCA4. Seahorse cartridges and media were prepared according to manufacturer instructions. Low phenol-red DMEM, pH 7.4 media was used for all Seahorse-based assays. Either vehicle control (<0.1% DMSO) or 30 µM CPA were pre-injected in addition to the designated reagents for the Mito and glycolysis stress test. Seahorse data obtained were analysed using Wave analysis software (Agilent Technologies, Santa Clara, USA).

**Statistics** – Data analysis was performed using Prism 7 software (GraphPad, San Diego, CA). Data are presented as means ± SEM. Parametric comparisons were performed using either Student's t-test or analysis of variance (ANOVA) with Bonferroni post-test. Non-parametric comparisons were performed using either the Kolmogorov-Smirnov test or Kruskal Wallis with multiple comparisons test. Two-factor comparisons were performed using Two-ANOVA with Dunnett's post-test. Statistical significance is defined as $p < 0.05$.

## 3.4 Results

### 3.4.1 Expression of PMCA4 gene, ATP2B4, is correlated with PDAC and poor patient survival

To determine whether alterations in ATP2B1-4 genes (encoding PMCA1-4 protein) in PDAC tumour are correlated to poor patient survival, data mining from open-source databases, Oncomine [23,24] and The Human Protein Atlas [25,26], was performed.

Gene chip microarray data from a study by Badea *et al.* (2008), comparing gene expression in PDAC tumour versus resected healthy tissue from the tumour margin, showed that ATP2B4 was overexpressed (2.65-fold, n=39, p<4.06-10) while ATP2B1 was less overexpressed (1.24-fold, n=39, p<0.035) in PDAC tumour. In contrast, expression of ATP2B2 (-1.44-fold, n=39, p<1.92-9) and ATP2B3 (-1.56-fold, n=39, p<1.95-8) were significantly reduced in PDAC. (Figure 3.1A-E)

Patient survival data was sourced from the cancer genomic atlas - pancreatic adenocarcinoma cohort (TGCA-PAAD). The cohort of PDAC patients was divided into quartiles based on the median-centred ATP2B1-4 tumour expression. Only patients with high expression of ATP2B4 had a higher risk of poor survival (hazard ratio= 1.83, n=45, p<0.04) whereas the expression of ATP2B1 had no effect. (Figure 3.1F-G) Expression of ATP2B2 and ATP2B3 were negligibly detected and could not be correlated to patient survival.

Collectively, elevated ATP2B4 and low ATP2B2-3 expressions are representative characteristics of resected PDAC tumours and high ATP2B4 expression is associated with poor PDAC patient survival.
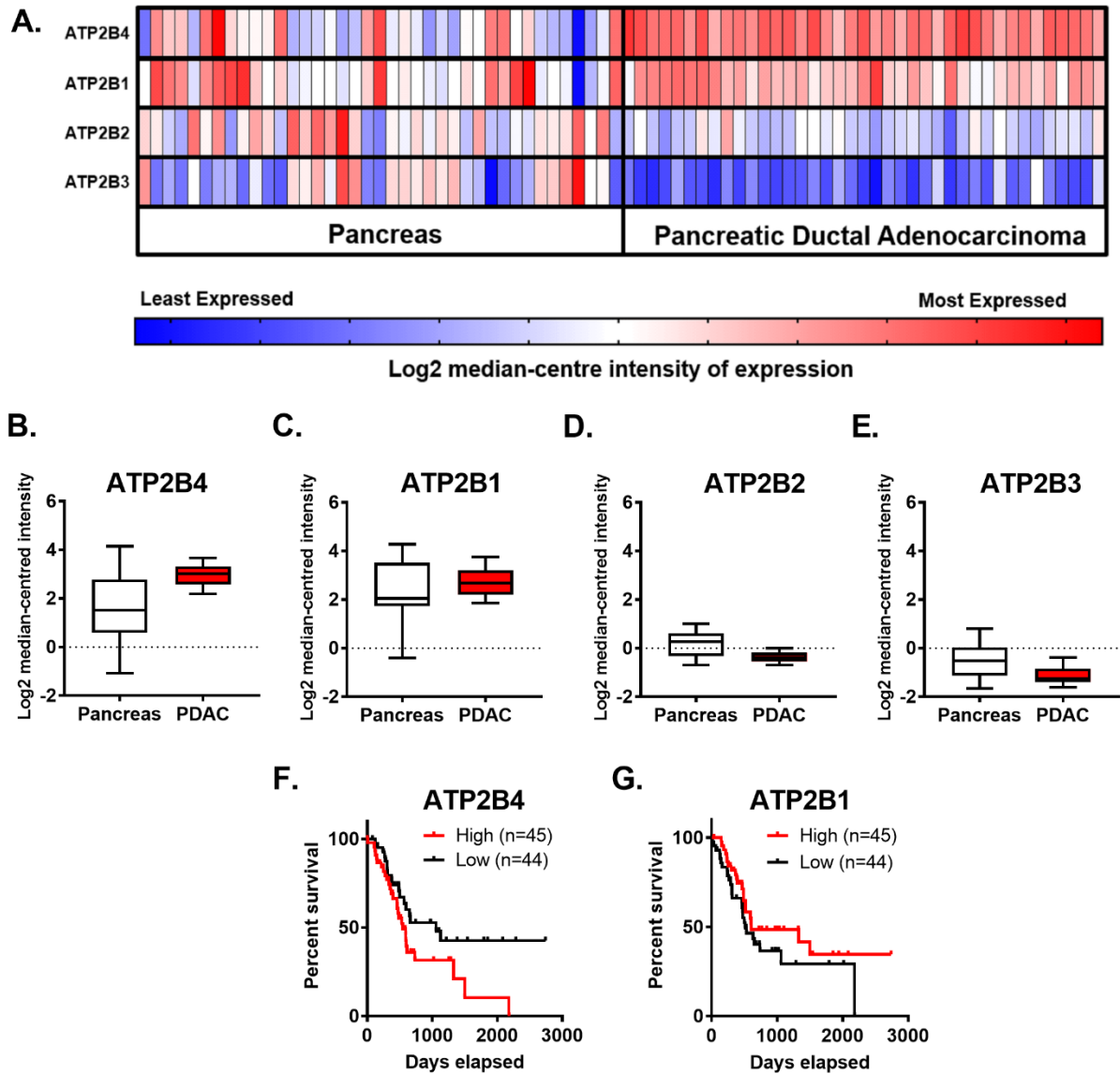
**Figure 3.1 – Elevated PMCA4 mRNA expression (ATP2B4) in PDAC is correlated with low patient survival.** A-E, Badea Pancreas (2008) gene chip microarray data, comparing resected PDAC tumour and healthy pancreatic tissue obtained from matching tumour margin (n=39), was obtained from Oncomine open-source database. **A,** The heat map of ATP2B1-4 gene expression in healthy pancreatic tissue (n=39) and PDAC tumour (n=39). Heat map colours, ranging from least expressed (blue) to most-expressed (red), depict relative Log2 median-centre intensity within rows. Heat map colours cannot be compared between rows. Comparison between PDAC and healthy pancreas tissue are shown as individual Log2 median-centre intensity of **B,** ATP2B4, **C,** ATP2B1, **D,** ATP2B2 and **E,** ATP2B3 gene expression. **F-G,** PDAC patient survival data was sourced from TGCA-PAAD (n=176), through The Human Protein Atlas database (January 2019, www.proteinatlas.org). The cohort of 176 PDAC patients was divided into quartiles based on the median-centred gene expression (fragments per kilobase of transcript per million mapped reads; FPKM) into either low (25 percentile) and high (75 percentile) gene expression. The survival outcomes of each group were compared using the log-rank test. Kaplan-Meier curves correlating the survival of PDAC patients to the low (black) or high (red) expression of F, ATP2B4 and G, ATP2B1.

### 3.4.2 PMCA4 is the major PMCA isoform expressed in MIAPaCa-2 pancreatic cancer cell line

Given that high expression of ATP2B4 correlates with poor PDAC patient survival, we sought to determine the expression PMCA1-4 isoforms in PDAC cell lines (MIAPaCa-2 and PANC-1) and related non-malignant pancreatic cells (human pancreatic ductal epithelial cells and human pancreatic stellate cells; HPDE and hPSC, respectively), at both protein and mRNA level.

Using Western immunoblotting, relative PMCA4 expression was the highest in both MIAPaCa-2 and hPSC compared to HPDE and PANC-1 (Figure 3.2A-B). PMCA2 was also detected in MIAPaCa-2 and hPSC to a greater extent than HPDE and PANC-1. However, despite high expression in the mouse brain lysate positive control, PMCA1 and PMCA3 were barely detected in any pancreatic cell lines screened. RT-qPCR further confirmed that ATP2B4 was almost exclusively expressed in MIAPaCa-2 cells with close to undetectable levels of ATP2B1-3 (Figure 3.2C). In relative terms, PANC-1 cells expressed low levels of ATP2B1-4 isoforms, also consistent with Western blot data. The non-malignant HPDE cells abundantly expressed ATP2B1 and ATP2B4 which was not necessarily consistent with the Western blot data, suggesting that either the primary antibody was relatively poor at detecting PMCA1 or that PMCA1 mRNA was silenced and not translated into protein in HPDE. hPSC expressed a similar pattern of mRNA expression to that observed in HPDE, albeit relatively lower and more variable than MIAPaCa-2.

It should be noted that the relative ratio of ATP2B4:ATP2B1 in hPSC, HPDE and PANC-1 cell lines were relatively similar (0.6-1.4 fold) whereas MIAPaCa-2 substantially expresses ATP2B4 by 48-fold more than ATP2B1. Since MIAPaCa-2 cells almost exclusively expressed PMCA4 at both the protein and mRNA level, this suggests that MIAPaCa-2 represent a good cellular model of PDAC that can be taken forward for further functional studies. Moreover, as MIAPaCa-2 is reported to exhibit a more glycolytic phenotype than PANC-1 [9,10], the MIAPaCa-2 cell line is a potentially good model to investigate the relationship between PMCA4 and glycolysis.
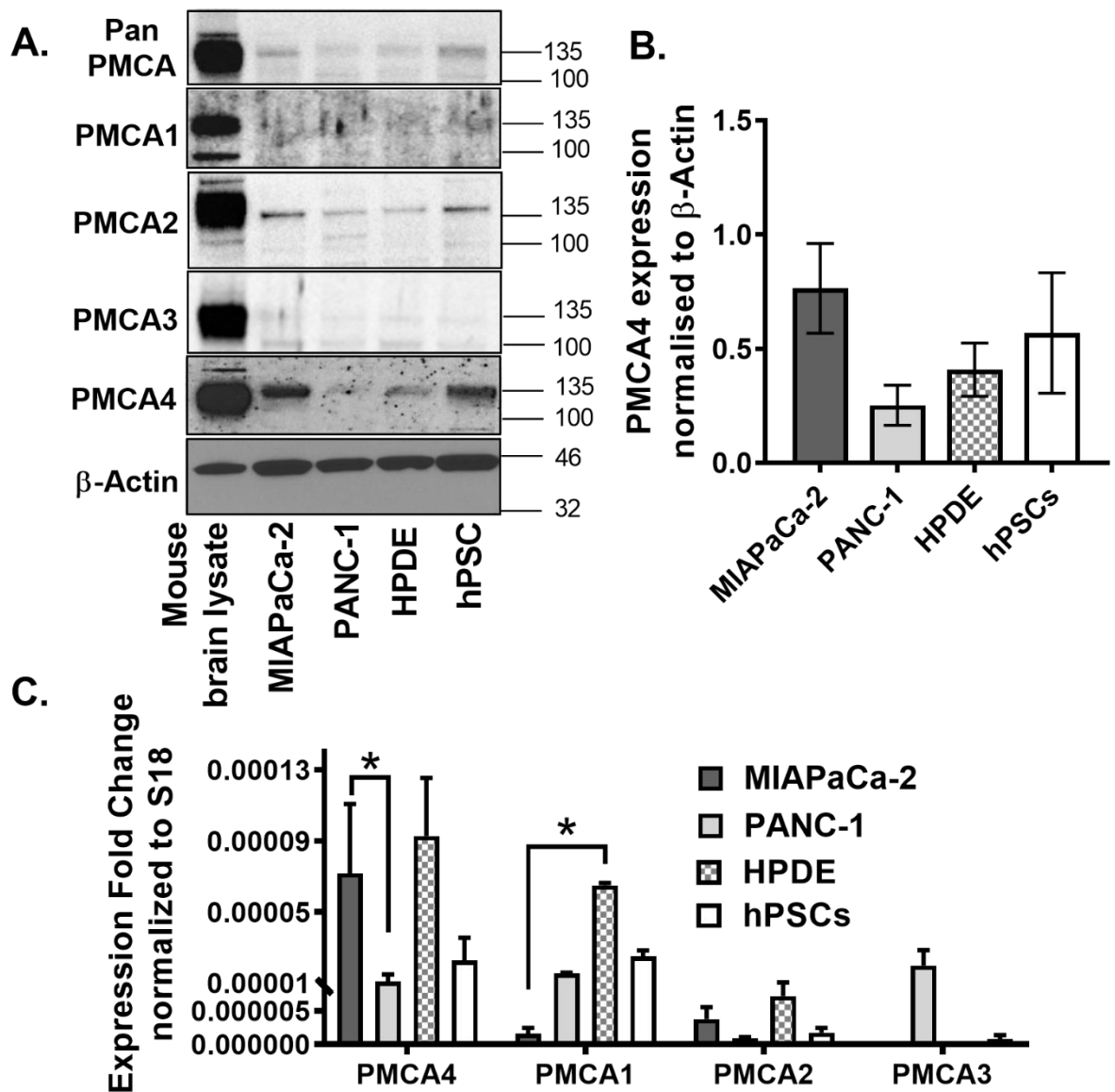
**Figure 3.2 – Expression of PMCA isoforms in multiple pancreatic cells lines. A,** Representative Western immunoblot shows the relative protein expression of total/pan PMCA and PMCA isoform 1-4 in pancreatic cancer (MIAPaCa-2 and PANC-1) and non-cancer pancreatic cells (HPDE and hPSC). Mouse brain lysate was used as a positive control for PMCA expressions and β-Actin was used as a protein loading control. **B,** PMCA4 protein expression in each cell line was quantified from Western blot bands and normalized to β-Actin housekeeping protein. **C,** The relative mRNA expressions of PMCA1-4 (ATP2B1-4) in each cell line was quantified by RT-qPCR. Data are expressed as relative mRNA expression normalized to corresponding S18 rRNA controls (2-ΔCт). Statistical comparisons were made using Kruskal-Wallis test with Dunn's multiple comparison test and two-way ANOVA with Dunnett's multiple comparison test. Data are expressed as mean ± SEM. (N=4-5, 4 replicates per treatment condition). * represents statistical significance where p<0.05.

### 3.4.3 siRNA knockdown of ATP2B4 mRNA and PMCA4 protein expression in MIAPaCa-2 cells

In order to test the functional effects of PMCA4 in MIAPaCa-2 cells, a pool of 4 siRNA was used to transiently knockdown the expression of ATP2B4 (siPMCA4). A similar pool of non-targeting siRNA (siNT) was used as a control. PMCA4 knockdown was then confirmed at the protein and mRNA level.

Using Western immunoblotting, results show that PMCA4 protein expression decreased in a time-dependent manner in comparison to the siNT control. PMCA4 expression decreased by 75% between 48-96 hours post-siPMCA4 treatment (Figure 3A-B, n =3, p<0.05). At mRNA level, the total ATP2B4 and splice variant ATP2B4b expressions were knocked down by at least 70% between 48-72 hour (Figure 3C-D, n =3, p<0.05). Moreover, there were no compensatory changes in ATP2B1-3 expression (data not shown). According to a previous study by Curry *et al.* (2012), conditions yielding ≥70% PMCA mRNA expression knockdown were sufficient to functionally inhibit cellular Ca$^{2+}$ clerance and influence cell death responses in MDA-MB-231 breast cancer cells [13]. Therefore, siRNA incubations between 48-96 hours, yielding ≥70% PMCA4 protein expression, were used for further experiments.
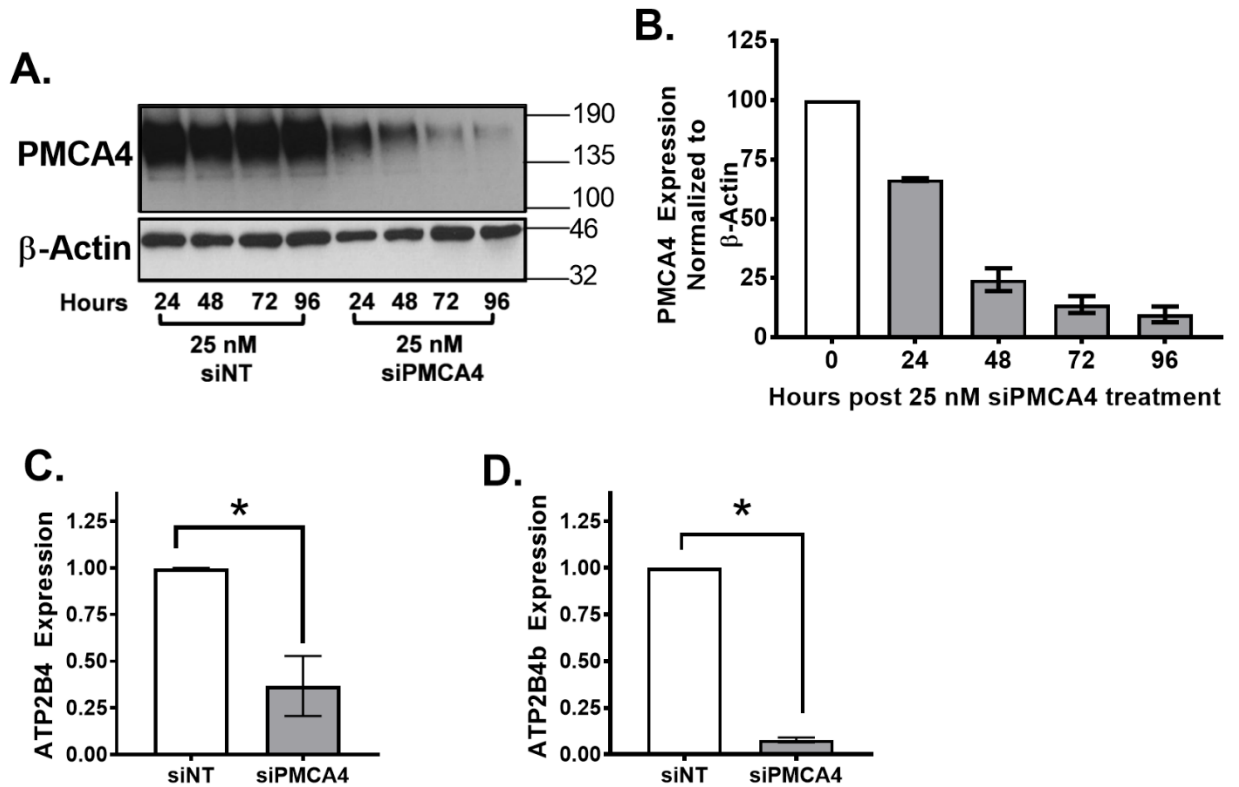


**Figure 3.3 – siRNA knockdown of PMCA4 in MIAPaCa-2 PDAC cells. A,** Representative western blot comparing PMCA4 protein expression in MIAPaCa-2 cells after 24-96 hours of treatment with siNT (control) and siPMCA4 (PMCA4 knockdown). **B,** PMCA44 protein expression of siPMCA4 treated cells were quantified from Western blot bands and normalized to β-Actin (N=4). **C,** The relative expression of ATP2B4 (PMCA4 mRNA) and D, ATP2B4b (PMCA4b mRNA) were examined after 48 hours of siRNA treatment by RT-qPCR. The expressions of target mRNA were normalized to S18 rRNA and expressed as 2-(ΔΔCт). Data are shown as mean ± SEM. (N=3) Comparisons were made between siNT control and siPMCA4 treated cells at matching time points post-drug treatment using Kolmogorov-Smirnov test (Unpaired, non-parametric cumulative distribution test). * represents statistically significant difference where P<0.05.

### 3.4.4 PMCA4 is the major functional Ca- efflux pathway in MIAPaCa-2 cells

Our previous study demonstrated that PMCA is the main mechanism of intracellular $Ca^{2+}$ ($[Ca^{2+}]_i$) efflux in MIAPaCa-2 cells. [9,10] As PMCA4 is the major PMCA isoform expressed in MIAPaCa-2, we predicted that PMCA4 is functionally critical for Ca- efflux. After establishing ≥70% of PMCA4 expression knockdown, we therefore wanted to confirm that this led to decreased PMCA activity using our *in situ* $Ca^{2+}$ clearance assay [9,10].

Cells loaded with $Ca^{2+}$ sensing fura-2 dye were perfused with $Ca^{2+}$-free HEPES-buffered physiological saline solution (HPSS) containing 1mM EGTA and 30 μM cyclopiazonic acid (CPA). CPA is an inhibitor of a sarco endoplasmic reticulum $Ca^{2+}$-ATPase (SERCA) that depletes endoplasmic reticulum $Ca^{2+}$ storage and activates store-operated $Ca^{2+}$ entry (SOCE) channels. The addition of 20 mM $Ca^{2+}$ HPSS leads to SOCE and a large increase in $[Ca^{2+}]_i$ which reaches a high steady-state. Subsequent removal of external $Ca^{2+}$ allows $[Ca^{2+}]_i$ clearance, almost exclusively due to PMCA [10] to be assessed and quantified by fitting the falling phase of a single exponential decay to yield a time constant (τ).

We found that knocking down PMCA4 led to profound inhibition of $[Ca^{2+}]_i$ clearance compared to siNT control (Figure 3.4 A-B). In siPMCA4-treated cells, the mean τ was significantly higher (τ = 472 ± 83.96 seconds) compared to siNT controls (τ = 126.8 ± 22.35 seconds), suggesting $Ca^{2+}$ clearance was dramatically delayed (Figure 3.4C-D). In addition, the transient increase in $[Ca^{2+}]_i$ following addition of CPA in zero external $Ca^{2+}$ (reported as area under the curve; AUC), which reflects ER $Ca^{2+}$ leak that is cleared from the cytosol by the PMCA, was also significantly greater in PMCA4 siRNA-treated cells (AUC = 525.8±65.9) compared to siNT controls (AUC = 211.6±24.8; Figure 3.4E-F). These results suggest that PMCA4 expression is an essential $Ca^{2+}$ efflux mechanism and loss of PMCA4 induces significantly impaired $Ca^{2+}$ clearance.
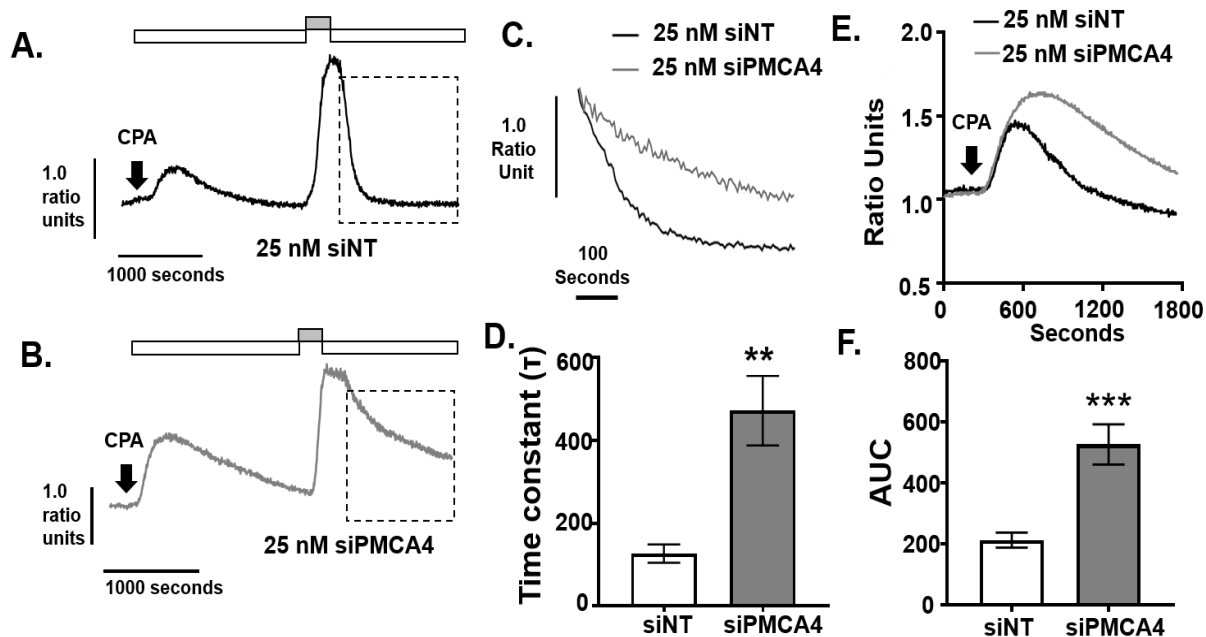
**Figure 3.4 – PMCA4 knockdown in MIAPaCa-2 reduces PMCA-mediated Ca²⁺ Clearance.**
MIAPaCa-2 cells were treated with 25 nM non-targeting siRNA (siNT) or 25 nM siRNA targeting PMCA4 mRNA (siPMCA4) for 48-72 hrs prior to performing in situ Ca²⁺ clearance assay using Fura-2 ratiometric dye. Representative *in situ* [Ca²⁺]ᵢ traces of MIAPaCa-2 incubated in either **A,** 25 nM siNT or **B,** 25 nM siPMCA4 for 48-72 hrs prior to imaging. Cells were perfused with 0 mM Ca²⁺ HPPS containing 30 µM CPA (white box) to induce ER intracellular Ca²⁺ storage depletion. Cells were then treated with 20 mM Ca²⁺ HPPS containing CPA (grey box) to induce store-operated Ca²⁺ entry. PMCA-associated Ca²⁺ efflux is triggered by subsequent removal of extracellular Ca²⁺ (0 mM Ca²⁺ HPPS). **C,** Representative clearance phase of siNT and siPMCA4 over 500 seconds are overlaid. **D,** The rate of [Ca²⁺]ᵢ clearance was fitted to a single exponential decay and the time constant (τ) was determined. **E,** Representative CPA traces of siNT and siPMCA4 over 1800 seconds is shown. **F,** The area under the curve of siNT and siPMCA4 following CPA treatment were compared. Data are shown as mean ± SEM. (N=5, data collected from at least 50 individual cells). Comparisons were made between siNT control and siPMCA4 treated cells at matching time points post-drug treatment using Kolmogorov-Smirnov test (Unpaired, non-parametric cumulative distribution test). ** and *** represents statistically significant difference where P<0.005 and P<0.001, respectively.

### 3.4.5 PMCA4 knockdown inhibits cell migration independent of cell proliferation

PMCA4 associated $Ca^{2+}$ efflux has been reported to be important for cell migration [15] as well as cell growth [27] – both important cancer hallmarks [16]. A gap closure assay was used to assess cell migration. As gap closure can result from both migration and cell proliferation, the anti-proliferative reagent mitomycin C (Mit C) was used to limit cell proliferation [28,29]. Sulforhodamine B (SRB) assay was used to confirm that mitomycin C successfully inhibited cell growth thereby removing any confounding effect on gap closure.

In untreated controls, gap closure attributed to both cell migration and proliferation was relatively similar between siPMCA4 and siNT control. (Figure 3.5A-B) Furthermore, no differences between the growth rate of siPMCA4 and siNT control were observed from SRB assays (Figure 3.5C). Upon treatment with Mit C to selectively monitor cell migration, siPMCA4-treated cells exhibited significantly reduced gap closure (65.61±4.43 % closure) compared to siNT controls after 48 hours (80.57±3.23% closure; Figure 3.5A-B). Mit C treatment inhibited cell growth of both siNT and siPMCA4 at 48 hours without any noticeable effect on cell viability. However, at 72 hours SRB absorbance declined, suggesting that Mit C was affecting cell viability beyond 48 hours. Nevertheless, this suggests that any changes in gap closure in Mit C-treated cells over 48 hours represent an effect on cell migration independent of cell viability. Overall, our results showed that PMCA4 knockdown significantly inhibited cell migration but had no effect on the growth rate of MIA PaCa-2 cells.
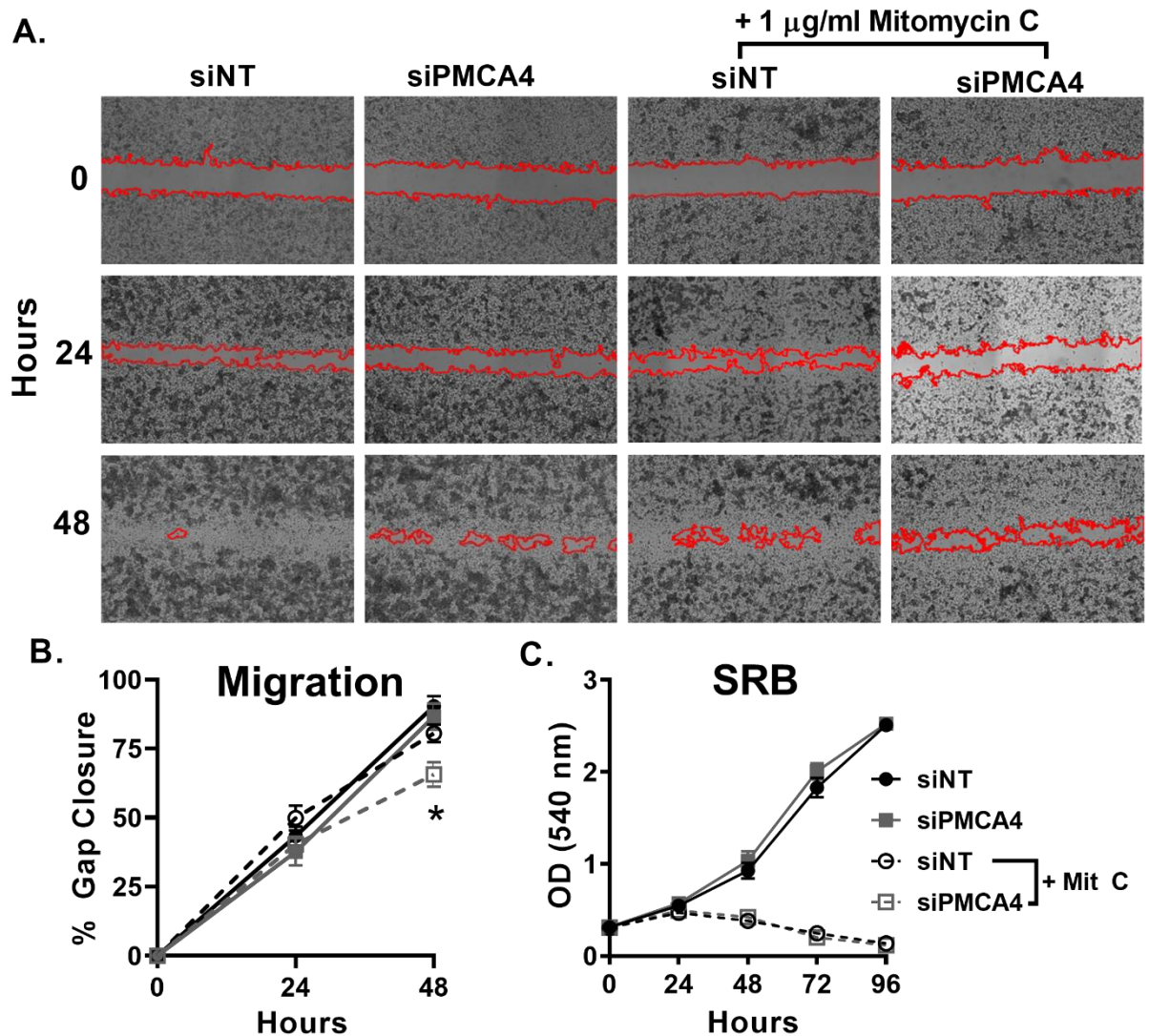
**Figure 3.5 – PMCA4 knockdown cells inhibits cell migration but does not affect cell proliferation.** MIAPaCa-2 cells seeded into Ibidi chambers were incubated with either 25 nM of non-targeting siRNA (siNT) or 25 nM siRNA targeting PMCA4 mRNA (siPMCA4). After 24 hours, the Ibidi chambers were removed to create a cell-free gap area at time 0 hour. The anti-proliferative agent, mitomycin C (Mit C), was added after Ibidi chamber removal to prevent gap closure by cell proliferation. **A,** Representative images of the gaps were imaged at 0, 24 and 48 hrs using an Olympus IX83 inverted microscope, on bright field mode with a 10x objective lens. Gap images were processed and analysed using ImageJ image processing software. **B,** Data are presented as % gap closure with respect to time 0 hour. **C,** SRB proliferation assays were run in parallel to the migration assay to ensure cell proliferation was sufficiently inhibited by Mit C. Data are shown as mean ± SEM. (N=4, at least 3 replicates were performed per treatment condition). Comparisons were made between siNT control and siPMCA4 treated cells at matching time points using Two-way ANOVA, Dunnett's multiple comparison post-hoc test. * represents statistically significant difference where P<0.05.

### 3.4.6 PMCA4 knockdown enhances apoptosis associated with Ca$^{2+}$ overload

PMCAs have been correlated with apoptotic resistance in multiple cancers [13,30]. Therefore, to investigate whether PMCA4 plays a role in apoptotic resistance, different stressor reagents were used in caspase 3/7 cleavage assay and Ca$^{2+}$ overload experiments.

Based on our previous studies, PMCA activity is modulated by glycolytic inhibitors but not mitochondrial inhibitors in MIAPaCa-2 cells [10]. Therefore, the stressors used in caspase 3/7 cleavage assay included glycolytic inhibitors (iodoacetate, IAA), mitochondrial inhibitor (oligomycin, OM) and Ca$^{2+}$ overload inducer (CPA). A classical apoptotic inducer, staurosporine (STS), was used as a positive control. Over a period of 12 hours, we found that STS significantly induced caspase 3/7 cleavage in both siNT (23.86 ± 2.07%) and siPMCA4 (37.47±2.71%) compared to DMSO vehicle control (11.5±1.38%; Figure 3.6A-B).

Our results showed that PMCA4 knockdown cells were significantly more susceptible to STS, CPA and OM induced apoptosis compared to siNT control. PMCA4 knockdown cells were noticeably sensitized to CPA-induced cell death (52.5±9.5% at 12 hours) and significant caspase 3/7 cleavage was observed from as little as 7 hours (32.4±7.6% at 7 hours; Figure 3.6C). Interestingly, OM induced significant apoptosis in siPMCA4 but had no effect on siNT controls. Conversely, IAA caused similar levels of apoptosis in both siPMCA4 (40.5±16.0%) and control (44.1±16.9%; Figure 3.6B). Overall, in comparison to vehicle control, CPA and OM had no effect on siNT control but significantly increased apoptosis in PMCA4 knockdown cells.

The impaired Ca$^{2+}$ efflux in PMCA4 knockdown cells likely facilitated Ca$^{2+}$ overload-associated apoptosis. Using the Ca$^{2+}$ overload assay, we showed that CPA treatment triggered a substantial increase in [Ca$^{2+}$]$_i$ which caused fura-2 signal saturation (R$_{max}$), making calibration of [Ca$^{2+}$]$_i$ difficult (Figure 3.6D). Therefore, the magnitude of these [Ca$^{2+}$]$_i$ responses were quantified by measuring the area under the curve (AUC) of uncalibrated fura-2 signal ratio (Figure 3.6E). The AUC of siPMCA4-treated condition was significantly higher than the PMCA4 positive siNT control by 1.5-fold. Although Ca$^{2+}$ calibration could not be applied to CPA responses, it was possible to calibrate and compare the resting [Ca$^{2+}$]$_i$. Interestingly, the resting [Ca$^{2+}$]$_i$ of siPMCA4 cells (286 ± 68 nM) was 3.6-fold higher than siNT controls resting [Ca$^{2+}$]$_i$ (79±12 nM; Figure 3.6F). These results suggest that PMCA4 knockdown cells had inherently higher resting [Ca$^{2+}$]$_i$ which may be due to impaired [Ca$^{2+}$]$_i$ efflux.

**A.**

siNT    siPMCA4

0.1%
DMSO

10 µM
STS

30 µM
CPA

10 µM
Oligomycin

10 µM
IAA
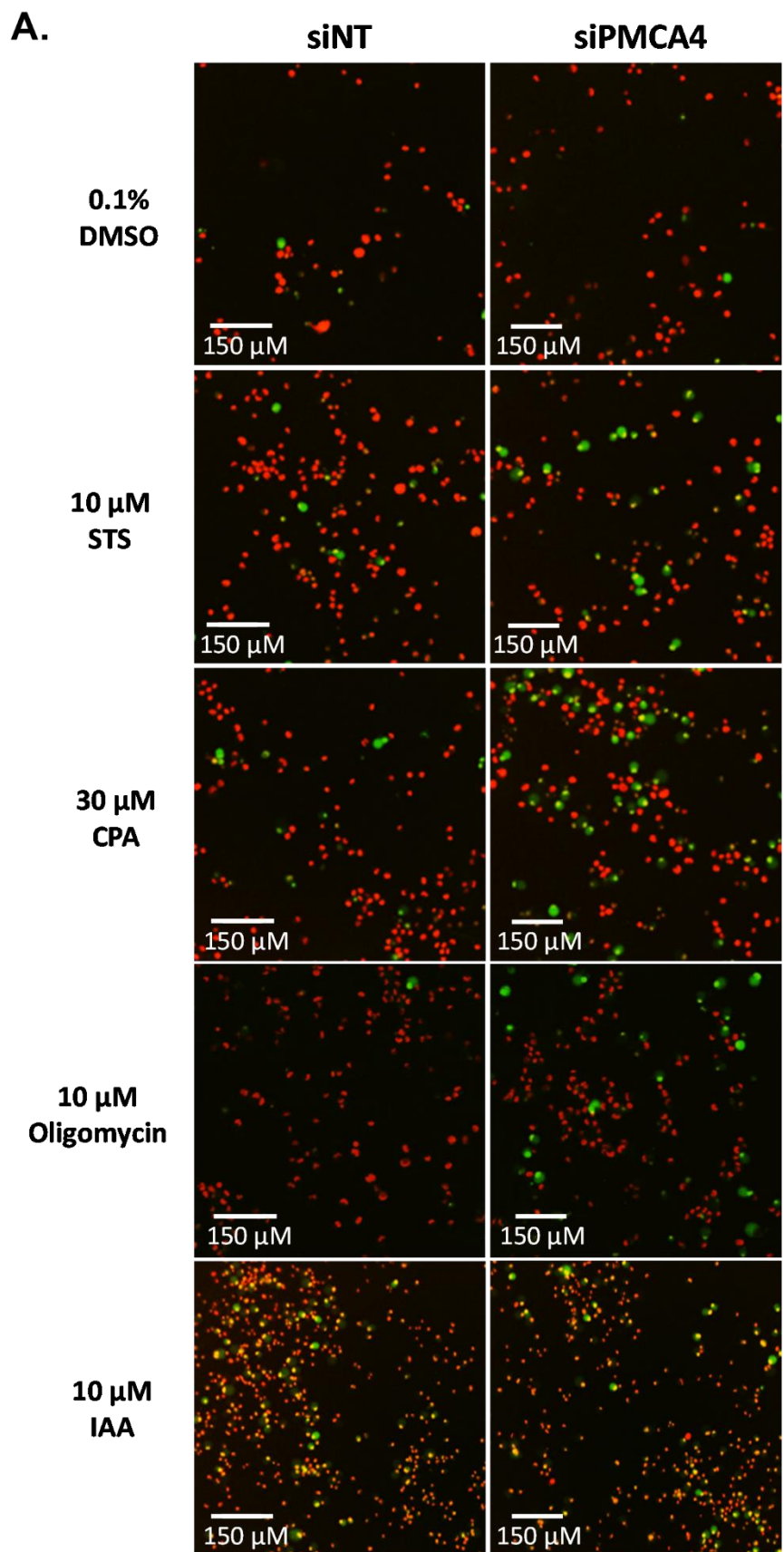
**Figure 3.6 – PMCA4 Knockdown enhances apoptosis associated with Ca$^{2+}$ overload.** (continuing next page)
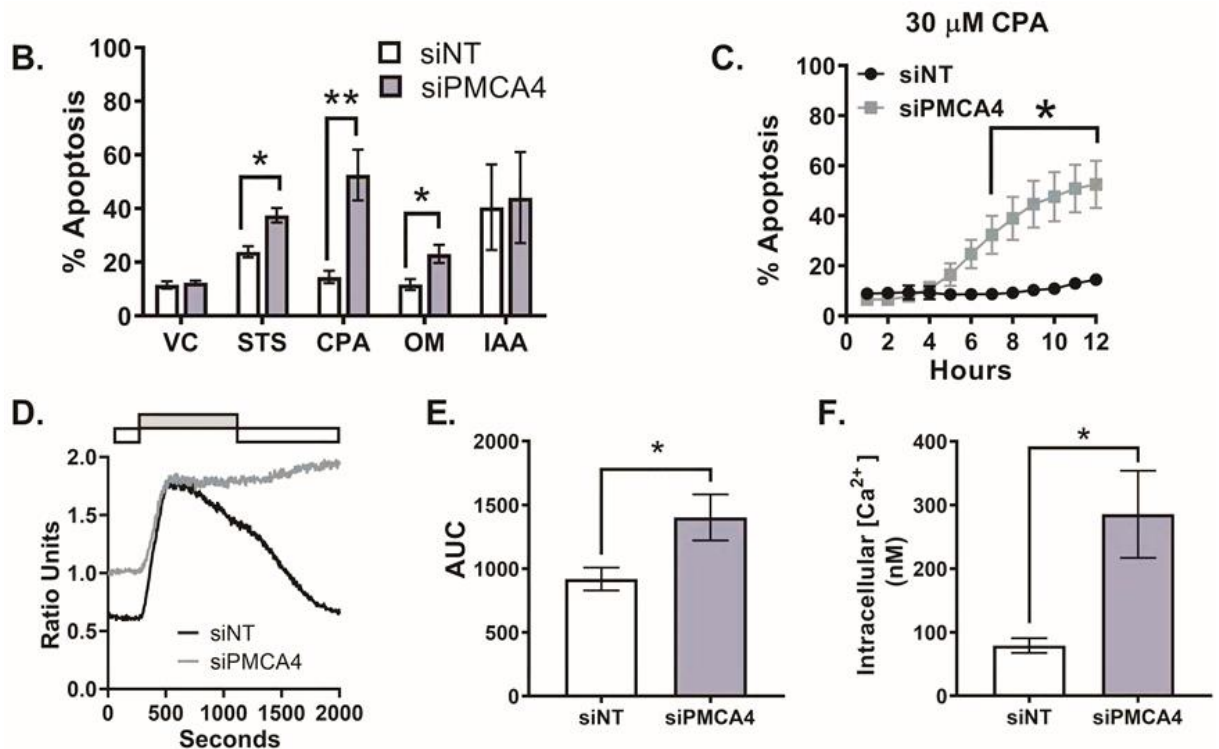
**Figure 3.6 Continued – PMCA4 Knockdown enhances apoptosis associated with Ca²⁺ overload.** MIAPaCa-2 cells were seeded in either non-targeting control (siNT) or siRNA targeting PMCA4 (siPMCA4) for 48 hours then treated with either 0.1% DMSO vehicle control (VC), apoptotic inducing staurosporine (STS), cyclopiazonic acid (CPA), oligomycin (OM) or iodoacetate (IAA). The cells are labelled with Nuclear ID red (red) and Caspase3/7 reagent (green). Cells were then imaged using the Incucyte, on the red and green channel, using a 10x objective lens. **A,** Representative images of cell death at 12 hours are shown and **B,** corresponding % apoptosis is shown as the percentage of caspase 3/7 cleavage with respect to total nucleus count. **C,** The effects of CPA induced apoptosis was further examined at 0.5-12 hr. **D,** Ca²⁺ overload assay was used to examine the relationship between CPA and Ca²⁺ overload associated cell death. Fura-2 loaded cells were perfused with HPPS (white box) for 200 seconds. After baseline signals stabilise, cells were perfused with 30 µM CPA added HPPS (black arrow and grey box) for 15 minutes then washed with HPPS for 15 minutes. Representative Ca²⁺ overload traces of siNT control (black) and siPMCA4 (grey) are shown. **E,** The area under the curve of the raw fura-2 fluorescence ratios and **F,** calibrated resting Ca²⁺ concentration were analysed. Comparisons were made between siNT and siPMCA4 treated conditions using the Kolmogorov-Smirnov test and unpaired t-test with Welch's correction. Data are shown as mean ± SEM. (N=3, 4 replicates per treatment condition) * represents statistically significant difference where $P < 0.05$.

### 3.4.7  PMCA4 is essential for metabolic flexibility during Ca$^{2+}$ overload

Ca$^{2+}$ is a known modulator of both glycolytic [31] and mitochondrial metabolic activity [32]. Moreover, we found that knocking down PMCA4 unexpectedly sensitized cells to mitochondrial ATP synthase inhibitor (OM), suggesting that mitochondrial respiration was altered in the absence of PMCA4. As PMCA is a crucial Ca$^{2+}$ efflux mechanism that is also functionally reliant on glycolytic ATP in PDAC cells [9,10], we hypothesized that PMCA4 knockdown will alter the metabolic phenotype of MIAPaCa-2 PDAC cells.

The Seahorse XFe96 Analyser was used to monitor real-time changes in oxygen consumption rate (OCR) and extracellular acidification rate (ECAR), indicative of baseline mitochondrial respiration (oxidative phosphorylation; OXPHOS) and glycolysis, respectively. The current study compared changes in both OXPHOS and glycolytic metabolism of siNT control versus siPMCA4 cells under basal (unstressed) and Ca$^{2+}$ overload conditions (Ca$^{2+}$ stressed). CPA was pre-injected to induce Ca$^{2+}$ overload stress, subsequently forcing PMCA4 to function at its maximum capacity.

In order to investigate the differences between the mitochondrial respiration of siNT control versus siPMCA4, key parameters of mitochondrial functions were measured using the Seahorse Mito stress test (Figure 3.7A-D). Under basal conditions, PMCA4 knockdown had no effect on all mitochondrial respiration parameters. However, we observed a 1.8-fold increase in mitochondrial membrane potential (ΔΨm), indicative of a larger driving force for mitochondrial ATP synthesis (Supplementary Figure 3.1).

Under Ca$^{2+}$ stress, siNT control showed decreased maximum respiration and spare respiratory capacity (Figure 3.7D). In contrast, siPMCA4 showed no changes in maximum respiration and spare respiratory capacity although mitochondria-linked ATP production was reduced (Figure 3.7D). Taken together, this suggests that knocking down PMCA4 abolished the effects of CPA on aerobic capacity.

Since CPA treatment reduced mitochondrial respiration capacity in siNT control, it could be argued that compensatory glycolysis may be responsible for sustaining PMCA4 activity. Therefore, the glycolysis stress test was used to measure changes in ECAR which reflect glycolytic flux (Figure 3.7E-H). Under basal conditions, PMCA4 knockdown had no effect on all glycolytic parameters. Under Ca$^{2+}$ stress, the glycolytic reserve was significantly lower in siPMCA4 compared to siNT, albeit the change is small and may not be physiologically relevant (Figure 3.7H). It should be noted that MIAPaCa-2 cells had a low glycolytic reserve which is indicative of metabolic reliance on glycolysis.

Finally, the simultaneous analysis of mitochondrial and glycolytic-linked ATP production rates was performed. The results revealed that over 70% of MIAPaCa-2 ATP production rate was glycolytically-linked and this pattern did not change under Ca$^{2+}$ stress condition (Figure 3.7I). This suggests that MIAPaCa-2 cells are heavily dependent on aerobic glycolysis regardless of PMCA4 expression. Under Ca$^{2+}$ stress, even though ATP production rate did not change in siNT control, PMCA4 knockdown cells showed significantly increased glycolysis-link ATP production rate, suggesting an increase in cellular ATP demand (Figure 3.7J).
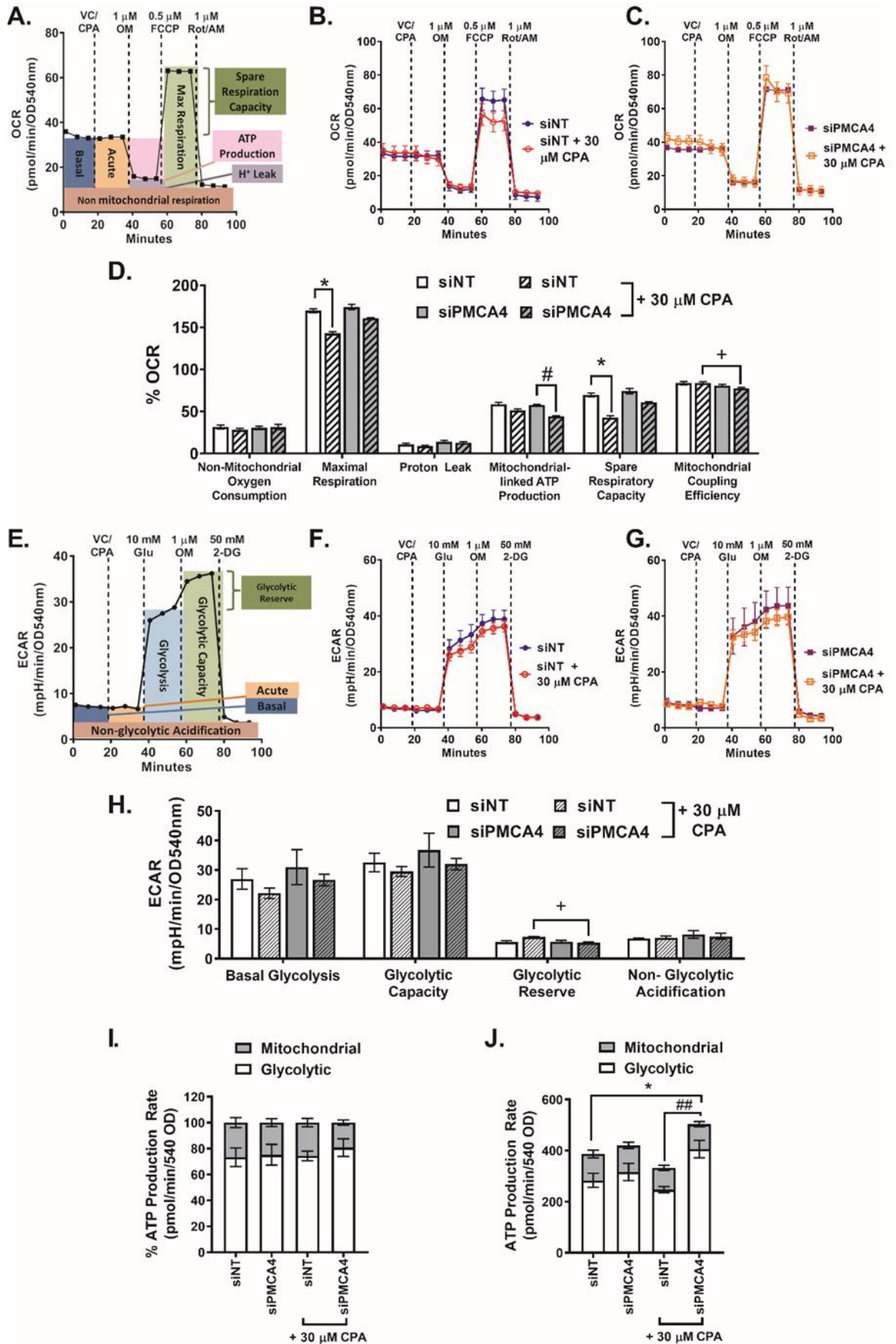
**Figure 3.7 – PMCA4 knockdown has no effect on basal metabolic phenotype.** MIAPaCa-2 cells were incubated with either 25 nM siNT control or siPMCA4 for 48 hours. (Continued next page)

**Figure 3.7 Continued – PMCA4 knockdown has no effect on basal metabolic phenotype. A,** Agilent Seahorse XF Mito stress test parameter profile. **B,** Representative Mito Stress test OCR graphs comparing non-treated and 30 µM CPA pre-treated siNT control and **C,** siPMCA4.**D,** Mito stress test data were normalized to protein content then normalized as % of OCR baseline. Statistical significance is determined by Kruskal Wallis; Post hoc multiple comparisons – Two-stage linear step-up procedure of Benjamini, Krieger and Yekutieli. **E,** Agilent Seahorse XF glycolysis stress test parameter profile. **F,** Representative Glyco Stress test ECAR traces are shown for control and **G,** CPA treated siRNA treated cells. **H,** Glyco stress test data were normalized to protein content (SRB; 540 OD). Statistical significance is determined One-way ANOVA with post-hoc Bonferroni. Agilent Seahorse ATP production rate was normalized to quantified protein content (540 OD). Data are shown as **I,** % ATP production rate and **J,** total ATP production rate. * represents a statistically significant difference between siNT and siNT + CPA, where $P<0.05$. (N≥3). # represents a statistically significant difference between siPMCA4 and siPMCA4 + CPA, where $P<0.05$. (N≥3). + and ++ represents statistically significant difference between siNT + CPA and siPMCA4 + CPA, where $P<0.05$ and $P<0.005$, respectively (N=3, 4 replicates per treatment condition).

Overall, we found that PMCA4 expression did not alter the basal metabolic phenotype of MIAPaCa-2 cells. Under $Ca^{2+}$ stress, PMCA4 positive cells showed decreased mitochondrial respiration capacity and increased the shift in glycolytic reserve while demonstrating unaltered ATP production rate. In contrast, all CPA effects observed were abolished when PMCA4 was knocked down and enhanced glycolytic-linked ATP production rate was observed.

## 3.5  Discussion

The current study has provided insights into the functional importance of PMCA4 on multiple cancer hallmarks in PDAC. Through data mining of available databases, we found that overexpression of ATP2B4 and under-expression of ATP2B1-3 are likely characteristics of PDAC tumours [24] correlated to poor PDAC patient survival prognosis [26]. ATP2B4 mRNA, in particular, has been reported to be overexpressed by 5-fold in PDAC compared to the healthy tissue margin [22]. Therefore, we consider ATP2B4 to be the single most important PMCA encoding gene linked with PDAC oncogenicity. We then identified MIAPaCa-2 as a representative cellular model of PDAC based on the almost exclusive expression of PMCA4 at both protein and mRNA level.

As our previous study demonstrated that PMCA is the main $Ca^{2+}$ efflux mechanism in PANC-1 and MIAPaCa-2 PDAC cells [10], the present study reveals that PMCA4 expression is essential for $Ca^{2+}$ efflux in MIAPaCa-2 cells and loss of PMCA4 expression significantly impairs $Ca^{2+}$ clearance, subsequently elevating resting $[Ca^{2+}]_i$. Similar observations were made where PMCA4 knockdown resulted in apparent inhibition of $[Ca^{2+}]_i$ clearance and elevated resting $[Ca^{2+}]i$ in PMCA4 knockdown mice sperm [33] and Jurkat cells [34]. The inhibition of critical $Ca^{2+}$ clearance mechanisms subsequently leads to impaired $Ca^{2+}$ signalling. PMCA4 mediated $Ca^{2+}$ signalling, in particular, has been reported to regulate cancer hallmarks including migration [15], cell cycle [27] and cell death [13].

As more than 40% of PDAC patients are diagnosed with metastasis [35,36], migration is an extremely important cancer hallmark for PDAC. Cell migration is a process regulated by the spatiotemporal distribution of $Ca^{2+}$ within the cell and transient $Ca^{2+}$ pulses which modulate the assembly and disassembly of the cytoskeleton and focal adhesion complexes [37,38]. With regards to resting cytosolic $[Ca^{2+}]_i$ (~100 nM), the migrating cell front maintains a lower $Ca^{2+}$ gradient (~30 nM) to facilitate $Ca^{2+}$ pulse signalling and focal adhesion assembly [37]. The current study finds that PMCA4 plays an important role in PDAC cell migration and this migration is inhibited in $Ca^{2+}$ clearance-impaired PMCA4 knockdown cells. Similarly, in human umbilical vein endothelial cells (HUVEC), low $Ca^{2+}$ is maintained by enrichment of PMCA4 at the migrating front [15] and knockdown of PMCA4 reduces cell migration in rabbit corneal epithelium cells [39]. This suggests that without efficient $Ca^{2+}$ clearance at the migration front, cell motility is compromised.

Cell proliferation is another cancer hallmark known to be modulated by $Ca^{2+}$ signalling. PMCA4, particularly the PMCA4b splice variant, has been associated with cell cycle progression and proliferation [13,21]. Furthermore, $Ca^{2+}$ efflux activity of PMCA4 is shown to be important for G1-phase progression and cell proliferation in mice-derived vascular smooth muscle cells [27]. We found that knocking down PMCA4 resulted in knockdown of PMCA4b variant but did not affect MIAPaCa-2 proliferation rate. Similar to our data, PMCA4 knockdown in MDA-MB-231 breast cells had no effect on cell cycle, proliferation and viability [13,40]. Moreover, while total PMCA1 knockout led to embryonic lethality, PMCA4 knockout selectively induced infertility in male mice [33]. This suggests that, albeit ubiquitously expressed, PMCA4 may potentially be used to selectively target PMCA4-overexpressing PDAC cells while sparing normal cells which express other PMCA isoforms.

Apoptosis resistance is a key cancer hallmark responsible for insensitivity to PDAC therapeutic treatment [41]. Elevated $[Ca^{2+}]_i$ induces apoptotic cell death by $Ca^{2+}$ overload, the subsequent release of cytochrome C from the mitochondria and activation of pro-apoptotic caspases. Overexpression of PMCAs in cancer prevents $[Ca^{2+}]_i$ overload under stress stimuli and subsequently leads to apoptotic resistance. [42] In MDA-MB-231 breast cancer cells, PMCA4 and PMCA1 distinctly mediate resistance to apoptotic and necrotic cell death, respectively [13]. Consistent with this observation, the current study shows that PMCA4 knockdown sensitized MIAPaCa-2 cells to apoptotic inducers, particularly CPA-mediated $Ca^{2+}$ overload. This suggests that PMCA4 is required for $Ca^{2+}$ overload-associated apoptotic resistance. Further study to examine whether PMCA4 knockdown would lead to sensitization against first-line chemotherapeutic drugs (e.g. gemcitabine, paclitaxel, cis-platin) would provide better insights into the clinical relevance of targeting PMCA4 activity in PDAC.

Moreover, both mitochondrial and glycolytic metabolism are known to be modulated by $Ca^{2+}$ [31,43,44]. The activity of key rate-limiting glycolytic enzyme 6-phosphofructo-1-kinase (PFK) is modulated by $Ca^{2+}$-dependent calmodulin binding [45]. Conversely, $Ca^{2+}$ is reported to promote the activity of the tricarboxylic acid cycle (TCA) dehydrogenases required for mitochondrial respiration [46]. Vice versa, PMCA may play a role in the metabolic shift towards glycolysis. In red blood cells, multiple glycolytic enzymes are localised to the plasma membrane, providing a privilege ATP supply to the PMCA [6,18]. Therefore, we hypothesized that PMCA4 may be functionally involved in PDAC metabolism. However, we found that PMCA4 expression had no effect on both basal mitochondrial and glycolytic metabolism.

Although PMCA4 knockdown did not alter mitochondrial respiration and ATP production rate, we observed a significant increase in resting cytosolic $Ca^{2+}$ and mitochondrial membrane potential (ΔΨm). Similar to our observations, a study in PC12 neuronal cells showed that PMCA2 and PMCA3 knockdown led to increased resting TMRE signal [47]. We suspect that PMCA4 knockdown cells adapted to elevated resting $[Ca^{2+}]_i$ by maintaining a higher ΔΨm to avoid mitochondrial membrane depolarization which subsequently triggers apoptotic cells death [5].

Under $Ca^{2+}$ stress, the reduced mitochondrial respiration in PMCA4 expressing MIAPaCa-2 cells may be related to SERCA inhibitor-mediated mitochondrial depolarization [48]. However, the mechanism of this impaired mitochondrial function remains unclear. In contrast, PMCA4 knockdown cells showed enhanced glycolytic-linked ATP production rate which suggests escalating demand for ATP. As PMCA4 knockdown cells maintained a higher resting ΔΨm, this increased glycolytic-linked ATP production rate during $Ca^{2+}$ stress may be associated to paradoxical hydrolysis of ATP by the ATP synthase to maintain ΔΨm [49], or apoptotic associate ATP demand [50]. However, the potential observations of ATP synthase functioning in reverse mode may be minimized due to the use of oligomycin (ATP synthase inhibitor) in Seahorse assays.

It should be noted, however, that PMCA4 is reported to exhibit contradictory roles in different cell types. For instance, although we observed that PMCA4 knockdown in PDAC cells led to inhibited cell migration, Kurusamy, S. *et al* (2017) and Baggott, R.R. *et al* (2014) had reported that inhibition or knockdown of PMCA4 in HUVEC cells led to enhanced cell migration by promoting calcineurin/NFAT

signalling [52-53]. Moreover, decreased PMCA4 expression has been correlated to enhance proliferation in colon cancer [21] while the expression of PMCA4 is reported to enhance apoptosis resistance in breast cancer cells [13]. These different responses could be due to the different $Ca^{2+}$ signalling machinery or remodelling present in different cellular models.

Taken together, PMCA4 has a distinct role in $Ca^{2+}$ clearance, cell migration and apoptotic resistance in PDAC. PMCA4 knockdown did not alter cell viability in PDAC cells. However, loss of PMCA4 expression sensitizes PDAC cells to $Ca^{2+}$ overload-associated apoptotic cell death. As PDAC is notoriously insensitive to current clinical therapies, acquiring the ability to selectively sensitize PMCA4-overexpressing PDAC cells to apoptotic inducing chemotherapy is crucial. Therefore, targeting PMCA4 may potentially be beneficial as a therapeutic adjuvant which selectively sensitizes PDAC cells to currently available clinical therapy while sparing healthy tissues.

## 3.6  Acknowledgements

## 3.7 References

1.    Office for National Statistics. Cancer Survival in England: adults diagnosed in 2009 to 2013, followed up to 2014. 2015;1–14.

2.    Le Large TYS, Bijlsma MF, Kazemier G, van Laarhoven HWM, Giovannetti E, Jimenez CR. Key biological processes driving metastatic spread of pancreatic cancer as identified by multi-omics studies. Semin Cancer Biol. 2017;44(January):153–69.

3.    Quaresma M, Coleman MP, Rachet B. 40-year trends in an index of survival for all cancers combined and survival adjusted for age and sex for each cancer in England and Wales, 1971–2011: a population-based study. Lancet. 2015 Mar;385(9974):1206–18.

4.    Monteith GR, Davis FM, Roberts-Thomson SJ. Calcium channels and pumps in cancer: Changes and consequences. J Biol Chem. 2012;287(38):31666–73.

5.    Gottlieb E, Armour SM, Harris MH, Thompson CB. Mitochondrial membrane potential regulates matrix configuration and cytochrome c release during apoptosis. Cell Death Differ. 2003;10(6):709–17.

6.    Bruce JIE. Metabolic regulation of the PMCA: Role in cell death and survival. Cell Calcium. 2018;69:28–36.

7.    Criddle DN, Gerasimenko J V., Baumgartner HK, Jaffar M, Voronina S, Sutton R, et al. Calcium signalling and pancreatic cell death: Apoptosis or necrosis? Cell Death Differ. 2007;14(7):1285–94.

8.    Brini M, Carafoli E. The plasma membrane Ca$^{2+}$ ATPase and the plasma membrane sodium calcium exchanger cooperate in the regulation of cell calcium. Cold Spring Harb Perspect Biol. 2011 Feb 1;3(2).

9.    James AD, Patel W, Butt Z, Adiamah M, Dakhel R, Latif A, et al. The Plasma Membrane Calcium Pump in Pancreatic Cancer Cells Exhibiting the Warburg Effect Relies on Glycolytic ATP. J Biol Chem. 2015 Oct 9;290(41):24760–71.

10.   James AD, Chan A, Erice O, Siriwardena AK, Bruce JIE. Glycolytic ATP fuels the plasma membrane calcium pump critical for pancreatic cancer cell survival. J Biol Chem. 2013 Dec 13;288(50):36007–19.

11.   Lopreiato R, Giacomello M, Carafoli E. The plasma membrane calcium pump: New ways to look at an old enzyme. J Biol Chem. 2014;289(15):10261–8.

12.   Zhao XS, Shin DM, Liu LH, Shull GE, Muallem S. Plasticity and adaptation of Ca$^{2+}$ signaling and Ca$^{2+}$-dependent exocytosis in SERCA2$^{+/-}$ mice. EMBO J. 2001;20(11):2680–9.

13.   Curry MC, Luk NA, Kenny PA, Roberts-Thomson SJ, Monteith GR. Distinct regulation of cytoplasmic calcium signals and cell death pathways by different plasma membrane calcium ATPase isoforms in MDA-MB-231 breast cancer cells. J Biol Chem. 2012 Aug 17;287(34):28598–608.

14.   Ono K, Wang X, Han J. Resistance to tumor necrosis factor-induced cell death mediated by PMCA4 deficiency. Mol Cell Biol. 2001 Dec;21(24):8276–88.

15.   Tsai FC, Seki A, Yang HW, Hayer A, Carrasco S, Malmersjö S, et al. A polarized Ca$^{2+}$, diacylglycerol and STIM1 signalling system regulates directed cell migration. Nat Cell Biol. 2014;16(2):133–44.

16.   Hanahan D, Weinberg RA. Hallmarks of cancer: the next generation. Cell. 2011 Mar 4;144(5):646–74.

17.   Guillaumond F, Leca J, Olivares O, Lavaut M-N, Vidal N, Berthezene P, et al. Strengthened glycolysis under hypoxia supports tumor symbiosis and hexosamine biosynthesis in pancreatic adenocarcinoma. Proc Natl Acad Sci. 2013;110(10):3919–24.

18.   Puchulu-Campanella E, Chu H, Anstee DJ, Galan JA, Tao WA, Low PS. Identification of the components of a glycolytic enzyme metabolon on the human red blood cell membrane. J Biol Chem. 2013 Jan 11;288(2):848–58.

19. Kemp RG, Gunasekera D. Evolution of the allosteric ligand sites of mammalian phosphofructo-1-kinase. Biochemistry. 2002 Jul 30;41(30):9426–30.

20. Jurica MS, Mesecar A, Heath PJ, Shi W, Nowak T, Stoddard BL. The allosteric regulation of pyruvate kinase by fructose-1,6-bisphosphate. Structure. 1998;6(2):195–210.

21. Aung CS, Ye W, Plowman G, Peters AA, Monteith GR, Roberts-Thomson SJ. Plasma membrane calcium ATPase 4 and the remodeling of calcium homeostasis in human colon cancer cells. Carcinogenesis. 2009 Nov 1;30(11):1962–9.

22. Nakamura T, Furukawa Y, Nakagawa H, Tsunoda T, Ohigashi H, Murata K, et al. Genome-wide cDNA microarray analysis of gene expression profiles in pancreatic cancers using populations of tumor cells and normal ductal epithelial cells selected for purity by laser microdissection. Oncogene. 2004 Mar 9;23(13):2385–400.

23. Oncomine [Internet]. [cited 2019 Jan 17]. Available from: www.oncomine.org

24. Badea L, Herlea V, Dima SO, Dumitrascu T, Popescu I. Combined gene expression analysis of whole-tissue and microdissected pancreatic ductal adenocarcinoma identifies genes specifically overexpressed in tumor epithelia. Hepatogastroenterology. 55(88):2016–27.

25. Uhlen M. Expression of ATP2B4 in pancreatic cancer - The Human Protein Atlas [Internet]. [cited 2019 Jan 17]. Available from: https://www.proteinatlas.org/ENSG00000058668-ATP2B4/pathology/tissue/pancreatic+cancer

26. Uhlen M, Zhang C, Lee S, Sjöstedt E, Fagerberg L, Bidkhori G, et al. A pathology atlas of the human cancer transcriptome. Science (80- ). 2017 Aug 18;357(6352):eaan2507.

27. Afroze T, Yang G, Khoshbin A, Tanwir M, Tabish T, Momen A, et al. Calcium efflux activity of plasma membrane $Ca^{2+}$ ATPase-4 (PMCA4) mediates cell cycle progression in vascular smooth muscle cells. J Biol Chem. 2014 Mar 7;289(10):7221–31.

28. Fu P, Thompson JA, Bach LA. Promotion of cancer cell migration: An insulin-like growth factor (IGF)-independent action of IGF-binding protein-6. J Biol Chem. 2007;282(31):22298–306.

29. Campbell L, Emmerson E, Davies F, Gilliver SC, Krust A, Chambon P, et al. Estrogen promotes cutaneous wound healing via estrogen receptor β independent of its antiinflammatory activities. J Exp Med. 2010;207(9):1825–33.

30. Aung CS, Kruger WA, Poronnik P, Roberts-Thomson SJ, Monteith GR. Plasma membrane $Ca^{2+}$-ATPase expression during colon cancer cell line differentiation. 2007;

31. Marinho-Carvalho MM, Costa-Mattos PV, Spitz GA, Zancan P, Sola-Penna M. Calmodulin upregulates skeletal muscle 6-phosphofructo-1-kinase reversing the inhibitory effects of allosteric modulators. Biochim Biophys Acta - Proteins Proteomics. 2009 Aug;1794(8):1175–80.

32. Marchi S, Patergnani S, Missiroli S, Morciano G, Rimessi A, Wieckowski MR, et al. Mitochondrial and endoplasmic reticulum calcium homeostasis and cell death. Cell Calcium. 2018;69:62–72.

33. Okunade GW, Miller ML, Pyne GJ, Sutliff RL, O'Connor KT, Neumann JC, et al. Targeted Ablation of Plasma Membrane $Ca^{2+}$ -ATPase (PMCA) 1 and 4 Indicates a Major Housekeeping Function for PMCA1 and a Critical Role in Hyperactivated Sperm Motility and Male Fertility for PMCA4. J Biol Chem. 2004 Aug 6;279(32):33742–50.

34. Ritchie MF, Samakai E, Soboloff J. STIM1 is required for attenuation of PMCA-mediated $Ca^{2+}$ clearance during T-cell activation. EMBO J. 2012 Mar 7;31(5):1123–33.

35. Frigeri M, De Dosso S, Castillo-Fernandez O, Feuerlein K, Neuenschwander H, Saletti P. Chemotherapy in patients with advanced pancreatic cancer: too close to death? Support Care Cancer. 2013 Jan 1;21(1):157–63.

36. Mukherjee S, Hudson E, Reza S, Thomas M, Crosby T, Maughan T. Pancreatic Cancer within a UK Cancer Network with Special Emphasis on Locally Advanced Non-metastatic Pancreatic Cancer. Clin Oncol. 2008 Sep;20(7):535–40.

37. Tsai F-C, Kuo G-H, Chang S-W, Tsai P-J. $Ca^{2+}$ signaling in cytoskeletal reorganization, cell migration, and cancer metastasis. Biomed Res Int. 2015 Apr 22;2015:409245.

38. Wei C, Wang X, Chen M, Ouyang K, Song L-S, Cheng H. Calcium flickers steer cell migration. Nature. 2009 Feb 12;457(7231):901–5.

39. Talarico EF. Plasma membrane calcium-ATPase isoform four distribution changes during corneal epithelial wound healing. Mol Vis. 2010;16(April):2259–72.

40. Peters AA, Milevskiy MJG, Lee WC, Curry MC, Smart CE, Saunus JM, et al. The calcium pump plasma membrane $Ca^{2+}$-ATPase 2 (PMCA2) regulates breast cancer cell proliferation and sensitivity to doxorubicin. Sci Rep. 2016 Jul 5;6(1):25505.

41. Modi S, Kir D, Banerjee S, Saluja A. Control of Apoptosis in Treatment and Biology of Pancreatic Cancer.

42. Stewart TA, Yapa KTDS, Monteith GR. Altered calcium signaling in cancer cells ☆. BBA - Biomembr. 2015;1848:2502–11.

43. Giorgi C, Agnoletto C, Bononi A, Bonora M, de Marchi E, Marchi S, et al. Mitochondrial calcium homeostasis as potential target for mitochondrial medicine. Mitochondrion. 2012;12(1):77–85.

44. Graier WF, Malli R. Mitochondrial calcium: a crucial hub for cancer cell metabolism? Transl Cancer Res. 2017;6(S7):S1124–7.

45. Sola-Penna M, Da Silva D, Coelho WS, Marinho-Carvalho MM, Zancan P. Regulation of mammalian muscle type 6-phosphofructo-1-kinase and its implication for the control of the metabolism. IUBMB Life. 2010 Nov;62(11):791–6.

46. Sola-Penna M, Da Silva D, Coelho WS, Marinho-Carvalho MM, Zancan P. Regulation of mammalian muscle type 6-phosphofructo-1-kinase and its implication for the control of the metabolism. IUBMB Life. 2010 Nov;62(11):791–6.

47. Reddy S, Zhao M, Hu D-Q, Fajardo G, Katznelson E, Punn R, et al. Physiologic and molecular characterization of a murine model of right ventricular volume overload. Am J Physiol Heart Circ Physiol. 2013 May 15;304(10):H1314-27.

48. Eaddy AC, Schnellmann RG. Visualization and quantification of endoplasmic reticulum $Ca^{2+}$ in renal cells using confocal microscopy and Fluo5F. Biochem Biophys Res Commun. 2011 Jan 7;404(1):424–7.

49. Zorova LD, Popkov VA, Plotnikov EJ, Silachev DN, Pevzner IB, Jankauskas SS, et al. Functional Significance of the Mitochondrial Membrane Potential. Biochem (Moscow), Suppl Ser A Membr Cell Biol. 2018;12(1):20–6.

50. Zamaraeva M V, Sabirov RZ, Maeno E, Ando-Akatsuka Y, Bessonova S V, Okada Y. Cells die with increased cytosolic ATP during apoptosis: a bioluminescence study with intracellular luciferase. Cell Death Differ. 2005 Nov 20;12(11):1390–7.

51. Vichai V, Kirtikara K. Sulforhodamine B colorimetric assay for cytotoxicity screening. Nat Protoc. 2006 Aug 17;1(3):1112–6.

52. Kurusamy S, López-Maderuelo D, Little R, Cadagan D, Savage AM, Ihugba JC, et al. Selective inhibition of plasma membrane calcium ATPase 4 improves angiogenesis and vascular reperfusion. J Mol Cell Cardiol. 2017;109:38–47.

53. Baggott RR, Alfranca A, López-Maderuelo D, Mohamed TMA, Escolano A, Oller J, et al. Plasma membrane calcium ATPase isoform 4 inhibits vascular endothelial growth factor-mediated angiogenesis through interaction with calcineurin. Arterioscler Thromb Vasc Biol. 2014;

# 3.8 Supplementary Data
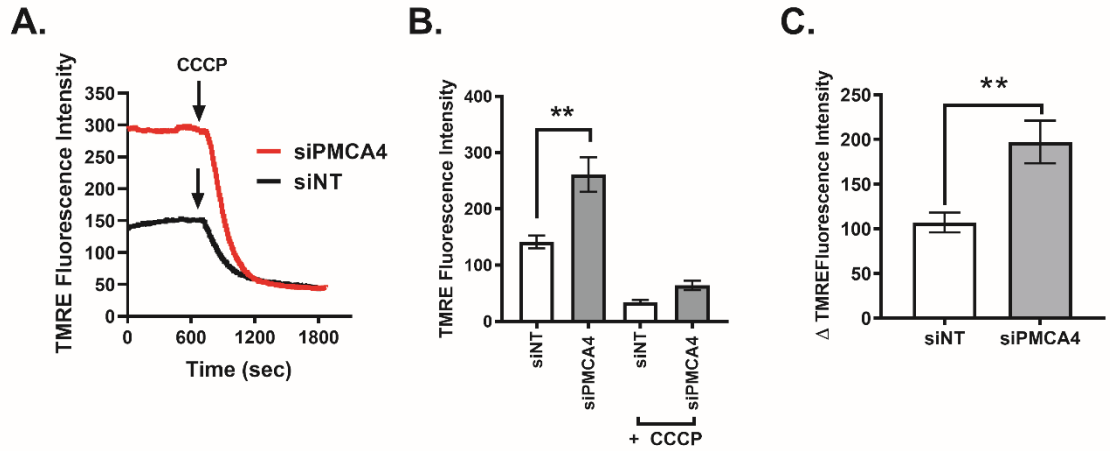


**Supplementary Figure 3.1 – PMCA4 knockdown increased basal mitochondrial membrane potential.** MIAPaCa-2 cells seeded with either 25 nM siNT control or siPMCA4 for 48 hours. **A,** Representative TMRE traces are shown with black arrows indicating the addition of CCCP. **B,** Raw TMRE fluorescence intensity of the basal and post-CCCP addition **C,** Mitochondrial membrane potential is shown as the change in TMRE fluorescence intensity. ** represents a statistically significant difference between siNT and siPMCA4, where $P<0.005$. (N=4, data collected from at least 40 individual cells).

# Chapter 4 –Plasma Membrane Calcium ATPase 4 (PMCA4) functional activity is dependent on Cav-1 expression in MIAPaCa-2 pancreatic cancer cell line

**Pishyaporn Sritangos[1], Andrew D. James[2], Daniel A. Richardson[1], Eduardo Pena Alarcon[1], Ahlam Sultan[1], Jason I.E. Bruce[1]**

[1] Division of Cancer Sciences, School of Medical Sciences, Faculty of Biology, Medicine and Health, University of Manchester, Manchester, M13 9PT, UK

[2] Department of Biology, University of York, Heslington, York, YO10 5DD, UK

## 4.1 Abstract

Overexpression of caveolin-1 (Cav-1) and plasma membrane calcium pump isoform 4 (PMCA4) have been observed in tumours resected from pancreatic ductal adenocarcinoma (PDAC) patients and could be correlated to poor patient survival. PMCA4 activity, associated with migration and apoptotic resistance in PDAC, is dependent on its localization in Cav-1-expressing caveolae compartment. However, the relationship between Cav-1 and PMCA4 in PDAC is currently unclear. This study selectively examined the functional relationship between Cav-1 expression and PMCA4 activity in MIAPaCa-2 PDAC cells which predominantly expresses PMCA4. The localisation of Cav-1 and PMCA4 was assessed using sucrose gradient ultracentrifugation and immunofluorescence labelling. Caveolae disruption was induced by either cholesterol depletion or siRNA targeting Cav-1. PMCA4-mediated $Ca^{2+}$ efflux, ATP-depletion, cell proliferation and metabolic parameters were examined using PMCA activity assay, $Ca^{2+}$ overload experiments, ATP-luciferase assay, sulforhodamine B/cell count kit-8, and Agilent Seahorse XFe96 Analyzer, respectively. We found that PMCA4 and Cav-1 colocalised in similar membrane fractions but were not exclusively colocalised spatially within the cell. Cholesterol depletion-mediated caveolae disruption led to markedly inhibited $Ca^{2+}$ clearance and $Ca^{2+}$ overload which occurred independently of ATP-depletion and cell death. To a lesser extent than cholesterol depletion, Cav-1 knockdown cells showed inhibited $Ca^{2+}$ clearance and $Ca^{2+}$ overload under $Ca^{2+}$ stress. However, knocking down Cav-1 had no effect on cell proliferation, glycolytic and mitochondrial respiration parameters. In conclusion, although Cav-1 expression is required for optimal PMCA4 activity, Cav-1 has no significant role in cell proliferation and metabolism in MIAPaCa-2 PDAC cells. Further experiments will be required to decipher the mechanism of how Cav-1 modulates PMCA4 activity.

**Keywords:** Pancreatic cancer, pancreatic ductal adenocarcinoma, caveolin-1, plasma membrane calcium ATPase isoform 4

## 4.2 Introductions

Pancreatic cancer is the 6th leading cause of cancer-related death [1] despite being only the 11th most common cancer with a 5-year survival rate of 6-8% [2]. Remodelling of calcium ($Ca^{2+}$) signalling machinery has been correlated to multiple cancer hallmarks including proliferation, apoptotic resistance and metastasis [3–5]. In PDAC cells, the plasma membrane calcium ATPases (PMCAs) is reported to be the primary ATP-consuming $Ca^{2+}$ efflux pathway which is heavily dependent on glycolysis-derived ATP [6,7]. PMCA4, in particular, has been correlated with migration and apoptotic resistance in PDAC cells (discussed in Chapter 3) and also reported to be overexpressed in PDAC patient-derived tumours [8].

Similar to PMCA4, Cav-1 is reported to be upregulated in PDAC and correlates to poor PDAC patient survival [9]. Interestingly, PMCAs are known to reside within the Cav-1-enriched caveolae – a lipid-rich "signalling hub" compartment of the plasma membrane [10].

Caveolae are omega or flask-shaped invaginations of the surface plasma membrane [11]. Key roles of the caveolae include compartmentalizing signal transduction including $Ca^{2+}$ signalling [12,13]. Caveolins, comprising of caveolin-1, 2 and 3, are integral membrane proteins necessary for the formation of the caveolae [11]. Caveolin-1 (Cav-1) and caveolin-2 are co-expressed within the caveolae of various tissues. On the other hand, Caveolin-3 is selectively expressed in muscle cells. Cav-1, in particular, is a crucial scaffolding component of the caveolae. Cav-1 has been reported to regulate cholesterol homeostasis [14,15], bind multiple signal transduction proteins (e.g. eNOS, protein kinase C, insulin receptor) [16–18] and the rate-limiting glycolytic enzyme – phosphofructokinase [19,20].

Although several studies have shown that PMCA activity is dependent on its localization in the Cav-1-enriched caveolae [21,22], limited reports have examined the localization and functional relationship between PMCA4 and Cav-1 in PDAC models. Since Cav-1 interacts with both $Ca^{2+}$ signal transducer as well as key glycolytic enzymes, we hypothesize that Cav-1 enriched domains may be important for PMCA4 activity in PDAC. The present study examined PMCA4 and Cav-1 colocalisation in MIAPaCa-2 PDAC cell which predominantly expresses PMCA4. We then examined the effects of chemical disruption of the caveolae, using methyl-β-cyclodextrin (MβC) or siRNA knockdown of Cav-1, on PMCA-mediated $Ca^{2+}$ efflux, cell proliferation and metabolism. As PMCA4-mediated $Ca^{2+}$ efflux and signalling are suggested to play an important role in maintaining PDAC cancer hallmark, understanding the functional relationship between Cav-1 and PMCA4 may provide beneficial insights to selectively sensitize or therapeutically target PDAC.

## 4.3 Materials and Methods

**Cell culture** – MIAPaCa-2 cells (purchased from ATCC) were cultured in DMEM media (D6429, Sigma Aldrich) with added 10% fetal bovine serum and 1% penicillin/streptomycin (P0781, Sigma Aldrich). Cultured cells were maintained in a temperature-controlled incubator at 5% $CO_2$ (g), 37°C. Cultured cells were screened for mycoplasma contaminations using either DAPI staining or PCR.

**Data mining** – Data mining of publicly available databases, including www.oncomine.org (ThermoFisher Scientific) and www.proteinatlas.org, version 18.1, were used to obtain Badea Pancreas (2008) gene chip microarray data and TGCA-PAAD Kaplan Meier survival data, respectively. All data used in this study were obtained in January 2019.

**Sucrose gradient ultracentrifugation** – MIAPaCa-2 cells were harvested in 0.5 M Na2CO3, pH 11, and homogenized using Omni blade homogenizer then sonicated. All homogenate samples were volume adjusted and mixed with 2-(N-Morpholino) ethanesulfonic acid-buffered saline containing 80% sucrose. Samples were loaded into 5-35% discontinuous sucrose gradient and centrifuged at 131,440 rcf, for 16 h, at 4°C, using a TL100 centrifuge (Beckman). 13 fractions obtained from centrifugation were individually precipitated using 10% trichloroacetic acid for 30 minutes. Precipitated pellets were denatured in Laemmli buffer for 5 minutes, at 90°C, and then used for Western immunoblotting.

**Sulforhodamine B (SRB)** – Cells were seeded at 5000 cells/well into 5 sets Corning 96-well plates (Sigma Aldrich). Cells were then fixed with 10% trichloroacetic acid every 24 hours for 96 hours post-siRNA treatment. 0.057% SRB was used to stain fixed adherent cells. 10 mM Tris, pH 10.5 was added to resuspend the SRB dye retained within fixed cells according to Vichai, V. *et al.* (2006) [23]. Absorbance at 540 nm was measured using Synergy HT microplate reader (BioTEK). The relative protein content was used to calculate the cell proliferation/growth in comparison to the control cells at time 0 hr.

**Cell count Kit-8 (WST-8)** – Cells were seeded at 5000 cells/well into 5 sets 96-well plates. The reduction potential, indicative of cell viability regardless of cell adherence, was quantified using water-soluble tetrazolium salt (WST-8) reagent (Dojindo Molecular Technologies) according to the manufacturer's instruction. In viable cells, dehydrogenases reduced the pink tetrazolium dye to orange-coloured formazan. 10 μl of WST-8 reagent were added per well into 96 well plates at 0, 24, 48, 72 and 96 hours. After 2 hours of WST-8 incubation at 37 C, absorbance at 450 nm was measured using Synergy HT microplate reader (BioTEK). Measurements obtained were used to calculate the relative cell viability was in comparison to the untreated control cells at time 0.

**ATP-luciferase assay** – Cells were seeded at 5000 cells/well into 96 well white-wall flat-bottom plates (Sigma Aldrich) and were allowed to attach for 24 hours prior to treatment. After incubation with designated treatments, cells were lysed with 50 μl of ViaLight® Plus cell lysis reagent (Lonza) for 10 minutes, releasing intracellular ATP. 100 μl of 'ATP monitoring regent Plus', containing luciferin substrate and firefly-luciferase enzyme, was added to the lysed cells. Luminescence signal was measured at 595 nm, using Synergy HT (BioTEK), according to ViaLight® Plus kit manufacturer's instructions. Relative cellular ATP was calculated after normalization to the ATP level of untreated control cells.

**GO-ATeam ATP-FRET reporter assay –** MIAPaCa-2 cells stably expressing GO-ATeam, a Förste resonance energy transfer (FRET)-based fluorescent ATP probe, were seeded on glass coverslips and mounted onto perfusion chamber. *In situ* ATP was measured by the ATP bound:ATP free ratio (565/510 nm fluorescence ratio; R) and fluorescence signals were collected using OptoSplit Image Splitter fitted with JC1 565 nm dichroic (Cairn Research). Cells were perfused with HEPES-buffer physiological saline solution (HPSS) for at least 200 seconds then the immediate fluorescence ratio was used as the basal *in situ* ATP signal (R0). After static incubation under control or 10 mM MβC treatment conditions, complete ATP depletion (Rmin) was demonstrated using metabolic inhibitor cocktail containing 2 mM iodoacetate, 500 µM bromopyruvate, 10 µM oligomycin and 2 µM antimycin. Data were expressed as % ATP = (Rt/ΔRmax) x 100 (Rt = the average of ratio values over 50 seconds at 0, 5, 10 ,20 and 30 minutes after treatment; ΔRmax= the maximum decrease in GO-ATeam signal (R0-Rmin)). [7]

**siRNA knockdown of caveolin-1 expression** – Cav-1 protein expression was knocked down using 12.5-25 nM ON-TARGETplus SMARTpool siRNA targeting CAV1 mRNA (siCav-1; L003467-00-0010). Non-targeting siRNA (siNT; D-001810-10-20) was used as a control. All knockdown conditions were performed using 0.1% DharmaFect1 transfection reagent (T-2001-03, Dharmacon). siRNA knockdowns were performed according to manufacturer instructions. Only conditions that produced ≥70% expression knockdown in MIAPaCa-2 cells were used in the current study. RT-qPCR and Western immunoblot were used to confirm Cav-1 expression knockdown at mRNA and protein level, respectively.

**Western immunoblotting** – Cells were harvested in RIPA buffer (50 mM Tris Base, 40 mM sodium pyrophosphate, 100 mM sodium fluoride, 150 mM sodium chloride, 1% Triton-X, 0.5 M EDTA and EGTA and 0.1 mM sodium orthovanadate, pH 7.4) supplemented with cOmplete, EDTA-free protease inhibitor cocktail (Sigma-Aldrich) and lysates were denatured for 5 minutes at 95$^\circ$C. Protein lysates were separated by electrophoresis using NuPAGE 4-12% Bis-Tris gel (ThermoFisher Scientific). Western immunoblotting was performed using PMCA4 (1:1000; clone JA9, Thermofisher Scientific) and Cav-1 (1:2000; #3238, Cell signaling) primary antibodies. Secondary anti-rabbit (1:2000) and anti-mouse (1:2000-1:5000) antibodies were purchased from Cell Signalling Technology. Protein bands were detected using Clarity Western ECL substrate (Bio-Rad) then imaged and quantified using the ChemiDoc Imaging System (Fisher Scientific).

**Fura-2 live cell Ca$^{2+}$ imaging** – Cells seeded onto sterilized glass coverslips (VWR) were transferred into HEPES physiological saline solution (HPSS 10 mM HEPES, 0.56 mM MgCl$_2$, 4.7 mM KCl, 138 mM NaCl, 1.28 mM CaCl$_2$, 5.5 mM Glucose, pH 7.4) then incubated with 4 µM fura-2 (AM, acetoxymethyl; TEFLabs) Ca$^{2+}$ ratiometric dye for 40 minutes. Fura-2 loaded cells were mounted onto a gravity-fed perfusion chamber (Harvard Apparatus). The 340/510 and 380/510 nm excitation/emission signal was separated using 400 nm dichroic with 505LP filter (Nikon). Images were collected on a Nikon TE2000 inverted microscope fitted with x40 oil immersion objective/1.3 numerical aperture and captured using a CoolSNAP HQ interline progressive-scan charge-coupled device-based camera (Roper Scientific Photometrics) through MetaFluor software (Molecular Devices).

**PMCA activity assay (Ca$^{2+}$ clearance assay)** – Fura-2 loaded cells were perfused with Ca$^{2+}$-free HPPS (1 mM EGTA and 30 µM cyclopiazonic acid; CPA) for 20 minutes before switching to 20 mM Ca$^{2+}$ HPPS

until a new signal plateau was reached. $Ca^{2+}$ clearance rate (R1) was obtained when switching 20 mM $Ca^{2+}$ to $Ca^{2+}$-free HPPS as described in our previous works [6,7]. To perform paired control experiments, a second clearance phase (R2) was performed after 30 minutes of designated treatment. Relative $[Ca^{2+}]_i$ clearance of paired (R2/R1) and unpaired (R1) designed $Ca^{2+}$ clearance experiments were determined using the fastest linear clearance (% R2/R1) and a single exponential decay fit (τ), respectively.

**$Ca^{2+}$ overload assay** – Fura-2-loaded cells were perfused with HPPS for 200 seconds to establish 340/380 nm fluorescence ratio baseline (R0), indicative of resting intracellular $Ca^{2+}$. Cells were perfused with 30 µM CPA for 15 minutes to inhibit SERCA, induce SOCE, and subsequently leading to $Ca^{2+}$ overload. $Ca^{2+}$ stress recovery was determined by washing the cells with HPPS for a further 15 minutes. All $[Ca^{2+}]_i$ calibrations were calculated using Neher, E. (1995) published equation [24]. All $[Ca^{2+}]$ values calculated in this study were calculated from the following $Ca^{2+}$ calibration equation: $[Ca^{2+}]_i$ nM = 541.6 nM * ((Ratio – 0.47)/(2.101 - Ratio)). $[Ca^{2+}]_i$ was quantified by the area under the curve (AUC) and maximum change in $[Ca^{2+}]_i$ (MaxΔ$[Ca^{2+}]_i$) during treatment and washing period as described in our previous works [6,7].

**RT-qPCR** – RNA samples were isolated using TRIzol Plus mRNA purification kit (Thermofisher Scientific) and samples were decontaminated with RQ-1 RNAse-free DNAase (Promega) according to manufacturers' instructions. Reverse transcription was performed using Taqman reverse transcription reagent (Thermofisher Scientific). Pre-designed KiCqStart®SYBR® Green primers targeting CAV1 and 18S rRNA (Sigma-Aldrich) and POWER SYBR green master mix were used for qPCR. qPCR experiments were performed on a StepOnePlus qPCR machine (Fisher Scientific). The relative quantification of CAV1 mRNA was done by S18 rRNA normalisation following by comparing the normalized CAV1 expression between siCav-1 and siNT control.

**Seahorse cell metabolism assays** – Cells were seeded at 5000 cells per well into 96-well Agilent Seahorse plates, containing either siNT or siCav-1 for 48 hours. Seahorse XFe96 sensor cartridges were hydrated overnight in ultrapure water (Thermofisher Scientific). Seahorse XF DMEM medium, pH 7.4 (#103575-100, Agilent Technologies) were used for both Mito stress test (supplemented with 1 mM pyruvate, 2 mM L-glutamine and 25 mM D-glucose) and glycolysis stress test (supplemented with 1mM L-glutamine). Pre-injections of either vehicle control (<0.1% dimethylsulfoxide; DMSO) or 30 µM CPA were prepared in addition to the Mito stress (1.5 µM oligomycin, 0.5 µM FCCP, and 0.5 µM rotenone/antimycin A) and glycolysis stress test (10 mM D-glucose, 1 µM oligomycin, and 50 mM 2-deoxyglucose) reagents which were prepared according to manufacturer's instructions. Seahorse data were collected using Agilent Seahorse XFe96 and analysed using Wave analysis software, version 2.3.0 (Agilent Technologies).

**Statistics** – Prism 7 software (GraphPad) was used for statistical data analysis. All processed data are presented as the mean of at least 3 independent ± standard error of means (SEM; error bars). Shapiro-Wilk normality test was performed prior to data analysis. Normally distributed parametric statistical comparisons were performed using Student's t-test or one-way analysis of variance (ANOVA) with Bonferroni post-test. Non-parametric statistical comparisons were performed using Kolmogorov-Smirnov test or Kruskal Wallis with multiple comparisons test was used for non-parametric statistical

comparisons. Two-way ANOVA with Dunnett's post-test was used for two-factor statistical comparisons. Statistical significance is defined as $p < 0.05$.

## 4.4  Results

### 4.4.1  Elevated co-expression of CAV1 and PMCA4 gene in PDAC tumours can be correlated to poor survival prognosis

Overexpression of PMCA4 encoding gene (ATP2B4) has been previously linked to poor PDAC patient survival (discussed in Chapter 3). PMCA4 is reported to reside within caveolin-1-enriched caveolae and may contribute to the assembly of PMCA4-containing signalling complexes. We, therefore, wanted to determine whether CAV1 gene expression in patient-derived PDAC tumours result in poor patient survival. This was achieved through data mining from publicly available databases including Oncomine [25,26] and the Human Protein Atlas [27–29].

Badea *et al.* (2008) gene chip microarray data were obtained from Oncomine. The results showed that CAV1 gene expression in PDAC tumour, versus resected healthy tissue from the tumour margin, was overexpressed by 1.67-fold (n=39, $p < 0.005$, Figure 4.1A) [26]. Patient survival data was sourced from the cancer genomic atlas - pancreatic adenocarcinoma cohort (TCGA-PAAD). PDAC patients were bifurcated into either low or high CAV1 expression based on the median-centred tumour expression. The Kaplan-Meier graph showed that patients expressing high tumour expression of CAV1 exhibited a significantly lower survival (hazard ratio= 1.61, n=88, $p < 0.021$, Figure 4.1B). This suggests that elevated CAV1 expression could be correlated to PDAC tumours and is associated with poor PDAC patient survival.

To further examine whether co-expression of CAV1 and ATP2B4 genes potentiates poor PDAC patient survival, the TCGA-PAAD patient cohort was divided into groups with either co-elevation or co-repression of CAV1 and ATP2B4 based on the median-centred gene expression. The Kaplan-Meier survival curves showed that co-elevation of PMCA4 and CAV1 leads to an enhanced risk of poor survival (hazard ratio = 1.93, n=52, $p < 0.015$, Figure 4.1C). Taken together, overexpression of ATP2B4 and CAV1 are relevant characteristics of PDAC tumours and enhances the risk of poor patient survival.
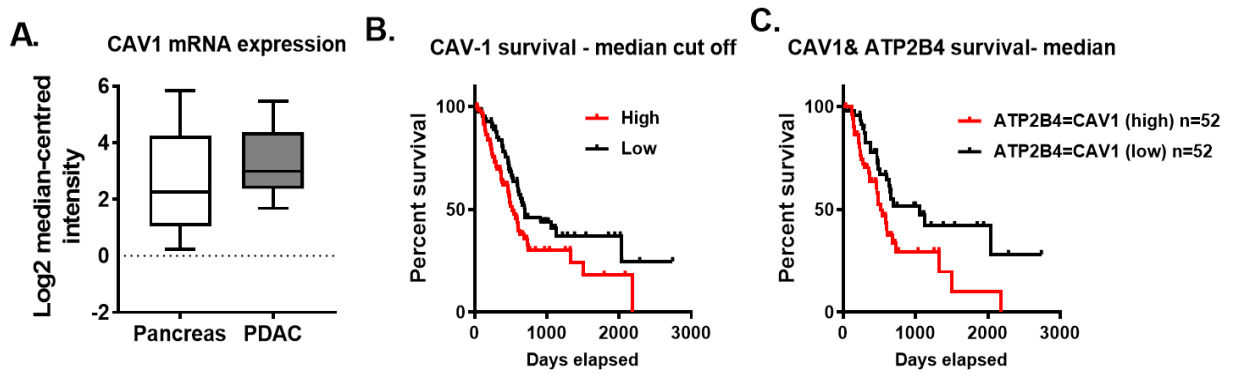
**Figure 4.1 – Elevated expression of CAV1 gene in PDAC is correlated to poor patient survival outcome.** (**A)** Comparison of CAV1 gene expression in healthy pancreatic tissue (n=39) and PDAC tumour (n=39) is shown as individual Log2 median-centre expression intensity of CAV1 gene expression. Data were obtained from Badea Pancreas (2008) through the Oncomine database. **(B)** Kaplan Meier curve correlating CAV1 expression to PDAC patient survival. PDAC Patients (n=176, TCGA-PAAD) were divided based on either low (black, n=88) or high (red, n=88) CAV1 gene expression. (**C**) Kaplan Meier curve correlating co-expression of CAV1 and ATP2B4 gene to PDAC patient survival. TCGA-PAAD PDAC patients were divided based on co-repression (black, n=52) or co-elevation (red, n=52) of CAV1 and ATP2B4. The survival outcomes of each group were compared using the log-rank test. Data were obtained from The Human Protein Atlas database (January 2019, www.proteinatlas.org).

## 4.4.2 Methyl-β-cyclodextrin-mediated cholesterol depletion disrupts PMCA4 from residing in Cav-1-rich caveolae fraction in MIAPaCa-2 PDAC cells

Since co-elevation of ATP2B4 and CAV1 genes are clinically relevant characteristics of PDAC, we aimed to investigate whether Cav-1 is co-expressed in MIAPaCa-2 PDAC cells in which PMCA4 is the predominant PMCA isoform (data presented in Chapter 3). Previous findings suggest that PMCA4 activity is enhanced when colocalised with Cav-1 in the murine small intestine [21] and sperm [22]. PMCA4 is reported to colocalise with caveolins in lipid-rich domains of the cell surface plasma membrane known as caveolae [10,21]. Therefore, we used sucrose gradient ultracentrifugation assay to separate the membrane fractions by density to identify Cav-1 enriched caveolae [11,30]. Western immunoblot showed that PMCA4 resides in the low-density sucrose fractions. Furthermore, PMCA4 expression coincides with Cav-1-enrich fractions (Figure 4.2A) which suggests that PMCA4 potentially reside in low-density Cav1-rich compartments – likely the caveolae.

To understand the relationship between PMCA4 and Cav-1, chemical disruption of the caveolae with a cholesterol depleting agent (methyl-β-cyclodextrin; MβC) [31] was performed. MβC-mediated cholesterol depletion led to the free distribution of PMCA4 and Cav-1 across multiple random density fractions, suggesting successful disruption of the caveolae (Figure 4.2B). Therefore, MβC treatment was chosen for further functional assessment of PMCA4 and Cav-1.
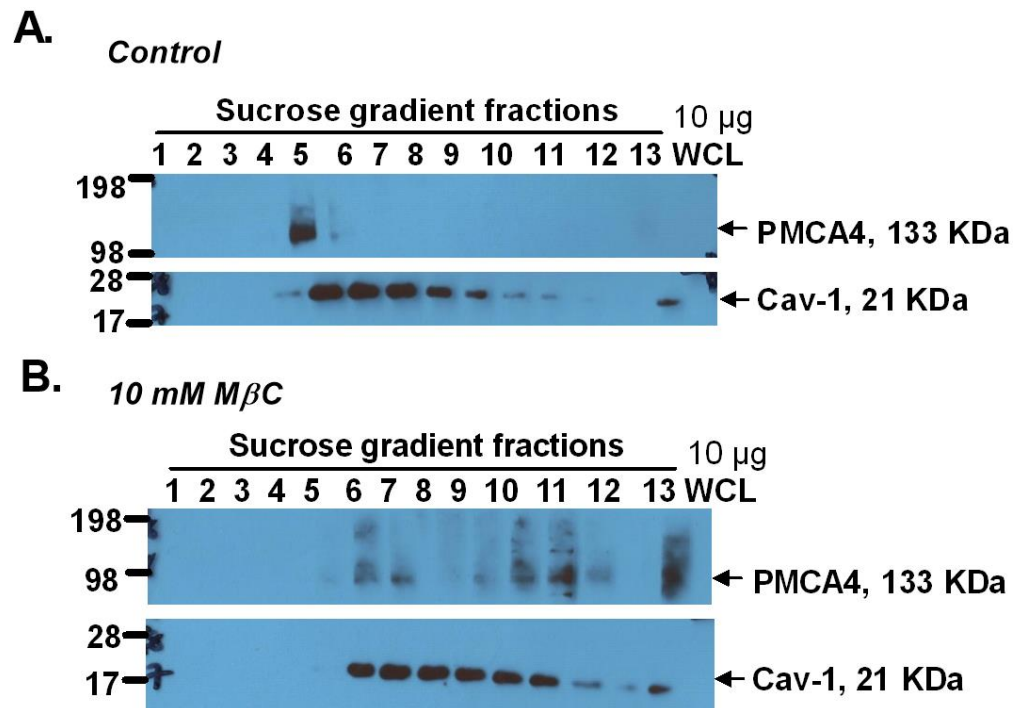


**Figure 4.2 – Chemical disruption of the caveolae and siRNA knockdown of Cav-1 (siCav-1).** Sucrose gradient ultracentrifugation was used to separate lysate fractions by density. Fractions 1-13 were collected, ranging from lowest density (low density; 1) to highest density (hydrophilic;13) fractions. **(A)** Representative Western immunoblot of PMCA4 localised in low-density caveolin-1-rich fraction. **(B)** Treatment with methyl-β-cyclodextrin (MβC) disrupted the colocalization between PMCA4 and caveolin-1 (Cav-1). (N=2)

### 4.4.3 Disruption of Cav1-rich caveolae impairs PMCA4-mediated Ca²⁺ clearance and causes Ca²⁺ overload in MIAPaCa-2 PDAC cell line

Our previous studies showed that PMCA, particularly PMCA4, is the primary $Ca^{2+}$ efflux mechanism in MIAPaCa-2 PDAC cells [6,7] (results are shown in Chapter 3). Furthermore, PMCA4 overexpression was correlated to poor PDAC patient survival [27–29] and multiple cancer hallmarks (discussed in Chapter 3). To investigate the functional importance of PMCA4 localization with Cav-1 enriched compartment, *in situ* $Ca^{2+}$ clearance (PMCA activity) and $Ca^{2+}$ overload experiments were performed in fura-2-loaded MIAPaCa-2 cells. Cells were perfused with $Ca^{2+}$ free HEPES-buffered physiological saline solution (HPSS) containing EGTA and cyclopiazonic acid (CPA), a sarco-endoplasmic reticulum $Ca^{2+}$-ATPase (SERCA) inhibitor. This facilitates depletion of intracellular $Ca^{2+}$ ($[Ca^{2+}]_i$) stores and activates store-operated $Ca^{2+}$ entry (SOCE) such that immediate perfusion with 20 mM $Ca^{2+}$ HPSS leads to rapid increase in $[Ca^{2+}]_i$ which reaches new steady state. Subsequent removal of external $Ca^{2+}$ then allows the assessment of $[Ca^{2+}]_i$ clearance that occurs almost exclusively due to PMCA [6,7]. After the first clearance phase, designated treatment of either 0.1% DMSO control, 10 mM MβC, or 1 μM carboxyeosin (pan PMCA inhibitor; CE) were added for 30 minutes. Repeating a second $Ca^{2+}$ influx-clearance phase in the presence of designated treatment then enables a "paired" comparison between the treated clearance rate (R2) and the untreated clearance rate (R1), giving the relative clearance (R2/R1 x 100%).

The results showed that MβC-induced cholesterol depletion decreased $[Ca^{2+}]_i$ clearance to 62.4±8.9% (p<0.005, n=6, Figure 4.3B) in comparison to the time-matched control (104±2.87%, n=7, p<0.005, Figure 4.3A). CE was used as a positive control to demonstrate maximal inhibition of the PMCA activity (21.4±6.43%, p<0.005, n=3, Figure 4.3C-D). These results suggest that disruption of the caveolae led to impairment of PMCA4 function but not complete inhibition of PMCA4 activity in MIAPaCa-2 PDAC cells.

Further $Ca^{2+}$ overload experiments were performed using fura-2 loaded MIAPaCa-2 cells treated with either 0.1% vehicle control or 10 mM MβC for 30 minutes under static conditions (Figure 3.4E-F). $Ca^{2+}$ responses were quantified by the area under the curve (AUC), mean maximum increase in $[Ca^{2+}]_i$ ($\Delta Max[Ca^{2+}]_i$), and the subsequent response to purinergic ATP (test of $Ca^{2+}$ response reversibility) were compared. The results demonstrated that MβC increased both AUC and maximum change in $[Ca^{2+}]_i$ without significantly affecting the % ATP response (Figure 4.3G-I). MβC treatment elevated the resting $[Ca^{2+}]_i$ (AUC = 206.5±81.43 μM.s, n=5, p< 0.0079) in comparison to the non-treated control (AUC = 55.16±4.15 μM.s, n=5, Figure 4.3G), indicative of $Ca^{2+}$ overload. MβC also increased the mean maximum $[Ca^{2+}]_i$ change ($\Delta Max[Ca^{2+}]_i$ = 408.1±210 nM, n=5, p< 0.0079) compared to time-matched control ($\Delta Max[Ca^{2+}]_i$ = 48.55±4.52 nM, n=5, Figure 4.3H). Although the numbers of cells responding to ATP were similar (Figure 4.2I), it should be noted that the MβC treated cells showed irreversible $Ca^{2+}$ response in comparison to the control (Figure 4.2E-F). This irreversible $Ca^{2+}$ response suggests that MβC treatment may lead to cell death.

Taken together, MβC-mediated cholesterol depletion leads to impaired PMCA4 $Ca^{2+}$ efflux and subsequent $Ca^{2+}$ overload, suggesting that PMCA4 activity may be modulated by its localization to Cav-1-rich low-density membrane compartment. However, it should be noted that MβC induces non-selective

cholesterol depletion which may disrupt the phospholipid environment required for the regulation of PMCA activity independent of its localisation within the caveolae.
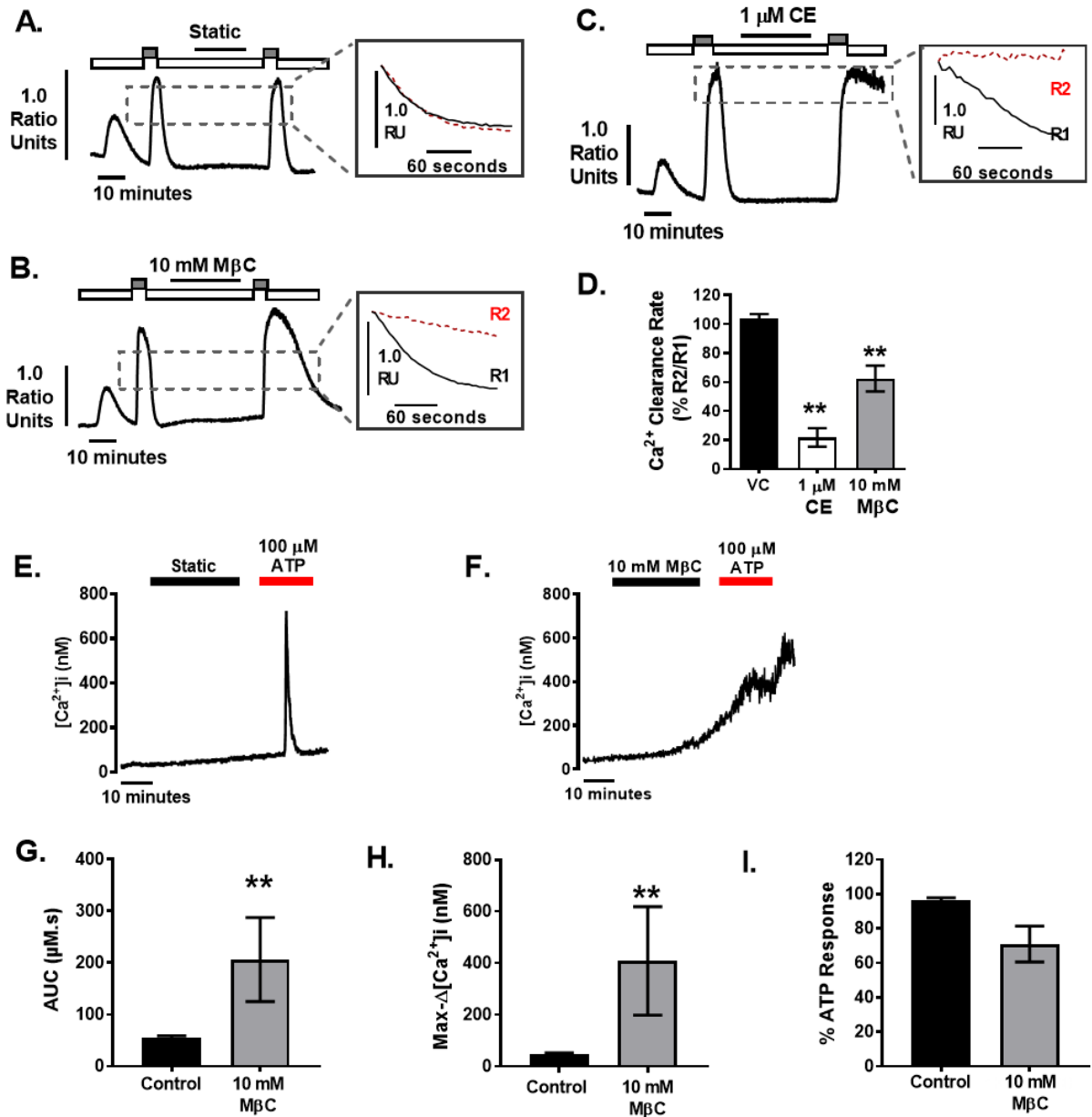


**Figure 4.3 – Disruption of caveolae leads to inhibition of Ca$^{2+}$ clearance.** Representative *in situ* Ca$^{2+}$ clearance traces of **(A)** control, **(B)** MβC, **(C)** Carboxyeosin (CE) are shown. Linear clearance phases are shown as an overlay in adjacent square boxes. PMCA-mediated [Ca$^{2+}$]$_i$ clearance is measured in fura-2 loaded MIAPaCa-2 cells perfused with Ca$^{2+}$-free HEPES containing 30 µM CPA and 1mM EGTA (white bar) to induce store-operated Ca$^{2+}$ influx upon perfusion with 20 mM Ca$^{2+}$ (grey bar). Subsequent Ca$^{2+}$ clearance was observed upon removal of external Ca$^{2+}$ (R1). Incubation of designated treatment was done prior to the second Ca$^{2+}$ influx-clearance phase (R2). All representative traces are presented as 340/380 fluorescence signal ratio units. **(D)** Relative Ca$^{2+}$ clearance rates are expressed as the mean of % Ca$^{2+}$ clearance (R2/R1). Representative Ca$^{2+}$ overload traces of **(E)** untreated control and **(F)** 10 mM MβC are shown. Black bar indicates treatment incubation under static conditions. Data were quantified as **(G)** area under the curve, **(H)** maximum change in [Ca$^{2+}$]$_i$ during this period (MaxΔ[Ca$^{2+}$]$_i$), and **(I)** % of cells responding to ATP. Data are presented as mean ± SEM of 3 independent experiments (data collected from at least 50 individual cells). Statistical comparisons were made between treatment group using Mann Whitney, non-parametric, Unpaired T-Test. ** represents statistically significant difference where p<0.01.

115

### 4.4.4 MβC-induced inhibition of PMCA activity is independent of global cellular ATP depletion

Our previous findings showed that glycolytic ATP depletion leads to inhibited PMCA-mediated $Ca^{2+}$ clearance, subsequent cytotoxic $Ca^{2+}$ overload and cell death. Moreover, overexpression of Cav-1 has been shown to enhance glycolytic enzyme (GEs) expression (phosphofructokinase and aldolase) at the plasma membrane [19] and enhanced glycolysis and ATP production in a panel of colon cancer cell lines [54]. From these studies, we hypothesized that Cav-1 may be important for GEs localization at the plasma membrane thereby providing privilege ATP supply to PMCA4. Hence, disrupting the caveolae may dissociate ATP-generating GEs near PMCA4, leading to local ATP depletion, thereby compromising PMCA activity and subsequently inducing cell death. Therefore, we further investigated the effects of MβC on ATP depletion using ATP-luciferase assay and further validated using SRB cell viability assay.

The results showed that MβC treatment had no effect on ATP depletion and cell viability over the 1 hour (Figure 4.4A-B). However, between 2-8 hours after treatment, MβC profoundly caused ATP depletion and loss of cell viability. This indicates that MβC induced cytotoxicity beyond 2 hours. The lack of effect on ATP depletion over the first hour was confirmed using MIAPaCa-2 cells transfected with FRET-based recombinant fluorescent ATP reporter (Go-ATeam) which provided real-time measurements of relative ATP within a single cell (Figure 4.4C-D). These data suggest that MβC has no effect on ATP that could account for the inhibition of $Ca^{2+}$ clearance and the subsequently observed $Ca^{2+}$ overload during the 1 hour experiment duration. However, progressive ATP-depletion and apoptosis were observed over the longer treatment duration of 2-8 hours.

In conclusion, these results suggest that MβC mediated $Ca^{2+}$ overload consequently resulted in decreased cell viability. However, the inhibition of PMCA activity was observed within 30 minutes of MβC exposure. Therefore, MβC-associated impairment of PMCA activity occurred independently of cellular ATP depletion. It should be noted that compartmental ATP depletion close to the caveolae could not be examined using either of these techniques.
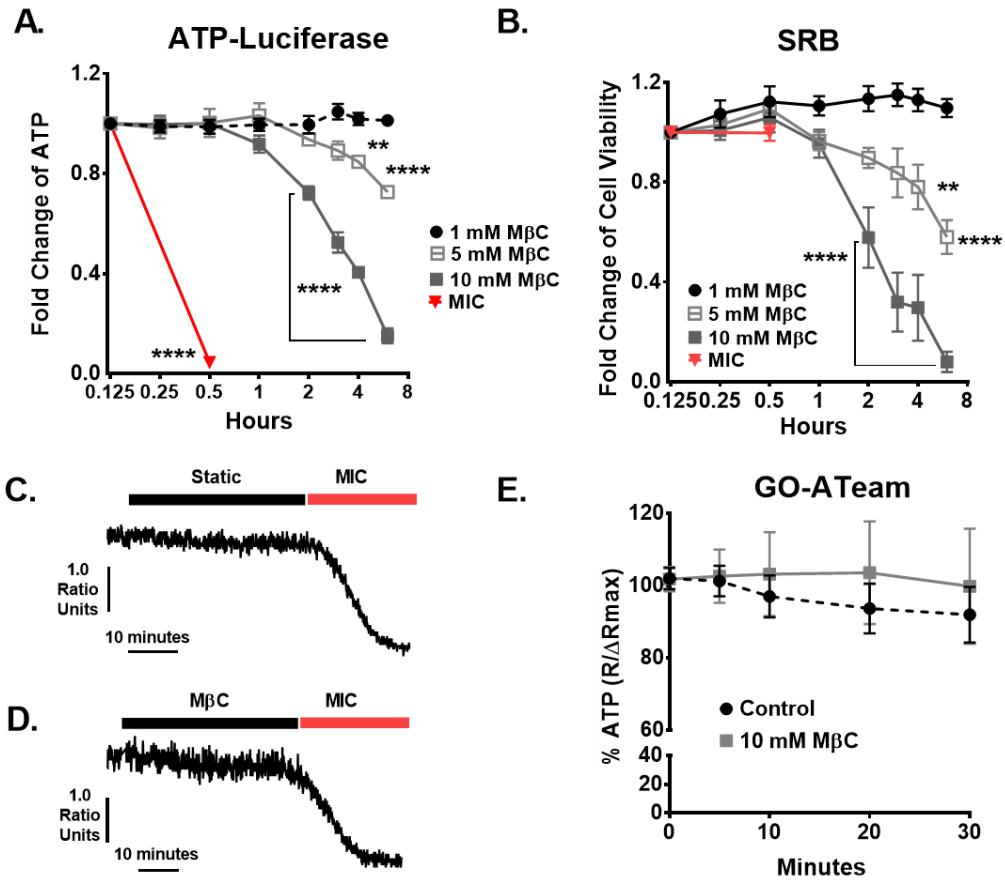
**Figure 4.4 – Disrupting the caveolae with methyl β-cyclodextrin induced ATP-depletion and cell death.** MIAPaCa-2 cells were treated with 1, 5, 10 mM MβC or metabolic inhibitor cocktail using (MIC). **A,** The effect of caveolae disruption on ATP-depletion was investigated using ATP-luciferase assay. **B,** SRB cell viability assay was performed in parallel to the ATP-luciferase assay. Data are expressed as fold change of untreated control. Real-time changes in cellular ATP were examined by live-fluorescence imaging of MIAPaCa-2 cells stably transfected with GO-ATeam FRET ATP-sensing construct. Representative *in situ* ATP traces of **C,** untreated and **D,** 10 mM MβC treated conditions are shown. Data are expressed as ATP bound:ATP free (565/510 nm) fluorescence ratio (R). **E,** Comparison of ATP changes between untreated control and MβC are expressed as % ATP. Basal ATP level (Rmax), obtained prior to MβC treatment, was normalized to the minimum R value post-MIC treatment (ΔRmax). All data are expressed as mean± SEM. (N=4, 4 replicates per treatment condition) Statistical comparisons between control and treatment groups were made using two-way ANOVA, with Bonferroni multiple comparison post-hoc test. ** and **** represents statistically significant difference where $p<0.01$ and $<0.001$, respectively.

### 4.4.5  Caveolin-1 knockdown does not alter cell viability and growth

Given that MβC induced non-specific cytotoxicity and loss of cell viability within a short period of 2 hours, an alternative method of disrupting the caveolae was considered to further functional studies which required longer experimental durations. As multiple studies have consistently shown that Cav-1 knockdown leads to disruption of caveolae [32,33], this study used a pool of 4 siRNA targeting CAV1 mRNA (siCav-1) to transiently knockdown the expression of Cav-1. A non-targeting pool of siRNA (siNT) was used as a control. Cav-1 knockdown was confirmed at protein and mRNA level, using western immunoblot and RT-qPCR, respectively (Figure 4.5A-C).

Western immunoblot showed that Cav-1 protein expression decreased in a time-dependent manner in comparison to the siNT control. Cav-1 expression was reduced by ≥75% between 48-96 hours post-siCav-1 treatment (Figure 4.5A-B, n=3, $p<0.05$). Similarly, CAV1 mRNA expression was knocked down by at least 70% between 48-72 hour (Figure 4.5C, n=3, $p<0.05$). As a previous study in mouse hepatoma cells reported that knocking down 76% of Cav-1 expression sufficiently inhibited colony formation and tumorigenesis [67], the following study used conditions that yielded at least 75% Cav-1 protein expression knockdown for subsequent functional experiments.

The effect of CAV-1 knockdown on cell viability was examined using both SRB and tetrazolium-formazan based cell count kit-8 (WST-8). Although SRB and WST-8 measurements were both used to assess similar outcomes of cell viability and proliferation, the principal of the methods differs slightly. To ensure that Cav-1 knockdown does not alter cellular attachment during further PMCA activity assays, SRB was used to assess adherent cells as the technical protocol requires multiple wash steps prior to protein staining. Conversely, WST-8 assay measured the reductive potential of live cells and took into account any live detached cells. The results showed no differences between the growth rate of siNT and siCav-1 treated cells assessed using both SRB and WST-8 (Figure 4.5D-E, n=4). These results suggest that Cav-1 knockdown had no effect on cell viability, growth rate and cell-surface adherence properties of MIAPaCa-2 PDAC cells, making Cav-1 knockdown cells suitable for further functional studies.
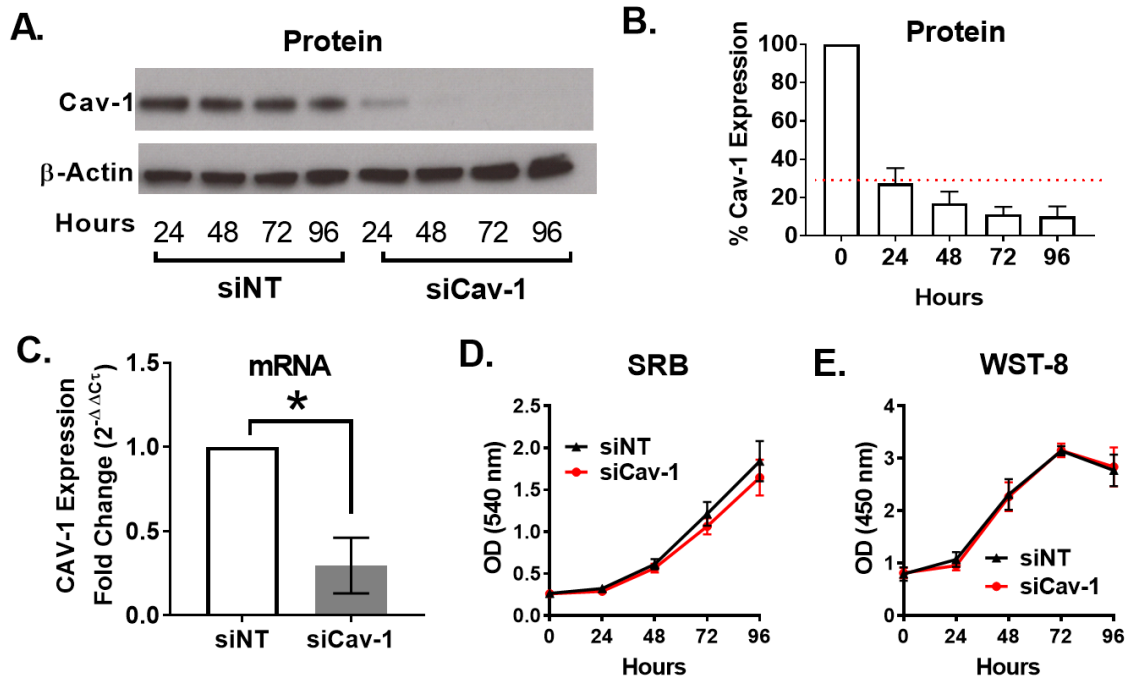
**Figure 4.5 – Caveolin-1 knockdown does not alter cell viability and growth. A,** Representative western blot comparing PMCA4 protein expression in MIAPaCa-2 cells after 24-96 hours of treatment with siNT control and siCav-1 (Cav-1 knockdown). **B,** Cav-1 protein expression of siCav-1 treated cells were quantified using band intensity normalized to corresponding time-matched β-Actin. **C,** The relative expression of CAV-1 mRNA was examined after 48 hours of siRNA treatment by RT-qPCR. The expressions of target mRNA were normalized to S18 rRNA and expressed as 2-(ΔΔCт). Statistical comparisons between siNT control and siPMCA4 treated cells were made using the Kolmogorov-Smirnov test (Unpaired, non-parametric cumulative distribution test). **D,** SRB proliferation assays were performed to monitor cell proliferation and adhesion while **E,** cell count kit-8 (WST-8) was performed to monitor cell viability independent of cell adhesion. Data are shown as mean ± SEM. (N=4). Statistical comparisons between siNT control and siPMCA4 treated cells were made using two-way ANOVA, Dunnett's multiple comparison post-hoc test. * represents statistically significant difference where P<0.05.

### 4.4.6 Caveolin-1 knockdown inhibits $Ca^{2+}$ clearance and $Ca^{2+}$ overload

To examine the importance of Cav-1 expression on PMCA4 functional activity, PMCA activity and CPA-induced $Ca^{2+}$ overload experiments were performed on siNT versus siCav-1 treated cells (Figure 4.6A-B). $[Ca^{2+}]_i$ clearance rate was assessed using an unpaired experimental design in which a single clearance rate was fitted to a single exponential decay to yield the time constant ($\tau$). The results showed that $Ca^{2+}$ clearance was significantly inhibited in Cav-1 knockdown cells ($\tau = 472 \pm 83.96$ seconds) in comparison to siNT control ($\tau = 126.8 \pm 22.35$ seconds; Figure 4.6C-D).

As impaired $Ca^{2+}$ efflux can lead to $Ca^{2+}$ overload [34], we further investigated the effects of CAV1 knockdown using a $Ca^{2+}$ overload assay in which fura-2 loaded cells were exposed to 30 µM CPA to induce ER depletion, activation of SOCE and subsequent cytotoxic $Ca^{2+}$ overload (Figure 4.6E). However, CPA induced fura-2 signal saturations (Rmax) which made $[Ca^{2+}]_i$ calibration very difficult. Therefore, only the AUC of uncalibrated fura-2 340/380 nm ratio could be used to quantify these $[Ca^{2+}]_i$ responses. The mean AUC of siCav-1-treated cells was significantly higher than the siNT control (Figure 4.6F). It should be noted that despite the impaired $Ca^{2+}$ clearance, no changes in resting $[Ca^{2+}]_i$ was observed (Figure 4.6G). Overall, these results suggest that although PMCA4-mediated $Ca^{2+}$ efflux was impaired in Cav-1 knockdown cells, the basal $Ca^{2+}$ homeostasis was not affected.
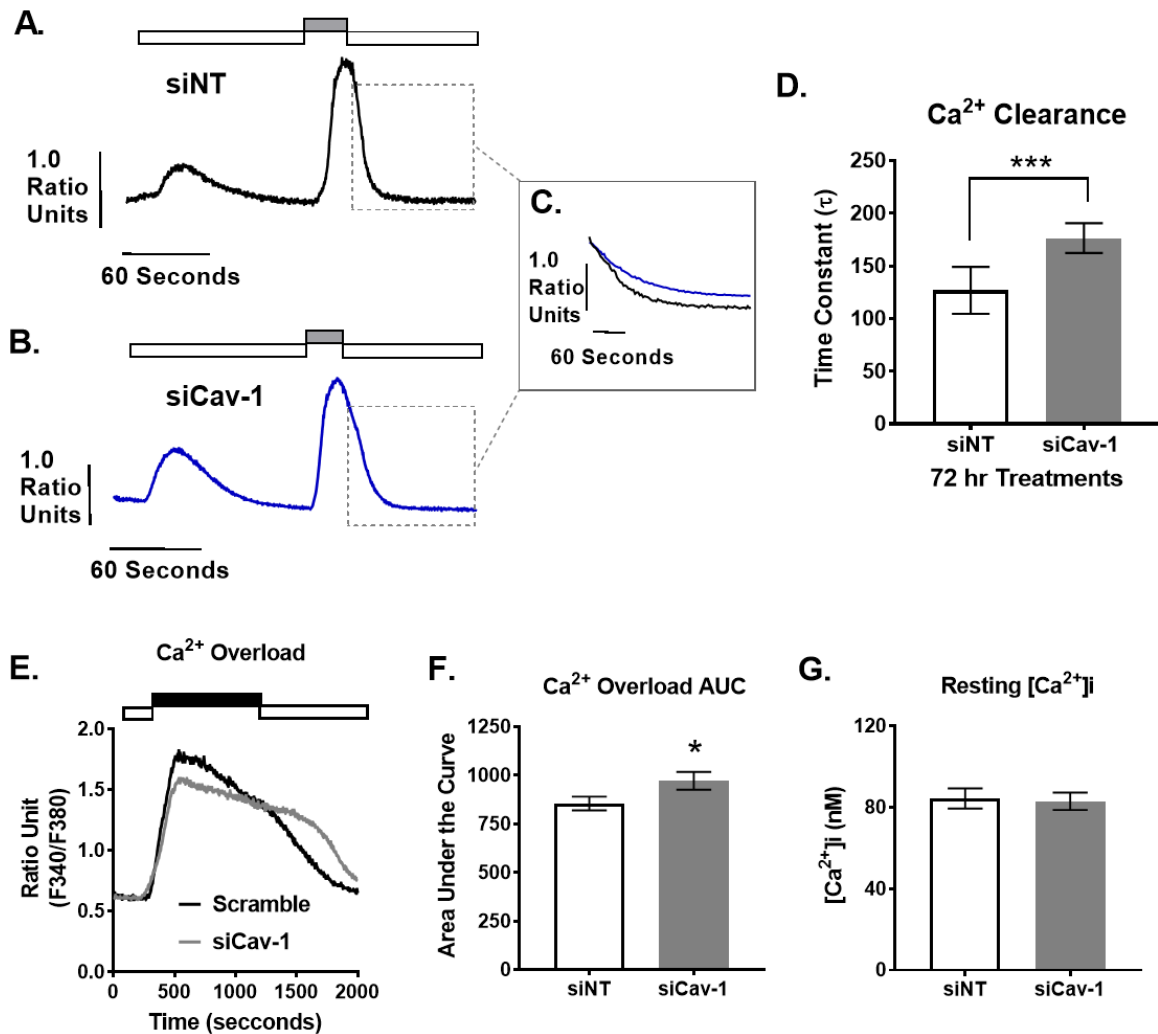
**Figure 4.6 – Cav-1 knockdown delays Ca$^{2+}$ clearance.** Representative *in situ* [Ca$^{2+}$]$_i$ clearance traces of MIAPaCa-2 cells incubated with either **A,** 25 nM siNT or **B,** 25 nM siCav-1 for 48-72 hrs prior to imaging. Fura2-loaded cells were sequentially perfused with 0 mM Ca$^{2+}$ HPPS containing 30 µM CPA (white box) to deplete intracellular Ca$^{2+}$ storage clearance and induce SOCE upon perfusion with 20 mM Ca$^{2+}$ HPPS (grey box). Switching back to 0 mM Ca$^{2+}$ HPPS then induced PMCA-mediated Ca$^{2+}$ efflux. **C,** Representative clearance phase of siNT (black) and siCav-1(blue) are shown as overlays. **D,** [Ca$^{2+}$]$_i$ clearance phases were fitted to single exponential decay and the results are shown as a time constant (τ). **E,** Representative CPA-mediated Ca$^{2+}$ overload traces of siNT (black) and siCav-1(grey) are shown. White and black bars represent perfusion with HPSS and 30 µM CPA, respectively. Data are expressed as **F,** the mean area under the curve (AUC) and **G,** calibrated resting [Ca$^{2+}$]$_i$. All representative traces are presented as 340/380 fluorescence signal ratio units. Data are shown as mean ± SEM (N=4, data collected from at least 50 individual cells). Statistical comparisons were made between siNT control and siCav-1 treated using the Kolmogorov-Smirnov test (Unpaired, non-parametric cumulative distribution test). * and *** represent statistically significant difference where P<0.05 and P<0.001, respectively.

### 4.4.7 Caveolin-1 knockdown had no effect on OXPHOS and glycolysis

Upregulation of Cav-1 has been associated to increase targeting of a key rate-limiting glycolytic enzyme (PFK-1) to the plasma membrane [20]. We hypothesized that Cav-1 targeting of PFK-1 to the plasma membrane, near the PMCAs, potentially prevents allosteric ATP inhibition of PFK-1 and subsequently drives glycolytic flux. In addition, $Ca^{2+}$ is reported to modulate both glycolytic [35] and mitochondrial metabolic activity [36]. Furthermore, our previous study showed that PMCA4 knockdown impaired mitochondrial respiration (results are shown in Chapter 3). Therefore, we next wanted to examine whether Cav-1 knockdown also alters the metabolic phenotype of MIAPaCa-2 PDAC cells.

Real-time changes in mitochondrial respiration (oxidative phosphorylation; OXPHOS) and glycolysis were measured using Mito stress test and glycolytic stress test with the Seahorse XFe96 Analyzer. This simultaneously measures oxygen consumption rate (OCR) and extracellular acidification rate (ECAR), following sequential treatments with metabolic inhibitors to reveal informative metabolic parameters. Changes in mitochondrial respiration and glycolytic metabolism of siCav-1 treated cells were compared to siNT control under basal (unstressed) and $Ca^{2+}$ stressed conditions following treatment with CPA which drives PMCA4 to function at its maximum capacity.

Under both basal and $Ca^{2+}$ stress conditions, siCav-1 treatment had no effect on all mitochondrial respiration parameters (Figure 4.7A-D), glycolytic metabolism (Figure 4.7E-H) and ATP production rate (Figure 4.7I). Compared to the basal condition, CPA-mediated $Ca^{2+}$ stress-induced a statistically significant decrease in mitochondrial maximal respiration and spare respiration capacity in siNT control. Conversely, siCav-1 treated cells showed a slightly blunted loss of mitochondrial respiration capacity under $Ca^{2+}$ stress. However, since knocking down Cav-1 had no effects on the ATP production rate under $Ca^{2+}$ stress (Figure 4.7I), the slightly blunted mitochondrial respiration parameters may not be biologically relevant.

Overall, we found that loss of Cav-1 expression did not alter the basal metabolic phenotype of MIAPaCa-2 cells. Under $Ca^{2+}$ stress, Cav-1 knockdown cells showed a slightly blunted decrease in mitochondrial respiration capacity, but the overall ATP production rate was not affected. Therefore, despite influencing PMCA4 activity, Cav-1 expression had a minimal role in glycolytic and mitochondrial respiration MIAPaCa-2 cells. This suggests that Cav-1 expression functionally modulates PMCA4 activity independent of ATP-depletion and changes in metabolic phenotype.
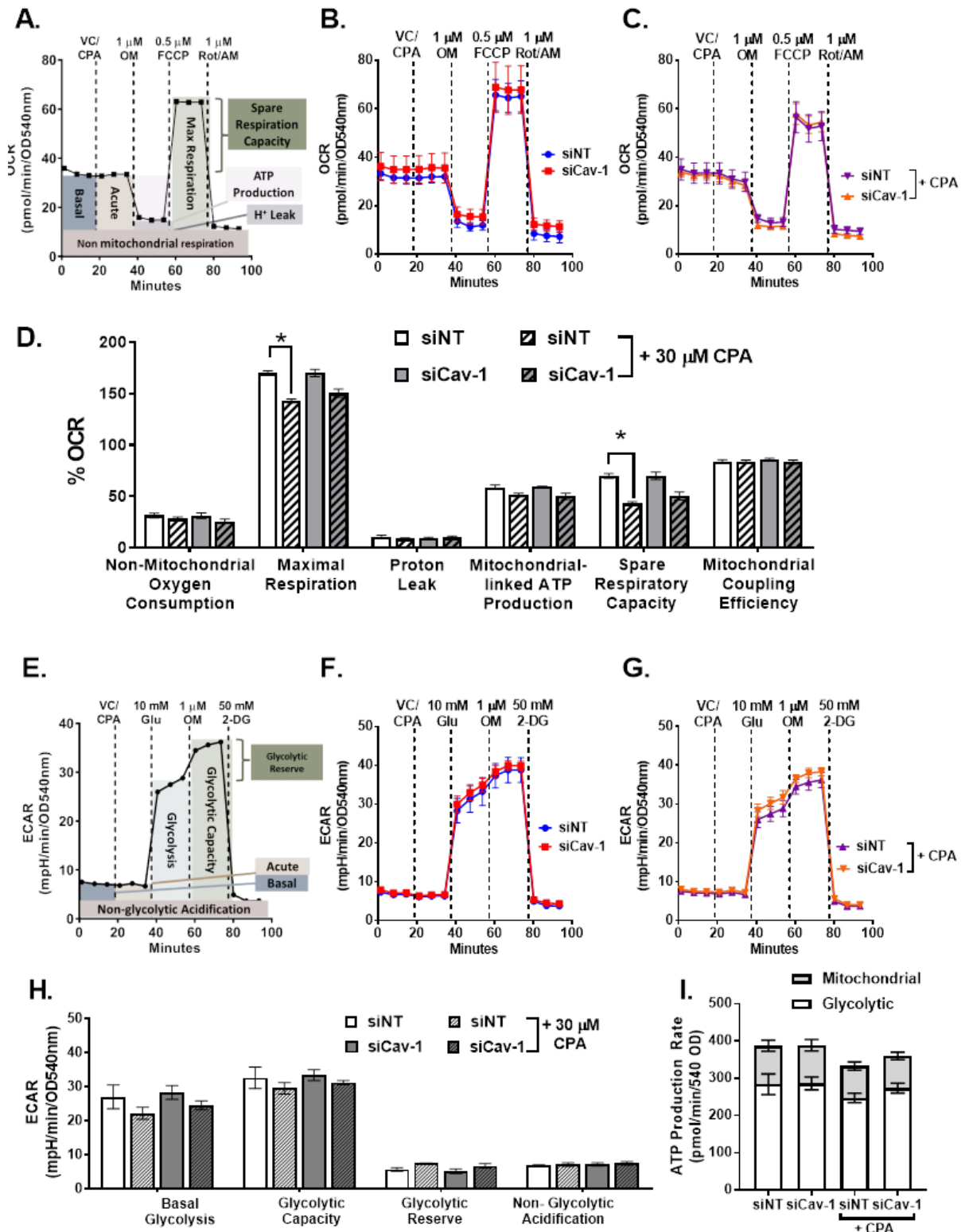
**Figure 4.7 – Cav-1 knockdown had no effect on OXPHOS and glycolysis.** MIAPaCa-2 cells were incubated with either 25 nM siNT control or siCav-1 for 48 hours. Representative Mito Stress test OCR graphs comparing non-treated and 30 µM CPA pre-treated **A,** siNT control and **B,** siPMCA4. **C,** Mito stress test data were normalized to protein content then normalized as % of OCR baseline. Representative Glycolysis Stress test ECAR traces are shown for **D,** control and **E,** CPA treated siRNA treated cells. **F,** Glycolysis stress test data were normalized to SRB and normalized as % of baseline. Statistical significance was determined using one-way ANOVA with post-hoc Bonferroni. (N=3, 4 replicates per treatment condition)

## 4.5 Discussion

Cav-1 and PMCA4 have been individually shown to play various roles in cancer hallmarks [9,37,38]. This study has provided evidence which links the importance of Cav-1 expression in modulating PMCA4 activity in PDAC. Although Cav-1 expression had no effect on PDAC cell proliferation and metabolic phenotype, we showed for the first time in MIA-PaCa2 PDAC cell line, which in the context of PMCA4 expression, is a good representative PDAC model, that either chemical disruption of the caveolae or knocking down Cav-1 consistently inhibited PMCA4 activity.

In PDAC, upregulation of Cav-1 expression has been correlated to multiple cancer hallmarks including tumour progression, apoptotic resistance, [9] migration, and invasion [39]. Consistent with previous findings by Chatterjee, M. *et al.* (2015) [9], our data mining of publicly available databases revealed that over-expression of Cav-1 mRNA (CAV1) in patient-derived PDAC tumours [25] is statistically correlated to poor patient survival [27]. Furthermore, co-elevation of ATP2B4 and CAV1 in resected PDAC tumours is clinically correlated to even worse PDAC patient survival [27], suggesting that PMCA4 and Cav-1 exhibit oncogenic cooperativity. Moreover, PMCAs are known to reside in the Cav-1-enriched caveolae [10,21,22], therefore this co-elevation of ATP2B4 and CAV1 (encoding PMCA4 and Cav-1) could potentially be important prognostic biomarkers of PDAC tumorigenicity.

Cav-1 is the major component and a well-recognized marker of the caveolae [40]. Caveolae are lipid-rich invagination of the surface membrane reported to facilitate assembly of signalling complexes associated with the insulin receptor, nitric oxide synthase, G-protein coupled receptors and ion channels [11,12,41]. Moreover, caveolae have been suggested to play an important role in compartmentalizing $Ca^{2+}$ signalling [13,42]; $Ca^{2+}$ pumps (PMCA; [21,30]), exchangers ($Na^+/Ca^{2+}$ exchanger [42]) and channels have been found localised within lipid-rich caveolae compartments [43]. Previous work in mouse small intestine [21] and ECV304 endothelial cells [30] demonstrated that PMCA4 is localised to caveolae. Although Cav-1 has been demonstrated to be overexpressed in PDAC cell lines, including MIAPaCa-2 [9], limited evidence was available on the colocalization of PMCA4 with caveolae in PDAC cells. The current study confirmed through sucrose density ultracentrifugation that PMCA4 and Cav-1 resided in similar low-density fractions, suggesting that PMCA4 may reside in Cav-1-enriched caveolae in MIAPaCa-2 PDAC cells. This is particularly important when considering the oncogenic cooperativity of the overexpressed PMCA4 (discussed in Chapter 3) and Cav-1 [9] in PDAC tumour. Similar to previous observations in pancreatic β-cells [11], we confirmed that the caveolae were successfully disrupted using MβC-mediated cholesterol depletion [30,44] which had a profound effect on PMCA4 activity. Since MIAPaCa-2 almost exclusively expresses PMCA4, we consider MIA-PaCa2 to be a suitable PDAC model to selectively study the functional relationship between Cav-1 and PMCA4.

PMCA is an ATP-dependent $Ca^{2+}$ efflux mechanism which plays a critical role in maintaining $Ca^{2+}$ homeostasis and $Ca^{2+}$-dependent cellular processes, including adhesion, migration, cell cycle, apoptosis and metabolism [3–5]. PMCA is functionally activated by $[Ca^{2+}]_i$-dependent calmodulin (CaM), protein kinase C (PKC), and phospholipids. Activated PMCA then requires ATP to initiate $Ca^{2+}$ efflux [4]. As PMCAs were found to be highly concentrated in the caveolae [10], the caveolae have been suggested

to act as a platform to optimally enable PMCA to maintain low $[Ca^{2+}]_i$ microdomain necessary for compartmentalizing $Ca^{2+}$ signal transduction [3,4,42]. Furthermore, similar to findings in vascular smooth muscle [20,45], we found that key glycolytic enzymes were found in all fractions including low-density PMCA4 and Cav-1-enriched fractions (S1 Fig), suggesting that some population of glycolytic enzymes may be membrane-associated. Localization of glycolytic enzymes at the plasma membrane has been suggested to provide a privilege ATP supply to the ATP-consuming PMCAs [46]. Moreover, the key rate-limiting glycolytic enzyme PFK1 and PKM2 are inhibited by high concentrations of ATP (>2.5 mM) [47]. Therefore, it could be argued that PMCA4 consumption of glycolytic ATP may drive glycolytic flux by preventing allosteric inhibition by glycolytic products (e.g. high ATP/ADP ratio) [47,48]. The current study hypothesized that the caveolae compartment facilitates targeting of glycolytic enzymes near the PMCA and thus disruption of the caveolae may potentially disassociate these glycolytic enzymes, thereby reducing the privileged ATP supply to the PMCA. Presumably, this would inhibit PMCA resulting in cytosolic $Ca^{2+}$ overload and the consequential cell death.

Our previous work showed that PMCA activity is indeed selectively dependent on glycolytic ATP in PDAC cells [6,7]. The present study confirmed that MβC-induced caveolae disruption led to significant inhibition of PMCA4-mediated $Ca^{2+}$ clearance and cytotoxic $Ca^{2+}$ overload, independent of ATP-depletion and cell death. Similar to our observations, a study by Zhang *et al.* (2009) showed that MβC-mediated caveolae disruption led to impaired PMCA activity in ECV304 epithelial cells [30]. In addition, the lack of cellular ATP-depletion and preserved cell viability after short-term MβC treatment were also observed in rat epithelial [49] and cerebellar granule neurons [50], respectively. Although cellular ATP-depletion was not observed during the duration of PMCA4 inhibition, it is plausible that caveolae disruption may dislodge glycolytic enzymes in proximity to the PMCA, leading to local ATP-depletion and subsequently reducing PMCA4 activity without any global changes in ATP. However, since we did not have the means to quantitatively measure localised ATP-depletion at the caveolae, it is not possible to confirm this and therefore we could only conclude that optimal PMCA4 functional activity is indeed dependent on its localisation in the caveolae compartment.

An important caveat to the interpretation of the effects of MβC on PMCA activity is that PMCA activity is regulated by acidic phospholipids (e.g. phosphatidylserine, phosphatidylinositol and phosphoinositide 4,5-bisphosphate) within the membrane which are particularly abundant within caveolae/lipid rafts [51–53]. Binding of phosphatidylserine and phosphatidylinositol to PMCA regulatory C-terminus strongly enhances PMCA affinity for $Ca^{2+}$ and facilitates ATP dephosphorylation [52,53]. Therefore, it is possible that MβC-mediated cholesterol depletion may indirectly inhibit PMCA4 activity by depriving essential acidic phospholipid from the PMCA microenvironment independent of ATP depletion [30]. Cav-1 knockdown is a subtle approach to alternatively inhibit caveolae formation in multiple models [21,32,54] without necessarily perturbing the phospholipid environment to the same extent as MβC. The current study therefore transiently knocked down Cav-1 to selectively inhibit caveolae formation without disturbing the membrane phospholipid microenvironment. Consistent with previous studies in mouse small intestine [21] and sperm [22], we showed that selective Cav-1 knockdown led to significantly impaired PMCA4-mediated $Ca^{2+}$ clearance and subsequently potentiated CPA-induced cytotoxic $Ca^{2+}$ overload. Therefore, these experiments reinforce the evidence that Cav-1

enriched caveolae compartment is essential for optimal PMCA4 activity independent of cholesterol depletion and disruption of the lipid environment surrounding the PMCA4.

Cav-1 has been implicated in glycolytic and mitochondrial metabolic processes [20,55]. Overexpression of Cav-1 has been shown to increase glycolytic enzyme expression (phosphofructokinase and aldolase) at the plasma membrane [20] and enhance glycolysis and ATP production in a panel of colon cancer cell lines [56]. Moreover, Cav-1 has been associated with mitochondrial function and loss of Cav-1 expression led to mitochondrial dysfunction and reduced ATP levels in fibroblasts [57,58]. Therefore, Cav-1 knockdown may potentially alter metabolism, reduce intracellular ATP, and thus inhibit PMCA4 activity. However, similar to previous findings in fibroblast [58], we found that knocking down Cav-1 had no effect on Seahorse XFe96 Analyzer derived ATP production rate, glycolytic or mitochondrial metabolic parameters in MIAPaCa-2 cells. This suggests that Cav-1 does not modulate basal metabolism in PDAC. Despite the impaired PMCA4-mediated $Ca^{2+}$ efflux in Cav-1 knockdown cells, under $Ca^{2+}$ stress, both Cav-1 knockdown and the control conditions showed similar decreases in mitochondrial respiration. However, thapsigargin, a SERCA inhibitor, has been shown to depolarize mitochondria and decrease basal OCR [47]. Although CPA has no effects on the basal OCR, it is possible that the CPA is similarly facilitating mitochondrial depolarization, thereby reducing mitochondrial respiration over the duration of the Mito Stress test experiment. Taken altogether, Cav-1 knockdown linked PMCA4 inhibition occurs independently of cellular metabolic changes in MIAPaCa-2 PDAC cells.

Although we postulate that compartmental ATP-depletion may be responsible for the impaired PMCA4 activity, this hypothesis cannot be tested under experimental conditions in this study and thus remains speculative. Multiple possibilities may also be responsible for PMCA4 inhibition in Cav-1 knockdown cells. For instance, since Cav-1 may serve as a docking site for glycolytic enzymes [20], it is plausible that the loss of Cav-1 resulted in less glycolytic enzymes being targeted to the membrane thereby reducing the privileged ATP supply to the PMCA4. Moreover, Cav-1 plays an important role in lipid homeostasis (cholesterol transport to the membrane) [14,15]. Knocking down Cav-1 is reported to reduce cholesterol in the plasma membrane and alter membrane lipid environments [14,59], which may interfere with PMCA4 activity in a similar manner to MβC. Furthermore, PKC, an activator of the PMCA, is known to be targeted to the caveolae [60]. Hence, Cav-1 knockdown associated loss of caveolae may reduce PKC activation of PMCA4.

Although the role of Cav-1 on cancer hallmarks had been extensively investigated in PDAC cells, the effect of Cav-1 knockdown in PDAC remains controversial as conflicting results were reported in similar PDAC cell lines across multiple studies. For instance, a study by Chatterjee *et al.* (2015) reported that Cav-1 knockdown led to inhibited cell migration and sensitized MIAPaCa-2 and BxPC3 PDAC cells to chemo and radiotherapy [9], suggesting that Cav-1 may be responsible for oncogenic cell migration and apoptotic resistance. In contrast, other studies showed that knocking down Cav-1 expression enhanced cell migration [39,61,62]. While Chatterjee *et al.* (2015) reported that knocking down Cav-1 (siCav-1 and shCav-1 treatment) inhibited cell proliferation in BxPC3 and MIAPaCa-2 cells (WST-1, 48 hours) and xenograft (tumour volume), a recent study by Kamposioras *et al.* (2019) showed that Cav-1

knockdown (shCav-1) in BxPC3 cells increased cell proliferation (BrdU and SRB) and enhanced cell migration [61]. These contradicting cell migration results were likely attributed to the different effects of Cav-1 knockdown on cell proliferation. At variance with these studies, our current data showed that Cav-1 knockdown had no significant effect on MIAPaCa-2 cell proliferation between 0-96 hours post-treatment as assessed using two separate assays (WST-8 and SRB). As knocking down Cav-1 may lead to compensatory redundancy of related proteins including Cav-2 or Cav-3. Moreover, Cav-2 and Cav-3 have been linked to the modulation of cell proliferation [63–66]. Therefore, the potential differences in caveolin redundancy may attribute to the differences in proliferation and migration responses in different PDAC cell lines.

In conclusion, co-elevation of Cav-1 and PMCA4 is correlated to PDAC patient survival. We have previously shown that PMCA4 plays an important role in migration and apoptotic resistance in PDAC. This study provides further evidence that, in MIAPaCa-2 PDAC model, Cav-1-rich caveolae play an important role in modulating PMCA4 activity, albeit the mechanism is unclear. Although no effects on cell proliferation and metabolic phenotype were observed, Cav-1 knockdown inhibited PMCA4-mediated $Ca^{2+}$ efflux independent of cellular ATP depletion and metabolic alteration. Since PMCA4 functional activity is dependent on Cav-1 expression in PDAC, further understanding the functional relationship between these PDAC markers may provide insights to selectively sensitize PDAC to therapeutic treatments.

## 4.6 Acknowledgements

## 4.7 References

1. Cancer Research UK [Internet]. [cited 2019 May 20]. Available from: https://www.cancerresearchuk.org/health-professional/cancer-statistics/statistics-by-cancer-type/pancreatic-cancer

2. John S, Broggio J. Cancer survival in England : national estimates for patients followed up to 2017 [Internet]. 2019.

3. Holton ML, Wang W, Emerson M, Neyses L, Armesilla AL. Plasma membrane calcium ATPase proteins as novel regulators of signal transduction pathways. World J Biol Chem. 2010 Jun 26;1(6):201–8.

4. Lopreiato R, Giacomello M, Carafoli E. The plasma membrane calcium pump: new ways to look at an old enzyme. J Biol Chem. 2014 Apr 11;289(15):10261–8.

5. Bruce JIE. Metabolic regulation of the PMCA: Role in cell death and survival. Cell Calcium. 2018;69:28–36.

6. James AD, Chan A, Erice O, Siriwardena AK, Bruce JIE. Glycolytic ATP fuels the plasma membrane calcium pump critical for pancreatic cancer cell survival. J Biol Chem. 2013 Dec 13;288(50):36007–19.

7. James AD, Patel W, Butt Z, Adiamah M, Dakhel R, Latif A, et al. The Plasma Membrane Calcium Pump in Pancreatic Cancer Cells Exhibiting the Warburg Effect Relies on Glycolytic ATP. J Biol Chem. 2015 Oct 9;290(41):24760–71.

8. Nakamura T, Furukawa Y, Nakagawa H, Tsunoda T, Ohigashi H, Murata K, et al. Genome-wide cDNA microarray analysis of gene expression profiles in pancreatic cancers using populations of tumor cells and normal ductal epithelial cells selected for purity by laser microdissection. Oncogene. 2004 Mar 9;23(13):2385–400.

9. Chatterjee M, Ben-Josef E, Thomas DG, Morgan MA, Zalupski MM, Khan G, et al. Caveolin-1 is Associated with Tumor Progression and Confers a Multi-Modality Resistance Phenotype in Pancreatic Cancer OPEN. Nat Publ Gr. 2015;

10. Fujimoto T. Calcium pump of the plasma membrane is localized in caveolae. J Cell Biol. 1993 Mar 1;120(5):1147–57.

11. Cheng JPX, Nichols BJ. Caveolae: One Function or Many? Trends Cell Biol. 2016 Mar;26(3):177–89.

12. Harvey RD, Calaghan SC. Caveolae create local signalling domains through their distinct protein content, lipid profile and morphology. J Mol Cell Cardiol. 2012 Feb;52(2):366–75.

13. Isshiki M, Anderson RGW. Function of caveolae in $Ca^{2+}$ entry and $Ca^{2+}$ -dependent signal transduction. Traffic. 2003;4(11):717–23.

14. Kuo A, Lee MY, Yang K, Gross RW, Sessa WC, Program T. Caveolin-1 regulates lipid droplet metabolism in endothelial cells via autocrine prostacyclin stimulated cAMP-mediated lipolysis. 2017;

15. Frank PG, Pavlides S, Cheung MW-C, Daumer K, Lisanti MP. Role of caveolin-1 in the regulation of lipoprotein metabolism. Am J Physiol Cell Physiol. 2008 Jul;295(1):C242-8.

16. Wang H, Wang AX, Barrett EJ. Caveolin-1 is required for vascular endothelial insulin uptake. Am J Physiol Endocrinol Metab. 2011 Jan;300(1):E134-44.

17. Rybin VO, Xu X, Steinberg SF. Activated Protein Kinase C Isoforms Target to Cardiomyocyte Caveolae. Circ Res. 1999 May 14;84(9):980–8.

18. Trane AE, Pavlov D, Sharma A, Saqib U, Lau K, Van Petegem F, et al. Deciphering the binding of Caveolin-1 to client protein endothelial nitric-oxide synthase (eNOS): Scaffolding subdomain identification, interaction modeling, and biological significance. J Biol Chem. 2014;289(19):13273–83.

19. Baudrand R, Gupta N, Garza AE, Vaidya A, Leopold JA, Hopkins PN, et al. Caveolin 1 Modulates Aldosterone-Mediated Pathways of Glucose and Lipid Homeostasis. J Am Heart Assoc. 2016;5(10).

20. Raikar LS, Vallejo J, Lloyd PG, Hardin CD. Overexpression of caveolin-1 results in increased plasma membrane targeting of glycolytic enzymes: The structural basis for a membrane associated metabolic compartment. J Cell Biochem. 2006 Jul 1;98(4):861–71.

21. El-Yazbi AF, Cho WJ, Schulz R, Daniel EE. Calcium extrusion by plasma membrane calcium pump is impaired in caveolin-1 knockout mouse small intestine. Eur J Pharmacol. 2008 Sep 4;591(1–3):80–7.

22. Olli KE, Li K, Galileo DS, Martin-DeLeon PA. Plasma membrane calcium ATPase 4 (PMCA4) co-ordinates calcium and nitric oxide signaling in regulating murine sperm functional activity. J Cell Physiol. 2018 Jan;233(1):11–22.

23. Vichai V, Kirtikara K. Sulforhodamine B colorimetric assay for cytotoxicity screening. Nat Protoc. 2006 Aug 17;1(3):1112–6.

24. Neher E. The use of fura-2 for estimating Ca buffers and Ca fluxes. Neuropharmacology. 1995 Nov;34(11):1423–42.

25. Oncomine [Internet]. [cited 2019 Jan 17]. Available from: www.oncomine.org

26. Badea L, Herlea V, Dima SO, Dumitrascu T, Popescu I. Combined gene expression analysis of whole-tissue and microdissected pancreatic ductal adenocarcinoma identifies genes specifically overexpressed in tumor epithelia. Hepatogastroenterology. 55(88):2016–27.

27. Uhlen M. Expression of CAV1 in pancreatic cancer - The Human Protein Atlas [Internet]. [cited 2019 Jan 19]. Available from: https://www.proteinatlas.org/ENSG00000105974-CAV1/pathology/tissue/pancreatic+cancer

28. Uhlen M. Expression of ATP2B4 in pancreatic cancer - The Human Protein Atlas [Internet]. [cited 2019 Jan 17]. Available from: https://www.proteinatlas.org/ENSG00000058668-ATP2B4/pathology/tissue/pancreatic+cancer

29. Uhlen M, Zhang C, Lee S, Sjöstedt E, Fagerberg L, Bidkhori G, et al. A pathology atlas of the human cancer transcriptome. Science (80- ). 2017 Aug 18;357(6352):eaan2507.

30. Zhang J, Xiao P, Zhang X. Phosphatidylserine externalization in caveolae inhibits $Ca^{2+}$ efflux through plasma membrane $Ca^{2+}$-ATPase in ECV304. Cell Calcium. 2009 Feb;45(2):177–84.

31. Rodal SK, Skretting G, Garred O, Vilhardt F, van Deurs B, Sandvig K. Extraction of cholesterol with methyl-beta-cyclodextrin perturbs formation of clathrin-coated endocytic vesicles. Mol Biol Cell. 1999 Apr;10(4):961–74.

32. Griffoni C, Spisni E, Santi S, Riccio M, Guarnieri T, Tomasi V. Knockdown of caveolin-1 by antisense oligonucleotides impairs angiogenesis in vitro and in vivo. Biochem Biophys Res Commun. 2000;276(2):756–61.

33. D'Alessio A, Al-Lamki RS, Bradley JR, Pober JS. Caveolae participate in tumor necrosis factor receptor 1 signaling and internalization in a human endothelial cell line. Am J Pathol. 2005;166(4):1273–82.

34. Orrenius S, Gogvadze V, Zhivotovsky B. Calcium and mitochondria in the regulation of cell death. 2015;

35. Marinho-Carvalho MM, Costa-Mattos PV, Spitz GA, Zancan P, Sola-Penna M. Calmodulin upregulates skeletal muscle 6-phosphofructo-1-kinase reversing the inhibitory effects of allosteric modulators. Biochim Biophys Acta - Proteins Proteomics. 2009 Aug;1794(8):1175–80.

36. Marchi S, Patergnani S, Missiroli S, Morciano G, Rimessi A, Wieckowski MR, et al. Mitochondrial and endoplasmic reticulum calcium homeostasis and cell death. Cell Calcium. 2018;69:62–72.

37. Elsheikh SE, Green AR, Rakha EA, Samaka RM, Ammar AA, Powe D, et al. Caveolin 1 and Caveolin 2 are associated with breast cancer basal-like and triple-negative immunophenotype. Br J Cancer. 2008 Jul 8;99(2):327–34.

38. Aung CS, Ye W, Plowman G, Peters AA, Monteith GR, Roberts-Thomson SJ. Plasma membrane calcium ATPase 4 and the remodeling of calcium homeostasis in human colon cancer cells. Carcinogenesis. 2009 Nov 1;30(11):1962–9.

39. Lin M, DiVito MM, Merajver SD, Boyanapalli M, van Golen KL. Regulation of pancreatic cancer cell migration and invasion by RhoC GTPase and caveolin-1. Mol Cancer. 2005 Jun 21;4(1):21.

40. Volonte D, Galbiati F, Lisanti MP. Visualization of caveolin-1, a caveolar marker protein, in living cells using green fluorescent protein (GFP) chimeras. The subcellular distribution of caveolin-1 is modulated by cell-cell contact. FEBS Lett. 1999 Feb 26;445(2–3):431–9.

41. Karlsson M, Thorn H, Parpal S, Strålfors P, Gustavsson J. Insulin induces translocation of glucose transporter GLUT4 to plasma membrane caveolae in adipocytes. FASEB J. 2002 Feb;16(2):249–51.

42. Pani B, Singh BB. Lipid rafts/caveolae as microdomains of calcium signaling. Cell Calcium. 2009 Jun;45(6):625–33.

43. Xia F, Leung YM, Gaisano G, Gao X, Chen Y, Fox JEM, et al. Targeting of voltage-gated $K^+$ and $Ca^{2+}$ channels and soluble N-ethylmaleimide-sensitive factor attachment protein receptor proteins to cholesterol-rich lipid rafts in pancreatic alpha-cells: effects on glucagon stimulus-secretion coupling. Endocrinology. 2007 May;148(5):2157–67.

44. Breen MR, Camps M, Carvalho-Simoes F, Zorzano A, Pilch PF. Cholesterol Depletion in Adipocytes Causes Caveolae Collapse Concomitant with Proteosomal Degradation of Cavin-2 in a Switch-Like Fashion. Martin S, editor. PLoS One. 2012 Apr 6;7(4):e34516.

45. Vallejo J, Hardin CD. Caveolin-1 Functions as a Scaffolding Protein for Phosphofructokinase in the Metabolic Organization of Vascular Smooth Muscle †. Biochemistry. 2004 Dec;43(51):16224–32.

46. Puchulu-Campanella E, Chu H, Anstee DJ, Galan JA, Tao WA, Low PS. Identification of the components of a glycolytic enzyme metabolon on the human red blood cell membrane. J Biol Chem. 2013 Jan 11;288(2):848–58.

47. Larsson C, Påhlman IL, Gustafsson L. The importance of ATP as a regulator of glycolytic flux in Saccharomyces cerevisiae. Yeast. 2000 Jun 30;16(9):797–809.

48. Moreno-Sánchez R, Marín-Hernández Á, Del Mazo-Monsalvo I, Saavedra E, Rodríguez-Enríquez S. Assessment of the low inhibitory specificity of oxamate, aminooxyacetate and dichloroacetate on cancer energy metabolism. Biochim Biophys Acta - Gen Subj. 2017 Jan;1861(1):3221–36.

49. Barnes K, Ingram JC, Bennett MDM, Stewart GW, Baldwin SA. Methyl-β-cyclodextrin stimulates glucose uptake in Clone 9 cells: a possible role for lipid rafts [Internet]. Vol. 378, Biochem. J. 2004.

50. Fortalezas S, Marques-da-Silva D, Gutierrez-Merino C, Fortalezas S, Marques-da-Silva D, Gutierrez-Merino C. Methyl-β-Cyclodextrin Impairs the Phosphorylation of the β2 Subunit of L-Type Calcium Channels and Cytosolic Calcium Homeostasis in Mature Cerebellar Granule Neurons. Int J Mol Sci. 2018 Nov 20;19(11):3667.

51. Hirama T, Das R, Yang Y, Ferguson C, Won A, Yip CM, et al. Phosphatidylserine dictates the assembly and dynamics of caveolae in the plasma membrane. J Biol Chem. 2017 Aug 25;292(34):14292–307.

52. Filomatori C V., Rega AF. On the mechanism of activation of the plasma membrane $Ca^{2+}$-ATPase by ATP and acidic phospholipids. J Biol Chem. 2003;278(25):22265–71.

53. Carafoli E. Calcium Pump of the Plasma Membrane [Internet]. Vol. 71, PHYSIOLOGICAL REVIEWS. 1991.

54. Drab M, Verkade P, Elger M, Kasper M, Lohn M, Lauterbach B, et al. Loss of Caveolae, Vascular Dysfunction, and Pulmonary Defects in Caveolin-1 Gene-Disrupted Mice. Science (80- ). 2001 Sep 28;293(5539):2449–52.

55. Niesman IR, Zemke N, Fridolfsson HN, Haushalter KJ, Levy K, Grove A, et al. Caveolin isoform switching as a molecular, structural, and metabolic regulator of microglia. Mol Cell Neurosci. 2013 Sep;56:283–97.

56. Ha T-K, Her N-G, Lee M-G, Ryu B-K, Lee J-H, Han J, et al. Caveolin-1 increases aerobic glycolysis in colorectal cancers by stimulating HMGA1-mediated GLUT3 transcription. Cancer Res. 2012 Aug 15;72(16):4097–109.

57. Yu D-M, Jung SH, An H-T, Lee S, Hong J, Park JS, et al. Caveolin-1 deficiency induces premature senescence with mitochondrial dysfunction. Aging Cell. 2017;16(4):773–84.

58. Volonte D, Liu Z, Shiva S, Galbiati F. Caveolin-1 controls mitochondrial function through regulation of m-AAA mitochondrial protease. Aging (Albany NY). 2016;8(10):2355–69.

59. Raggi C, Diociaiuti M, Caracciolo G, Fratini F, Fantozzi L, Piccaro G, et al. Caveolin-1 Endows Order in Cholesterol-Rich Detergent Resistant Membranes. Biomolecules. 2019 Jul 17;9(7):287.

60. Mineo C, Ying YS, Chapline C, Jaken S, Anderson RG. Targeting of protein kinase Calpha to caveolae. J Cell Biol. 1998 May 4;141(3):601–10.

61. Kamposioras K, Tsimplouli C, Verbeke C, Anthoney A, Daoukopoulou A, Papandreou CN, et al. Silencing of caveolin-1 in fibroblasts as opposed to epithelial tumor cells results in increased tumor growth rate and chemoresistance in a human pancreatic cancer model. Int J Oncol. 2019 Feb 1;54(2):537–49.

62. Han F, Zhu HG. Caveolin-1 Regulating the Invasion and Expression of Matrix Metalloproteinase (MMPs) in Pancreatic Carcinoma Cells. J Surg Res. 2010;159(1):443–50.

63. Shang L, Chen T, Deng Y, Huang Y, Huang Y, Xian J, et al. Caveolin-3 promotes glycometabolism, growth and proliferation in muscle cells. Fan G-C, editor. PLoS One. 2017 Dec 5;12(12):e0189004.

64. Hu S, Li L, Huang W, Liu J, Lan G, Yu S, et al. CAV3.1 knockdown suppresses cell proliferation, migration and invasion of prostate cancer cells by inhibiting AKT. Cancer Manag Res. 2018 Oct;Volume 10:4603–14.

65. Sowa G. Novel insights into the role of caveolin-2 in cell- and tissue-specific signaling and function. Biochem Res Int. 2011 Dec 20;2011:809259.

66. Pak S, Kwon H, Jeong K, Pak Y. Regulation of cancer cell proliferation by caveolin-2 down-regulation and re-expression. Int J Oncol. 2011 May 1;38(5):1395–402.

67. Wang S, Jia L, Zhou H, Shi W, Zhang J. Knockdown of Caveolin-1 by siRNA Inhibits the Transformation of Mouse Hepatoma H22 Cells In Vitro and In Vivo . Oligonucleotides. 2009;19(1):81–8.

# 4.8 Supplementary Data
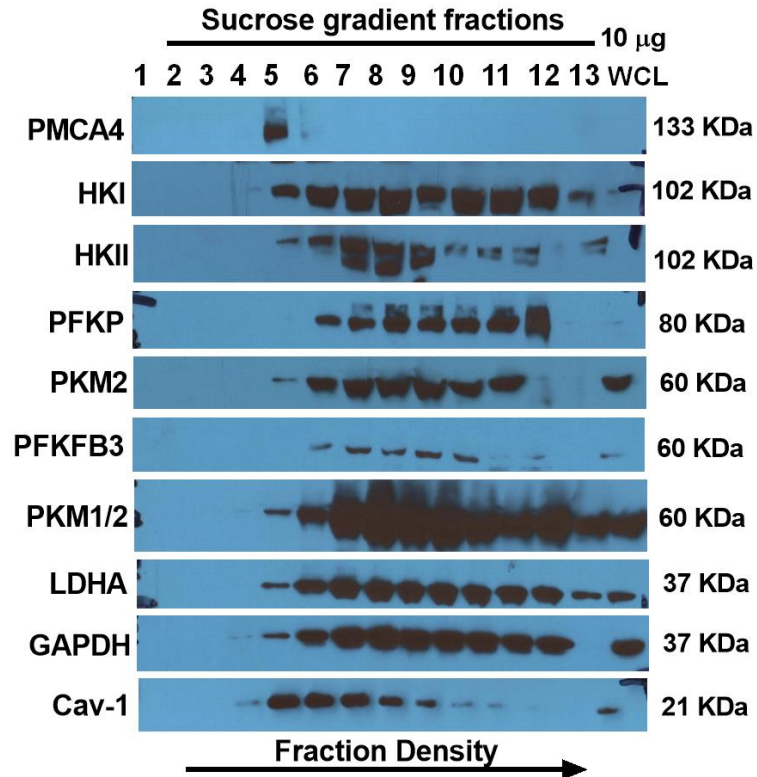


**Supplementary Figure 4.1 – Colocalization of glycolytic enzymes in Cav-1-enriched low-density fraction.** Sucrose gradient ultracentrifugation was used to separate lysate fractions by density. Fractions from lowest density (low density; 1) to highest density (hydrophilic; 13) fraction were collected. Whole-cell lysate (WCL; 10 µg) was loaded as control. Proteins from each fraction were loaded into 4-12% Bis-Tris gel and protein bands were separated using electrophoresis. Representative Western immunoblot of plasma membrane $Ca^{2+}$ ATPase isoform 4 (PMCA4), hexokinase I (HKI), hexokinase II (HKII), phosphofructokinase-platelet type (PFKP), pyruvate kinase M2 (PKM2), 6-phosphofructo-2-kinase/fructose-2,6-biphosphatase 3 (PFKFB3), pan pyruvate kinase M1&2 isoforms (PKM1/2), lactate dehydrogenase A (LDHA), glyceraldehyde 3-phosphate dehydrogenase (GAPDH), and caveolin-1 (Cav-1) are shown. (N=2)

# Chapter 5 – Bio-identification of PKM2 interaction in MIAPaCa-2 pancreatic ductal adenocarcinoma cells

**Pishyaporn Sritangos[1], Andrew D. James[2] and Jason I.E. Bruce[1]**

[1] Division of Cancer Sciences, School of Medical Sciences, Faculty of Biology, Medicine and Health, University of Manchester, Manchester, M13 9PT, United Kingdom

[2] Department of Biology, University of York, Heslington, York, YO10 5DD, United Kingdom

## 5.1 Abstract

A shift towards aerobic glycolysis and overexpression of oncogenic PKM2 has been observed in multiple cancers including pancreatic ductal adenocarcinoma (PDAC). Our previous studies showed that key glycolytic enzymes were associated with the plasma membrane fraction and that glycolytic ATP was shown to be important for fuelling plasma membrane $Ca^{2+}$ ATPase (PMCA) activity. Previous studies have introduced the concept of a membrane-associated glycolytic metabolon that provides a privilege ATP supply to the ATP consuming pumps (e.g. PMCA) at the plasma membrane in multiple models. The aim of the current study was to investigate the potential interaction of pyruvate kinase (PKM2), a key ATP-generating glycolytic enzyme, with membrane-binding proteins responsible for associating this glycolytic metabolon at the plasma membrane of PDAC cells. Moreover, as datamining of publicly available databases suggest that PKM2 overexpression in PDAC tumours has been correlated to poor patient survival, the current study used proximity-dependent biotinylation identification (BioID) technique to screen for potential interactors of PKM2. MIAPaCa-2 PDAC cells were stably transfected with a designated protein bait (mouse PKM2 wildtype, mouse PKM2 K433E mutant or non-targeting Venus fluorophore) fused to a mutant E. Coli biotin ligase (BirA*) and the expression of these fusion proteins were confirmed by Western immunoblot and immunofluorescence imaging. In the presence of exogenous biotin, these BirA* fusion proteins can promiscuously biotinylate proteins within 10-20 nm of the bait. Biotin-labelled proteins were separated from unlabelled proteins using streptavidin affinity purification. Biotinylated proteins were then identified by LC-MS/MS using Progenesis QI software. Enrichment of PKM2 interacting partners was categorized based on using PANTHER (protein analysis through evolutionary relationships) database. Compared to the Venus-BirA*, we showed that mPKM2-BirA* exhibited significantly enriched interactions with a transmembrane voltage-channel potassium channel (KCNH4) subunit. Moreover, mPKM2-BirA* also significantly interacted with a canonical glycolytic enzyme, aldolase (ALDOA). A further qualitative screening revealed that the Venus bait had a high degree of non-specific interaction which potentially led to an underestimation of relevant PKM2 interacting partners. In contrast, the mutant PKM2 bait (mPKM2-K433E) had lower non-specific interactions and, therefore, may serve as a better control bait to identify relevant interacting partners of PKM2. The current study provides preliminary results indicating that PKM2 interacts with transmembrane protein and other glycolytic enzymes in MIAPaCa-2 PDAC cells. Additional work stemming from this study will provide novel insights into the role of PKM2 in PDAC and may reveal potential therapeutic targets for selective targeting of PDAC treatment.


**Key Words:** pyruvate kinase M2, PKM2, pancreatic cancer, pancreatic ductal adenocarcinoma, glycolysis, BioID, BirA*, protein-protein interaction

## 5.2 Introduction

Pancreatic ductal adenocarcinoma is one of the most common cancers with the worst patient survival rate of 9 % [1]. As the rate of patient PDAC survival has negligibly improved over the past three decades [1], it is crucial to understand the 'mechanistic vulnerability' of PDAC in order to identify effective therapeutic strategies to improve PDAC patient survival. The majority of PDAC tumour overexpresses oncogenic pyruvate kinase muscle isoform 2 (PKM2) [2] associated with a metabolic shift towards glycolysis (Warburg effect) [3] - a key cancer hallmark [4].

Pyruvate kinase (PK) is the final ATP-generating glycolytic enzyme responsible for converting phosphoenolpyruvate into pyruvate while yielding two ATP molecules per molecule of glucose. Four tissue-selective isoforms of PK are known, including PKL (liver), PKR (erythrocytes), PKM1 (skeletal muscle) and PKM2 (embryonic). Encoded from the same PKM gene, PKM1 and PKM2 are splice variants which exclusively contained either exon 9 or exon 10, respectively. PKM1 is ubiquitously expressed in differentiated cells, including skeletal muscles. In contrast, PKM2 is found in highly proliferative cells, embryonic stem cells as well as cancer cells and some differentiated tissues, including pancreatic islets, adipose tissue and lungs [5].

PKM1 is considered to have high PK activity whereas PKM2 is generally considered to possess lower PK activity. This is because while PKM1 exists as a permanently active tetramer, PKM2 dynamically switches between the inactive monomeric/dimeric states to the active tetrameric state [6]. The active PKM2 tetramer state is stabilized by the presence of allosteric activators (e.g. fructose-1,6-bisphosphate (F1,6BP) and serine) whereas the inactive dimeric state is regulated by post-translational modifications (phosphorylation, acetylation, oxidation) [7]. In highly proliferative cells and cancer cells, a high dimeric:tetrameric PKM2 ratio generates a bottleneck at the terminal end of glycolysis which facilitates the accumulation of biosynthetic glycolytic intermediates required for rapidly dividing cells. However, this is at the expense of ATP which is essential to maintain cellular function and survival. For instance, evidence from mitochondria-lacking erythrocytes suggests that key glycolytic enzymes are present [8] and are anchored to the cell membrane via a transmembrane protein (band-3) [9]. Therefore, it is hypothesized that ATP-generating PKM2 needs to be in close proximity to provide privileged ATP supply to critical ATP consumers.

Our previous findings suggest that glycolytic ATP is required for maintaining PMCA activity in MIAPaCa-2 PDAC cells to prevent $Ca^{2+}$ overload and cell death [10,11]. Furthermore, our previous cell surface biotinylation data revealed the presence of key glycolytic enzymes that likely associated with the cell membrane (e.g. transmembrane protein; results shown in Chapter 4). Therefore, in glycolysis dependent PDAC cells, we hypothesized that PKM2 potentially interacts with cell membrane proteins, likely in close proximity to key cellular ATP consumers such as PMCAs. In order to investigate the potential interaction of PKM2 with cell membrane proteins, the present study used proximity-dependent biotinylation (BioID) technique to screen for potential cell membrane interactions in MIAPaCa-2 PDAC cells. The current study also screened for PKM2 interactions with other canonical glycolytic enzymes and broadly examined the general interacting partners of PKM2 in MIAPaCa-2 PDAC cells. The current

work provides preliminary evidence showing that PKM2 exhibited a significant interaction with a transmembrane protein (voltage-gated K$^+$ channel; KCNH4)) and a canonical glycolytic enzyme (aldolase A; ALDOA). Further studies based on this preliminary work may provide a better understanding of PKM2-cell membrane interactions and if proven to be functionally valid, may represent a novel therapeutic target.

## 5.3 Materials and Methods

**Cell culture** – MIAPaCa-2 cell line was purchased from ATCC and was cultured in DMEM media (D6429, Sigma Aldrich) with added 10% fetal bovine serum and 1% of penicillin/streptomycin (Sigma Aldrich). Cultured cells were maintained in a temperature-controlled incubator at 37°C, 5% $CO_2$ (g). Mycoplasma contaminations were tested using either DAPI staining or PCR.

**Materials and reagents** – All chemical, reagents and materials were obtained from Sigma Aldrich, if not otherwise specified.

**Data mining** – Badea Pancreas (2008) gene chip microarray data sets and TCGA-PAAD Kaplan Meier survival data sets were obtained from www.oncomine.org (ThermoFisher Scientific) and www.proteinatlas.org, version 18.1. All data used in this study were publicly available and were obtained in June 2019.

**Lentiviral plasmids** – Sequences of wild type mPKM2 (catalogue # 42512) and mPKM2-K433E (catalogue # 42514) as well as the -MycBirA*-blue fluorescence protein (BFP) containing lentiviral plasmid vector were obtained and purchased from Addgene (www.addgene.org). Venus-MycBirA*-BFP lentiviral plasmid was a kind gift from Dr Andrew Gilmore, University of Manchester.

**Establishing cell lines stably expressing bait-BirA***

**Plasmid amplification** – NEB® stable competent E. Coli containing lentiviral plasmids encoding either mPKM2-WT, mPKM2-K433E, or Venus fused to Myc-BirA* were grown in LB broth containing 100 µg/ml ampicillin at 37°C, on a shaker, overnight (14-16 hours). DNA plasmids were isolated using QIAGEN Plasmid Midi DNA Purification Kit according to the manufacturer's instructions.

**Lentiviral packaging** – A mixture of non-supplemented DMEM media (serum-free and penicillin/streptomycin free) containing 1x PEI, 4.5 µg PSpax2, 3 µg pMD2G and 6 µg of designated BirA* plasmid was prepared and incubated at room temperature for 30 minutes prior to usage. HEK 293T cells grown to 70% confluence were used for transfection. Culture media was replaced with fresh non-supplemented DMEM media then the cocktail containing the plasmid and lentiviral packaging was added. After overnight incubation, replace the media with DMEM containing 10 mM sodium butyrate for 8 hours then replace the media with normal supplemented DMEM (10% FBS). After a further 48 hours, media containing lentiviral were filtered using a 45 µm PES filter then transferred to a VIVASPIN® tube (Sartorius AG). Lentiviral was concentrated by ultracentrifugation (Beckman Coulter) at 30,000 rcf, 4°C, for 1 hour. Stocks of lentivirus were frozen at -80°C until required.

**Lentiviral transfection** – MIAPaCa-2 cells were seeded at 40% confluence into 6 well culture plates. Polybrene (1:2000 dilution) and 2 drops of harvested lentivirus concentrate were added per well. After 48 hours of lentiviral transfection, viral containing media was replaced with normal culture media. As the plasmid containing bait-MycBirA* also contained BFP, bait-BirA* and BFP were expressed on a 1:1 ratio. Cells were passaged normally over 2-3 weeks, checked for fluorescence expression under the microscope, then sorted for plasmid expression levels using FACs (e.g. blue fluorescence protein).

**BirA\* Bio-identification**

**BirA\* labelling of proximal proteins** – MIAPaCa-2 cells stably expressing either mPKM2-WT, mPKM2-K433E or Venus fused to MycBirA\* were incubated with culture media containing 100 µM biotin for a period of 14-16 hours overnight. Cells were rinsed with Dulbecco's Phosphate-Buffered Saline (DPBS) twice then harvested with modified radioimmunoprecipitation assay (RIPA) buffer (150 mM NaCl, 50 mM Tris, 5mM EDTA, 5 mM EGTA, 1% Triton-X, 0.1% SDS, pH 7.6) supplemented with cOmplete\TM, EDTA-free protease inhibitor cocktail protease inhibitor cocktail and PhosSTOP™. Harvested cells were sonicated and incubated on ice for 30 minutes. Protein concentration was determined using Bradford assay.

**Streptavidin affinity purification** – Biotinylated proteins were enriched by adding 1 mg of each sample lysates were added to individual microtubes containing 100 µl of streptavidin agarose beads (Life Technologies). Samples were mixed using rotatory mixer overnight, at 4°C. Lysate portions unbound to the agarose beads were collected, labelled as "flow-through", and kept aside at -80°C until used. Streptavidin agarose beads were washed, and biotinylated proteins were eluted using 80 µl elution buffer then incubated at 95°C for 5 minutes. Collected samples were labelled as "biotinylated fraction", and then stored at -80°C until used.

**Liquid chromatography-tandem mass spectrometry** – Equal volumes of each biotinylated fraction were loaded into 10 well, 10% Bolt Bis-Tris Plus gels (Thermo Fisher Scientific). Electrophoresis was performed at 200 V, 3 minutes, until the samples ran 0.5-0.8 cm into the gel top, without resolving the band. Gel top samples were then stained by InstantBlueTM gel stain then submitted for LC-MS/MS processing by the University of Manchester Biological Mass Spectrometry facility, using Thermo Orbitrap Elite coupled with Thermo nanoRSLC system (Thermo Fisher Scientific).

**Identification of biotinylated proteins** – LC-MS/MS data obtained were processed and analysed by the University of Manchester Biological Mass Spectrometry facility, using the Mascot database and Progenesis QI Nonlinear Dynamic software. Quantitative LC-MS/MS data were analysed based on the 3 independent sample preparations. The interaction enrichment was determined based on statistical significance ($p<0.05$) and the maximum fold change of mPKM2-BirA\* samples with respect to the Venus-BirA\* controls. Qualitative LC-MS/MS data indicated the confidence of protein identity present in the sample. The unique peptide hit suggests the following: 1 = possible identification, 2-3 = probable identification and ≥4 = almost certain identification. PANTHER (protein analysis through evolutionary relationships) database was used for categorization of identified proteins based on three aspects: 1) biological process (protein associated function), 2) protein class (enzymatic activity and structure), and 3) cell component (cellular localisation).

**Western immunoblotting** – Cells were harvested in RIPA buffer supplemented with cOmplete, EDTA-free protease inhibitor cocktail (Sigma-Aldrich) and lysates were denatured for 5 minutes at 95°C. Protein bands were resolved by electrophoresis using NuPAGE 4-12% Bis-Tris gel (ThermoFisher Scientific). Proteins were transferred onto either nitrocellulose (GE Healthcare Life Sciences) or PVDF membrane (Bio-Rad) using a Trans-Blot® TurboTM blotting system (Bio-Rad). Western immunoblotting was performed using anti-Myc (1:1000, Sigma Aldrich), anti-biotin (1:1000, Sigma Aldrich), PMCA4 (1:1000;

clone JA9, Thermofisher Scientific), PKM2 (1:5000), PFK-L (1:1000), PFK-M (1:1000), PFKFB3 (1:1000), GAPDH (1:2000), Cav-1 (1:2000), and β-Actin (1:5000) primary antibodies were purchased from Cell Signalling Technology. Secondary anti-rabbit (1:2000) and anti-mouse (1:2000-1:5000) antibodies were purchased from Cell Signalling Technology. Protein bands were detected using Clarity Western ECL substrate (Bio-Rad) then imaged and quantified using the ChemiDoc Imaging System (Fisher Scientific).

**Near-infrared (NIF) Western blot detection** – Cells stably transfected with mPKM2-WT, mPKM2-K433E and Venus fused to MycBirA* were either treated with 0.1% DMSO control or 100 μM biotin. Cells were harvested in RIPA buffer supplemented with cOmplete, EDTA-free protease inhibitor cocktail (Sigma-Aldrich) and lysates were denatured at 95 °C, for 5 minutes. Biotinylated proteins were enriched using streptavidin affinity purification. Protein samples in non-biotinylated and biotinylated fractions were resolved by electrophoresis using NuPAGE 4-12% Bis-Tris gel (ThermoFisher Scientific). Proteins were transferred onto either nitrocellulose (GE Healthcare Life Sciences) or polyvinylidene difluoride (PDVF) membrane (Bio-Rad) using a Trans-Blot® TurboTM blotting system (Bio-Rad). Anti-Myc (1:1000, clone 4A6) and anti-biotin (1:1000) primary antibodies were purchased from Sigma Aldrich. Corresponding secondary antibodies, IRDye® 680RD (1:5000) and 800CW (1:5000), were obtained from LI-COR. NIF signals were detected using Odyssey® CLx (LI-COR).

**Immunofluorescences** – MIAPaCa-2 cells stably transfected with mPKM2-WT, mPKM2-K433E and Venus fused to MycBirA* were either treated with 0.1% DMSO control or 100 μM biotin. Cells were fixed with 4% paraformaldehyde and incubated with either anti-Myc (1:400) or anti-biotin/streptavidin (1:400) primary antibody overnight. Corresponding Alexa Fluor 488 (1:400) and 594 (1:400) secondary antibodies were obtained from Thermo Fisher Scientific. Images were obtained using a Zeiss Axioimager.D2 upright microscope using a 63x / 1.4 Plan Apochromat (Oil, DIC) objective and captured using a Coolsnap HQ2 camera (Photometrics) through Micromanager software v1.4.23. Specific bandpass filter sets for FITC and Texas red were used to prevent bleed-through from one channel to the next. Images were then processed and analysed using Fiji ImageJ (http://imagej.net/Fiji/Downloads).

**Statistical analysis** – Prism 7 software (GraphPad) was used for some graphing and statistical data analysis. Progenesis QI Nonlinear Dynamic software was used for quantitative LC-MS/MS small molecule discovery analysis. Proteins identified by quantitative LC-MS/MS were analysed for statistical significance using one-way ANOVA and data are presented as the mean of 3 independent samples ± standard error of means (SEM). Qualitative LC-MS/MS data only indicated the potential presence of the protein identified and therefore, no statistical analysis was performed (N=1). Statistical significance is defined as $p < 0.05$.

## 5.4 Results

### 5.4.1 PKM2 overexpression in PDAC tumours is correlated to poor PDAC patient survival

Elevation of the PKM gene, encoding for PKM1 and PKM2 protein expression, has been previously linked to poor PDAC patient survival [12]. Overexpression of PKM2, in particular, had been associated with a malignant shift towards aerobic glycolysis (Warburg effect) in multiple cancers [3]. To determine whether PKM2 overexpression is clinically relevant in PDAC, data mining from publicly available databases including Oncomine [13,14] and the Human Protein Atlas [15,16] was carried out.

Using Oncomine.org database, Badea *et al.* (2008) gene chip microarray data showed that PKM gene expression is elevated in PDAC tumour by 1.48-fold (n=39, p<0.0001, Figure 5.1A) in comparison to resected healthy tissue from the tumour margin [13,14]. Moreover, patient survival data obtained from the cancer genomic atlas - pancreatic adenocarcinoma cohort (TCGA-PAAD) through the Human Protein Atlas database revealed that PKM overexpression is significantly correlated to poor PDAC patient survival [15,16]. PDAC patients were divided into two groups depending on the low or high PKM expression of the resected tumour. Kaplan-Meier survival curve suggested high tumour expression of PKM resulted in a significantly lower PDAC patient survival (hazard ratio= 1.60, n=88, p<0.025, Figure 5.1B). This indicates that the elevation of PKM gene is a clinical characteristic of malignant PDAC tumours and is linked to poor PDAC patient survival.
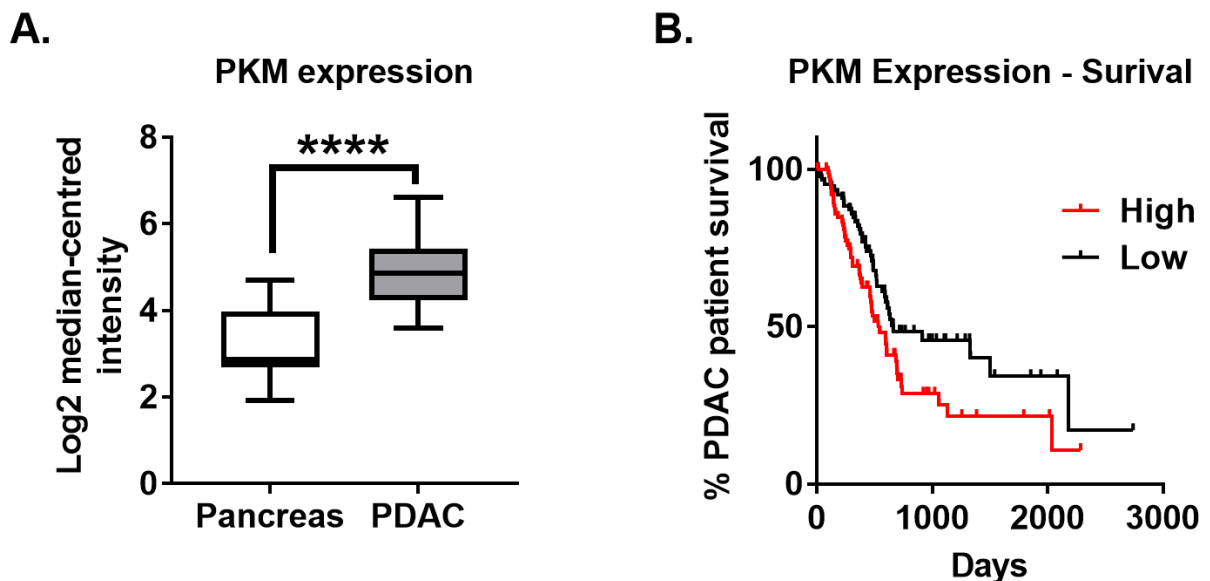


**Figure 5.1 – Overexpression of PKM gene in PDAC tumour is correlated to poor patient survival.** Badea Pancreas (2008) gene chip microarray data, comparing resected PDAC tumour and healthy pancreatic tissue obtained from matching tumour margin (n=39), was obtained from Oncomine open-source database (June 2019, www.oncomine.org). **A,** Comparison of PKM gene expression in healthy pancreatic tissue (n=39) and PDAC tumour (n=39) is shown as individual Log2 median-centre intensity of PKM gene expression. **B,** PDAC patient survival data was sourced from TCGA-PAAD (n=176), through The Human Protein Atlas database (June 2019, www.proteinatlas.org). 176 PDAC patients in the TCGA-PAAD cohort was divided into two groups based on the median-centred gene expression (fragments per kilobase of transcript per million mapped reads; FPKM) into either low or high PKM gene expression. The survival outcomes of each group were compared using the log-rank test. Kaplan-Meier curves correlating the survival of PDAC patients to the low (black) or high (red) expression of the PKM gene.

## 5.4.2 Establishing MIAPaCa-2 PDAC cells stably expressing mouse-derived mPKM2-BirA* fusion protein

Our previous studies showed that the activity of plasma membrane $Ca^{2+}$ ATPases (PMCAs) in MIAPaCa-2 PDAC cells is dependent on glycolytic-ATP [10,11]. Furthermore, glycolytic enzymes were found in cell surface membrane biotinylation fractions (Supplementary Figure 5.1), suggesting that at least a sub-population of PKM2 and possibly other glycolytic enzymes may be associated with plasma membrane protein(s) where they may provide a privileged ATP supply to the ATP consuming pumps (e.g. PMCA4). As the key oncogenic and ATP-generating glycolytic enzyme, the potential interactions of PKM2 with the plasma membrane protein of PDAC cells may be therapeutically important. This is because the identification of such a protein potentially means that novel drugs could be designed to disrupt the binding of PKM2 with the cell membrane, cutting off the glycolytic ATP supply to ATP consumers. Such a strategy may be selective for PDAC cells that are highly dependent on glycolytic ATP.

The current study employed bio identification (BioID) technique to identify PKM2 protein interactions in MIAPaCa-2 PDAC cells. BioID technique generally involves the expression of a designated bait protein fused with a mutant R118G Escherichia coli biotin ligase (BirA*). As described in Figure 5.2, in the presence of biotin, BirA* fusion proteins would generate a short-lived reactive biotinyl-5' AMP which would promiscuously biotinylate proteins within ~10-20 nm distance of the bait [17,18]. Our experimental strategy involved stably expressing a mouse-derived wild-type PKM2 (mPKM2) bait or a constitutively active PKM2 mutant (mPKM2-K433E) bait fused to BirA* containing a myc-tagged epitope in MIAPaCa-2 cells. The PKM2 mutation at the phosphotyrosine binding site, achieved by replacing the lysine 433 residue with glutamate [19,20], was employed to investigate whether the active tetrameric and inactive dimeric PKM2 exhibited different binding interactions. To ensure that BirA* selectively biotinylates protein specific to the bait, cells stably expressing Venus yellow fluorescent protein fused to BirA* were used as a non-targeting control (Venus).

Plasmids containing either mPKM2, mPKM2-K433E or non-targeting Venus fluorophore fused to myc-BirA* were transfected into MIAPaCa-2 PDAC cells using lentivirus (Figure 5.3A-B). Since the plasmid used for the bait-BirA* expression also co-expressed mTagBFP under the same EF1a promoter, the bait-BirA* and mTagBFP should be equally expressed at a 1:1 ratio. Therefore, equivalent expressions of each bait-BirA* could be selected through BFP expression via fluorescence-activated cell sorting (FACS) (Figure 5.3C).
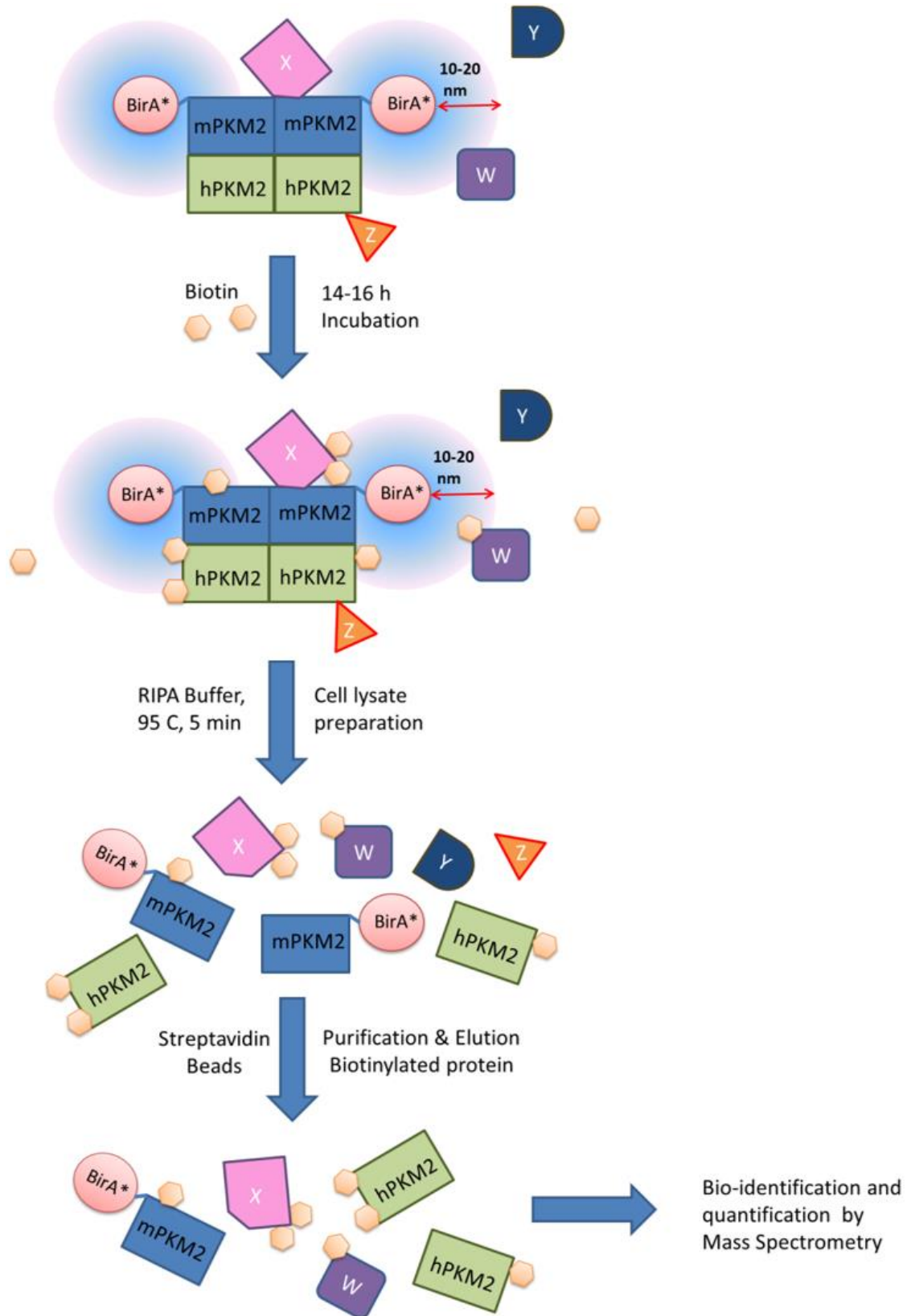
**Figure 5.2 –Bio-identification assay using mPKM2-BirA\*.** MIAPaCa-2 PDAC cells stably expressing mPKM2-BirA\* proteins were incubated with 100 µM biotin for 14-16 hours. Proteins interacting with mPKM2-BirA\* within the proximity of 10-20 nm will be biotinylated via BirA\*. Biotinylated proteins were separated by incubation with streptavidin agarose beads and which allowed further qualitative or quantitative bio-identification using mass spectrometry. W-Z, indicates unknown proteins near PKM2; mPKM2 = mouse-derived PKM2; hPKM2 = inherently expressed human PKM2
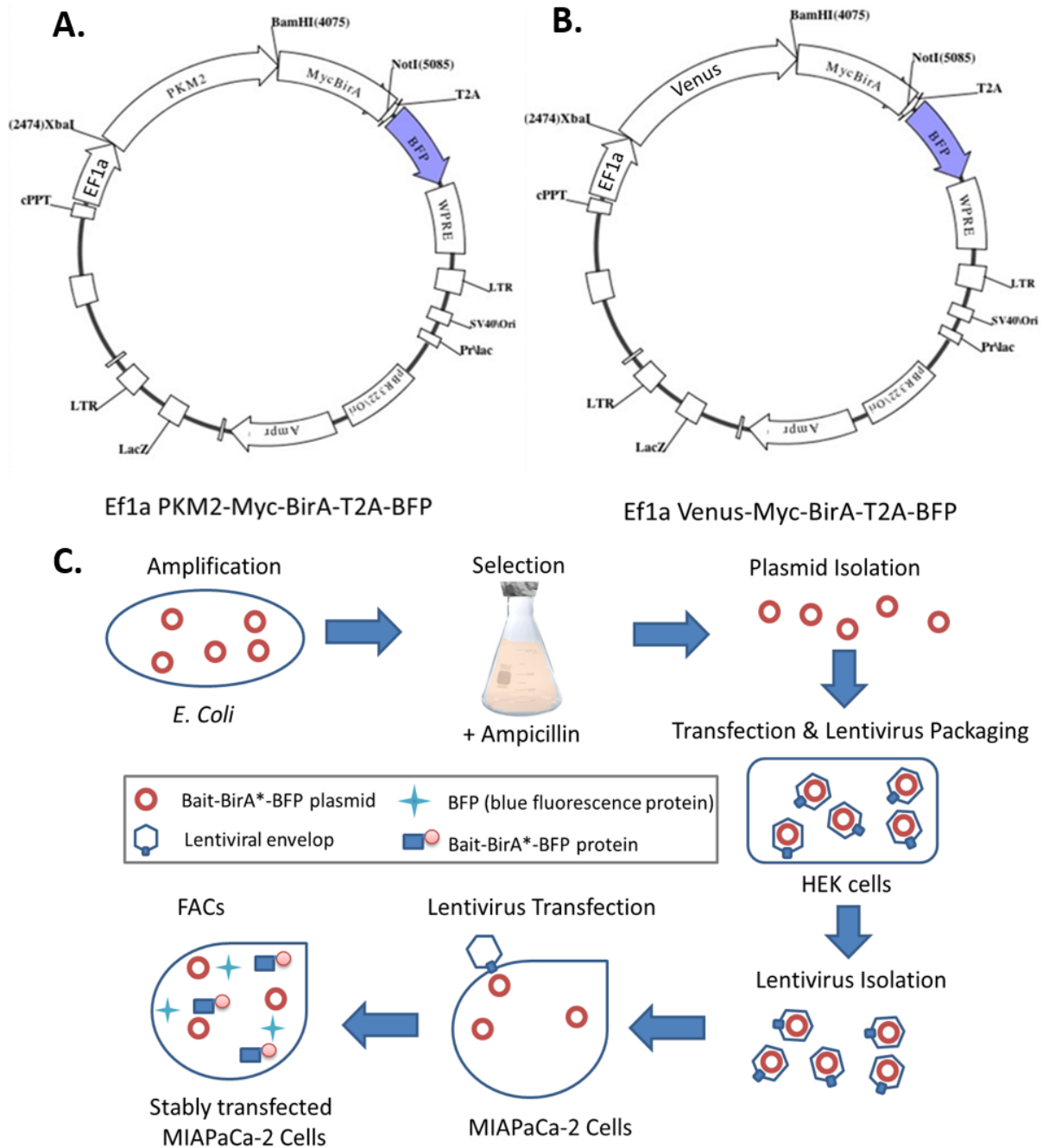
**Figure 5.3 – Plasmid construct designs and establishing stably transfected MIAPaCa-2 PDAC cell line. A-B,** Diagram depicts Myc-tagged BirA* plasmid construct containing either **A,** PKM2-wild type (mPKM2-WT; W) and PKM2-mutant (mPKM2-K433E; M), or **B,** non-specific Venus fluorophore (Venus; V). **C,** Steps required to established stably transfected MIAPaCa-2 cells using lentivirus. Transfection process includes amplification of plasmid in *E. Coli,* selection with ampicillin, plasmid isolation, lentivirus packaging in HEK cells, isolation of lentivirus containing plasmid, transfection of lentivirus into MIAPaCa-2 cells and selecting successfully transfected cells using FACs. Abbreviations: PKM2= pyruvate kinase muscle isoform 2; MycBirA*=Myc-tagged BirA*; BamHI=restriction enzyme site; NotI=rare restriction enzyme site; T2A=self-cleavage sequence; BFP=blue fluorescence protein; WPRE=Woodchuck hepatitis virus posttranscriptional regulatory element; LTR = long terminal repeat promoter; SV40\Ori=origin of replication; Pr\Lac = lytic promoter; pBR332\ori = origin of replication; Ampr= ampicillin resistance gene; LacZ = promoter; cPPT=central polypurine tract; EF1a=promoter; Xbal=restriction site. (Refer to Supplementary Table 5.1 for further vector component description)

### 5.4.3 Validation of MIAPaCa-2 PDAC cells stably expressing mouse-derived mPKM2-BirA* fusion protein

To confirm the bait-BirA* expression post-transfection, the expression of myc-tagged BirA* was detected by immunofluorescence (Figure 5.4A) and near-infrared western immunoblotting using anti-Myc antibody (Figure 5.4B). To confirm biotinylation of protein by BirA*, transfected cells were treated with 100 µM biotin for 12-16 hours then biotinylated proteins were probed using anti-biotin antibody. Immunofluorescence results showed that myc-tags were present in cell lines stably expressing mPKM2-WT, mPKM2-K433E and Venus control, indicative of successful bait-BirA* fusion protein expression (Figure 5.4A). Cells not treated with biotin (negative control) had minimal basal anti-biotin signal, suggesting that BirA* was incapable of biotinylating proteins without exogenous biotin. In contrast, apparent anti-biotin signals were detected after cells were treated with 100 µM biotin. This suggests that myc-tagged BirA* associated with all baits (mPKM2-WT, mPKM2-K433E and Venus) were functional and were capable of biotinylating other proteins in the presence of biotin.

To determine whether myc-tagged BirA* is associated with the bait proteins, Western immunoblotting of Myc and biotinylated proteins was performed (Figure 5.4B). Streptavidin beads were used to purify and enrich biotinylated proteins. In the streptavidin bead purified fraction (biotinylated fraction), both anti-Myc and streptavidin (anti-biotin) antibodies revealed similar molecular weight bands at approximately 70 and 100 kDa which corresponds to Venus-BirA* and mPKM2-WT-BirA*, respectively. Moreover, biotin treated cells purified with streptavidin beads show an additional band at 100 and 130 kDa which corresponds to Venus-BirA*-BFP and mPKM2-WT-BirA*-BFP, respectively. It should be noted that basal biotinylation was detected in non-transfected MIAPaCa-2 cells whereas Myc tagged proteins were not detected.

Taken together this suggests that PKM-2-WT, mPKM2-K433E, and Venus fused to Myc-tagged BirA* were successfully expressed and the BirA* expressed was able to initiate protein biotinylation in the presence of added biotin.
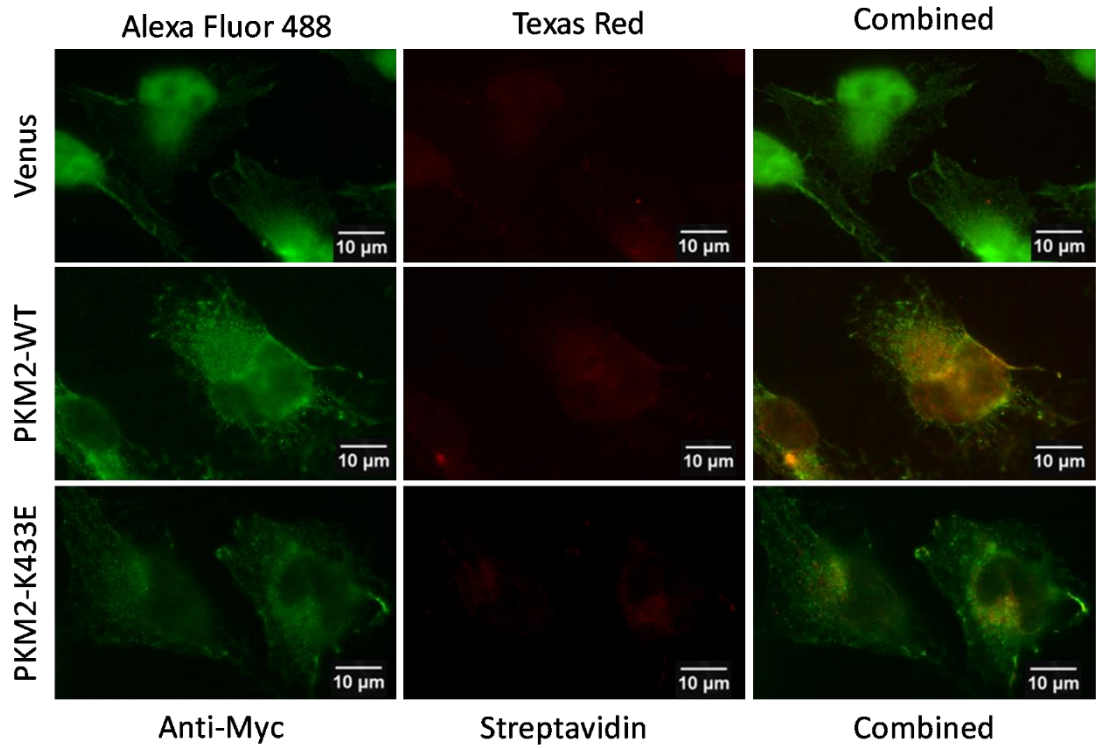
## A(i).     Labelled (-) Biotin
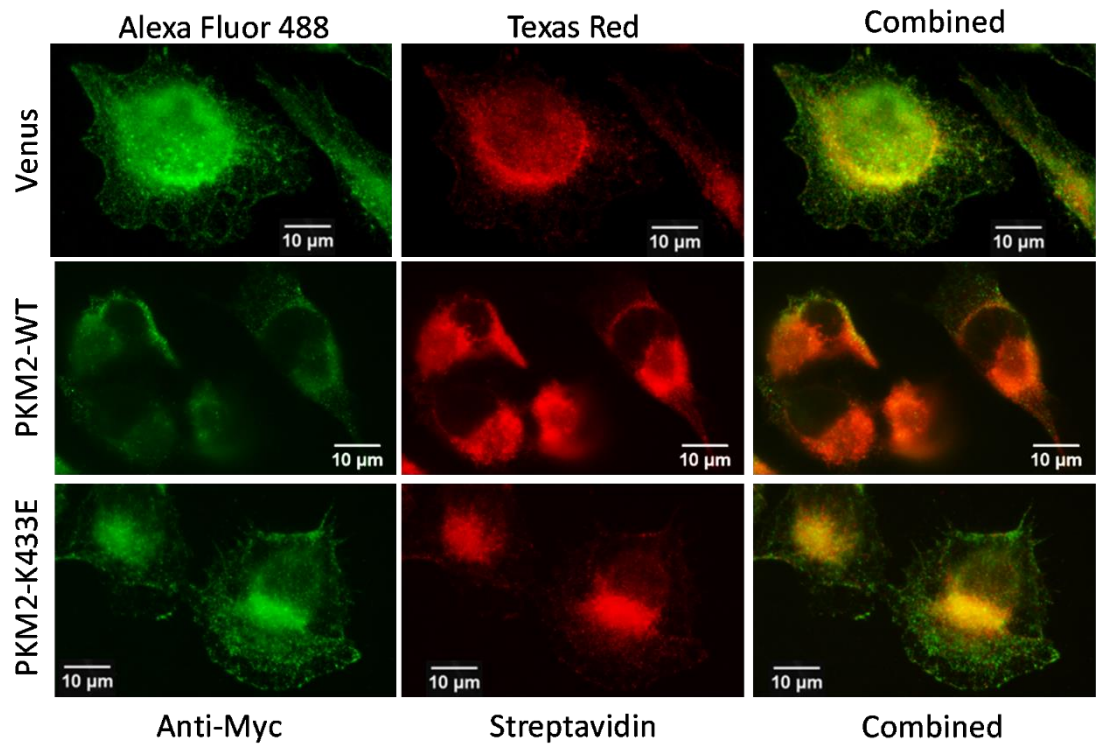


**Figure 5.4 – Validation of plasmid transfection and BirA* activity.** (Continued next page)
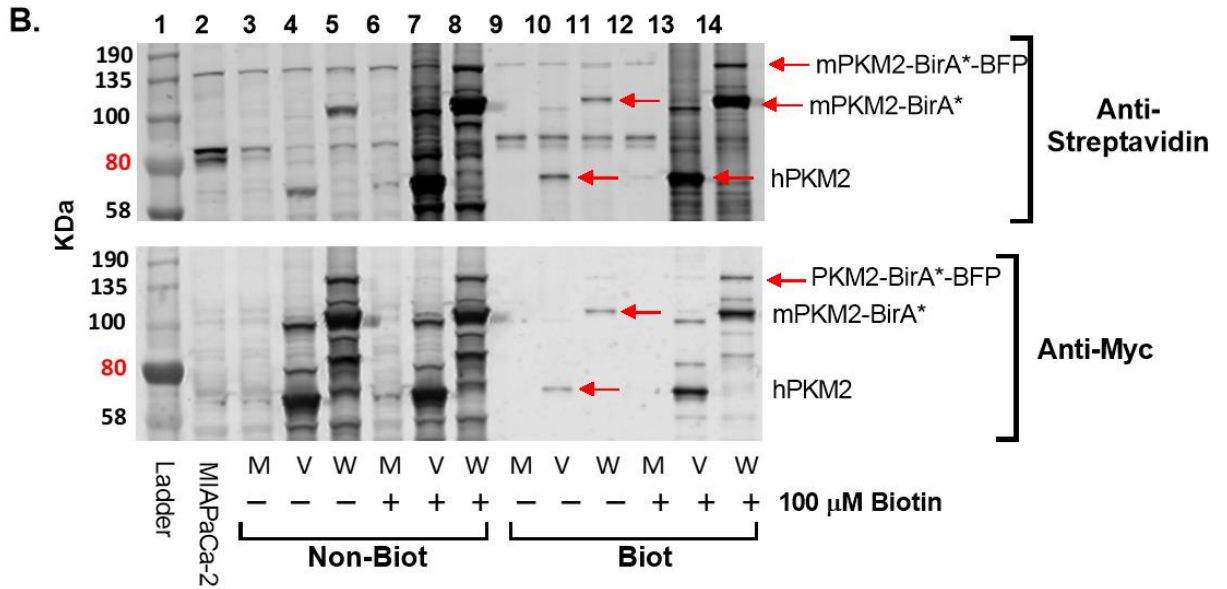
**Figure 5.4 Continued – Validation of plasmid transfection and BirA\* activity.** After lentiviral transfection, ampicillin selection and FAC sorting, stably transfected MIAPaCa-2 cells were validated for plasmid expression using anti-biotin and anti-Myc primary antibodies to detect biotin and Myc tag, respectively. Venus (control), mPKM2-WT, and mPKM2-K433E stably transfected cell lines were either not treated (control) or treated with 100 μM biotin overnight to validate transfected BirA\* activity. **A,** Immunofluorescence staining of Myc-tag (green), biotin (red) and merged (green and red overlay) images, at 63x magnification, are shown. **B,** Biotinylated proteins in both non-treated (–) and biotin treated (+) of non-transfected MIAPaCa-2 and stably transfected cell lines were purified using streptavidin beads. Proteins were detected by Near-infrared fluorescence imaging detection of biotin and Myc-tag in non-transfected MIAPaCa-2 control, a non-biotinylated fraction (Non-Biot), and a biotinylated fraction (Biot). Red arrows are indicative of bands with molecular weight which corresponds to hPKM2, mPKM2-BirA\* and mPKM2-BirA\*-BFP at 60, 99 and 125 kDa, respectively. PKM2=phosphokinase M isoform 2; MycBirA\*=Myc-tagged BirA\*

### 5.4.4 Endogenous human PKM2 and other glycolytic enzymes in PDAC cells are biotinylated by both mPKM2-BirA* and Venus-BirA*

Although the molecular weights of the myc-tagged BirA* corresponds to the predicted molecular weight of the PKM2 bait, further confirmation was required to demonstrate that PKM2 was indeed fused to BirA* (mPKM2 -BirA*) through Western immunoblot of PKM2 protein (Figure 5.5A). Both untreated and biotin treated mPKM2-BirA* cells had three prominent PKM2 bands at 60, 99 and 125 kDa which corresponds to endogenous hPKM2, mPKM2-BirA* and mPKM2-BirA*-BFP, respectively. After streptavidin bead purification, only biotin treated mPKM2-WT-BirA* expressing cells demonstrated biotinylation of endogenous hPKM2 whereas the untreated control showed negligible biotinylation. This suggests that the mPKM2-BirA* expressed was capable of interacting, and likely forming complexes, with the endogenous human PKM2 in the MIAPaCa-2 PDAC cells. In contrast, Venus-BirA* samples expressed native PKM2 but no apparent biotinylation of PKM2 was observed after streptavidin bead enrichment. This indicates that the non-specific Venus bait interacted less with PKM2, making Venus a suitable control for randomized BirA* biotinylation.

Puchulu-Campanella et al. (2013) proposed that a membrane-associated glycolytic metabolon exists in order to provide a privileged ATP supply for the plasma membrane ATPases in red blood cell [8]. Similarly, the current study hypothesized that PKM2 may potentially interact with other glycolytic enzymes in PDAC cells. A panel of key glycolytic enzymes, caveolae-1 (Cav-1) surface membrane marker and PMCA4 in PDAC cells were screened using Western immunoblot (Figure 5.5B). We found that the mPKM2-WT-BirA* biotinylated key glycolytic enzymes including the endogenous human PKM2, phosphofructokinase-liver isoform (PFK-L) and glyceraldehyde 3-phosphate dehydrogenase (GAPDH). However, as Venus-BirA* was also found to biotinylate PFK-L, PFK-muscle isoform (PFK-M) and GAPDH, this suggested that these GEs were likely abundantly expressed in MIAPaCa-2 cells.

Contradicting our hypothesis, Cav-1 and PMCA4 were not biotinylated by either mPKM2-WT-BirA* and Venus-BirA*expressing cells. This suggests that either: i) both mPKM2 and the Venus baits did not interact with these surface membrane proteins screened, or ii) Western immunoblotting was not sensitive enough to detect this interaction. The protein detection limit of Western immunoblot is dependent on multiple factors including: i) the protein transfer efficiency, ii) primary/secondary antibodies binding efficiency, iii) the sensitivity of enhanced chemiluminescence (ECL) substrate used, and iv) sensitivity of chemiluminescence detection method used. Moreover, Western immunoblot is low throughput method unsuitable for broad sample screening. Therefore, a more rigorous method, capable of high-throughput bio-identification was required to examine interaction enrichments in mPKM2-BirA* versus the non-specific Venus-BirA* control.
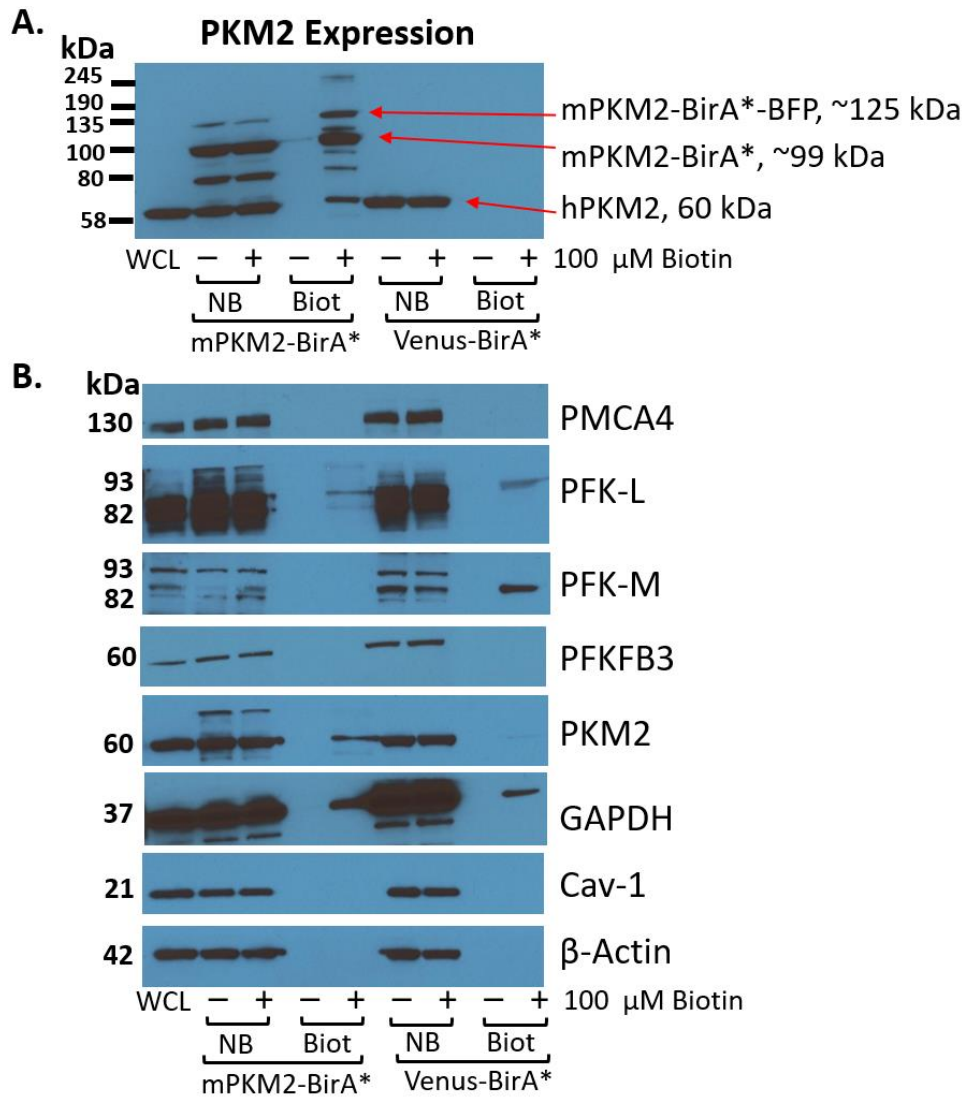
**Figure 5.5 – Biotinylation screening of cell surface membrane and glycolytic enzymes using Western immunoblot.** MIAPaCa-2 stably transfected with mPKM2-BirA* (mPKM2) and non-specific Venus- BirA* (Venus) were either non-treated (–) or 100 µM biotin (+). Biotinylated proteins were purified using streptavidin beads overnight. Non-streptavidin bound proteins were classified as non-biotinylated (NB) and streptavidin bead-associated proteins were biotinylated (Biot) protein fraction. A whole-cell lysate (WCL) was provided to demonstrate endogenous expression of proteins in the sample prior to streptavidin affinity purification. Western immunoblot of **A,** PKM2 is shown. Red arrows are indicative of bands with molecular weight which corresponds to hPKM2, mPKM2-BirA* and mPKM2-BirA*-BFP at 60, 99 and 125 kDa, respectively. **B,** Western immunoblot screening of target proteins, including: PMCA4, PFK-L, PFK-M, PFKFB3, PKM2, GAPDH, Cav-1, and β-Actin.

### 5.4.5 Bio-identification of protein interacting partners and biological processes enriched in mPKM2-BirA* in comparison to the non-targeting Venus control

Although we previously showed that mPKM2-BirA* biotinylated other glycolytic enzymes through Western immunoblot, the screening throughput was low and the enrichment in mPKM2 vs Venus could not be compared. To quantitatively examine the PKM2 interactome in PDAC cells, biotinylated proteins from mPKM2-BirA* and Venus-BirA* were compared using mass spectrometry. All proteins identified using the Ingenuity Pathway Analysis (IPA) database were classified according to gene name then categorized according to their associated canonical pathway. Three independent sets of mPKM2 -BirA* and Venus-BirA* cells were used for data analysis.

A list of 1387 proteins was identified through quantitative mass spectrometry (LC-MS/MS), out of which 1106 proteins were present in both samples and could be compared for biotinylated proteins enriched in mPKM2-BirA* and Venus-BirA* control samples. To identify PKM2-associated protein interaction enrichments in PDAC cells, mPKM2 interaction partners were compared with respect to the non-specific Venus control. Using IPA ingenuity, 72 out of 509 identified targets were found to be significantly enriched in mPKM2-BirA* compared to the Venus-BirA* control (mPKM2>Venus, $p<0.05$; Supplementary Table 5.2). The current study focuses on comparing significantly enriched "proteins" of mPKM2 versus Venus control (mPKM2>Venus; $p<0.05$) and is primarily interested in PKM2 protein-protein interactions with membrane-associated proteins.

Comparing the biotinylated proteins in mPKM2 to the Venus samples, the IPA database suggested that the top 5 significant canonical pathways associated with PKM2 protein-protein interactions in PDAC were: 1) DNA methylation, 2) cell cycle control, 3) DNA double-strand break repair, 4) glycolysis and 5) caveolar mediated endocytosis (Figure 5.6A). Based on this initial analysis, we screened all identified targets significantly enriched in mPKM2-BirA (mPKM2>Venus, $p<0.05$) and Venus-BirA (Venus>mPKM2, $p<0.05$) samples using PANTHER (Protein ANalysis THrough Evolutionary Relationships database) to further categorized the significantly enriched proteins according to their cellular location (cellular components) and associated biological processes (Figure 5.6B-D). Interestingly, PANTHER identified KCNH4 (voltage-gated $K^+$ channel, subfamily H, member) as the single plasma membrane protein. Moreover, KCNH4 is a subunit of voltage-gated $K^+$ channel – a transmembrane protein primarily localised at the cell plasma membrane [21], suggesting that KCNH4 may be the plasma membrane interacting partner of PKM2. Consistent with the other IPA results, PANTHER database categorization revealed that mPKM2 interacted more with cytoskeletal proteins, nucleic acid binding proteins and enzyme modulators. mPKM2 also interacted frequently with organelle-specific proteins and complex associated proteins as well as proteins associated with metabolism, biogenesis, and cellular regulation.

Based on the maximal fold change of proteins enriched in mPKM2>Venus, the top 10 proteins significantly enriched in mPKM2-BirA* samples were identified as shown in Table 5.1. Interestingly, KCNH4, the only transmembrane protein identified, was enriched by 38-fold and was identified as the 9th most enriched protein in mPKM2 samples in comparison to Venus control. Out of the top 10 most enriched mPKM2 interacting partner, two proteins were found to be mitochondrial-linked. Ranked 1st in

terms of PKM2 interaction enrichment, COQ6 (Coenzyme Q6, monooxygenase) is a conserved mitochondrial monooxygenase required for the biosynthesis of ubiquinone (coenzyme Q10) – a critical electron transport chain moiety essential for mitochondrial oxidative phosphorylation [22]. Another mitochondrial linked protein, MRPL23 (mitochondrial ribosomal protein L23, isoform CRA_a) was ranked 5th on the mPKM2>Venus enrichment list. MRPL23 plays a role in mitochondrial protein biosynthesis [23]. These enriched interactions of PKM2 with mitochondrial linked protein may hint at a potential regulatory relationship between glycolysis and the mitochondria.
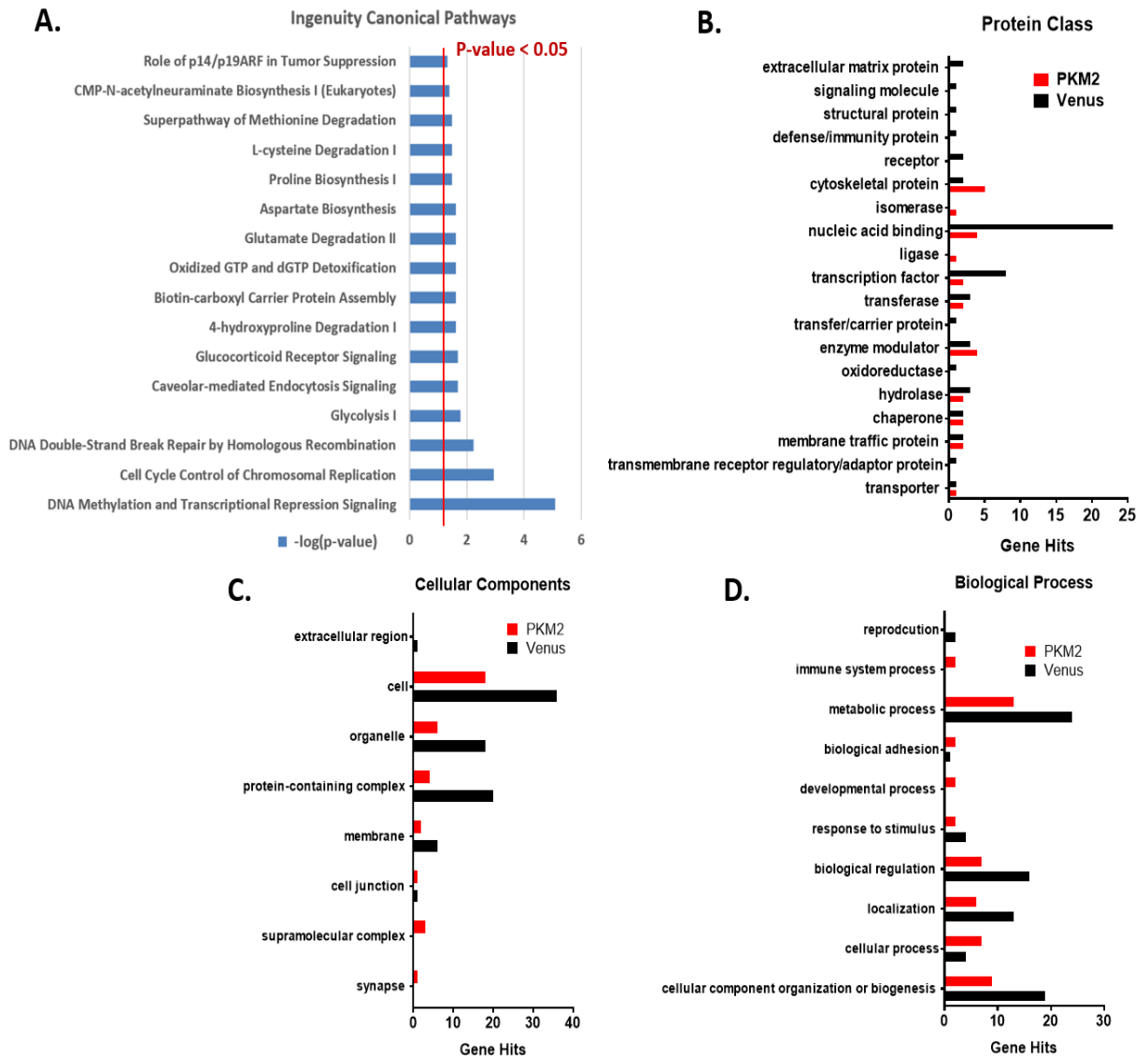


**Figure 5.6 – Bio-identification categorization of enriched processes associated with PKM2 in comparison to Venus BirA\*.** MIAPaCa-2 stably transfected with mPKM2-WT (PKM2) and non-specific Venus (Venus) BirA* constructs were treated with 100 µM biotin overnight then biotinylated proteins were purified with streptavidin beads. Biotinylated proteins were identified using quantitative mass spectrometry. Bio-identification results were analysed using Ingenuity Pathway Analysis to yield **A**, Canonical pathways of proteins interactions enriched in mPKM2>Venus, data expressed as -log (p-value). Significant protein interaction (p<0.05) results identified were further analysed using Panther version 14.1. Proteins were identified by gene name and were classified according to **B,** protein class, **C,** cellular components, and **D,** biological process. Data are expressed as a number of individual genes identified (gene hits). N=3. Statistical significance, defined as p<0.05, was determined using one-way ANOVA.

| Gene ID | Protein Name | Max fold change WT>V | ANOVA (p-value) | Functional Role | Ref |
|---|---|---|---|---|---|
| COQ6 | Ubiquinone biosynthesis monooxygenase COQ6, mitochondrial | 688.27 | 9.36E-03 | biosynthesis of ubiquinone (Coenzyme Q10), required for electron transport chain | [22] |
| PPP1R10 | Serine/threonine-protein phosphatase 1 regulatory subunit 10 | 282.09 | 7.05E-04 | regulator of phosphatase 1, involved in cell cycle progression, DNA repair and apoptosis | [24] |
| ACACA | Acetyl-CoA carboxylase 1 | 150.23 | 1.05E-04 | ATP-dependent enzyme involved in the rate-limiting step of fatty acid synthesis | [25] |
| PKM | Pyruvate kinase PKM | 123.33 | 3.78E-04 | key ATP-generating glycolytic enzymes which participate in various moonlighting functions | [19] |
| MRPL23 | Mitochondrial ribosomal protein L23, isoform CRA_a | 105.93 | 7.7E-06 | mitochondrial protein synthesis biosynthesis | [23] |
| HSPA4 | Heat shock 70 kDa protein 4 | 78.49 | 9.01E-05 | ATP-dependent molecular chaperone which assists protein folding and transport | [26,27] |
| POLE | DNA polymerase epsilon catalytic subunit A | 67.33 | 2.61E-03 | a catalytic subunit of DNA polymerase ε, required for DNA replication and repair | [28] |
| PCLO | Protein piccolo | 53.22 | 3.37E-03 | vesicle trafficking, often associated with active synaptic zone; $Ca^{2+}$sensor | [29] |
| KCNH4 | Potassium voltage-gated channel subfamily H member 4 | 38.24 | 9.3E-05 | transmembrane protein regulation of insulin secretion, muscle contraction and cell volume | [21] |
| PACS1 | Phosphofurin acidic cluster sorting protein 1, isoform CRA_a | 28.16 | 1.03E-03 | associated to the localization of trans-Golgi network (TGN) membrane proteins | [30] |

**Table 5.1 – Top 10 proteins enriched in mPKM2-BirA\* samples in comparison to Venus-BirA\* control.**

As an ATP-producing protein, it was interesting that the top 10 PKM2 interaction enrichments also included ATP-dependent proteins involved in biosynthesis (ACACA, acetyl-CoA carboxylase 1), transportation/trafficking (HSPA4, heat shock protein 4; PCLO, protein piccolo; PACS1, phosphofurin acidic cluster sorting protein 1) and cell cycle (PPP1R10, serine/threonine-protein phosphatase 1 regulatory subunit 10; POLE, DNA polymerase epsilon catalytic subunit A). Another interesting observation from this screening was the interaction of mPKM2-BirA* with other canonical glycolytic enzymes. mPKM2-WT-BirA* interacted with endogenous human PKM (encoding either PKM1 or PKM2) by 188-fold, suggesting that mPKM2 could potentially form polymeric structures with inherent human PKM2 (hPKM2). The only non-bait canonical glycolytic enzyme significantly enriched in mPKM2-WT-BirA* by 3.65-fold was ALDOA (fructose-bisphosphate aldolase A) – the enzyme involved in the fourth step of glycolysis (Figure 5.7A and Table 5.2). GOT2, encoding glutamic-oxaloacetic transaminase-2, which plays an important role in the tricarboxylic acid cycle (TCA) cycle and glycolysis, was also found to be enriched in mPKM2-WT samples by 13.5-fold with respect to Venus control.

PKM2 has been demonstrated to play several "moonlighting" functions [31–33]. In addition to glucose metabolic processes, PKM2 also interacted with 13 proteins involved with cell cycle regulation (Figure 5.7B and Table 5.2). The top 3 PKM2-cell cycle protein interactions were POLE (DNA polymerase Epsilon catalytic subunit A), PSMD2 (Proteasome 26S Subunit Non-ATPase 2) and SYNE2 (Spectrin Repeat Containing Nuclear Envelope Protein 2). PKM2 also interacted with 28 proteins associated with biogenesis/metabolic processes (Figure 5.7C and Table 5.2). These 28 proteins associated to biogenesis/metabolism were localised to the nucleus (50%), cytosol (44%) and mitochondria (9%), indicating the dynamic and ubiquitous role of PKM2 in cellular process regulation.

However, it should be noted that the Venus-BirA* robustly biotinylated more protein hits than mPKM2-WT-BirA* in all PANTHER categorized processes (Figure 5.6B-D), potentially adding more noise/background to the data. This made it relatively difficult to discern 'significant enrichment' of mPKM2-BirA* interaction partner, potentially favouring false negatives. For instance, although 509 proteins were found to be enriched in mPKM2-WT samples in comparison to Venus samples, only 70 proteins were significantly enriched. However, although some proteins identified had shown 2 to 8-fold of enrichments, these other 438 proteins were not statistically significant.

Taken together, mPKM2-BirA* exhibited enriched interactions with plasma membrane protein KCNH4, other glycolytic enzymes as well as proteins associated with cell cycle and biogenesis/metabolism. PKM2 ubiquitously interacted with proteins localised in multiple sites of the cells including the cytosol, nucleus and organelles. As non-targeting Venus control was used for comparison of mPKM2 interaction, we were able to discern mPKM2 selective enrichment from random cytosolic biotinylation. However, the high degree of biotinylated proteins detected by Venus-BirA* likely led to an underestimation of the mPKM2-specific protein enrichments identified. This suggests that Venus does not represent the most appropriate control and may lead to an underestimation of bona fide PKM2-binding proteins.
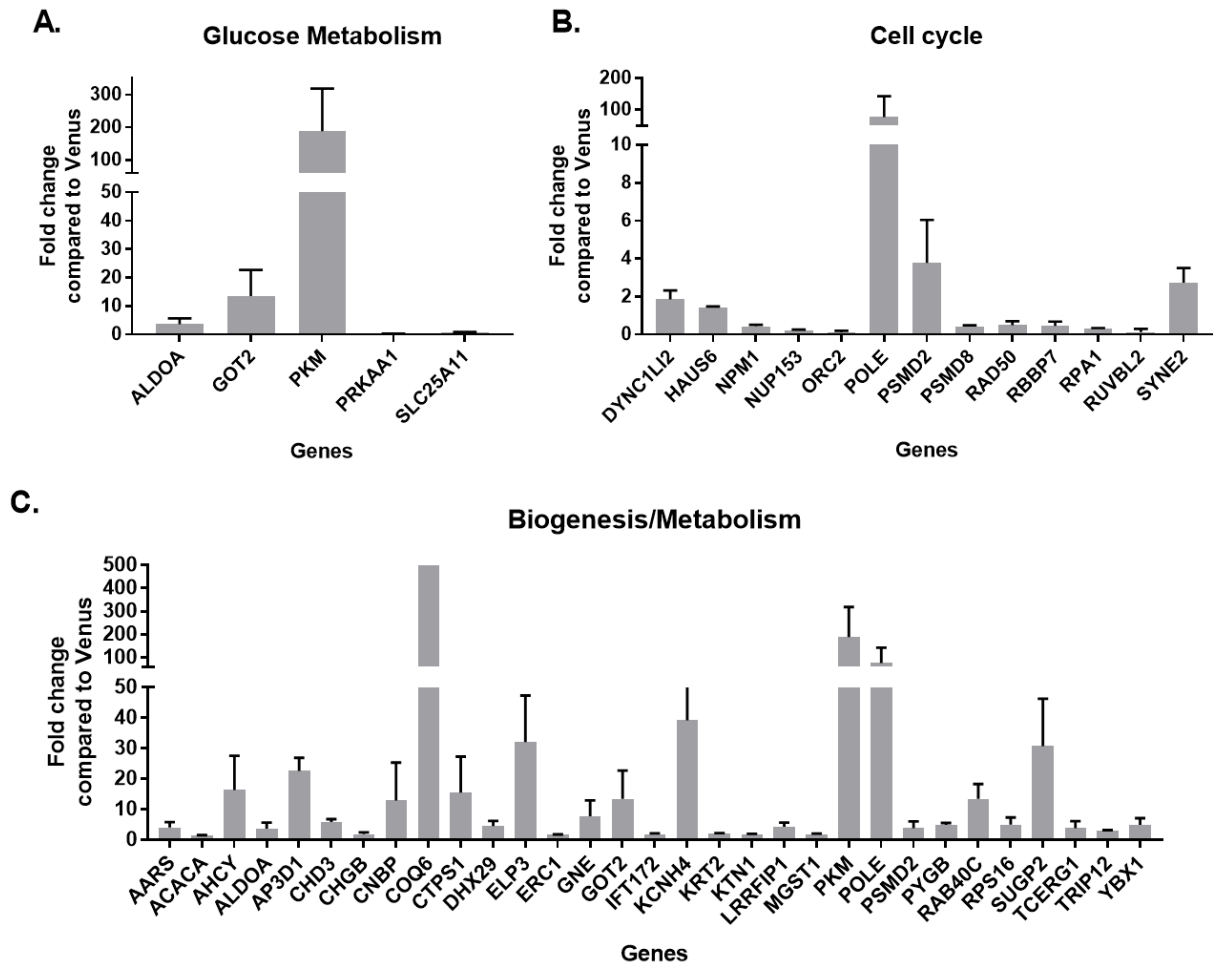
**Figure 5.7 – Enrichment of protein interaction in mPKM2-Wildtype with respect to non-specific Venus control.** MIAPaCa-2 cells were stably transfected with mPKM2-BirA* and non-targeting Venus-BirA*. Biotinylated proteins were identified using mass spectrometry. Biotinylated proteins were identified using gene name and further classified using Panther version 14.1. Significant protein interaction enrichments in mPKM2-WT with respect to Venus control associated with **A,** metabolism, **B,** glucose metabolism, and **C,** cell cycle are shown. Gene names listed are explained in Table 5.2. Data are expressed fold change of mPKM2-WT enrichment in comparison to Venus control. N=3, data are shown as mean ± SEM.

| Gene name | Protein name | Fold Change of WT compared to Venus | | | |
|---|---|---|---|---|---|
| | | N1 | N2 | N3 | Mean |
| **Glucose metabolism** | | | | | |
| ALDOA | Fructose-bisphosphate aldolase A | 2.90 | 5.96 | 2.09 | 3.65 |
| GOT2 | Aspartate aminotransferase, mitochondrial | 15.75 | 21.34 | 3.26 | 13.45 |
| PKM | Pyruvate kinase PKM | 193.74 | 315.72 | 54.68 | 188.05 |
| PRKAA1 | 5'-AMP-activated protein kinase catalytic subunit alpha-1 | 0.06 | 0.11 | 0.39 | 0.19 |
| SLC25A11 | Mitochondrial 2-oxoglutarate/malate carrier protein | 0.90 | 0.80 | 0.71 | 0.80 |
| **Cell cycle** | | | | | |
| DYNC1LI2 | Dynein, cytoplasmic 1, light intermediate chain 2, isoform CRA_a | 1.59 | 2.40 | 1.56 | 1.85 |
| HAUS6 | HAUS augmin-like complex subunit 6 | 1.35 | 1.40 | 1.48 | 1.41 |
| NPM1 | Nucleophosmin isoform 2 (Fragment) | 0.50 | 0.34 | 0.46 | 0.43 |
| NUP153 | Nucleoporin 153kDa, isoform CRA_a | 0.26 | 0.19 | 0.16 | 0.20 |
| ORC2 | Origin recognition complex, subunit 2-like (Yeast) | 0.20 | 0.11 | 0.06 | 0.12 |
| POLE | DNA polymerase epsilon catalytic subunit A | 68.88 | 146.28 | 13.92 | 76.36 |
| PSMD2 | 26S proteasome non-ATPase regulatory subunit 2 | 4.79 | 5.37 | 1.19 | 3.78 |
| PSMD8 | 26S proteasome non-ATPase regulatory subunit 8 | 0.37 | 0.48 | 0.43 | 0.43 |
| RAD50 | DNA repair protein RAD50 | 0.52 | 0.69 | 0.27 | 0.50 |
| RBBP7 | RBBP7 protein | 0.72 | 0.35 | 0.30 | 0.45 |
| RPA1 | Replication protein A 70 kDa DNA-binding subunit | 0.23 | 0.32 | 0.33 | 0.29 |
| RUVBL2 | RuvB-like 2 | 0.02 | 0.03 | 0.33 | 0.13 |
| SYNE2 | Nesprin-2 | 2.04 | 3.57 | 2.57 | 2.73 |
| **Biogenesis/Metabolism** | | | | | |
| AARS | Alanine--tRNA ligase, cytoplasmic | 5.59 | 4.46 | 2.05 | 4.04 |
| ACACA | Acetyl-CoA carboxylase 1 | 1.33 | 1.58 | 1.32 | 1.41 |
| AHCY | Adenosylhomocysteinase | 20.71 | 24.74 | 3.62 | 16.36 |
| ALDOA | Fructose-bisphosphate aldolase A | 2.90 | 5.96 | 2.09 | 3.65 |
| AP3D1 | AP-3 complex subunit delta-1 | 17.66 | 24.85 | 25.36 | 22.62 |
| CHD3 | Chromodomain-helicase-DNA-binding protein 3 | 4.95 | 6.82 | 5.71 | 5.83 |
| CHGB | Secretogranin-1 | 1.53 | 2.57 | 1.39 | 1.83 |
| CNBP | CCHC-type zinc finger nucleic acid binding protein isoform 3 | 11.49 | 26.00 | 1.22 | 12.90 |
| COQ6 | Ubiquinone biosynthesis monooxygenase COQ6, mitochondrial | 2029.15 | 166071.00 | 209.31 | 56103.15 |
| CTPS1 | CTP synthase 1 | 12.73 | 28.46 | 5.39 | 15.53 |
| DHX29 | ATP-dependent RNA helicase DHX29 | 4.48 | 6.20 | 3.02 | 4.57 |
| ELP3 | Elongator complex protein 3 | 33.10 | 46.78 | 16.38 | 32.09 |
| ERC1 | ELKS/Rab6-interacting/CAST family member 1 | 1.44 | 1.80 | 1.49 | 1.58 |
| GNE | Bifunctional UDP-N-acetylglucosamine 2-epimerase /N-acetylmannosamine kinase | 9.81 | 11.55 | 1.67 | 7.68 |
| GOT2 | Aspartate aminotransferase, mitochondrial | 15.75 | 21.34 | 3.26 | 13.45 |
| IFT172 | Intraflagellar transport protein 172 homolog | 1.21 | 1.60 | 2.16 | 1.66 |
| KCNH4 | Potassium voltage-gated channel subfamily H member 4 | 22.17 | 38.90 | 56.66 | 39.24 |
| KRT2 | Keratin, type II cytoskeletal 2 epidermal | 2.06 | 2.25 | 1.93 | 2.08 |
| KTN1 | Kinectin 1 (Kinesin receptor), isoform CRA_a | 2.03 | 1.40 | 1.58 | 1.67 |
| LRRFIP1 | Leucine rich repeat (In FLII) interacting protein 1, isoform CRA_c | 3.68 | 5.86 | 3.52 | 4.35 |
| MGST1 | Microsomal glutathione S-transferase 1, isoform CRA_a | 1.96 | 1.91 | 1.27 | 1.71 |
| PKM | Pyruvate kinase PKM | 193.74 | 315.72 | 54.68 | 188.05 |
| POLE | DNA polymerase epsilon catalytic subunit A | 68.88 | 146.28 | 13.92 | 76.36 |
| PSMD2 | 26S proteasome non-ATPase regulatory subunit 2 | 4.79 | 5.37 | 1.19 | 3.78 |
| PYGB | Glycogen phosphorylase, brain form | 4.55 | 4.70 | 5.60 | 4.95 |
| RAB40C | Ras-related protein Rab-40C | 17.88 | 14.27 | 8.35 | 13.50 |
| RPS16 | 40S ribosomal protein S16 | 6.02 | 6.64 | 2.39 | 5.02 |
| SUGP2 | SURP and G-patch domain-containing protein 2 | 19.90 | 23.87 | 48.52 | 30.76 |
| TCERG1 | Transcription elongation regulator 1 | 2.63 | 2.35 | 6.48 | 3.82 |
| TRIP12 | E3 ubiquitin-protein ligase TRIP12 | 3.14 | 2.94 | 3.14 | 3.07 |
| YBX1 | Nuclease-sensitive element-binding protein 1 | 5.44 | 6.81 | 2.57 | 4.94 |

**Table 5.2 – Gene names and protein description with respect to Figure 5.7**

## 5.4.6 Characterizing protein interaction enrichment between mPKM2-wildtype, mPKM2-K433E mutant and Venus-non targeting control

Due to the high degree of biotinylated protein detected and thus non-specific binding of Venus, it was decided that a PKM2 mutant might be a more appropriate alternative bio-identification control. Exclusive to exon 10 encoding PKM2, the lysine residue 433 (K433) is located in F1,6BP binding pocket and the binding of F1,6BP stabilizes tetrameric PKM2 [34]. Binding of phosphotyrosine to the K433 residue leads to the release of F1,6BP from PKM2 and inhibition of PKM2 activity by destabilizing the tetrameric state [19]. Mutating the K433 by replacing the lysine with glutamate (K433E), resulted in phosphotyrosine-resistant PKM2, stabilizing tetrameric PKM2 which exhibited high PK activity [19,20]. Therefore, using this PKM2 mutant (PKM2-K433E-BirA*) as a control, might potentially identify more specific populations of proteins which interact with tetrameric mPKM2-K433E in comparison to the mPKM2-WT which could interchange between oligomeric states. To examine whether PKM2-mutant would serve as a better control bait, the current study performed a preliminary qualitative bio-identification experiment to compare the variety (gene hits) of proteins biotinylated by mPKM2-WT-BirA*, mPKM2-K433E-BirA* and Venus-BirA* baits (Figure 5.8). It should be noted, however, that qualitative bio-identification is a screening technique which favours the broad identification of proteins without quantifying the interaction enrichment.

Since dimeric PKM has been shown to participate in moonlighting functions [35] rather than PK activity in comparison to the tetrameric PKM2, we anticipated that wild-type PKM2 would interact with different populations of proteins. The current study qualitatively identified interacting partners of different BirA* fused baits, including the mPKM2-WT, pro-tetrameric mPKM2-K433E, and the non-targeting Venus. The identity of biotinylated proteins was assessed by the number of unique peptides matched, where 4 or more unique peptides indicated an almost certain identification. Identified interacting partners were then categorized using PANTHER to broadly screen for the variation of potential interactors, indicative of interaction selectivity.

A list of 544 interacting partners of mPKM2-WT, mPKM2-K433E and non-targeting Venus baits was collectively identified through qualitative bio-identification via LC-MS/MS (unique peptide match ≥ 2; Supplementary Table 5.3). Screening for only proteins almost certainty identified in all samples (unique peptide match ≥ 4), we found that Venus-BirA* interacted with 175 proteins while mPKM2-WT-BirA* and mPKM2-K433E-BirA* interacted with 130 and 131 proteins, respectively. Consistent with previous observations, we found that Venus control generally biotinylated more proteins than mPKM2-WT and mPKM2-K433E in most PANTHER categorized processes. This indicated that the Venus bait produced high non-specific binding. It should be noted that subtle differences between mPKM2-WT and mPKM2-K433E could be observed. For instance, mPKM2-WT interacted more with nucleic acid-binding proteins whereas mPKM2-WT interacted more with chaperones and cytoskeletal proteins (Figure 5.8A). Surprisingly, pro-tetrameric mPKM2-K433E biotinylated more proteins associated with biogenesis while mPKM2-WT biotinylated more proteins associated with the extracellular region/space outside the plasma membrane (PGK2 and annexin A1; Figure 5.8B-C). This suggests that dimer and tetramer PKM2 have different regulatory roles in PDAC.
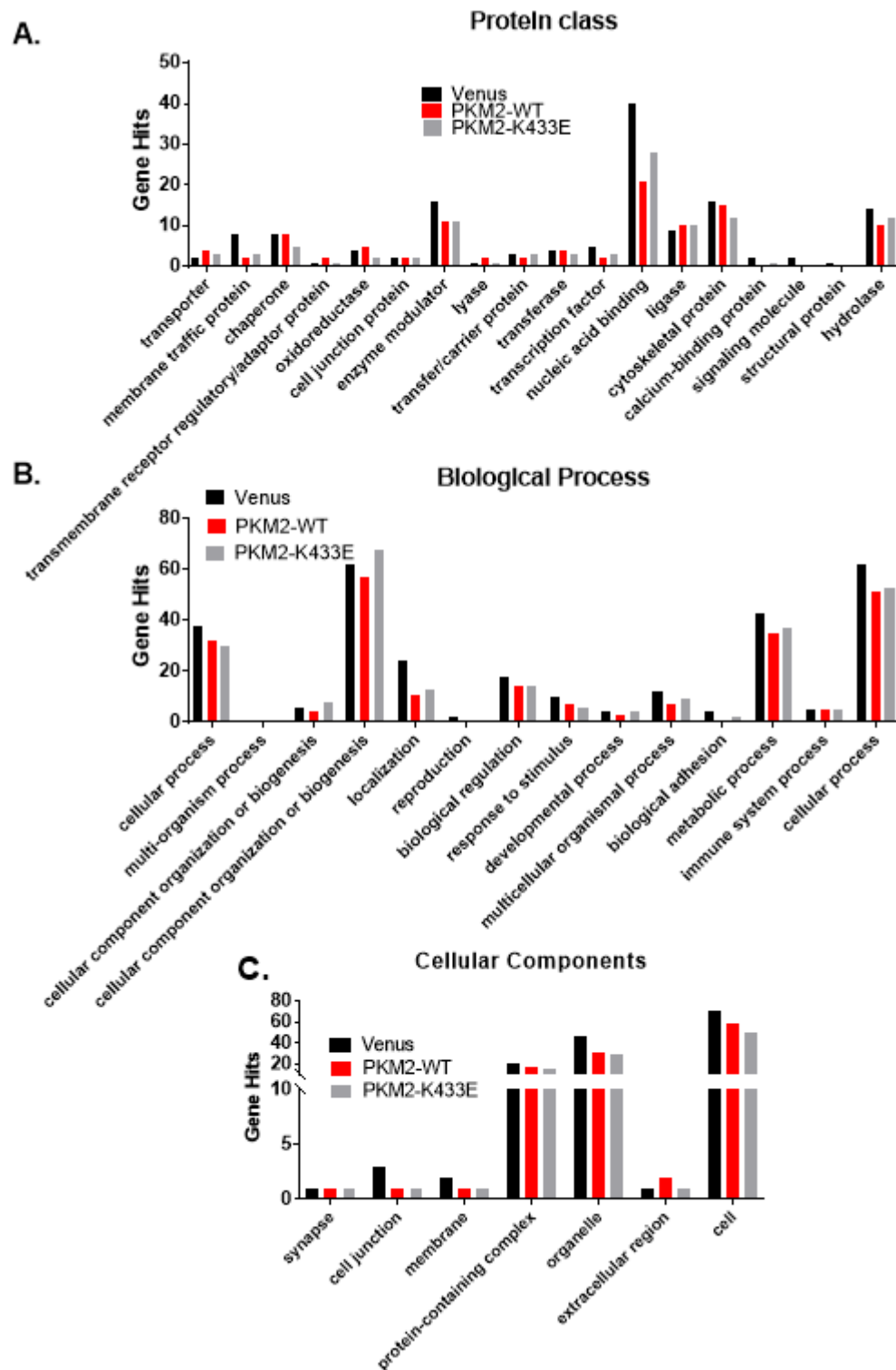
**Figure 5.8 – Categorization of biotinylated protein identified in non-specific Venus, mPKM2-Wildtype and mPKM2-K433E.** MIAPaCa-2 stably transfected with non-specific Venus, mPKM2-WT and mPKM2-K433E BirA* constructs were treated with 100 µM biotin overnight. Biotinylated proteins were separated from non-biotinylated proteins using streptavidin beads then identified using qualitative mass spectrometry. Proteins were identified by gene name and raw data are expressed as the number of unique peptides hits where the higher the unique peptide hits, the more certain the identification. Proteins with almost certain identification (unique peptide ≥4) were categorized using Panther version 14.1 according to: **A,** protein class, **B,** biological process and **C,** cellular components. Data are expressed as the number of individual genes identified (gene hits). N=1. No statistical analysis was performed.

To further identify the distinct differences between dimeric and tetrameric PKM2 interactions, all probable identifications (unique protein≥2) were compared. Identified proteins were then divided into three distinct groups as follow: 1) unique to mPKM2-WT, 2) present in both mPKM2-WT and mPKM2-K433E and 3) unique to mPKM2-K433E (Supplementary Table 5.3). The unique differences between protein enrichment in mPKM2-WT (dimer/tetramer) and pro-tetrameric mPKM2-K433E were compared based on protein class, cellular components and biological processes (Figure 5.9). Out of a total 380 protein detected between both samples, 86 proteins were uniquely identified in the mPKM2-WT whereas 90 proteins were uniquely found in mPKM2-K433E mutant. Based on PANTHER categorization, mPKM2-WT interacted more with organelle associated proteins, hydrolase and transporters. On the other hand, mPKM2-K433E mutant was shown to distinctly interact with more nucleic acid bind proteins, membrane-associated proteins and metabolic processes (Figure 5.9A-C; additional proteins identity available in Supplementary Table 5.4.1-5.4.3). Interestingly, a family member of the 14-3-3 protein (tyrosine 3-monooxygenase/tryptophan 5-monooxygenase activation protein theta isoform; YWHAQ) reported to exhibit inhibitory interaction with the N-terminus of PMCA4 (plasma membrane Ca$^{2+}$ ATPase isoform 4) [36], was identified as a unique chaperone interactor of mPKM2-WT. However, the importance of these biotinylated proteins associated processes cannot be determined until further quantitative enrichment analysis is performed, and the biological functions of these individual proteins are considered.
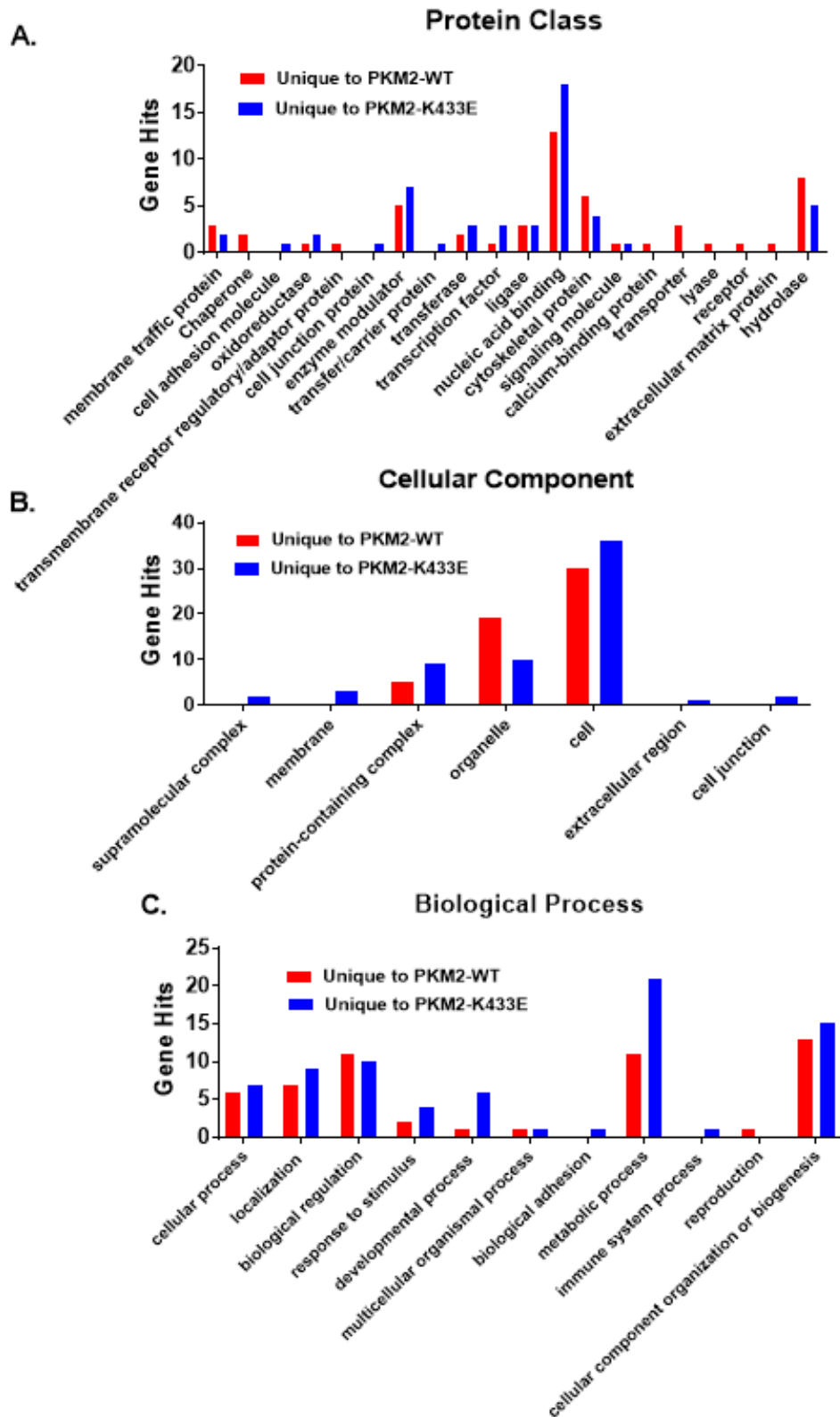
**Figure 5.9 – Categorization of biotinylated proteins unique in mPKM2-Wild type in comparison to pro-tetrameric mutant mPKM2-K433E.** MIAPaCa-2 stably transfected mPKM2-WT (WT) and mPKM2-K433E (MUT) BirA* constructs were treated with 100 µM biotin overnight. Biotinylated proteins were separated from non-biotinylated fraction using streptavidin beads then identified using qualitative mass spectrometry. Identified proteins were categorized using Panther version 14.1, based on: **A,** protein class, **B,** cellular components and **C,** biological process. A comparison was made between biotinylated proteins either: i) unique to mPKM2-WT (red) and ii) unique to mPKM2-K433E (blue). Data are expressed as the number of individual genes identified (gene hits). N=1. No statistical analysis was performed on the data.

## 5.5 Discussion & Future work

### 5.5.1 Discussion

Overexpression of PKM2 plays an important role in the metabolic shift towards aerobic glycolysis [3]. In PDAC, PKM2 overexpression in PDAC tumour is reported to correlate with poor PDAC patient survival [2,13,15]. In relation to our hypothesis that PKM2 potentially interacts with cell membrane proteins in order to provide a privileged ATP supply in close proximity to fuel PMCA4 activity, the present study attempted to examine the potential protein-protein interactions (interactome) of PKM2 with potential plasma membrane-associated proteins and other key glycolytic enzymes. Proximity-dependent biotinylation labelling technique (BioID) has been used previously to identify multiple protein-protein interactions, for instance, insulin signalling [1], focal adhesion complexes [2], caveolae [3] and carbonic anhydrase IX metabolic interactome [4]. However, to our current knowledge, no previous studies have used BioID to decipher protein-protein interactions between PKM2-binding partners.

Compartmentalization of glycolytic enzymes (GEs), in mitochondria-free erythrocyte and the cell migration front, has been proposed by multiple studies [8,37–39]. This indicates that GEs may associate to membrane proteins as a complex thereby potentially providing a privileged microdomain of ATP in close proximity to fuel ATP consuming machineries, including the PMCAs. In erythrocytes which lack the mitochondria, band 3 transmembrane protein (solute carrier family 4 member 1; SLC4A1) has been identified as the plasma membrane binding site of the glycolytic metabolon [8]. Raikar, L.S., *et al.* (2006) reported that the overexpression of caveolin 1 (Cav-1) led to enhanced membrane targeting of key glycolytic enzymes, PFK and aldolase (ALD), in rat aorta vascular smooth muscle [39]. Moreover, a study by Wei, Y. *et al.* (2017) suggested that PKM2 is targeted to the plasma membrane by SNAP23, a vesicular transport protein, in Hela and A549 pulmonary adenocarcinoma cells [40]. As PMCA has been reported to reside within the lipid rafts/caveolae compartment, we initially anticipated to identify some caveolae marker proteins or membrane-targeting chaperone proteins, although to our surprised, this was not the case.

As PKM2 is the major ATP generating glycolytic enzyme associated with malignant transformation, potentially responsible for fuelling PMCA activity, the current study used PKM2 as the BioID bait and screened for potential interactions of PKM2 with plasma membrane-associated proteins. We found that PKM2 had significantly enriched interactions with a transmembrane protein (voltage-gated K$^+$ channel subfamily H member 4; KCNH4) and a canonical glycolytic enzyme (fructose-bisphosphate aldolase, muscle isoform; ALDOA) in comparison to the Venus control ($p<0.05$). However, our results suggested that PKM2 did not interact with any caveolae markers in MIAPaCa-2 PDAC cells. Interestingly, we identified a few members of the 14-3-3 protein isoforms (e.g. YWHAQ, 14-3-3 theta; YWHAZ, 14-3-3 zeta/delta; YWHAE, 14-3-3 epsilon) known to mediate inhibition of PMCA4 by binding at the N-terminus. Although these 14-3-3 proteins were enriched in PKM2 samples and were reported to interact with PKM2 [41,42], none of these proteins was statistically significant upon comparison to Venus control. Similarly, although we found that SNAP29 (synaptosome associated protein 29) was 1.6-fold enriched in mPKM2-WT with respect to Venus control, the data was not statistically significant ($p>0.05$). However, as the

current study could only present data obtained from three independent samples (N=3) of mPKM2-BirA* and Venus-BirA*, care must be taken not to over interpret the data.

KCNH4 is a gene encoding a member of voltage-gated $K^+$ (Kv) channel known as Kv 12.3 channel. Kv channels play an important role in excitable tissue (e.g. cardiac) and are suggested to play a role in insulin secretion in pancreatic β-cells [43]. While KCNH2 overexpression has been correlated to pancreatic cancer [44], the role of KCNH4 in the pancreas is currently unclear. A study by Yoshida, M. *et al.* (2009) report an observation that glucose metabolism is associated with the enhanced amplitude of Kv channels in rat pancreatic β cells [45], suggesting that PKM2 may play a potential role in modulating Kv channel, although the actual mechanism is currently unknown. Since KCNH4 is a transmembrane protein intrinsically expressed at the cell membrane which significantly interacted with PKM2, we postulated that KCNH4 is likely the key PKM2-binding plasma membrane protein. However, further investigation with proximity-ligation assay and co-immunoprecipitation of KCNH4-PKM2 may be necessary to examine the nature of PKM2-KCNH4 protein-protein interaction. If KCNH4 and PKM2 do indeed interact, the functional role of KCNH4 in metabolism, particularly its role in providing privileged ATP supply to the PMCAs, could be further explored using KCNH4 inhibitors or selective siRNA knockdown.

Glycolytic enzymes (GEs) have been suggested to interact with other glycolytic enzymes to form a glycolytic metabolon/ multiprotein complex [8,31,46]. In glycolysis-reliant erythrocyte cells, lacking the mitochondria, Puchulu-Campanella, E., *et al.* (2013) employed LC-MS/MS of cell surface biotinylation assay to identify cell membrane-associated GEs, including pyruvate kinase, ALD, GADPH and lactate dehydrogenase [8]. This led to the proposal that these GEs potentially forms a glycolytic metabolon near the site of ATP consuming $Na^+/K^+$ and $Ca^{2+}$ pumps on erythrocyte membrane [8,47]. Another study by Kohnhorst, C.L, *et al.* (2017), using FRET tags and immunofluorescence imaging, suggested that key rate-liming glycolytic enzymes, comprised of PFKL, PKM2, FBP (fructose-1,6 bisphosphatase) and PEPCK1 (phosphoenolpyruvate carboxykinase 1), form multi-enzyme complex in human cervical adenocarcinoma Hela cell and Hs578T breast cancer cell lines [46]. Consistent with previous finding [8], we found that PKM2 had significantly enriched interactions with ALDOA in MIAPaCa-2 PDAC cells. Moreover, although not significantly enriched, PKM2 also interacted with PFKL, PFKP, GAPDH and LDHA. Our present data suggest that PKM2 does indeed interact with other canonical GEs but as we did not address the spatio-temporal colocalization of these GEs within live cells, the nature of these GE interactions remain inconclusive.

Collectively, as PKM2 had significant interactions with KCNH4 and some interaction with SNAP29, this indicates that PKM2 is potentially targeted to the surface plasma membrane. However, further colocalization studies (e.g. confocal immunofluorescence and co-immunoprecipitation) of these GEs will be required to test this hypothesis.

### 5.5.2 Future work

As the present study serves as preliminary BioID screening to identify putative PKM2 plasma membrane binding partners and its neighbouring proteins, further studies will be required to confirm our hypothesis of whether PKM2 fuels the PMCAs by interacting with membrane proteins in the proximity of PMCA in PDAC. (Figure 5.10) It is important to narrow down our identified proteins of interest and validate whether these significantly identified 'prey' proteins are genuine functional interacting partners of PKM2. PKM2 is an oligomeric protein which dynamically interchanges between monomer, dimer and tetrameric forms [5,19]. As different oligomeric forms have been correlated to different functional activities, the interactome enrichment is expected to be dependent on the proportion/ratio of each PKM2 oligomers. Therefore, it is critical to understand that the identified 'prey' interactions obtained from our mPKM2-WT bait are likely a combination of all the dynamic changes in PKM2 forms, hence generating a large variability in LC-MS/MS data obtained. To identify specific oligomeric PKM2 interaction enrichments, mutations which restrain PKM2 to a certain oligomeric confirmation may prove to be more beneficial to decipher the dynamic nature of PKM2 interactomes. For example, PKM2-Y105F which locks PKM2 tetrameric form [20] and exon-10 mutation variants which result in reduced allostery which favours the formation of dimeric PKM2 conformation [48]. Alternatively, the constitutive tetrameric PKM1, encoded from the same PKM gene as PKM2, could be possibly used as a BirA* bait to examine the tetrameric pyruvate kinase protein-protein interactions. This is because PKM1 and FBP-bound PKM2 exhibit the same tetrameric conformation and almost identical kinetic activities [49,50].

In order to probe the existence of a PKM2 glycolytic metabolon, it is essential to identify other glycolytic enzymes that significantly interact with PKM2. Since our data had revealed that ALDOA is a significant interacting partner of PKM2, suggesting that it is likely "closest" interacting GE with PKM2, ALDOA may be used as the next bait to identify other GEs which may belong to this glycolytic interactome as well as to validate ALD-PKM2 interaction enrichment. Other GEs identified using mPKM2-BirA* that were not significantly enriched could also potentially be used as BirA* baits, particularly PFK and PGK. PFK is a well-established rate-limiting glycolytic enzyme which is allosterically regulated by ATP and citrate ratio [51]. On the other hand, PGK is a critical ATP-producing GE in the glycolytic pay-off phase which, like PKM, has been linked to tumorigenesis [52]. Therefore, ALD, PFK and PGK may serve as suitable baits for further investigation of glycolytic metabolon existence in PDAC.
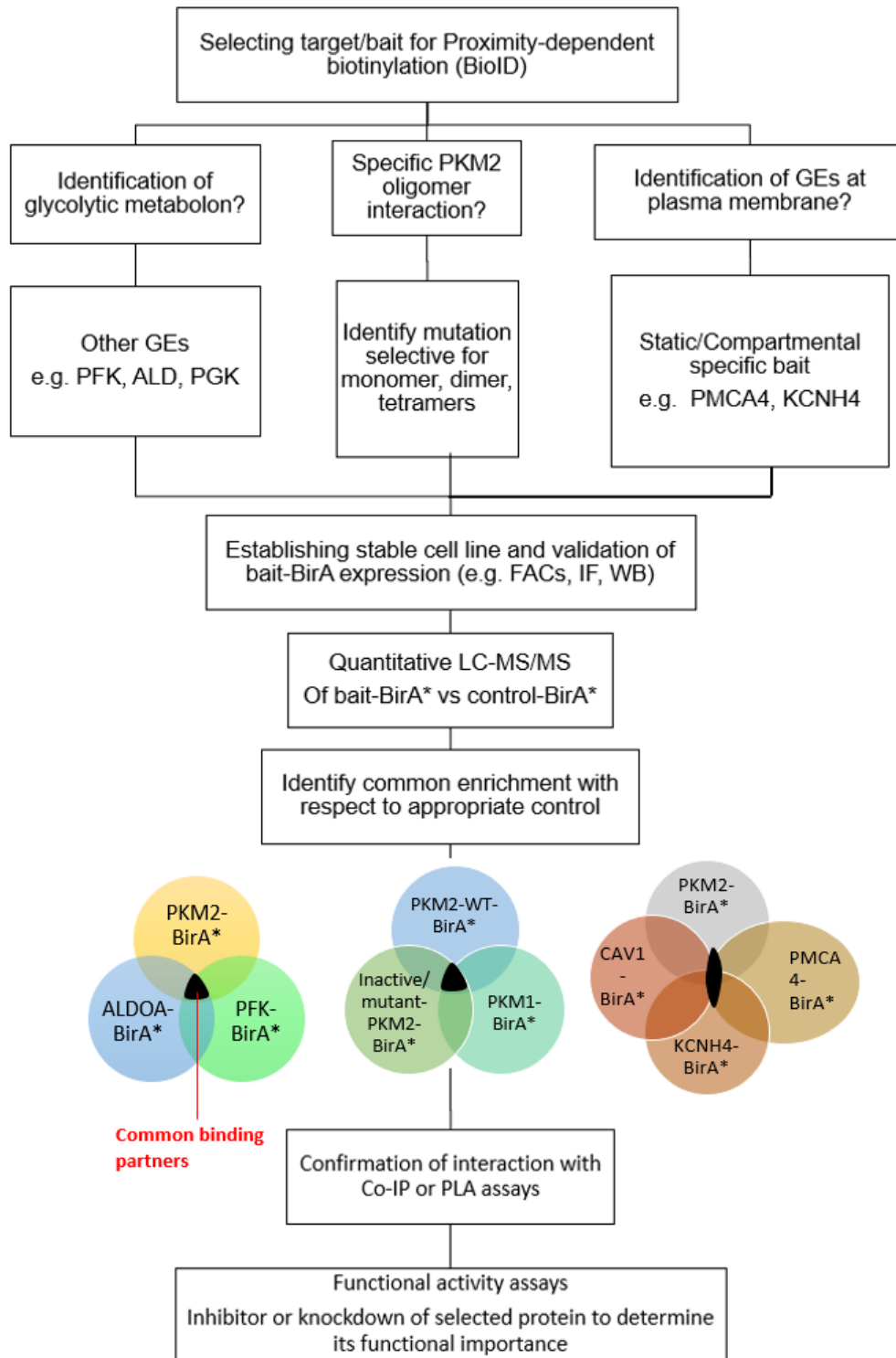
**Figure 5.10 – Potential options for future proximity-dependent biotinylation experiments.** The following flow chart lists the logical sequence of potential BioID experiments which could further expand on the existing work. Depending on the experimental objectives of interest, different sets of bait-BirA* fusion proteins should be considered for the identification of common interacting/binding protein partners (highlighted black on the Venn diagram). Abbreviations: BioID: bio-identification; PKM2: pyruvate kinase M2; GEs: glycolytic enzymes; PFK: phosphofructokinase; ALD: aldolase; PGK: phosphoglycerate kinase; PMCA4: plasma membrane $Ca^{2+}$ ATPase isoform 4; KCNH4: voltage-gated potassium channel subfamily H member 4; FACs: fluorescence-activated cell sorting; IF: immunofluorescence; WB: Western immunoblot; LC-MS/MS: liquid chromatography with tandem mass spectrometry; ALDOA: aldolase A; PKM1: pyruvate kinase M1; CAV1: caveolin-1; WT: wild type; PLA: proximity ligation assay; Co-IP: co-immunoprecipitation.

162

To examine potential compartmentalization of glycolytic enzymes at the surface plasma membrane, it is critical to identify static BioID baits which are intrinsic plasma membrane proteins and/or well-established sub-membrane domain markers (e.g. caveolae/lipid rafts). As our data revealed that KCNH4 significantly interacted with PKM2, KCNH4 may be used as a potential bait to investigate plasma membrane-associated GEs. In addition, since PMCA4 has been our oncogenic target of interest, PMCA4 may serve as a good plasma membrane marker as well as a relevant bait for ATP-producing GE associated to the plasma membrane. Although no caveolae markers were found in our current data, Cav-1 is suggested to serve as a binding site for ALD [39] and was identified as a significant interacting partner of PKM2. Therefore, Cav-1 could potentially serve as useful BirA* bait to identify GEs as well as signalling machineries found in the caveolae signalling hub. Furthermore, proximity ligation assays and co-immunoprecipitation assays of these membrane-associated proteins (e.g. KCNH4, PMCA4, Cav-1) with PKM2 should be performed to confirm the protein-protein interaction identified in this study.

In conclusion, the overexpression of PKM2 in PDAC tumour is a relevant clinical marker associated with poor PDAC patient survival. Using PKM2 as a protein bait for BioID, the current study provides some preliminary data which identified KCNH4 and ALDOA as the interacting partners of PKM2. We have shown that PKM2 significantly interact with KCNH4, potentially indicating a subpopulation of PKM2 residing near the plasma membrane in a PDAC model. Although inconclusive, these data suggested that PKM2 likely interacted with a bona fide plasma membrane protein as well as other canonical GEs. Since the majority of PDAC tumour demonstrated a metabolic shift towards glycolysis and PKM2 is a clinically relevant marker for PDAC, further understanding of the glycolytic interactome may provide beneficial insights to therapeutically target PDAC more efficiently.

## 5.6 Acknowledgements

## 5.7 References

1.  Siegel RL, Miller KD, Jemal A. Cancer statistics, 2019. CA Cancer J Clin. 2019;69(1):7–34.

2.  Tian S, Li P, Sheng S, Jin X. Upregulation of pyruvate kinase M2 expression by fatty acid synthase contributes to gemcitabine resistance in pancreatic cancer. Oncol Lett. 2018 Feb;15(2):2211–7.

3.  Christofk HR, Vander Heiden MG, Harris MH, Ramanathan A, Gerszten RE, Wei R, et al. The M2 splice isoform of pyruvate kinase is important for cancer metabolism and tumour growth. Nature. 2008;452(7184):230–3.

4.  Hanahan D, Weinberg RA. Hallmarks of cancer: the next generation. Cell. 2011 Mar 4;144(5):646–74.

5.  Mazurek S. Pyruvate kinase type M2: A key regulator of the metabolic budget system in tumor cells. Int J Biochem Cell Biol. 2011;43(7):969–80.

6.  Dombrauckas JD, Santarsiero BD, Mesecar AD. Structural basis for tumor pyruvate kinase M2 allosteric regulation and catalysis. Biochemistry. 2005;44(27):9417–29.

7.  Gupta V, Bamezai RNK. Human pyruvate kinase M2: a multifunctional protein. Protein Sci. 2010 Nov;19(11):2031–44.

8.  Puchulu-Campanella E, Chu H, Anstee DJ, Galan JA, Tao WA, Low PS. Identification of the components of a glycolytic enzyme metabolon on the human red blood cell membrane. J Biol Chem. 2013 Jan 11;288(2):848–58.

9.  Campanella ME, Chu H, Wandersee NJ, Peters LL, Mohandas N, Gilligan DM, et al. Characterization of glycolytic enzyme interactions with murine erythrocyte membranes in wild-type and membrane protein knockout mice. Blood. 2008;112(9):3900–6.

10. James AD, Patel W, Butt Z, Adiamah M, Dakhel R, Latif A, et al. The Plasma Membrane Calcium Pump in Pancreatic Cancer Cells Exhibiting the Warburg Effect Relies on Glycolytic ATP. J Biol Chem. 2015 Oct 9;290(41):24760–71.

11. James AD, Chan A, Erice O, Siriwardena AK, Bruce JIE. Glycolytic ATP fuels the plasma membrane calcium pump critical for pancreatic cancer cell survival. J Biol Chem. 2013 Dec 13;288(50):36007–19.

12. Azoitei N, Becher A, Steinestel K, Rouhi A, Diepold K, Genze F, et al. PKM2 promotes tumor angiogenesis by regulating HIF-1α through NF-κB activation. Mol Cancer. 2016 Dec 6;15(1):3.

13. Oncomine [Internet]. [cited 2019 Jun 20]. Available from: www.oncomine.org

14. Rhodes DR, Yu J, Shanker K, Deshpande N, Varambally R, Ghosh D, et al. ONCOMINE: A Cancer Microarray Database and Integrated Data-Mining Platform. Neoplasia. 2004;6(1):1–6.

15. Uhlen M. Expression of PKM in pancreatic cancer - The Human Protein Atlaso Title [Internet]. [cited 2019 Jun 20]. Available from: https://www.proteinatlas.org/ENSG00000067225-PKM/pathology/tissue/pancreatic+cancer

16. Uhlen M, Zhang C, Lee S, Sjöstedt E, Fagerberg L, Bidkhori G, et al. A pathology atlas of the human cancer transcriptome. Science (80- ). 2017 Aug 18;357(6352):eaan2507.

17. Varnaitė R, MacNeill SA. Meet the neighbors: Mapping local protein interactomes by proximity-dependent labeling with BioID. Proteomics. 2016;16(19):2503–18.

18. Roux KJ, Kim DI, Burke B, May DG, Falls NS, Dakota S, et al. BioID : A Screen for Protein-Protein Interactions. 2019;(2):1–20.

19. Christofk HR, Vander Heiden MG, Wu N, Asara JM, Cantley LC. Pyruvate kinase M2 is a phosphotyrosine-binding protein. Nature. 2008;452(7184):181–6.

20. Hitosugi T, Kang S, Vander Heiden MG, Chung T-W, Elf S, Lythgoe K, et al. Tyrosine Phosphorylation Inhibits PKM2 to Promote the Warburg Effect and Tumor Growth. Bönig H, editor. Sci Signal. 2009 Nov 17;2(97):ra73–ra73.

21. Morais-Cabral JH, Robertson GA. The enigmatic cytoplasmic regions of KCNH channels. J Mol Biol. 2015 Jan 16;427(1):67–76.

22. Ozeir M, Mü U, Webert H, Lill R, Fontecave M, Pierrel F. Article Coenzyme Q Biosynthesis: Coq6 Is Required for the C5-Hydroxylation Reaction and Substrate Analogs Rescue Coq6 Deficiency. Chem Biol. 2011;18:1134–42.

23. Sylvester JE, Fischel-Ghodsian N, Mougey EB, O'brien TW. Mitochondrial ribosomal proteins: Candidate genes for mitochondrial disease. Genet Med. 2004 Apr;6(2):73–80.

24. Kavela S, Shinde SR, Ratheesh R, Viswakalyan K, Bashyam MD, Gowrishankar S, et al. PNUTS Functions as a Proto-Oncogene by Sequestering PTEN. Cancer Res. 2013 Jan 1;73(1):205–14.

25. Hunkeler M, Hagmann A, Stuttfeld E, Chami M, Guri Y, Stahlberg H, et al. Structural basis for regulation of human acetyl-CoA carboxylase. Nature. 2018 Jun 13;558(7710):470–4.

26. Mayer MP, Bukau B. Hsp70 chaperones: cellular functions and molecular mechanism. Cell Mol Life Sci. 2005 Mar;62(6):670–84.

27. Multhoff G. Heat shock protein 70 (Hsp70): Membrane location, export and immunological relevance. Methods. 2007 Nov;43(3):229–37.

28. Chae YK, Anker JF, Oh MS, Bais P, Namburi S, Agte S, et al. Mutations in DNA repair genes are associated with increased neoantigen burden and a distinct immunophenotype in lung squamous cell carcinoma. Sci Rep. 2019 Dec 1;9(1):3235.

29. Fujimoto K, Shibasaki T, Yokoi N, Kashima Y, Matsumoto M, Sasaki T, et al. Piccolo, a $Ca^{2+}$ sensor in pancreatic beta-cells. Involvement of cAMP-GEFII.Rim2. Piccolo complex in cAMP-dependent exocytosis. J Biol Chem. 2002 Dec 27;277(52):50497–502.

30. Thomas G, Aslan JE, Thomas L, Shinde P, Shinde U, Simmen T. Caught in the act – protein adaptation and the expanding roles of the PACS proteins in tissue homeostasis and disease. J Cell Sci. 2017 Jun 1;130(11):1865–76.

31. Menard L, Maughan D, Vigoreaux J, Menard L, Maughan D, Vigoreaux J. The Structural and Functional Coordination of Glycolytic Enzymes in Muscle: Evidence of a Metabolon? Biology (Basel). 2014 Sep 22;3(3):623–44.

32. Prakasam G, Iqbal MA, Bamezai RNK, Mazurek S. Posttranslational Modifications of Pyruvate Kinase M2: Tweaks that Benefit Cancer. Front Oncol. 2018;8(February):1–12.

33. Snaebjornsson MT, Schulze A. Non-canonical functions of enzymes facilitate cross-talk between cell metabolic and regulatory pathways. Exp Mol Med. 2018 Apr 16;50(4):34.

34. Dombrauckas JD, Santarsiero BD, Mesecar AD. Structural Basis for Tumor Pyruvate Kinase M2 Allosteric Regulation and Catalysis † , ‡. Biochemistry. 2005 Jul;44(27):9417–29.

35. Gao X, Wang H, Yang JJ, Liu X, Liu ZR. Pyruvate Kinase M2 Regulates Gene Transcription by Acting as a Protein Kinase. Mol Cell. 2012;45(5):598–609.

36. Rimessi A, Coletto L, Pinton P, Rizzuto R, Brini M, Carafoli E. Inhibitory Interaction of the 14-3-3 Protein with Isoform 4 of the Plasma Membrane Ca 2-ATPase Pump *. 2005;

37. Campanella ME, Chu H, Low PS. Assembly and regulation of a glycolytic enzyme complex on the human erythrocyte membrane. Proc Natl Acad Sci. 2005 Feb 15;102(7):2402–7.

38. Gooptu M, Whitaker-Menezes D, Sprandio J, Domingo-Vidal M, Lin Z, Uppal G, et al. Mitochondrial and glycolytic metabolic compartmentalization in diffuse large B-cell lymphoma. Semin Oncol. 2017 Jun 1;44(3):204–17.

39. Raikar LS, Vallejo J, Lloyd PG, Hardin CD. Overexpression of caveolin-1 results in increased plasma membrane targeting of glycolytic enzymes: The structural basis for a membrane associated metabolic compartment. J Cell Biochem. 2006 Jul 1;98(4):861–71.

40. Wei Y, Wang D, Jin F, Bian Z, Li L, Liang H, et al. Pyruvate kinase type M2 promotes tumour cell exosome release via phosphorylating synaptosome-associated protein 23. Nat Commun. 2017 Apr 9;8(1):14041.

41. Pozuelo Rubio M, Geraghty KM, Wong BHC, Wood NT, Campbell DG, Morrice N, et al. 14-3-3-Affinity purification of over 200 human phosphoproteins reveals new links to regulation of cellular metabolism, proliferation and trafficking. Biochem J. 2004;379(2):395–408.

42. Meek SEM, Lane WS, Piwnica-Worms H. Comprehensive proteomic analysis of interphase and mitotic 14-3-3-binding proteins. J Biol Chem. 2004;279(31):32046–54.

43. Rosati B, Marchetti P, Crociani O, Lecchi M, Lupi R, Arcangeli A, et al. Glucose- and arginine-induced insulin secretion by human pancreatic beta-cells: the role of HERG K$^+$ channels in firing and release. FASEB J. 2000 Dec;14(15):2601–10.

44. Feng J, Yu J, Pan X, Li Z, Chen Z, Zhang W, et al. HERG1 functions as an oncogene in pancreatic cancer and is downregulated by miR-96. Oncotarget. 2014 Jul 30;5(14):5832–44.

45. Yoshida M, Dezaki K, Yamato S, Aoki A, Sugawara H, Toyoshima H, et al. Regulation of voltage-gated K$^+$ channels by glucose metabolism in pancreatic β-cells. FEBS Lett. 2009 Jul 7;583(13):2225–30.

46. Kohnhorst CL, Kyoung M, Jeon M, Schmitt DL, Kennedy EL, Ramirez J, et al. Identification of a multienzyme complex for glucose metabolism in living cells. J Biol Chem. 2017 Jun 2;292(22):9191–203.

47. Chu H, Puchulu-Campanella E, Galan JA, Tao WA, Low PS, Hoffman JF. Identification of cytoskeletal elements enclosing the ATP pools that fuel human red blood cell membrane cation pumps. Proc Natl Acad Sci U S A. 2012 Jul 31;109(31):12794–9.

48. Chen T-J, Wang H-J, Liu J-S, Cheng H-H, Hsu S-C, Wu M-C, et al. Mutations in the PKM2 exon-10 region are associated with reduced allostery and increased nuclear translocation. Commun Biol. 2019 Dec 15;2(1):105.

49. Israelsen WJ, Vander Heiden MG. Pyruvate kinase: Function, regulation and role in cancer. Semin Cell Dev Biol. 2015 Jul;43:43–51.

50. Ibsen KH, Chiu RHC, Park HR, Sanders DA, Roy S, Garratt KN, et al. Purification and Properties of Mouse Pyruvate Kinases K and M and of a Modified K Subunit. Biochemistry. 1981;20(6):1497–506.

51. Mulukutla BC, Yongky A, Daoutidis P, Hu W-S. Bistability in Glycolysis Pathway as a Physiological Switch in Energy Metabolism. Dzeja P, editor. PLoS One. 2014 Jun 9;9(6):e98756.

52. Li X, Jiang Y, Meisenhelder J, Yang W, Hawke DH, Zheng Y, et al. Mitochondria-Translocated PGK1 Functions as a Protein Kinase to Coordinate Glycolysis and the TCA Cycle in Tumorigenesis. Mol Cell. 2016 Mar 3;61(5):705–19.

## 5.8 Supplementary Data
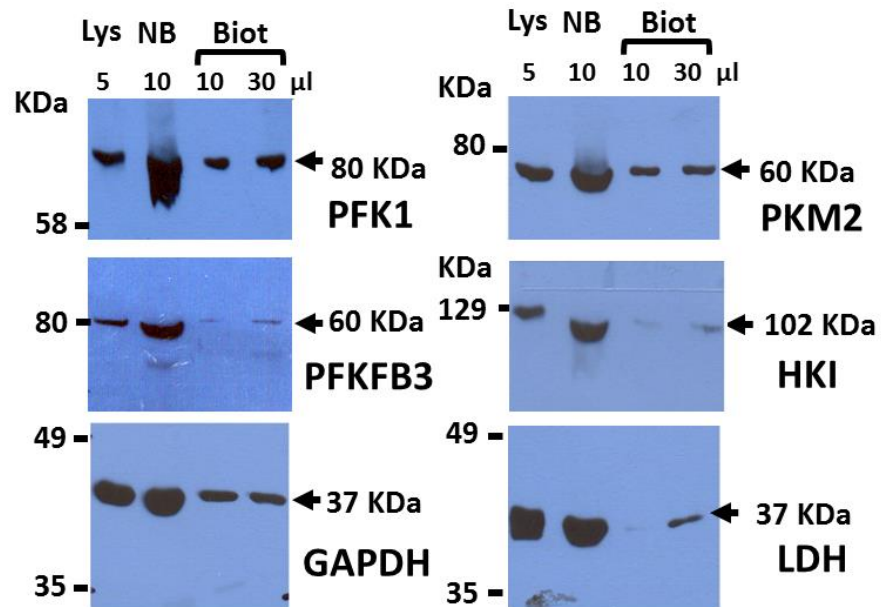


**Supplementary Figure 5.1 – Membrane-associated glycolytic enzymes in MIAPaCa-2 PDAC cells**.
Cell surface biotinylation assay was used to isolate plasma-membrane protein and any associated proteins. The extracellular glycosylated transmembrane proteins of MIAPaCa-2 cells were labelled with Sulfo-NHS-SS-Biotin. NeutrAvidin agarose column was used to bind the biotinylated sample and separate the non-biotinylated fractions by centrifugation at 10000 relative centrifugal force (rcf). Biotinylated proteins were eluted from the agarose column using 1x Laemmli sample buffer containing 50 mM dithiothreitol (DTT). SDS-PAGE of whole-cell lysates (Lys), non-biotinylated (NB) and biotinylated protein (Biot) fractions were Western blotted for key glycolytic enzymes, including: phosphofructokinase-1 (PFK1), phosphofructokinase fructose bisphosphatase-3 (PFKFB3), glyceraldehyde 3-phosphate dehydrogenase (GAPDH), pyruvate kinase M2 (PKM2), hexokinase I (HKI) and lactate dehydrogenase (LDH). [Data was provided by Dr Andrew James]

| Vector Components | Description |
| --- | --- |
| PKM2 | Pyruvate Kinase Muscle isoform 2 |
| MycBirA* | Myc-tagged BirA* |
| BamHI | Restriction enzyme site |
| NotI | Rare restriction enzyme site |
| T2A | Self-cleavage sequence |
| BFP | Blue fluorescence protein |
| WPRE | Woodchuck hepatitis virus posttranscriptional regulatory element |
| LTR | Long terminal repeat promoter |
| SV40\Ori | Origin of replication |
| Pr\Lac | Lytic promoter |
| pBR332\ori | Origin of replication |
| Ampr | Ampicillin resistance gene |
| LacZ | Promoter |
| cPPT | Central polypurine tract |
| EF1a | Promoter |
| Xbal | Restriction site |

**Supplementary Table 5.1 – Plasmid vector component description**

| Gene ID | Description | Max fold change | ANOVA (p) |
|---|---|---|---|
| FLNA* | cDNA FLJ57890, highly similar to Filamin-A | 18754.67 | 2.69E-03 |
| COQ6 | Ubiquinone biosynthesis monooxygenase COQ6, mitochondrial | 688.27 | 9.36E-03 |
| PPP1R10 | Serine/threonine-protein phosphatase 1 regulatory subunit 10 | 282.09 | 7.05E-04 |
| ACACA | Acetyl-CoA carboxylase 1 | 150.23 | 1.05E-04 |
| PKM | Pyruvate kinase PKM | 123.33 | 3.78E-04 |
| MRPL23 | Mitochondrial ribosomal protein L23, isoform CRA_a | 105.93 | 7.7E-06 |
| ZC3H11A* | cDNA FLJ58196, highly similar to Zinc finger CCCH domain-containing protein 11A | 86.61 | 1.1E-05 |
| HSPA4 | Heat shock 70 kDa protein 4 | 78.49 | 9.01E-05 |
| POLE | DNA polymerase epsilon catalytic subunit A | 67.33 | 2.61E-03 |
| PCLO | Protein piccolo | 53.22 | 3.37E-03 |
| KCNH4 | Potassium voltage-gated channel subfamily H member 4 | 38.24 | 9.3E-05 |
| ACTN2* | cDNA FLJ50104, highly similar to Alpha-actinin-2 | 31.08 | 1.08E-03 |
| PACS1 | Phosphofurin acidic cluster sorting protein 1, isoform CRA_a | 28.16 | 1.03E-03 |
| FGFR2-AHCYL1 | Adenosylhomocysteinase | 27.85 | 1.72E-04 |
| SUGP2 | SURP and G-patch domain-containing protein 2 | 27.81 | 1.11E-04 |
| ELP3 | Elongator complex protein 3 | 25.91 | 1.43E-03 |
| AP3D1 | AP-3 complex subunit delta-1 (Fragment) | 23.16 | 3.87E-04 |
| ZC3H15 | Zinc finger CCCH domain-containing protein 15 | 23.11 | 1.99E-03 |
| MGC16703 | Alpha tubulin-like, isoform CRA_a | 19.76 | 1.89E-03 |
| RAB40C | Ras-related protein Rab-40C (Fragment) | 12.50 | 1.86E-04 |
| CTPS1 | CTP synthase 1 | 12.12 | 2.60E-03 |
| KRT78 | Keratin, type II cytoskeletal 78 | 9.95 | 0.0326 |
| MYO9B | Myosin IXB variant protein | 8.89 | 0.0345 |
| RPL22 | Heparin-binding protein HBp15 | 8.27 | 0.0428 |
| AHCY | Adenosylhomocysteinase | 8.12 | 0.0158 |
| TTI1 | TELO2-interacting protein 1 homolog (Fragment) | 7.83 | 6.72E-04 |
| ASAP2 | PH domain-containing protein 1 | 7.38 | 5.78E-04 |
| ASAP1 | Arf-GAP with SH3 domain, ANK repeat and | 6.38 | 5.78E-04 |
| STXBP5 | Syntaxin-binding protein 5 | 6.24 | 7.30E-04 |
| GOT2 | Aspartate aminotransferase, mitochondrial | 6.09 | 0.0362 |
| CHD3 | Chromodomain-helicase-DNA-binding protein 3 | 5.68 | 2.85E-03 |
| SPATA19 | Spermatogenesis-associated protein 19, mitochondrial | 5.54 | 0.0496 |
| TBC1D2B | TBC1 domain family, member 2B | 5.26 | 3.92E-04 |
| LRRFIP2 | isoform CRA_c | 5.20 | 3.05E-04 |

**Supplementary Table 5.2 – continuing next page**

| Gene ID | Description | Max fold change | ANOVA (p) |
|---|---|---|---|
| GIT1 | ARF GTPase-activating protein GIT1 | 5.16 | 0.0149 |
| PYGB | Glycogen phosphorylase, brain form | 5.16 | 0.0277 |
| SPATA5 | Spermatogenesis-associated protein 5 | 5.12 | 0.0468 |
| DAAM1* | dishevelled associated activator of morphogenesis 1, mRNA | 5.01 | 7.20E-03 |
| CNBP | CCHC-type zinc finger nucleic acid binding protein isoform 3 (Fragment) | 5.00 | 0.0480 |
| GNE | Bifunctional UDP-N-acetylglucosamine 2-epimerase /N-acetylmannosamine kinase | 4.36 | 0.0325 |
| DHX29 | ATP-dependent RNA helicase DHX29 | 4.36 | 5.60E-04 |
| LRRFIP1 | Leucine rich repeat (In FLII) interacting protein 1, | 4.20 | 3.05E-04 |
| RPS16 | 40S ribosomal protein S16 | 4.01 | 0.0125 |
| DAAM1* | cDNA FLJ78680, highly similar to Homo sapiens | 4.01 | 7.20E-03 |
| TCERG1 | Transcription elongation regulator 1 | 3.97 | 0.0341 |
| YBX1 | Nuclease-sensitive element-binding protein 1 | 3.72 | 0.0397 |
| PSMD2 | 26S proteasome non-ATPase regulatory subunit 2 | 3.34 | 0.0463 |
| AARS | Alanine--tRNA ligase, cytoplasmic | 3.19 | 0.0302 |
| TRIP12 | E3 ubiquitin-protein ligase TRIP12 | 3.06 | 3.62E-04 |
| ALDOA | Fructose-bisphosphate aldolase A (Fragment) | 2.89 | 0.0486 |
| BCAR3* | cDNA FLJ30880 fis, clone FEBRA2004767, highly similar to Breast cancer anti-estrogen resistance protein 3 | 2.73 | 0.0117 |
| SYNE2 | Nesprin-2 | 2.56 | 0.0175 |
| TUBB4Q | Beta-tubulin 4Q isoform 1 (Fragment) | 2.51 | 4.56E-03 |
| DST | Dystonin | 2.20 | 0.0419 |
| KRT2 | Keratin, type II cytoskeletal 2 epidermal | 2.05 | 0.0407 |
| C15orf38 -AP3S2 | Protein C15orf38-AP3S2 | 1.96 | 0.0122 |
| RSN | Restin, isoform CRA_b (Reed-Steinberg cell-expressed intermediate filament-associated protein) | 1.93 | 0.0249 |
| DYNC1LI2 | Dynein, cytoplasmic 1, light intermediate chain 2, isoform CRA_a | 1.81 | 0.0101 |
| ARFGAP1 | ADP-ribosylation factor GTPase-activating protein 1 | 1.79 | 0.0154 |
| MSN | Moesin | 1.75 | 0.0149 |
| CHGB | Secretogranin-1 | 1.74 | 0.0378 |
| MGST1 | Microsomal glutathione S-transferase 1, isoform CRA_a | 1.68 | 6.46E-03 |
| VDAC3 | Voltage-dependent anion-selective channel protein 3 | 1.65 | 0.0454 |
| DNAAF2 | Protein kintoun | 1.64 | 0.0317 |
| KTN1 | Kinectin 1 (Kinesin receptor), isoform CRA_a | 1.63 | 0.0111 |
| SRGAP1 | SLIT-ROBO Rho GTPase-activating protein 1 | 1.62 | 0.0122 |
| IFT172 | Intraflagellar transport protein 172 homolog | 1.61 | 0.0184 |
| ERC1 | ELKS/Rab6-interacting/CAST family member 1 | 1.56 | 6.87E-03 |
| KRT7 | Keratin, type II cytoskeletal 7 | 1.55 | 0.0309 |
| TNS1 | Tensin-1 | 1.43 | 4.99E-03 |

| Gene ID | Description | | 1.42 | 0.0443 |
|---------|-------------|---|------|--------|
| HAUS6 | HAUS augmin-like complex subunit 6 | | 1.42 | 0.0443 |

**Supplementary Table 5.2 – continuing next page**

| Gene ID | Description | Max fold change | ANOVA (p) |
|---------|-------------|-----------------|-----------|
| CEP170 | Centrosomal protein of 170 kDa | 1.35 | 0.0163 |
| CDV3 | CDV3 homolog (Mouse), isoform CRA_a | 1.33 | 0.0140 |

**Supplementary Table 5.2 – mPKM2-wildtype protein interaction enrichment in comparison to non-specific Venus control.** 70 proteins were identified to be significantly enriched in mPKM2-WT in comparison to the Venus bait control. * indicates the most likely gene name corresponding to the proteins/cDNA identified (p<0.05, Unique peptide ≥1).

| Unique to mPKM2-K433E | | | |
|---|---|---|---|
| Gene | Identified Proteins | Unique Peptide | |
| | | WT | K433E |
| HIST1H2BJ | Histone H2B | | 35 |
| HIST1H2BM | Histone H2B type 1-M | | 26 |
| HIST1H4J | Histone H4 | | 16 |
| | cDNA FLJ75154, highly similar to Homo sapiens heterogeneous nuclear ribonucleoprotein C (C1/C2), mRNA | | 9 |
| HIST2H2AA3 | Histone H2A type 2-A | | 8 |
| DHX9 | ATP-dependent RNA helicase A | | 7 |
| HNRNPA2B1 | Heterogeneous nuclear ribonucleoproteins A2/B1 | | 5 |
| | Kinesin-like protein | | 5 |
| TANGO6 | Transport and Golgi organization protein 6 homolog | | 5 |
| NOP56 | NOP56 protein (Fragment) | | 5 |
| PTPN12 | Tyrosine-protein phosphatase non-receptor type 12 | | 4 |
| UBE2O | E2 ubiquitin-conjugating enzyme | | 4 |
| IRAK1 | Interleukin-1 receptor-associated kinase 1 | | 4 |
| H3F3A | Histone H3 | | 4 |
| MATR3 | Matrin-3 | | 4 |
| DDX21 | Nucleolar RNA helicase 2 | | 4 |
| RPL6 | 60S ribosomal protein L6 | | 4 |
| RPS9 | 40S ribosomal protein S9 | | 4 |
| CACYBP | Calcyclin binding protein, isoform CRA_a | | 4 |
| RPL7A | 60S ribosomal protein L7a (Fragment) | | 3 |
| | cDNA, FLJ94136, highly similar to Homo sapiens synaptotagmin binding, cytoplasmic RNA interacting protein (SYNCRIP), mRNA | | 3 |
| PDLIM7 | PDZ and LIM domain protein 7 | | 3 |
| UBAP2L | Ubiquitin-associated protein 2-like | | 3 |
| | cDNA FLJ11308 fis, clone PLACE1010074, highly similar to Sorting nexin-2 | | 3 |
| KIF4A | Chromosome-associated kinesin KIF4A | | 3 |
| DNAJB1 | DnaJ homolog subfamily B member 1 | | 3 |
| ATXN2L | Ataxin-2-like protein | | 3 |
| RPS18 | 40S ribosomal protein S18 | | 3 |
| RPL8 | 60S ribosomal protein L8 (Fragment) | | 3 |
| RPS8 | 40S ribosomal protein S8 | | 3 |
| HNRNPM | Heterogeneous nuclear ribonucleoprotein M | | 3 |
| RBMX | RNA-binding motif protein, X chromosome | | 3 |
| ALDH18A1 | Delta-1-pyrroline-5-carboxylate synthase | | 3 |
| ILF3 | Interleukin enhancer binding factor 3, 90kDa, isoform CRA_d | | 3 |
| DVL3 | Segment polarity protein dishevelled homolog DVL-3 | | 3 |

**Supplementary Table 5.3 – continuing next page**

| Unique to mPKM2-K433E | | | |
|---|---|---|---|
| | | **Unique Peptide** | |
| **Gene** | **Identified Proteins** | **WT** | **K433E** |
| | DNA-directed RNA polymerase subunit beta | | 3 |
| CLTC | Clathrin heavy chain | | 3 |
| SRP72 | Signal recognition particle subunit SRP72 | | 3 |
| STMN1 | Stathmin | | 3 |
| RACGAP1 | Rac GTPase activating protein 1, isoform CRA_a | | 3 |
| LMNA | Prelamin-A/C | | 3 |
| AARS | Alanine--tRNA ligase, cytoplasmic | | 3 |
| HNRPF | Heterogeneous nuclear ribonucleoprotein F, isoform CRA_a | | 3 |
| NUDC | Nuclear migration protein nudC | | 3 |
| COPB1 | Coatomer subunit beta | | 2 |
| GAF1 | Putative uncharacterized protein GAF1 (Fragment) | | 2 |
| RANBP2 | E3 SUMO-protein ligase RanBP2 | | 2 |
| LUZP1 | Leucine zipper protein 1, isoform CRA_a | | 2 |
| HN1 | Haematological and neurological expressed 1 protein | | 2 |
| MGEA5 | Protein O-GlcNAcase | | 2 |
| EDC4 | Enhancer of mRNA-decapping protein 4 | | 2 |
| | cDNA FLJ59508, highly similar to Homo sapiens ubiquitin associated protein 2 (UBAP2), transcript variant 1, mRNA | | 2 |
| G3BP1 | Ras GTPase-activating protein-binding protein 1 | | 2 |
| FAM62A | Family with sequence similarity 62 (C2 domain containing), member A, isoform CRA_a | | 2 |
| XRN1 | 5'-3' exoribonuclease 1 | | 2 |
| | cDNA FLJ78677, highly similar to Homo sapiens splicing factor 3b, subunit 3, 130kDa (SF3B3), mRNA | | 2 |
| CTNND1 | Catenin delta-1 | | 2 |
| ERC1 | ELKS/Rab6-interacting/CAST family member 1 | | 2 |
| TNKS1BP1 | Tankyrase 1 binding protein 1, 182kDa, isoform CRA_a | | 2 |
| | cDNA FLJ75500, highly similar to Homo sapiens EH domain binding protein 1, mRNA | | 2 |
| | cDNA, FLJ94025, highly similar to Homo sapiens tripartite motif-containing 28 (TRIM28), mRNA | | 2 |
| RPS13 | 40S ribosomal protein S13 | | 2 |
| HNRPA1 | Heterogeneous nuclear ribonucleoprotein A1, isoform CRA_b | | 2 |
| | cDNA FLJ35376 fis, clone SKMUS2004044, highly similar to Homo sapiens ribosomal protein L3 (RPL3), transcript variant 2, mRNA | | 2 |

**Supplementary Table 5.3 – continuing next page**

| Unique to mPKM2-K433E | | Unique Peptide | |
|---|---|---|---|
| Gene | Identified Proteins | WT | K433E |
| HNRNPUL2 | Heterogeneous nuclear ribonucleoprotein U-like protein 2 | | 2 |
| | cDNA FLJ77421, highly similar to Homo sapiens autoantigen p542 mRNA | | 2 |
| | cDNA FLJ51983, highly similar to Phosphoglycerate mutase 1 (EC 5.4.2.1) | | 2 |
| RSL1D1 | RSL1D1 protein (Fragment) | | 2 |
| VCP | VCP protein (Fragment) | | 2 |
| PTPN11 | Tyrosine-protein phosphatase non-receptor type 11 | | 2 |
| DBN1 | Drebrin | | 2 |
| | cDNA, FLJ94229, highly similar to Homo sapiens heterogeneous nuclear ribonucleoprotein L (HNRPL),mRNA | | 2 |
| DDX18 | DEAD (Asp-Glu-Ala-Asp) box polypeptide 18, isoform CRA_b | | 2 |
| GTPBP4 | Nucleolar GTP-binding protein 1 | | 2 |
| TBK1 | Serine/threonine-protein kinase TBK1 | | 2 |
| OCRL | Inositol polyphosphate 5-phosphatase OCRL-1 | | 2 |
| H2AFY | Core histone macro-H2A.1 | | 2 |
| NOP2 | Probable 28S rRNA (cytosine(4447)-C(5))-methyltransferase | | 2 |
| BZW2 | Basic leucine zipper and W2 domains 2, isoform CRA_a | | 2 |
| DST | Dystonin | | 2 |
| EIF5B | Eukaryotic translation initiation factor 5B | | 2 |
| ATG3 | Ubiquitin-like-conjugating enzyme ATG3 | | 2 |
| | cDNA FLJ60461, highly similar to Peroxiredoxin-2 (EC 1.11.1.15) | | 2 |
| EPB41 | Protein 4.1 | | 2 |
| | cDNA FLJ77615, highly similar to Homo sapiens nucleolar complex associated 3 homolog (S. cerevisiae) (NOC3L), mRNA | | 2 |
| | cDNA FLJ43948 fis, clone TESTI4014924, highly similar to Homo sapiens cytoplasmic FMR1 interacting protein 1 (CYFIP1), transcript variant 1, mRNA | | 2 |
| HNRNPAB | Heterogeneous nuclear ribonucleoprotein A/B | | 2 |
| | cDNA FLJ10273 fis, clone HEMBB1001137, highly similar to SEC23-interacting protein | | 2 |
| CBL | E3 ubiquitin-protein ligase CBL | | 2 |
| NANP | N-acylneuraminate-9-phosphatase | | 2 |

**Supplementary Table 5.3 – continuing next page**

| Present in both mPKM2-K433E and mPKM2-WT | | Unique Peptide | |
|---|---|---|---|
| Gene | Identified Proteins | WT | K433E |
| PKM | Pyruvate kinase PKM | 164 | 242 |
| HEL113 | Epididymis luminal protein 113 | 7 | 65 |
| ACACA | Acetyl-CoA carboxylase 1 | 45 | 51 |
| CCT8 | T-complex protein 1 subunit theta | 24 | 29 |
| HSPA8 | Heat shock cognate 71 kDa protein | 27 | 29 |
| AHNAK | Neuroblast differentiation-associated protein AHNAK | 23 | 26 |
| ACTB | Actin, cytoplasmic 1 | 25 | 26 |
| EIF4G1 | EIF4G1 protein | 22 | 25 |
| | cDNA FLJ32131 fis, clone PEBLM2000267, highly similar to Tubulin alpha-ubiquitous chain | 18 | 22 |
| PC | Pyruvate carboxylase | 15 | 21 |
| HSP90AA1 | Heat shock protein HSP 90-alpha | 10 | 20 |
| | cDNA FLJ53619, highly similar to Heat shock protein HSP 90-beta | 16 | 19 |
| CKAP5 | Cytoskeleton-associated protein 5 | 16 | 19 |
| TUBB | Beta 5-tubulin | 16 | 17 |
| GEMIN5 | GEMIN5 protein | 14 | 16 |
| EEF1A1 | Elongation factor 1-alpha 1 | 13 | 14 |
| CORO1B | Coronin | 12 | 13 |
| ANXA2 | Annexin | 11 | 12 |
| ACTN4 | Actinin alpha 4 isoform 1 (Fragment) | 2 | 11 |
| CD2AP | CD2-associated protein | 7 | 11 |
| KIAA1524 | Protein CIP2A | 7 | 10 |
| | Heat shock 70kDa protein 1A variant (Fragment) | 7 | 10 |
| CSDE1 | Cold shock domain containing E1, RNA-binding, isoform CRA_a | 8 | 10 |
| RAPH1 | Ras association (RalGDS/AF-6) and pleckstrin homology domains 1, isoform CRA_b | 8 | 10 |
| DNMBP | Dynamin-binding protein | 4 | 9 |
| DDX3X | ATP-dependent RNA helicase DDX3X | 6 | 9 |
| LIMA1 | LIM domain and actin-binding protein 1 | 6 | 9 |
| SLK | STE20-like serine/threonine-protein kinase | 6 | 9 |
| KRT16 | Keratin, type I cytoskeletal 16 | 8 | 9 |
| STAT3 | Signal transducer and activator of transcription | 5 | 8 |
| CORO1C | Coronin | 6 | 8 |
| GART | Trifunctional purine biosynthetic protein adenosine-3 | 2 | 7 |
| TNS3 | Tensin-3 | 3 | 7 |
| CEP170 | Centrosomal protein 170kDa | 5 | 7 |
| KIF5B | Kinesin-like protein | 6 | 7 |
| STAT1 | Signal transducer and activator of transcription | 2 | 6 |
| | cDNA FLJ78740, highly similar to Homo sapiens sperm associated antigen 5 (SPAG5), mRNA | 3 | 6 |
| | cDNA FLJ54020, highly similar to Heterogeneous nuclear ribonucleoprotein U | 4 | 6 |

**Supplementary Table 5.3 – continuing next page**

| Present in both mPKM2-K433E and mPKM2-WT | | | |
|---|---|---|---|
| **Gene** | **Identified Proteins** | **Unique Peptide** | |
| | | **WT** | **K433E** |
| | cDNA FLJ75516, highly similar to Xenopus tropicalis ubiquitin C, mRNA | 4 | 6 |
| HSPD1 | Heat shock 60kDa protein 1 (Chaperonin), isoform CRA_a | 4 | 6 |
| | cDNA FLJ78413, highly similar to Homo sapiens albumin, mRNA | 5 | 6 |
| MYH9 | Myosin, heavy polypeptide 9, non-muscle, isoform CRA_a | 5 | 6 |
| | Ribosomal protein L4 variant (Fragment) | 2 | 5 |
| USP15 | Ubiquitin carboxyl-terminal hydrolase 15 | 2 | 5 |
| RPS14 | 40S ribosomal protein S14 | 2 | 5 |
| SNX1 | Sorting nexin-1 | 3 | 5 |
| | cDNA FLJ76121, highly similar to Homo sapiens zinc finger CCCH-type, antiviral 1 (ZC3HAV1), transcript variant 1, mRNA | 3 | 5 |
| COPG2 | Coatomer subunit gamma-2 | 3 | 5 |
| PCBP2 | Poly(rC)-binding protein 2 | 3 | 5 |
| | cDNA FLJ59571, highly similar to Eukaryotic translation initiation factor 4 gamma 2 | 4 | 5 |
| NCAPG | Condensin complex subunit 3 | 2 | 4 |
| CALD1 | Caldesmon | 2 | 4 |
| RPS4X | 40S ribosomal protein S4 | 2 | 4 |
| CLINT1 | Clathrin interactor 1 isoform 2 (Fragment) | 3 | 4 |
| C9orf88 | Chromosome 9 open reading frame 88, isoform CRA_a | 3 | 4 |
| STK38 | Serine/threonine kinase 38, isoform CRA_a | 3 | 4 |
| HNRPK | Heterogeneous nuclear ribonucleoprotein K, isoform CRA_d | 3 | 4 |
| | cDNA, FLJ92620, highly similar to Homo sapiens staphylococcal nuclease domain containing 1 (SND1),mRNA | 3 | 4 |
| EEF1G | Elongation factor 1-gamma | 3 | 4 |
| TP53BP2 | Apoptosis-stimulating of p53 protein 2 | 2 | 3 |
| TXNRD1 | Thioredoxin reductase 1 | 2 | 3 |
| HNRNPH1 | Heterogeneous nuclear ribonucleoprotein H | 2 | 3 |
| SNAP29 | Synaptosomal-associated protein 29 | 2 | 3 |
| EMD | Emerin | 2 | 3 |
| EPS15L1 | Epidermal growth factor receptor pathway substrate 15-like 1, isoform CRA_a | 2 | 3 |
| TRIP12 | E3 ubiquitin-protein ligase TRIP12 | 2 | 3 |
| RPL9 | NPC-A-16 | 2 | 3 |
| IFIT5 | Interferon-induced protein with tetratricopeptide repeats 5 | 2 | 3 |
| | Peptidyl-prolyl cis-trans isomerase | 2 | 3 |

**Supplementary Table 5.3 – continuing next page**

| Present in both mPKM2-K433E and mPKM2-WT | | | |
|---|---|---|---|
| Gene | Identified Proteins | Unique Peptide | |
| | | WT | K433E |
| | cDNA, FLJ96156, highly similar to Homo sapiens leucyl-tRNA synthetase (LARS), mRNA | 2 | 3 |
| HDLBP | High density lipoprotein binding protein (Vigilin), isoform CRA_a | 13 | 13 |
| | cDNA, FLJ92973, highly similar to Homo sapiens villin 2 (ezrin) (VIL2), mRNA | 11 | 11 |
| EIF5 | Eukaryotic translation initiation factor 5, isoform CRA_b | 9 | 9 |
| NEK9 | NIMA (Never in mitosis gene a)-related kinase 9, isoform CRA_a | 9 | 9 |
| EIF3A | Eukaryotic translation initiation factor 3 subunit A | 6 | 6 |
| RPS16 | 40S ribosomal protein S16 | 6 | 6 |
| | cDNA FLJ51907, highly similar to Stress-70 protein, mitochondrial | 6 | 6 |
| ZYX | Zyxin | 5 | 5 |
| ATP5B | ATP synthase subunit beta, mitochondrial | 4 | 4 |
| ALDOA | Fructose-bisphosphate aldolase A | 4 | 4 |
| TIPRL | TIP41-like protein | 4 | 4 |
| RPL11 | Cell growth-inhibiting protein 34 | 4 | 4 |
| | T-complex protein 1 subunit delta | 4 | 4 |
| CPSF3 | Cleavage and polyadenylation specificity factor subunit 3 | 4 | 4 |
| CRKL | Crk-like protein | 3 | 3 |
| STAU1 | Double-stranded RNA-binding protein Staufen homolog 1 | 3 | 3 |
| DBNL | Drebrin-like protein | 3 | 3 |
| PXN | Paxillin | 3 | 3 |
| EIF3D | Eukaryotic translation initiation factor 3 subunit D | 3 | 3 |
| SERBP1 | SERPINE1 mRNA binding protein 1, isoform CRA_d | 3 | 3 |
| IARS | Isoleucine--tRNA ligase, cytoplasmic | 3 | 3 |
| LASP1 | LIM and SH3 protein 1, isoform CRA_b | 3 | 3 |
| ERCC6L | DNA excision repair protein ERCC-6-like | 2 | 2 |
| EXOC4 | Exocyst complex component 4 | 2 | 2 |
| FARSA | Phenylalanine--tRNA ligase alpha subunit | 2 | 2 |
| | Transketolase (Fragment) | 2 | 2 |
| PDLIM1 | PDZ and LIM domain protein 1 | 2 | 2 |
| SNX4 | Sorting nexin-4 | 2 | 2 |
| ARCN1 | Archain 1, isoform CRA_b | 2 | 2 |
| EIF3S8 | Eukaryotic translation initiation factor 3 subunit C | 2 | 2 |
| NCL | Nucleolin, isoform CRA_b | 2 | 2 |
| USP10 | Ubiquitin carboxyl-terminal hydrolase 10 | 2 | 2 |
| PRKDC | DNA-dependent protein kinase catalytic subunit | 2 | 2 |
| RPL13 | 60S ribosomal protein L13 | 2 | 2 |

**Supplementary Table 5.3 – continuing next page**

| | | Unique Peptide | |
|---|---|---|---|
| Present in both mPKM2-K433E and mPKM2-WT | | | |
| Gene | Identified Proteins | WT | K433E |
| RPL10 | 60S ribosomal protein L10 | 2 | 2 |
| MYPN | Myopalladin | 2 | 2 |
| ARFGAP2 | ADP-ribosylation factor GTPase-activating protein 2 | 2 | 2 |
| CIAPIN1 | Anamorsin | 2 | 2 |
| EPS15 | Epidermal growth factor receptor substrate 15 | 2 | 2 |
| | cDNA FLJ76981, highly similar to Homo sapiens Golgi autoantigen, golgin subfamily a, 5 (GOLGA5), mRNA | 2 | 2 |
| MKL2 | MKL/myocardin-like protein 2 | 2 | 2 |
| FLNA | Filamin A | 126 | 113 |
| FASN | Fatty acid synthase | 116 | 112 |
| KRT8 | Keratin, type II cytoskeletal 8 | 60 | 46 |
| KRT18 | Keratin 18, isoform CRA_a | 50 | 47 |
| KRT1 | Keratin 1 | 48 | 37 |
| KRT2 | Keratin, type II cytoskeletal 2 epidermal | 37 | 24 |
| FLNB | Filamin-B | 35 | 26 |
| KRT9 | Keratin, type I cytoskeletal 9 | 31 | 16 |
| PRIC295 | Peroxisome proliferator activated receptor interacting complex protein | 29 | 18 |
| EEF2 | Elongation factor 2 | 26 | 23 |
| TLN1 | Talin-1 | 26 | 21 |
| KRT10 | Keratin, type I cytoskeletal 10 | 26 | 20 |
| MCCC1 | Methylcrotonoyl-CoA carboxylase 1 isoform 1 (Fragment) | 25 | 23 |
| SEPT9 | Septin-9 | 19 | 10 |
| TUBB2C | Tubulin, beta 2C | 17 | 15 |
| KRT6C | Keratin, type II cytoskeletal 6C | 17 | 12 |
| RARS | Arginine--tRNA ligase, cytoplasmic | 16 | 13 |
| ANXA1 | Annexin A1 | 16 | 9 |
| | Dihydropyrimidinase-like 2 variant (Fragment) | 14 | 11 |
| KRT14 | Keratin, type I cytoskeletal 14 | 14 | 10 |
| PLIN3 | Perilipin-3 | 14 | 9 |
| TPR | Nucleoprotein TPR | 13 | 12 |
| | Cortactin isoform a variant (Fragment) | 12 | 10 |
| VCL | Vinculin, isoform CRA_c | 12 | 10 |
| KRT5 | Keratin, type II cytoskeletal 5 | 12 | 9 |
| MCCC2 | Methylcrotonoyl-CoA carboxylase beta chain, mitochondrial | 12 | 6 |
| DNAJC13 | DnaJ (Hsp40) homolog, subfamily C, member 13 | 12 | 6 |
| GAPDH | Glyceraldehyde-3-phosphate dehydrogenase | 12 | 4 |

**Supplementary Table 5.3 – continuing next page**

| Present in both mPKM2-K433E and mPKM2-WT | | | |
|---|---|---|---|
| **Gene** | **Identified Proteins** | **Unique Peptide** | |
| | | **WT** | **K433E** |
| RPS3 | 40S ribosomal protein S3 | 11 | 10 |
| UBE1 | Ubiquitin-activating enzyme E1 (A1S9T and BN75 temperature sensitivity complementing), isoform CRA_a | 11 | 10 |
| SLC25A5 | ADP/ATP translocase 2 | 11 | 7 |
| KEAP1 | Kelch-like ECH-associated protein 1, isoform CRA_a | 11 | 6 |
| TAGLN2 | Transgelin-2 | 10 | 7 |
| PAK2 | Serine/threonine-protein kinase PAK 2 | 10 | 6 |
| MRE11A | MRE11 meiotic recombination 11 homolog A (S. cerevisiae), isoform CRA_a | 9 | 8 |
| MAP4 | Microtubule-associated protein | 9 | 7 |
| HSPA5 | 78 kDa glucose-regulated protein | 9 | 6 |
| ENO1 | Enolase 1, (Alpha), isoform CRA_a | 9 | 5 |
| CRK | V-crk sarcoma virus CT10 oncogene-like protein isoform 1 (Fragment) | 9 | 5 |
| ATP5A1 | ATP synthase subunit alpha, mitochondrial | 9 | 4 |
| WARS | Tryptophanyl-tRNA synthetase, isoform CRA_a | 8 | 6 |
| EPRS | Bifunctional glutamate/proline--tRNA ligase | 8 | 4 |
| GAPVD1 | GTPase activating protein and VPS9 domains 1, isoform CRA_b | 8 | 4 |
| TCP1 | T-complex protein 1 subunit alpha | 7 | 6 |
| PCCA | Propionyl-CoA carboxylase alpha chain, mitochondrial | 7 | 5 |
| PDLIM5 | PDZ and LIM domain 5, isoform CRA_c | 7 | 5 |
| VCPIP1 | Deubiquitinating protein VCIP135 | 7 | 5 |
| HSPH1 | Heat shock 105kDa/110kDa protein 1, isoform CRA_a | 7 | 5 |
| TNRC15 | Trinucleotide repeat containing 15, isoform CRA_a | 7 | 5 |
| RUVBL1 | RuvB-like helicase (Fragment) | 7 | 5 |
| PABPC1 | Polyadenylate-binding protein | 7 | 4 |
| PRDX1 | Peroxiredoxin-1 (Fragment) | 7 | 3 |
| | T-complex protein 1 subunit gamma | 7 | 2 |
| | cDNA FLJ50778, highly similar to Protein flightless-1 homolog | 6 | 5 |
| SRP68 | Signal recognition particle subunit SRP68 | 6 | 5 |
| RANGAP1 | Ran GTPase activating protein 1, isoform CRA_d | 6 | 5 |
| CCT6A | Chaperonin containing TCP1, subunit 6A (Zeta 1), isoform CRA_a | 6 | 5 |
| HAUS5 | HAUS augmin-like complex subunit 5 | 6 | 4 |
| HSPB1 | Heat shock protein beta-1 | 6 | 3 |
| VASP | Vasodilator-stimulated phosphoprotein isoform 1 | 6 | 3 |
| ABCF2 | ATP-binding cassette, sub-family F (GCN20), member 2 | 5 | 4 |

**Supplementary Table 5.3 – continuing next page**

| Present in both mPKM2-K433E and mPKM2-WT | | | |
|---|---|---|---|
| **Gene** | **Identified Proteins** | **Unique Peptide** | |
| | | **WT** | **K433E** |
| PCBP1 | Poly(rC)-binding protein 1 | 5 | 4 |
| TJP1 | Tight junction protein ZO-1 | 5 | 4 |
| PTBP1 | Polypyrimidine tract-binding protein 1 | 5 | 3 |
| | cDNA FLJ59206, highly similar to Eukaryotic translation initiation factor 4B | 5 | 3 |
| LARP1 | La-related protein 1 | 5 | 3 |
| LDHA | L-lactate dehydrogenase A chain | 5 | 3 |
| | Chaperonin containing TCP1, subunit 7 (Eta) variant (Fragment) | 5 | 2 |
| EIF4A2 | Eukaryotic initiation factor 4A-II | 4 | 3 |
| CAPZB | Capping protein (Actin filament) muscle Z-line, beta, isoform CRA_d | 4 | 3 |
| | cDNA FLJ61233, highly similar to Kinesin light chain 1 | 4 | 3 |
| ALDH1A1 | Retinal dehydrogenase 1 | 4 | 3 |
| | Alpha-1,4 glucan phosphorylase | 4 | 3 |
| PSMD2 | 26S proteasome non-ATPase regulatory subunit 2 | 4 | 3 |
| EIF2A | Eukaryotic translation initiation factor 2A | 4 | 3 |
| CCT2 | T-complex protein 1 subunit beta | 4 | 3 |
| RPS11 | 40S ribosomal protein S11 | 4 | 3 |
| RACK1 | Receptor of-activated protein C kinase 1 | 4 | 3 |
| NME2 | Nucleoside diphosphate kinase B | 4 | 2 |
| PGK1 | Phosphoglycerate kinase | 4 | 2 |
| NCK1 | NCK adaptor protein 1 isoform 3 (Fragment) | 4 | 2 |
| RAN | GTP-binding nuclear protein Ran | 3 | 2 |
| MTHFD1 | Methylenetetrahydrofolate dehydrogenase (NADP$^+$ dependent) 1, methenyltetrahydrofolate cyclohydrolase, formyltetrahydrofolate synthetase, isoform CRA_a | 3 | 2 |
| FARSB | Phenylalanine--tRNA ligase beta subunit | 3 | 2 |
| | AP-3 complex subunit beta | 3 | 2 |
| ETF1 | Eukaryotic peptide chain release factor subunit 1 | 3 | 2 |
| FXR1 | Fragile X mental retardation autosomal homolog variant p2K | 3 | 2 |
| AHSA1 | Activator of 90 kDa heat shock protein ATPase homolog 1 | 3 | 2 |
| | cDNA, FLJ95650, highly similar to Homo sapiens karyopherin (importin) beta 1 (KPNB1), mRNA | 3 | 2 |
| USP14 | Ubiquitin specific peptidase 14 (TRNA-guanine transglycosylase), isoform CRA_a | 3 | 2 |

**Supplementary Table 5.3 – continuing next page**

| Present in both mPKM2-K433E and mPKM2-WT | | | |
|---|---|---|---|
| **Gene** | **Identified Proteins** | **Unique Peptide** | |
| | | **WT** | **K433E** |
| GSTP1 | Glutathione S-transferase P | 3 | 2 |
| RPS3A | 40S ribosomal protein S3a | 3 | 2 |
| AAK1 | AP2-associated protein kinase 1 (Fragment) | 3 | 2 |
| **Unique to mPKM2-WT** | | | |
| **Gene** | **Identified Proteins** | **Unique Peptide** | |
| | | **WT** | **K433E** |
| TUBA1C | Tubulin alpha-1C chain | 21 | |
| KRT19 | Keratin, type I cytoskeletal 19 | 9 | |
| TUBB6 | TUBB6 protein | 9 | |
| COPA | Coatomer subunit alpha | 6 | |
| STRAP | Serine-threonine kinase receptor-associated protein | 5 | |
| RUFY1 | RUN and FYVE domain-containing protein 1 | 5 | |
| PAICS | Phosphoribosylaminoimidazole carboxylase, isoform CRA_c phosphoribosylaminoimidazole succinocarboxamide synthetase, | 5 | |
| YWHAQ | 14-3-3 protein theta | 5 | |
| NPM1 | Nucleophosmin isoform 2 (Fragment) | 5 | |
| ACLY | ATP-citrate synthase | 4 | |
| TTC28 | Tetratricopeptide repeat protein 28 | 4 | |
| AAK1 | AP2-associated protein kinase 1 | 4 | |
| | cDNA FLJ56381, highly similar to Dynamin-1-like protein (EC 3.6.5.5) | 4 | |
| PABPC4 | Polyadenylate-binding protein | 4 | |
| EIF2S3 | Eukaryotic translation initiation factor 2 subunit 3 | 4 | |
| ATP6V1A | V-type proton ATPase catalytic subunit A | 4 | |
| ANKRD17 | Ankyrin repeat domain-containing protein 17 | 4 | |
| KIF15 | Kinesin-like protein KIF15 | 3 | |
| | cDNA FLJ50442, highly similar to T-complex protein 1 subunit epsilon | 3 | |
| RTCB | tRNA-splicing ligase RtcB homolog | 3 | |
| EFHD2 | EF-hand domain family, member D2, isoform CRA_a | 3 | |
| ANKHD1 | Ankyrin repeat and KH domain-containing protein 1 | 3 | |
| UNC45A | Protein unc-45 homolog A | 3 | |
| INF2 | Inverted formin-2 | 3 | |
| | cDNA FLJ55542, highly similar to Ran-binding protein 3 | 3 | |
| MYOF | Myoferlin | 3 | |
| | Importin subunit alpha | 3 | |
| | cDNA FLJ57604, highly similar to GMP synthase (glutamine-hydrolyzing) (EC 6.3.5.2) | 3 | |

**Supplementary Table 5.3 – continuing next page**

| Unique to mPKM2-WT | | | |
|---|---|---|---|
| Gene | Identified Proteins | Unique Peptide | |
| | | WT | K433E |
| PUF60 | Poly(U)-binding-splicing factor PUF60 (Fragment) | 3 | |
| NONO | Non-POU domain containing octamer-binding isoform 1 (Fragment) | 3 | |
| KRT78 | Keratin, type II cytoskeletal 78 | 3 | |
| RPS20 | 40S ribosomal protein S20 | 3 | |
| | cDNA FLJ61538, highly similar to Switch-associated protein 70 | 3 | |
| | cDNA FLJ75085, highly similar to Homo sapiens glutaminyl-tRNA synthetase (QARS), mRNA | 3 | |
| PFN1 | Profilin 1, isoform CRA_b | 3 | |
| COPG1 | Coatomer subunit gamma-1 | 3 | |
| RPL5 | Ribosomal protein L5 | 3 | |
| | Septin 7 variant 4 | 3 | |
| OLA1 | Obg-like ATPase 1 | 3 | |
| SEPT2 | Septin-2 | 3 | |
| RPS5 | Ribosomal protein S5, isoform CRA_a | 2 | |
| | cDNA FLJ76789, highly similar to Homo sapiens methionine-tRNA synthetase (MARS), mRNA | 2 | |
| | Condensin complex subunit 1 | 2 | |
| DFNA5 | Deafness, autosomal dominant 5, isoform CRA_a | 2 | |
| ABCF3 | ATP-binding cassette sub-family F member 3 isoform 1 (Fragment) | 2 | |
| LRRFIP1 | Leucine rich repeat (In FLII) interacting protein 1, isoform CRA_c | 2 | |
| | cDNA FLJ53366, highly similar to Probable ATP-dependent RNA helicase DDX5 (EC 3.6.1.-) | 2 | |
| PSMC1 | 26S protease regulatory subunit 4 | 2 | |
| HSPA4 | Heat shock 70 kDa protein 4 | 2 | |
| SH3GL1 | SH3 domain GRB2-like 1 | 2 | |
| PSMC2 | 26S protease regulatory subunit 7 | 2 | |
| SHC1 | SHC-transforming protein 1 | 2 | |
| | cDNA FLJ50985, highly similar to Segment polarity protein dishevelled homologDVL-2 | 2 | |
| RUVBL2 | RuvB-like 2 | 2 | |
| HAUS6 | HAUS augmin-like complex subunit 6 | 2 | |
| | cDNA FLJ30049 fis, clone ADRGL1000033, highly similar to 26S proteasome non-ATPase regulatory subunit 3 | 2 | |
| SLC3A2 | 4F2 cell-surface antigen heavy chain | 2 | |
| NUFIP2 | Nuclear fragile X mental retardation protein interacting protein 2 | 2 | |

**Supplementary Table 5.3 – continuing next page**

| Unique to mPKM2-WT | | Unique Peptide | |
| --- | --- | --- | --- |
| Gene | Identified Proteins | WT | K433E |
| DOCK7 | Dedicator of cytokinesis protein 7 | 2 | |
| SFPQ | Splicing factor proline/glutamine-rich (Polypyrimidine tract binding protein associated) | 2 | |
| HCFC1 | Host cell factor 1 | 2 | |
| DYNC1H1 | Cytoplasmic dynein 1 heavy chain 1 | 2 | |
| FLG2 | Filaggrin-2 | 2 | |
| RPS29 | 40S ribosomal protein S29 | 2 | |
| | Triosephosphate isomerase (Fragment) | 2 | |
| ATP5O | ATP synthase subunit O, mitochondrial | 2 | |
| | Adenylyl cyclase-associated protein | 2 | |
| KIAA1468 | KIAA1468, isoform CRA_b | 2 | |
| | cDNA, FLJ95525, highly similar to Homo sapiens synapse associated protein 1, SAP47 homolog (SYAP1), mRNA | 2 | |
| AHCY | Adenosylhomocysteinase | 2 | |
| CLUH | Clustered mitochondria protein homolog | 2 | |
| | cDNA, FLJ94230, highly similar to Homo sapiens thioredoxin-like 1 (TXNL1), mRNA | 2 | |
| DHX29 | ATP-dependent RNA helicase DHX29 | 2 | |
| PSMD8 | 26S proteasome non-ATPase regulatory subunit 8 | 2 | |
| | cDNA, FLJ92583, highly similar to Homo sapiens glycogenin (GYG), mRNA | 2 | |
| ZFYVE16 | Zinc finger, FYVE domain containing 16, isoform CRA_a | 2 | |
| NARS | Asparagine--tRNA ligase, cytoplasmic | 2 | |
| JTV1 | JTV1 gene, isoform CRA_a | 2 | |
| | cDNA, FLJ96812, highly similar to Homo sapiens threonyl-tRNA synthetase (TARS), mRNA | 2 | |
| GIT1 | ARF GTPase-activating protein GIT1 | 2 | |
| BUB3 | Mitotic checkpoint protein BUB3 | 2 | |
| HN1L | Hematological and neurological-expressed 1-like protein | 2 | |
| DRG1 | Developmentally-regulated GTP-binding protein 1 | 2 | |
| ATP5J2 | ATP synthase subunit f, mitochondrial | 2 | |
| AP3M1 | Adaptor-related protein complex 3, mu 1 subunit, isoform CRA_a | 2 | |
| ALDH7A1 | Alpha-aminoadipic semialdehyde dehydrogenase | 2 | |

**Supplementary Table 5.3** – **mPKM2-WT versus mPKM2-K433E mutant protein-protein interaction enrichment comparisons.** 380 proteins were identified in total from both mPKM2-WT (WT) and mPKM2-K433E (K433E) samples. 86 and 90 proteins were uniquely identified in WT and K433E mutant, respectively. 204 mutual proteins were identified in both WT and K433E. Data are expressed as the number of unique peptides hits where the higher the unique peptide hits, the more certain the identification. Unique peptide hit suggests the following: 1 = possible identification, 2-3 = probable identification, ≥4 = almost certain identification. N=1

| Gene name | Protein name | Unique Peptides | | |
|---|---|---|---|---|
| | | Venus | WT | Mutant |
| **Metabolic Pathways** | | | | |
| ACACA | Acetyl-CoA carboxylase 1 | 44 | 45 | 51 |
| ACLY | ACLY variant protein | | 5 | 3 |
| AHCY | Adenosylhomocysteinase | | 2 | |
| ALDH1A1 | Retinal dehydrogenase 1 | 4 | 4 | 3 |
| ALDH7A1 | Alpha-aminoadipic semialdehyde dehydrogenase | | 2 | |
| ALDOA | Fructose-bisphosphate aldolase A | 3 | 4 | 4 |
| ATP5A1 | ATP synthase subunit alpha, mitochondrial | 5 | 9 | 4 |
| ATP5B | ATP synthase subunit beta, mitochondrial | 2 | 4 | 4 |
| ATP5J2 | ATP synthase subunit f, mitochondrial | | 2 | |
| ATP5O | ATP synthase subunit O, mitochondrial | | 2 | |
| ATP6V1A | V-type proton ATPase catalytic subunit A | | 4 | |
| ENO1 | Enolase 1, (Alpha), isoform CRA_a | 6 | 9 | 5 |
| EPRS | Bifunctional glutamate/proline--tRNA ligase | 6 | 8 | 4 |
| GAPDH | Glyceraldehyde-3-phosphate dehydrogenase | 8 | 12 | 4 |
| GART | Trifunctional purine biosynthetic protein adenosine-3 | 5 | 2 | 7 |
| LDHA | L-lactate dehydrogenase A chain | | 5 | 3 |
| MCCC1 | Methylcrotonoyl-CoA carboxylase 1 isoform 1 | 15 | 25 | 23 |
| MCCC2 | Methylcrotonoyl-CoA carboxylase beta chain, mitochondrial | 12 | 12 | 6 |
| MTHFD1 | Methylenetetrahydrofolate dehydrogenase (NADP+ dependent) 1, methenyltetrahydrofolate cyclohydrolase, formyltetrahydrofolate synthetase, isoform CRA_a | 2 | 3 | 2 |
| NME2 | Nucleoside diphosphate kinase B | 2 | 4 | 2 |
| PAICS | Phosphoribosylaminoimidazole carboxylase, isoform CRA_c phosphoribosylaminoimidazole succinocarboxamide synthetase, | 3 | 5 | |
| PC | Pyruvate carboxylase | 18 | 15 | 21 |
| PCCA | Propionyl-CoA carboxylase alpha chain, mitochondrial | 3 | 7 | 5 |
| PGK2 | Phosphoglycerate kinase 2 | 3 | 4 | 2 |
| PKM | Pyruvate kinase PKM | 17 | 164 | 242 |

**Supplementary Table 5.4.1 – Bio-identification of metabolic proteins interacting with mPKM2-WT, mPKM2-K433E mutant and non-targeting Venus control.** mPKM2-WT (WT), mPKM2-K433E mutant (Mutant) and non-targeting Venus control (Venus). Proteins involved in cell cycles were classified using Pather.org database. Data are expressed as the number of unique peptides hits where the higher the unique peptide hits, the more certain the identification. Unique peptide hit suggests the following: 1 = possible identification, 2-3 = probable identification, ≥4 = almost certain identification. N=1

| Gene name | Protein name | Unique Peptides | | |
|---|---|---|---|---|
| | | Venus | WT | Mutant |
| **Cell cycle** | | | | |
| CKAP5 | Cytoskeleton-associated protein 5 | 27 | 16 | 19 |
| CLTC | Clathrin heavy chain | | | 3 |
| EMD | Emerin | 3 | 2 | 3 |
| EPB41 | Protein 4.1, Erythrocyte Membrane Protein Band 4.1 | | | 2 |
| ERCC6L | DNA excision repair protein ERCC-6-like | 2 | 2 | 2 |
| FLNA | Filamin A | 119 | 126 | 113 |
| GIGYF2 | GRB10 Interacting GYF Protein 2, Trinucleotide repeat containing 15, isoform CRA_a | 9 | 7 | 5 |
| RACK1 | Receptor of-activated protein C kinase 1 | | 4 | 3 |
| HAUS5 | HAUS augmin-like complex subunit 5 | 6 | 6 | 4 |
| HSP90AA1 | Heat shock protein HSP 90-alpha | 10 | 10 | 20 |
| KIF4A | Chromosome-associated kinesin KIF4A | 4 | | 3 |
| KRT18 | Keratin 18, isoform CRA_a | 42 | 50 | 47 |
| LMNA | Prelamin-A/C | | | 3 |
| MAP4 | Microtubule-associated protein | 19 | 9 | 7 |
| MRE11A | MRE11 meiotic recombination 11 homolog A, isoform CRA_a | 7 | 9 | 8 |
| MYH9 | Myosin, heavy polypeptide 9, non-muscle, isoform CRA_a | 7 | 5 | 6 |
| NCAPG | Condensin complex subunit 3 | 2 | 2 | |
| NEK9 | NIMA (Never in mitosis gene a)-related kinase 9, isoform CRA_a | 9 | 9 | 9 |
| NUDC | Nuclear migration protein nudC | | | 3 |
| PRKDC | DNA-dependent protein kinase catalytic subunit | | 2 | 2 |
| PTPN11 | Tyrosine-protein phosphatase non-receptor type 11 | | | 2 |
| RACGAP1 | Rac GTPase activating protein 1, isoform CRA_a | | | 2 |
| RAN | GTP-binding nuclear protein Ran | | 4 | |
| RANBP2 | E3 SUMO-protein ligase RanBP2 | 2 | | 2 |
| RPS3 | 40S ribosomal protein S3 | | 3 | 2 |
| RUVBL1 | RuvB-like helicase | 11 | 7 | 5 |
| SEPT9 | Septin-9 | 19 | 19 | 10 |
| STMN1 | Stathmin | | | 3 |
| TNKS1BP1 | Tankyrase 1 binding protein 1, 182kDa, isoform CRA_a | 6 | | 2 |
| TP53BP2 | Apoptosis-stimulating of p53 protein 2 | 2 | 2 | 3 |
| TPR | Nucleoprotein TPR | 14 | 13 | 12 |
| TUBB | Beta 5-tubulin | 11 | 16 | 17 |
| TUBB4B | Tubulin, beta 2C; Tubulin Beta 4B Class Ivb | 10 | 17 | 15 |
| VCPIP1 | Deubiquitinating protein VCIP135 | 6 | 7 | 5 |

**Supplementary Table 5.4.2 – Bio-identification of cell cycle proteins interacting with mPKM2-WT, mPKM2-K433E mutant and non-targeting Venus control.** mPKM2-WT (WT), mPKM2-K433E mutant (Mutant) and non-targeting Venus control (Venus). Proteins involved in cell cycles were classified using Pather.org database. Data are expressed as the number of unique peptides hits where the higher the unique peptide hits, the more certain the identification. Unique peptide hit suggests the following: 1 = possible identification, 2-3 = probable identification, ≥4 = almost certain identification. N=1

| Gene name | Protein name | Unique Peptides | | |
|---|---|---|---|---|
| | | Venus | WT | Mutant |
| **Glycolytic Enzymes** | | | | |
| PKM | Pyruvate kinase PKM | 17 | 164 | 242 |
| PC | Pyruvate carboxylase | 18 | 15 | 21 |
| GAPDH | Glyceraldehyde-3-phosphate dehydrogenase | 8 | 12 | 4 |
| ENO1 | Enolase 1, (Alpha), isoform CRA_a | 6 | 9 | 5 |
| LDHA | L-lactate dehydrogenase A-like 6A | | 5 | 3 |
| ALDOA | Fructose-bisphosphate aldolase A | 3 | 4 | 4 |
| PGK1 | Phosphoglycerate Kinase 1 | 3 | 4 | 2 |
| ALDH7A1 | Alpha-aminoadipic semialdehyde dehydrogenase | | 2 | |
| ACACA | Acetyl-CoA carboxylase 1 | 44 | 45 | 51 |
| **Calcium binding** | | | | |
| EPS15L1 | Epidermal growth factor receptor pathway substrate 15-like 1, isoform CRA_a | 4 | 2 | 3 |
| STK38 | Serine/threonine kinase 38, isoform CRA_a | 5 | 3 | 4 |
| EPS15 | Epidermal growth factor receptor substrate 15 | | 2 | 2 |
| **Cell adhesion** | | | | |
| CTNND1 | Catenin delta-1 | 5 | | 2 |
| TNS3 | Tensin-3 | 9 | 3 | 7 |
| ANXA1 | Annexin A1 | 11 | 16 | 9 |
| MYPN | Myopalladin | | 2 | 2 |
| **Gap Junction** | | | | |
| ZYX | Zyxin | 4 | 5 | 5 |
| TJP1 | Tight junction protein ZO-1 | 8 | 5 | 4 |

**Supplementary Table 5.4.3 – Bio-identification of functional proteins interacting with mPKM2-WT, mPKM2-K433E mutant and non-targeting Venus control.** mPKM2-WT (WT), mPKM2-K433E mutant (Mutant) and non-targeting Venus control (Venus). Proteins were classified by biological processes using Pather.org database. Data are expressed as the number of unique peptides hits where the higher the unique peptide hits, the more certain the identification. Unique peptide hit suggests the following: 1 = possible identification, 2-3 = probable identification, ≥4 = almost certain identification. N=1

# Chapter 6 – Conclusion and Future work

## 6.1 Concluding discussion

Pancreatic cancer, particularly pancreatic ductal adenocarcinoma (PDAC), is a fatal cancer with limited therapeutic treatment options and successes, this malignancy has one of the poorest patient survival prognoses amongst all cancers [1,2]. Over the past three decades, PDAC patient survival prognosis has marginally improved by a few months with current treatment regimens [1,8], suggesting the need to identify novel targets and strategies to therapeutically target the disease. As multiple cancers exhibit metabolic reprogramming towards glycolysis (Warburg effect) and remodelling of $Ca^{2+}$ signalling machinery, intensive research has been ongoing to strategically exploit these vulnerabilities [50,109,230,341]. Indeed, the majority of PDAC tumours overexpress oncogenic PKM2 [304] which drives the Warburg phenomenon as well as upregulates the expression of PMCA4 [118], a major ATP-consuming $Ca^{2+}$ efflux machinery often remodelled in multiple cancers [124]. Although controversial, the role of PKM2 has been extensively studied in PDAC [304,342]. However, less is known about the role of PMCAs in PDAC. The previous study by James, A.D et al (2015) showed that NCX minimally contributes towards $Ca^{2+}$ clearance whereas PMCA functions as primary $Ca^{2+}$efflux mechanism, suggesting that PMCAs play a critical role in $Ca^{2+}$ homeostasis role in both MIAPaCa-2 and PANC-1 PDAC cell lines [114,121,123]. Further linking glycolysis and PMCA, James, A.D *et al* (2013, 2015) also reported glycolytic ATP is essential for fuelling PMCA activity, preventing cytotoxic $Ca^{2+}$ overload and potentially driving PDAC cell growth and survival [114]. The current thesis presents evidence which suggests that overexpression of plasma membrane $Ca^{2+}$ ATPase isoform 4 (PMCA4) is essential for the maintenance of $Ca^{2+}$ homeostasis and cancer hallmarks in PDAC cells, therefore, strategies which impair PMCA4 activity may therapeutically benefit PDAC treatment. These strategies, explored in parts in this thesis, include the disruption of Cav-1 enrich membrane subdomains and identification of putative PKM2-plasma membrane binding protein which may potentially be inhibited to cut-off privileged glycolytic ATP supply to the PMCA4.

Focusing on the role of PMCA on cancer hallmarks, Chapter 3 of this thesis firstly highlights the clinical relevance of PMCA isoforms, particularly correlating PMCA4 overexpression in PDAC tumour with poor patient survival prognosis, through data mining of publicly available databases [343–345]. Furthermore, this work has identified MIAPaCa-2 as a clinically relevant PDAC model which exhibits overexpression PMCA4 and the Warburg phenomenon, both of which are typical characteristics of patient-derived PDAC tumours [118,302]. In line with findings by James, A.D *et al* (2013,2015) that PMCA is the major $Ca^{2+}$ efflux mechanism in PDAC cells [121,123], we demonstrated that PMCA4 plays a key role in PDAC $Ca^{2+}$ clearance and regulation of $Ca^{2+}$ homeostasis. As glycolysis-derived ATP is required to fuel PMCA activity in PDAC cells [121,123], it could be inferred that overexpression of PMCA4 requires enhanced glycolytic flux to fulfil this increased ATP-demand at the plasma membrane. Hypothetically, this ATP-consumption also symbiotically limits metabolite-induced inhibition of key GEs which drive the glycolytic flux, particularly PFK-1 and PKM2. Therefore, we predicted that inhibition of PMCA4, reducing the ATP-consumption at the plasma membrane, could potentially reduce glycolytic flux. Unexpectedly, knocking down PMCA4 expression had no effect on basal mitochondrial respiration

and glycolysis metabolic phenotypes, as assessed by Agilent Mito stress and glycolytic stress tests. This suggests that remodelling of PMCA4 expression in PDAC cells have minimal effect on basal cellular metabolic phenotype, including glycolytic flux. However, regardless of its lack of involvement in regulating metabolic phenotype, we showed that PMCA4 expression in MIAPaCa-2 PDAC cells plays a role in facilitating cell migration and enhanced apoptosis resistance. These observations were consistent with previous studies in corneal epithelial wound healing [245] and breast cancer cells [249], respectively. Therefore, the overexpression of PMCA4 in PDAC remains an important oncogenic alteration which facilitates the manifestation of cancer hallmarks, particularly cell migration and apoptosis resistance.

Although inhibition of PMCA4 may provide a means to inhibit PDAC, currently reported selective inhibitors of PMCA4, including aurintricarboxylic acid (ATA) and caloxin 1c2, had minimal inhibitory effects on PMCA4 activity at concentrations reported to exhibit negligible non-specific effects (described in Chapter 2, section 2.2.3). As previous findings suggest that PMCA4 and key GEs potentially co-localise at the Cav-1-enriched plasma membrane (PM) "caveolae" subdomain [113,116,228,229], the work in Chapter 4 of this thesis broadly examined the relevance of this Cav-1-enriched subdomain in PDAC and whether it could be exploited to target PMCA4 activity. Consistent with previous studies [117,346], we showed through data mining of public databases that Cav-1 is overexpressed could be correlated to poor PDAC patient survival. In addition, we highlighted that co-elevation of PMCA4 and Cav-1 had a worse impact on PDAC patient survival outcome, suggesting potential functional cooperation of these two genes in PDAC. In line with previous findings in mouse small intestine [113] and sperm cells [347], this work presented in Chapter 4 provides the evidence that the Cav-1 expression knockdown led to impaired PMCA activity in glycolysis-reliant MIAPaCa-2 PDAC cells. This disruption of Cav-1-enriched caveolae, induced by either methyl-β-cyclodextrin (MβC) or siRNA knockdown of Cav-1 expression, leads to impaired PMCA-mediated $Ca^{2+}$ clearance in MIAPaCa-2 cells, albeit these disruptions induce a minimal effect on $Ca^{2+}$ homeostasis. This suggests that $Ca^{2+}$ homeostasis was sufficiently maintained despite the modest impairment of PMCA4 activity in MIAPaCa-2 cells. Potential explanations for this PMCA4 impairment includes compartmental ATP-depletion due to the loss of favourable Cav-1 docking sites for glycolytic enzymes [116], and/or, the loss of Cav-1-mediated lipid transport (cholesterol and acidic phospholipids) to the plasma membrane [257,348] which disrupts the membrane lipid microenvironment [257,281] required for optimum PMCA function [349–351]. As the effect of Cav-1 knockdown on PMCA4 activity was very modest, it might be that PMCA4 functions independently of Cav-1 expression, possibly due to the non-exclusive PMCA4 expression in lipid rafts [112] as well as the caveolae [113,352]. This line of enquiry could be clarified by further immunoprecipitation and/or immunofluorescence confocal microscopy of PMCA4 and Cav-1. Overall, Cav-1 expression had no effect on PDAC cell viability, proliferation, glycolysis and mitochondrial respiration metabolic phenotypes.

As plasma membrane-associated glycolytic enzymes (PM-GEs) may be important for providing a privileged ATP supply to fuel the PMCA, we hypothesized that PMCA activity could be inhibited by the disruption of GEs binding to the plasma membrane, cutting-off this privileged ATP supply. Compartmentalization of glycolytic enzymes (GEs), in erythrocytes (lacking mitochondria) and at the leading edge of migrating cells, has been proposed by multiple studies [116,296,298,353]. In

erythrocytes, band 3 transmembrane protein (solute carrier family 4 member 1; SLC4A1) has been identified as the plasma membrane binding site of the glycolytic metabolon [296]. In nucleated cells, however, Cav-1 has been suggested to target PFK and ALD to the plasma membrane in rat vascular smooth muscle [116] whereas PKM2 is targeted to the plasma membrane by SNAP23, an important component of the exosome, in Hela and A549 pulmonary adenocarcinoma cells [354]. However, limited evidence is available on the protein which binds or targets GEs to the plasma membrane in PDAC cells. As an attempt to identify this putative PM-GE binding protein, the work presented in Chapter 5 used an unbiased screening technique to identify putative interacting partners of PKM2, using BirA* proximity-ligation fusion protein. Providing the first preliminary evidence that voltage-gated $K^+$ channel subfamily H member 4 (KCNH4) is a putative intrinsic plasma membrane protein which significantly interacts with PKM2, this work strongly suggests that a subpopulation PKM2 resided near the plasma membrane in PDAC. In addition, we showed that PKM2 interacted with other GEs, particularly aldolase A (ALDOA), known to bind to Cav-1 and localised at the caveolae [116]. This screening also revealed the putative moonlighting functions of PKM2 in PDAC which includes processes (e.g. regulation of DNA replication)[306]. However, the results presented in Chapter 5, suggests that PKM2 did not interact with any caveolae markers and had an insignificant interaction enrichment with SNAP29 (synaptosome associated protein 29) in MIAPaCa-2 PDAC cells. As the results presented in Chapter 5 are very preliminary in nature, further extensive experimentation will be required to validate the physical interaction of KCNH4 and PKM2 and investigate the biological implication of disrupting this putative interaction in PDAC.

In conclusion, the results presented in this current thesis suggest that PMCA4 overexpression plays a critical role in $Ca^{2+}$ homeostasis and cancer hallmarks in PDAC. We, therefore, propose that strategies which enable selective inhibition or impairment of PMCA4 function may selectively sensitize PDAC cells to apoptotic cell death. Based on this work, future studies may be done to dissect the mechanistic regulation of PMCA4 in PDAC cancer hallmarks, and understand whether inhibition of PMCA4 could indeed be exploited to therapeutically sensitize PDAC to currently available first-line treatments, validate the relationship between KCNH4 and PKM2 (PM-GEs binding proteins), and identify whether the disruption of this interaction could be exploited to selectively target PDAC which overexpresses PMCA4.
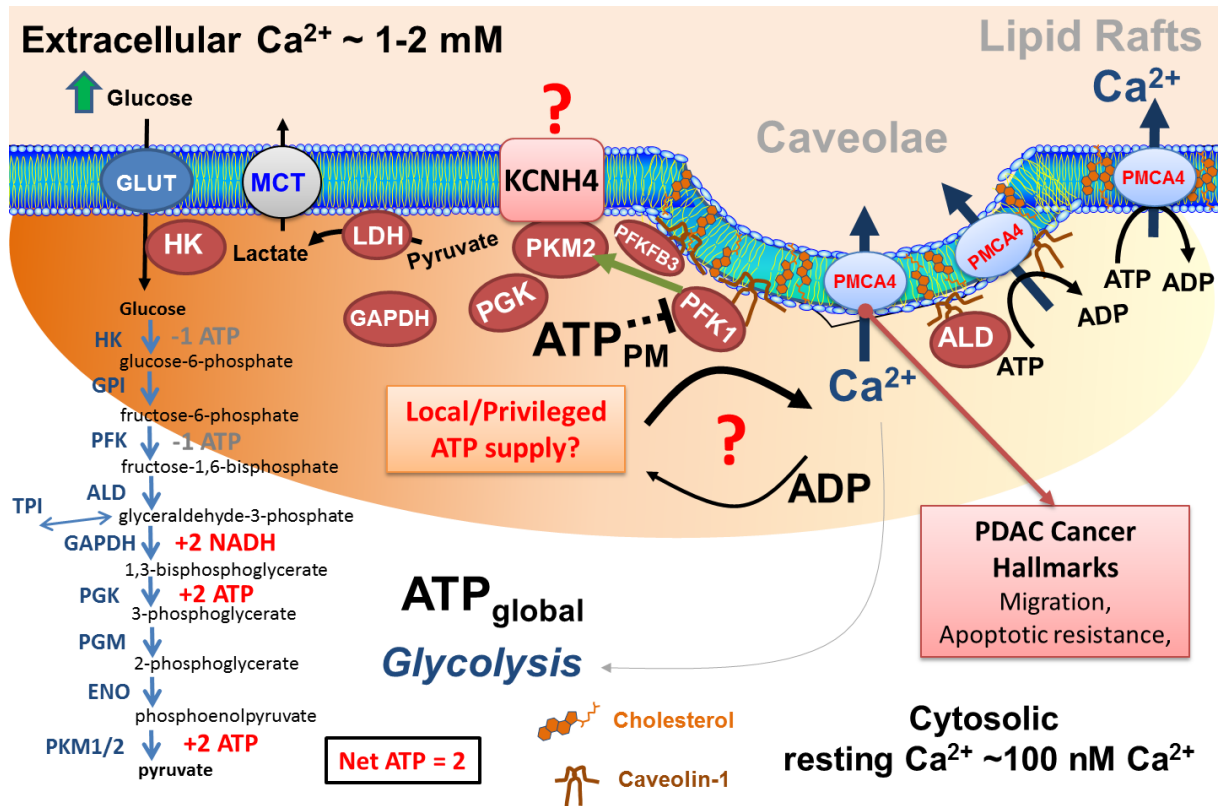
**Figure 6.1 – Proposed relationship between PMCA4 and putative glycolytic ATP supply at the membrane.** In MIAPaCa-2 PDAC cells, PMCA4 is the critical $Ca^{2+}$ efflux mechanism required for the maintenance of low resting $[Ca^{2+}]_i$ and contributes towards cancer hallmarks, including enhanced migration and apoptotic resistance. PMCA4 potentially resides in lipid-rich membrane subdomains, not exclusive to Cav-1-enriched caveolae, but likely includes lipid rafts. KCNH4 potentially serves as an intrinsic transmembrane protein which binds ATP-producing PKM2 to the plasma membrane subdomains, in close proximity to PMCA4, providing privileged ATP supply which drives PMCA-mediated maintenance of $Ca^{2+}$ homeostasis. This consumption of local ATP ($ATP_{PM}$), however, does not impact global glycolytic flux and ATP ($ATP_{global}$).

## 6.2 Future work

Based on the current evidence presented in this thesis, many potential experiments could be done to extensively expand on the findings:

### Chapter 3 – PMCA4 paper

- Overexpress PMCA4 in normal pancreas cell lines (e.g. HPDE and HPNE) and/or alternative PDAC cell lines (e.g. PANC-1) which express low levels of PMCA4 to examine whether this remodelling results in cancer phenotype observed in MIAPaCa-2, particularly migration and apoptotic resistance.

- Dissecting the signalling pathways involved in PMCA4 mediated cell migration and apoptosis resistance. As the majority of PMCA4 overexpression in MIAPaCa-2 cells are PMCA4b variant, known to possess PDZ binding site and is involved in mediating signal transduction via multiple effectors (e.g. NOS). Therefore, identification of PMCA4-mediating signalling pathway that is responsible for modulating these cancer phenotypes may provide insights into PDAC disease progression.

- To investigate whether PMCA4 knockdown would lead to sensitization (e.g. caspase 3/7 cleavage apoptotic assay) against first line PDAC chemotherapeutic drugs (e.g. gemcitabine, paclitaxel, cis-platin) as this would provide insights into the clinical relevance of targeting PMCA4 activity in PDAC.

*Chapter 4 – Plasma Membrane Calcium ATPase 4 (PMCA4) functional activity is dependent on Cav-1 expression in pancreatic ductal adenocarcinoma cells*

- To validate the co-localisation of Cav-1 and PMCA4 within the same plasma membrane subdomain compartment, immunofluorescence confocal microscopy could be employed to image the co-localisation of Cav-1 and PMCA4 within the same plane of view.
- To verify whether the knockdown of Cav-1 expression could lead to the disruption of caveolae, scanning electron microscopy could be used to image the caveolae.
- As Cav-1 expression had been linked to cancer hallmarks in PDAC, particularly migration and apoptosis resistance, further caspase 3/7 cleavage apoptosis assay and gap closure migration assays could be performed, respectively.
- Overexpression of Cav-1 in normal pancreatic cell lines could be done to identify potential manifestation of cancer phenotypes such as growth (SRB/WST-8), cell migration (gap closure), alterations in PMCA4 expression (Western immunoblot) and metabolic phenotype (Agilent Seahorse XFe96 Mito stress, glycolysis stress and ATP production rate assay).
- To investigate whether Cav-1 knockdown associated PMCA4 impairment could sensitize PDAC cells to apoptotic stimuli and/or first line PDAC therapeutics. If yes, understand how Cav-1 mediate this impairment could provide a novel strategy to target PDAC.
- To understand whether PMCA4 activity impairment occurred due to Cav-1 knockdown associated dysregulation of membrane lipid content, measurement of cholesterol content in the plasma membrane could be performed. If the cholesterol content has been reduced due to the loss of Cav-1 mediated lipid transport, we could test whether the addition of exogenous cholesterol could rescue PMCA4 activity.

*Chapter 5 – PKM2 chapter*

- Validation of KCNH4 interaction with PKM2 using techniques such as co-immunoprecipitation, proximity ligation assay, and immunofluorescence confocal microscopy.
- KCNH4 knockdown to examine whether this putative PM-GE binding protein serves to modulate glycolytic flux (Agilent Seahorse XFe96 Mito stress, glycolysis stress, and ATP production rate assay) and/or PMCA4 activity (PMCA activity and $Ca^{2+}$ overload experiments). If KCNH4 knockdown does indeed inhibit PMCA activity or alter glycolytic flux, further efforts may be put into the identification of PKM2 binding site on KCNH4. This is because the disruption of PKM2-KCNH4 interaction could potentially provide a novel therapeutic target for the treatment of PDAC.
- The functional role of PKM2 in PDAC can be further investigated by interrogating present mass spectrometry data through proteomics programs (e.g. Ingenuity Pathway Analysis, PANTHER and Strings databases) to categorize moonlighting functions associated with cancer hallmarks.

- Alternative baits could be used for bio-identification to strengthen the integrity of PKM2-BirA* data, particularly for the identification of putative plasma membrane proteins which binds GEs. For instance, intrinsic plasma membrane proteins of interest could be used as baits: PMCA4b and KCNH4.
- Examine the effects of PKM2-BirA overexpression in MIAPaCa-2 cell line, particularly on cell viability and proliferation (WST-8/ SRB) and metabolic status (Agilent Seahorse XFe96 Mito stress, glycolysis stress, and ATP production rate assay).

# Chapter 7 – References

1. Pancreatic cancer statistics | Cancer Research UK [Internet]. [cited 2019 Jul 19]. Available from: https://www.cancerresearchuk.org/health-professional/cancer-statistics/statistics-by-cancer-type/pancreatic-cancer#heading-Zero

2. John S, Broggio J. Cancer survival in England : national estimates for patients followed up to 2017 [Internet]. 2019. Available from: https://www.ons.gov.uk/peoplepopulationandcommunity/healthandsocialcare/conditionsanddiseases/bulletins/cancersurvivalinengland/nationalestimatesforpatientsfollowedupto2017

3. Yadav D, Lowenfels AB. The Epidemiology of Pancreatitis and Pancreatic Cancer. Gastroenterology [Internet]. 2013 May 1 [cited 2019 Jul 19];144(6):1252–61. Available from: https://linkinghub.elsevier.com/retrieve/pii/S0016508513001686

4. Smyth D, Smyth T. The relationship between diabetes and cancer. J Diabetes Nurs. 2005;9(7):269.

5. Mena S, Ortega A, Estrela JM. Oxidative stress in environmental-induced carcinogenesis. Mutat Res Toxicol Environ Mutagen [Internet]. 2009 Mar 31 [cited 2019 Jul 19];674(1–2):36–44. Available from: http://www.ncbi.nlm.nih.gov/pubmed/18977455

6. Adami H-O, Hunter D, Trichopoulos D, editors. Textbook of Cancer Epidemiology [Internet]. Oxford University Press; 2008. Available from: http://www.oxfordscholarship.com/view/10.1093/acprof:oso/9780195311174.001.0001/acprof-9780195311174

7. WAGNER M, LUHRS H, KLOPPEL G, ADLER G, SCHMID R. Malignant transformation of duct-like cells originating from acini in transforming growth factor α transgenic mice. Gastroenterology [Internet]. 1998 Nov 1 [cited 2019 Jul 19];115(5):1254–62. Available from: https://linkinghub.elsevier.com/retrieve/pii/S0016508598700988

8. Quaresma M, Coleman MP, Rachet B. Articles 40-year trends in an index of survival for all cancers combined and survival adjusted for age and sex for each cancer in England and Wales, 1971-2011: a population-based study. www.thelancet.com [Internet]. 2015 [cited 2019 Jul 19];385. Available from: http://dx.doi.org/10.1016/

9. Mönkemüller K, Fry LC, Malfertheiner P. Pancreatic Cancer Is 'Always Non-Resectable.' Dig Dis [Internet]. 2007 [cited 2019 Jul 19];25(3):285–8. Available from: http://www.ncbi.nlm.nih.gov/pubmed/17827959

10. Perera RM, Bardeesy N. Pancreatic Cancer Metabolism: Breaking It Down to Build It Back Up. Cancer Discov [Internet]. 2015 Dec 1 [cited 2019 Aug 17];5(12):1247–61. Available from: http://www.ncbi.nlm.nih.gov/pubmed/26534901

11. Shibata W, Kinoshita H, Hikiba Y, Sato T, Ishii Y, Sue S, et al. Overexpression of HER2 in the pancreas promotes development of intraductal papillary mucinous neoplasms in mice. Sci Rep [Internet]. 2018 Dec 18 [cited 2019 Aug 17];8(1):6150. Available from: http://www.nature.com/articles/s41598-018-24375-2

12. van Heek NT, Meeker AK, Kern SE, Yeo CJ, Lillemoe KD, Cameron JL, et al. Telomere shortening is nearly universal in pancreatic intraepithelial neoplasia. Am J Pathol [Internet]. 2002 Nov [cited 2019 Aug 17];161(5):1541–7. Available from: http://www.ncbi.nlm.nih.gov/pubmed/12414502

13. Hanahan D, Weinberg RA. Hallmarks of cancer: the next generation. Cell [Internet]. 2011 Mar 4;144(5):646–74. Available from: http://dx.doi.org/10.1016/j.cell.2011.02.013

14. Miwa H, Numata K, Sugimori K, Kaneko T, Sakamaki K, Ueda M, et al. Differential diagnosis of solid pancreatic lesions using contrast-enhanced three-dimensional ultrasonography. Abdom Imaging [Internet]. 2014 Oct 8 [cited 2019 Aug 17];39(5):988–99. Available from: https://link-springer-com.manchester.idm.oclc.org/content/pdf/10.1007%2Fs00261-014-0135-8.pdf

15. Campbell PJ, Yachida S, Mudie LJ, Stephens PJ, Pleasance ED, Stebbings LA, et al. The patterns and dynamics of genomic instability in metastatic pancreatic cancer. Nature [Internet]. 2010 Oct 27 [cited 2019 Jul 19];467(7319):1109–13. Available from: http://www.nature.com/articles/nature09460

16. Sousa CM, Kimmelman AC. The complex landscape of pancreatic cancer metabolism. Carcinogenesis [Internet]. 2014 Jul [cited 2019 Jul 19];35(7):1441–50. Available from: http://www.ncbi.nlm.nih.gov/pubmed/24743516

17. Chan AKC, Bruce JIE, Siriwardena AK. Glucose metabolic phenotype of pancreatic cancer. World J Gastroenterol [Internet]. 2016 Mar 28 [cited 2019 Jul 19];22(12):3471–85. Available from: http://www.ncbi.nlm.nih.gov/pubmed/27022229

18. Erkan M, Michalski CW, Rieder S, Reiser–Erkan C, Abiatari I, Kolb A, et al. The Activated

Stroma Index Is a Novel and Independent Prognostic Marker in Pancreatic Ductal Adenocarcinoma. Clin Gastroenterol Hepatol [Internet]. 2008 Oct 1 [cited 2019 Jul 19];6(10):1155–61. Available from: https://linkinghub.elsevier.com/retrieve/pii/S1542356508004989

19.  Hwang RF, Moore T, Arumugam T, Ramachandran V, Amos KD, Rivera A, et al. Cancer-associated stromal fibroblasts promote pancreatic tumor progression. Cancer Res [Internet]. 2008 Feb 1 [cited 2019 Jul 19];68(3):918–26. Available from: http://www.ncbi.nlm.nih.gov/pubmed/18245495

20.  Li J, Wientjes MG, Au JL-S. Pancreatic cancer: pathobiology, treatment options, and drug delivery. AAPS J [Internet]. 2010 Jun [cited 2019 Jul 19];12(2):223–32. Available from: http://www.ncbi.nlm.nih.gov/pubmed/20198462

21.  Ueno H, Kosuge T. Adjuvant treatments for resectable pancreatic cancer. J Hepatobiliary Pancreat Surg [Internet]. 2008 Sep 4 [cited 2019 Jul 19];15(5):468–72. Available from: http://link.springer.com/10.1007/s00534-008-1357-3

22.  Pokorny AMJ, Chin VT, Nagrial AM, Yip D, Chantrill LA. Metastatic pancreatic ductal adenocarcinoma: diagnosis and treatment with a view to the future. Intern Med J [Internet]. 2018 Jun 1 [cited 2019 Jul 20];48(6):637–44. Available from: http://doi.wiley.com/10.1111/imj.13810

23.  Uccello M, Moschetta M, Mak G, Alam T, Henriquez CM, Arkenau H-T. Towards an optimal treatment algorithm for metastatic pancreatic ductal adenocarcinoma (PDA). Curr Oncol [Internet]. 2018 Feb [cited 2019 Jul 20];25(1):e90–4. Available from: http://www.ncbi.nlm.nih.gov/pubmed/29507500

24.  Zimmerman JJ, von Saint André-von Arnim A, McLaughlin J. Cellular Respiration [Internet]. Fourth Edi. Pediatric Critical Care. Elsevier; 2011. 1058–1072 p. Available from: http://dx.doi.org/10.1016/B978-0-323-07307-3.10074-6

25.  Cooper GM. The Cell: A Molecular Approach. 2nd; The Mechanism of Oxidative Phosphorylation [Internet]. 2nd ed. Sunderland (MA): Sinauer Associates; 2000. Available from: https://www.ncbi.nlm.nih.gov/books/NBK9885

26.  Matthew G. Vander Heiden, Lewis C. Cantley, Craig B. Thompson. Understanding the Warburg Effect: The Metabolic Requirements of Cell Proliferation. Science (80- ) [Internet]. 2009;324(may):1029–1033. Available from: https://www.ncbi.nlm.nih.gov/pubmed/2204486

27.  Pfeiffer T, Schuster S, Bonhoeffer S. Cooperation and Competition in the Evolution of ATP-Producing Pathways. Science (80- ) [Internet]. 2001 Apr 20 [cited 2019 Aug 17];292(5516):504–7. Available from: http://www.ncbi.nlm.nih.gov/pubmed/13298683

28.  Scott CB. Contribution of anaerobic energy expenditure to whole body thermogenesis. 2005 [cited 2019 Aug 17]; Available from: http://www.nutritionandmetabolism.com/content/2/1/14

29.  Abdel-Haleem AM, Lewis NE, Jamshidi N, Mineta K, Gao X, Gojobori T. The Emerging Facets of Non-Cancerous Warburg Effect. Front Endocrinol (Lausanne) [Internet]. 2017 [cited 2019 Aug 18];8:279. Available from: http://www.ncbi.nlm.nih.gov/pubmed/29109698

30.  Lunt SY, Vander Heiden MG. Aerobic Glycolysis: Meeting the Metabolic Requirements of Cell Proliferation. Annu Rev Cell Dev Biol [Internet]. 2011 Nov 10 [cited 2019 Aug 18];27(1):441–64. Available from: http://www.annualreviews.org/doi/10.1146/annurev-cellbio-092910-154237

31.  De Berardinis RJ, Chandel NS. Fundamentals of cancer metabolism. Sci Adv. 2016;2(5).

32.  Warburg O. On the Origin of Cancer Cells. Science (80- ) [Internet]. 1956 Feb 24 [cited 2019 Aug 18];123(3191):309–14. Available from: http://science.sciencemag.org/

33.  Porporato PE, Filigheddu N, Pedro JMB-S, Kroemer G, Galluzzi L. Mitochondrial metabolism and cancer. Cell Res [Internet]. 2018 Mar 8 [cited 2019 Aug 18];28(3):265–80. Available from: http://www.nature.com/articles/cr2017155

34.  Cairns RA, Harris IS, Mak TW. Regulation of cancer cell metabolism. Nat Rev Cancer [Internet]. 2011;11(2):85–95. Available from: http://dx.doi.org/10.1038/nrc2981

35.  Vander Heiden MG, DeBerardinis RJ. Understanding the Intersections between Metabolism and Cancer Biology. Cell [Internet]. 2017 Feb [cited 2019 Aug 18];168(4):657–69. Available from: http://dx.doi.org/10.1016/j.cell.2016.12.039

36.  Cairns RA, Harris IS, Mak TW. Regulation of cancer cell metabolism. Nat Rev Cancer [Internet]. 2011 Feb 24 [cited 2019 Aug 18];11(2):85–95. Available from: http://www.nature.com/articles/nrc2981

37.  Vaupel P, Schmidberger H, Mayer A. The Warburg effect: essential part of metabolic reprogramming and central contributor to cancer progression. Int J Radiat Biol [Internet]. 2019 Jul 3 [cited 2019 Aug 18];95(7):912–9. Available from: http://www.ncbi.nlm.nih.gov/pubmed/30822194

38. Tanner LB, Goglia AG, Wei MH, Sehgal T, Parsons LR, Park JO, et al. Four Key Steps Control Glycolytic Flux in Mammalian Cells. Cell Syst. 2018 Jul 25;7(1):49-62.e8.

39. Mellati AA, Yücel M, Altinörs N, Gündüz U. Regulation of M2-type pyruvate kinase from human meningioma by allosteric effectors fructose 1,6 diphosphate and L-alanine. Cancer Biochem Biophys [Internet]. 1992 Oct;13(1):33–41. Available from: http://www.ncbi.nlm.nih.gov/pubmed/1343845

40. Christofk HR, Vander Heiden MG, Wu N, Asara JM, Cantley LC. Pyruvate kinase M2 is a phosphotyrosine-binding protein. Nature. 2008;452(7184):181–6.

41. Xie J, Dai C, Hu X. Evidence That Does Not Support Pyruvate Kinase M2 (PKM2)-catalyzed Reaction as a Rate-limiting Step in Cancer Cell Glycolysis. J Biol Chem [Internet]. 2016 Apr 22 [cited 2019 Aug 18];291(17):8987–99. Available from: http://www.ncbi.nlm.nih.gov/pubmed/26917721

42. Christofk HR, Vander Heiden MG, Harris MH, Ramanathan A, Gerszten RE, Wei R, et al. The M2 splice isoform of pyruvate kinase is important for cancer metabolism and tumour growth. Nature. 2008;452(7184):230–3.

43. Mazurek S, Boschek CB, Hugo F, Eigenbrodt E. Pyruvate kinase type M2 and its role in tumor growth and spreading. Semin Cancer Biol. 2005;15(4):300–8.

44. Mazurek S. Pyruvate kinase type M2: A key regulator of the metabolic budget system in tumor cells. Int J Biochem Cell Biol. 2011;43(7):969–80.

45. Berg JM, Tymoczko JL SL. Biochemistry. 5th edition; Section 16.2 - The Glycolytic Pathway Is Tightly Controlled. [Internet]. New York: W H Freeman; 2002. Available from: https://www.ncbi.nlm.nih.gov/books/NBK22395/

46. Ureta T, Lazo PA, Sols A. Allosteric inhibition of brain hexokinase by glucose 6-phosphate in the reverse reaction. Arch Biochem Biophys [Internet]. 1985 Jun;239(2):315–9. Available from: http://www.ncbi.nlm.nih.gov/pubmed/4004267

47. Muniyappa K, Mendicino J. Binding and regulatory properties of phosphofructokinase from swine kidney. Mol Cell Biochem [Internet]. 1984 Aug;63(1):21–32. Available from: http://www.ncbi.nlm.nih.gov/pubmed/6092905

48. Ros S, Schulze A. Balancing glycolytic flux: the role of 6-phosphofructo-2-kinase/fructose 2,6-bisphosphatases in cancer metabolism. Cancer Metab. 2013;1(1):1.

49. Jenkins CM, Yang J, Sims HF, Gross RW. Reversible high affinity inhibition of phosphofructokinase-1 by acyl-CoA: a mechanism integrating glycolytic flux with lipid metabolism. J Biol Chem [Internet]. 2011 Apr 8 [cited 2019 Aug 18];286(14):11937–50. Available from: http://www.ncbi.nlm.nih.gov/pubmed/21258134

50. Luengo A, Gui DY, Vander Heiden MG. Targeting Metabolism for Cancer Therapy. Cell Chem Biol [Internet]. 2017;24(9):1161–80. Available from: http://dx.doi.org/10.1016/j.chembiol.2017.08.028

51. Porporato PE, Dhup S, Dadhich RK, Copetti T, Sonveaux P. Anticancer targets in the glycolytic metabolism of tumors: a comprehensive review. Front Pharmacol [Internet]. 2011 [cited 2019 Aug 22];2:49. Available from: http://www.ncbi.nlm.nih.gov/pubmed/21904528

52. Gambhir SS. Molecular imaging of cancer with positron emission tomography. Nat Rev Cancer [Internet]. 2002 Sep [cited 2019 Aug 19];2(9):683–93. Available from: http://www.nature.com/articles/nrc882

53. Benjamin D, Robay D, Hindupur SK, Pohlmann J, Colombi M, El-Shemerly MY, et al. Dual Inhibition of the Lactate Transporters MCT1 and MCT4 Is Synthetic Lethal with Metformin due to NAD+ Depletion in Cancer Cells. Cell Rep [Internet]. 2018 Dec 11 [cited 2019 Aug 19];25(11):3047-3058.e4. Available from: https://www-sciencedirect-com.manchester.idm.oclc.org/science/article/pii/S2211124718318060

54. Benej M, Pastorekova S, Pastorek J. Carbonic Anhydrase IX: Regulation and Role in Cancer. In 2014. p. 199–219. Available from: http://link.springer.com/10.1007/978-94-007-7359-2_11

55. Fischer K, Voelkl S, Meidenbauer N, Ammer J, Gottfried E, Schwarz S, et al. Inhibitory effect of tumor cell-derived lactic acid on human T cells. Blood [Internet]. 2007;109(9):3812–9. Available from: http://eutils.ncbi.nlm.nih.gov/entrez/eutils/elink.fcgi?dbfrom=pubmed&amp;id=17255361&amp;retmode=ref&amp;cmd=prlinks

56. Koukourakis MI, Giatromanolaki A, Harris AL, Sivridis E. Comparison of metabolic pathways between cancer cells and stromal cells in colorectal carcinomas: A metabolic survival role for tumor-associated stroma. Cancer Res. 2006;66(2):632–7.

57. Pylayeva-Gupta Y, Grabocka E, Bar-Sagi D. RAS oncogenes: Weaving a tumorigenic web. Nat Rev Cancer [Internet]. 2011;11(11):761–74. Available from: http://dx.doi.org/10.1038/nrc3106

58. Rajalingam K, Schreck R, Rapp UR, Albert Š. Ras oncogenes and their downstream targets. Biochim Biophys Acta - Mol Cell Res [Internet]. 2007 Aug 1 [cited 2019 Aug 19];1773(8):1177–95. Available from: https://www-sciencedirect-com.manchester.idm.oclc.org/science/article/pii/S0167488907000286

59. di Magliano MP, Logsdon CD. Roles for KRAS in Pancreatic Tumor Development and Progression. Gastroenterology [Internet]. 2013 May [cited 2019 Aug 19];144(6):1220–9. Available from: http://www.ncbi.nlm.nih.gov/pubmed/23622131

60. Morris JP, Wang SC, Hebrok M. KRAS, Hedgehog, Wnt and the twisted developmental biology of pancreatic ductal adenocarcinoma. Nat Rev Cancer [Internet]. 2010 Oct;10(10):683–95. Available from: http://www.ncbi.nlm.nih.gov/pubmed/20814421

61. Hruban RH, Brune K, Fukushima N, Maitra A. Pancreatic Intraepithelial Neoplasia. In: Pancreatic Cancer [Internet]. Boston, MA: Springer US; 2008 [cited 2019 Aug 17]. p. 41–51. Available from: http://link.springer.com/10.1007/978-0-387-69252-4_3

62. Ying H, Kimmelman AC, Lyssiotis CA, Hua S, Chu GC, Fletcher-Sananikone E, et al. Oncogenic Kras Maintains Pancreatic Tumors through Regulation of Anabolic Glucose Metabolism. Cell [Internet]. 2012 [cited 2019 Aug 19];149:656–70. Available from: https://www-cell-com.manchester.idm.oclc.org/cell/pdfExtended/S0092-8674(12)00352-2

63. Criscimanna A, Duan LJ, Rhodes JA, Fendrich V, Wickline E, Hartman DJ, et al. PanIN-specific regulation of Wnt signaling by HIF2a during early pancreatic tumorigenesis. Cancer Res. 2013;73(15):4781–90.

64. Hoffmann A-C, Mori R, Vallbohmer D, Brabender J, Klein E, Drebber U, et al. High expression of HIF1a is a predictor of clinical outcome in patients with pancreatic ductal adenocarcinomas and correlated to PDGFA, VEGF, and bFGF. Neoplasia [Internet]. 2008 Jul [cited 2019 Aug 19];10(7):674–9. Available from: http://www.ncbi.nlm.nih.gov/pubmed/18592007

65. Ye L-Y, Zhang Q, Bai X-L, Pankaj P, Hu Q-D, Liang T-B. Hypoxia-inducible factor 1α expression and its clinical significance in pancreatic cancer: A meta-analysis. Pancreatology [Internet]. 2014 Sep 1 [cited 2019 Aug 19];14(5):391–7. Available from: https://www-sciencedirect-com.manchester.idm.oclc.org/science/article/pii/S142439031400934X?via%3Dihub

66. Zhong H, De Marzo AM, Laughner E, Lim M, Hilton DA, Zagzag D, et al. Overexpression of hypoxia-inducible factor 1alpha in common human cancers and their metastases. Cancer Res [Internet]. 1999 Nov 15 [cited 2019 Aug 19];59(22):5830–5. Available from: https://cancerres-aacrjournals-org.manchester.idm.oclc.org/content/59/22/5830

67. Ziello JE, Jovin IS, Huang Y. Hypoxia-Inducible Factor (HIF)-1 regulatory pathway and its potential for therapeutic intervention in malignancy and ischemia. Yale J Biol Med [Internet]. 2007 Jun [cited 2019 Aug 19];80(2):51–60. Available from: http://www.ncbi.nlm.nih.gov/pubmed/18160990

68. Lee J-W, Bae S-H, Jeong J-W, Kim S-H, Kim K-W. Hypoxia-inducible factor (HIF-1)alpha: its protein stability and biological functions. Exp Mol Med [Internet]. 2004 Feb 29;36(1):1–12. Available from: http://www.ncbi.nlm.nih.gov/pubmed/15031665

69. Papandreou I, Cairns RA, Fontana L, Lim AL, Denko NC. HIF-1 mediates adaptation to hypoxia by actively downregulating mitochondrial oxygen consumption. Cell Metab. 2006;3(3):187–97.

70. Kim JW, Tchernyshyov I, Semenza GL, Dang C V. HIF-1-mediated expression of pyruvate dehydrogenase kinase: A metabolic switch required for cellular adaptation to hypoxia. Cell Metab. 2006;3(3):177–85.

71. Yuen A, Díaz B. The impact of hypoxia in pancreatic cancer invasion and metastasis. Hypoxia (Auckland, NZ) [Internet]. 2014 [cited 2019 Aug 19];2:91–106. Available from: http://www.ncbi.nlm.nih.gov/pubmed/27774469

72. Cui X-G, Han Z-T, He S-H, Wu X, Chen T-R, Shao C-H, et al. HIF1/2α mediates hypoxia-induced LDHA expression in human pancreatic cancer cells. Oncotarget [Internet]. 2017 Apr 11 [cited 2019 Aug 19];8(15):24840–52. Available from: http://www.ncbi.nlm.nih.gov/pubmed/28193910

73. Singh D, Arora R, Kaur P, Singh B, Mannan R, Arora S. Overexpression of hypoxia-inducible factor and metabolic pathways: possible targets of cancer. Cell Biosci [Internet]. 2017 Dec 13 [cited 2019 Aug 19];7(1):62. Available from: https://cellandbioscience.biomedcentral.com/articles/10.1186/s13578-017-0190-2

74. Luo W, Semenza GL. Pyruvate kinase M2 regulates glucose metabolism by functioning as a coactivator for hypoxia-inducible factor 1 in cancer cells. Oncotarget [Internet]. 2011 Jul [cited 2019 Aug 19];2(7):551–6. Available from: http://www.ncbi.nlm.nih.gov/pubmed/21709315

75. Zhang H, Gao P, Fukuda R, Kumar G, Krishnamachary B, Zeller KI, et al. HIF-1 Inhibits

Mitochondrial Biogenesis and Cellular Respiration in VHL-Deficient Renal Cell Carcinoma by Repression of C-MYC Activity. Cancer Cell. 2007;11(5):407–20.

76. Rajeshkumar N V., Dutta P, Yabuuchi S, de Wilde RF, Martinez G V., Le A, et al. Therapeutic Targeting of the Warburg Effect in Pancreatic Cancer Relies on an Absence of p53 Function. Cancer Res [Internet]. 2015 Aug 15 [cited 2019 Jul 10];75(16):3355–64. Available from: http://cancerres.aacrjournals.org/cgi/doi/10.1158/0008-5472.CAN-15-0108

77. Vousden KH, Prives C. Blinded by the Light: The Growing Complexity of p53. Cell [Internet]. 2009 May;137(3):413–31. Available from: https://linkinghub.elsevier.com/retrieve/pii/S0092867409004590

78. Wei X, Wu S, Song T, Chen L, Gao M, Borcherds W, et al. Secondary interaction between MDMX and p53 core domain inhibits p53 DNA binding. Proc Natl Acad Sci U S A [Internet]. 2016 May 10;113(19):E2558-63. Available from: http://www.ncbi.nlm.nih.gov/pubmed/27114532

79. Brooks CL, Gu W. New insights into p53 activation. Cell Res [Internet]. 2010;20(6):614–21. Available from: http://dx.doi.org/10.1038/cr.2010.53

80. Brady CA, Attardi LD. P53 At a Glance. J Cell Sci. 2010;123(15):2527–32.

81. Mello SS, Valente LJ, Raj N, Seoane JA, Flowers BM, McClendon J, et al. A p53 Super-tumor Suppressor Reveals a Tumor Suppressive p53-Ptpn14-Yap Axis in Pancreatic Cancer. Cancer Cell [Internet]. 2017;32(4):460-473.e6. Available from: https://doi.org/10.1016/j.ccell.2017.09.007

82. Schwartzenberg-Bar-Yoseph F, Armoni M, Karnieli E. The tumor suppressor p53 down-regulates glucose transporters GLUT1 and GLUT4 gene expression. Cancer Res [Internet]. 2004 Apr 1;64(7):2627–33. Available from: http://www.ncbi.nlm.nih.gov/pubmed/15059920

83. Kondoh H, Lleonart ME, Gil J, Wang J, Degan P, Peters G, et al. Glycolytic enzymes can modulate cellular life span. Cancer Res [Internet]. 2005 Jan 1;65(1):177–85. Available from: http://www.ncbi.nlm.nih.gov/pubmed/15665293

84. Bensaad K, Tsuruta A, Selak MA, Vidal MNC, Nakano K, Bartrons R, et al. TIGAR, a p53-inducible regulator of glycolysis and apoptosis. Cell [Internet]. 2006 Jul 14;126(1):107–20. Available from: http://www.ncbi.nlm.nih.gov/pubmed/16839880

85. Jiang P, Du W, Wang X, Mancuso A, Gao X, Wu M, et al. P53 regulates biosynthesis through direct inactivation of glucose-6-phosphate dehydrogenase. Nat Cell Biol [Internet]. 2011;13(3):310–6. Available from: http://dx.doi.org/10.1038/ncb2172

86. Matoba S, Kang J-G, Patino WD, Wragg A, Boehm M, Gavrilova O, et al. p53 regulates mitochondrial respiration. Science [Internet]. 2006 Jun 16;312(5780):1650–3. Available from: http://www.ncbi.nlm.nih.gov/pubmed/16728594

87. Lüttges J, Galehdari H, Bröcker V, Schwarte-Waldhoff I, Henne-Bruns D, Klöppel G, et al. Allelic loss is often the first hit in the biallelic inactivation of the p53 and DPC4 genes during pancreatic carcinogenesis. Am J Pathol [Internet]. 2001 May;158(5):1677–83. Available from: http://www.ncbi.nlm.nih.gov/pubmed/11337365

88. Cicenas J, Kvederaviciute K, Meskinyte I, Meskinyte-Kausiliene E, Skeberdyte A. KRAS, TP53, CDKN2A, SMAD4, BRCA1, and BRCA2 mutations in pancreatic cancer. Cancers (Basel). 2017;9(5).

89. Zhang C, Liu J, Liang Y, Wu R, Zhao Y, Hong X, et al. Tumour-associated mutant p53 drives the Warburg effect. Nat Commun. 2013;4.

90. Butera G, Pacchiana R, Mullappilly N, Margiotta M, Bruno S, Conti P, et al. Mutant p53 prevents GAPDH nuclear translocation in pancreatic cancer cells favoring glycolysis and 2-deoxyglucose sensitivity. Biochim Biophys Acta - Mol Cell Res [Internet]. 2018;1865(12):1914–23. Available from: https://doi.org/10.1016/j.bbamcr.2018.10.005

91. Nagarajan A, Dogra SK, Sun L, Gandotra N, Ho T, Cai G, et al. Paraoxonase 2 Facilitates Pancreatic Cancer Growth and Metastasis by Stimulating GLUT1-Mediated Glucose Transport. Mol Cell [Internet]. 2017 Aug 17;67(4):685-701.e6. Available from: http://www.ncbi.nlm.nih.gov/pubmed/28803777

92. Yang J, Ren B, Yang G, Wang H, Chen G, You L, et al. The enhancement of glycolysis regulates pancreatic cancer metastasis. Cell Mol Life Sci [Internet]. 2019;(0123456789). Available from: http://link.springer.com/10.1007/s00018-019-03278-z

93. Wilentz RE, Geradts J, Maynard R, Offerhaus GJ, Kang M, Goggins M, et al. Inactivation of the p16 (INK4A) tumor-suppressor gene in pancreatic duct lesions: loss of intranuclear expression. Cancer Res [Internet]. 1998 Oct 15;58(20):4740–4. Available from: http://www.ncbi.nlm.nih.gov/pubmed/9788631

94. Attri J, Srinivasan R, Majumdar S, Radotra BD, Wig J. Alterations of tumor suppressor gene p16INK4a in pancreatic ductal carcinoma. BMC Gastroenterol. 2005;5:1–10.

95. Schutte M, Hruban RH, Geradts J, Maynard R, Hilgers W, Rabindran SK, et al. Abrogation of the Rb/p16 tumor-suppressive pathway in virtually all pancreatic carcinomas. Cancer Res [Internet]. 1997 Aug 1;57(15):3126–30. Available from: http://www.ncbi.nlm.nih.gov/pubmed/9242437

96. Zhao R, Choi BY, Lee MH, Bode AM, Dong Z. Implications of Genetic and Epigenetic Alterations of CDKN2A (p16 INK4a ) in Cancer. EBioMedicine [Internet]. 2016;8(127):30–9. Available from: http://dx.doi.org/10.1016/j.ebiom.2016.04.017

97. Bardeesy N, Aguirre AJ, Chu GC, Cheng K-H, Lopez L V, Hezel AF, et al. Both p16(Ink4a) and the p19(Arf)-p53 pathway constrain progression of pancreatic adenocarcinoma in the mouse. Proc Natl Acad Sci U S A [Internet]. 2006 Apr 11;103(15):5947–52. Available from: http://www.ncbi.nlm.nih.gov/pubmed/16585505

98. Ju HQ, Ying H, Tian T, Ling J, Fu J, Lu Y, et al. Mutant Kras- and p16-regulated NOX4 activation overcomes metabolic checkpoints in development of pancreatic ductal adenocarcinoma. Nat Commun. 2017;8.

99. Bardeesy N, Cheng KH, Berger JH, Chu GC, Pahler J, Olson P, et al. Smad4 is dispensable for normal pancreas development yet critical in progression and tumor biology of pancreas cancer. Genes Dev. 2006;20(22):3130–46.

100. Ryan DP, Hong TS, Bardeesy N. Pancreatic Adenocarcinoma. N Engl J Med [Internet]. 2014 Sep 11;371(11):1039–49. Available from: http://www.nejm.org/doi/10.1056/NEJMra1404198

101. Shen W, Tao G-Q, Zhang Y, Cai B, Sun J, Tian Z-Q. TGF-β in pancreatic cancer initiation and progression: two sides of the same coin. Cell Biosci [Internet]. 2017 [cited 2019 Aug 22];7:39. Available from: http://www.ncbi.nlm.nih.gov/pubmed/28794854

102. Dennler S, Ten Dijke P. Smad Proteins in TGF-Beta Signaling. In: Encyclopedia of Cancer [Internet]. Berlin, Heidelberg: Springer Berlin Heidelberg; 2011 [cited 2019 Aug 22]. p. 3440–3. Available from: http://link.springer.com/10.1007/978-3-642-16483-5_5364

103. Schwarte-Waldhoff I, Volpert O V, Bouck NP, Sipos B, Hahn SA, Klein-Scory S, et al. Smad4/DPC4-mediated tumor suppression through suppression of angiogenesis. Proc Natl Acad Sci U S A [Internet]. 2000 Aug 15 [cited 2019 Aug 22];97(17):9624–9. Available from: http://www.ncbi.nlm.nih.gov/pubmed/10944227

104. Basso D, Gnatta E, Padoan A, Fogar P, Furlanello S, Aita A, et al. PDAC-derived exosomes enrich the microenvironment in MDSCs in a *SMAD4*-dependent manner through a new calcium related axis. Oncotarget [Internet]. 2017 Oct 17;8(49):605–11. Available from: http://www.ncbi.nlm.nih.gov/pubmed/16319880

105. Guido C, Whitaker-Menezes D, Capparelli C, Balliet R, Lin Z, Pestell RG, et al. Metabolic reprogramming of cancer-associated fibroblasts by TGF-β drives tumor growth: connecting TGF-β signaling with "Warburg-like" cancer metabolism and L-lactate production. Cell Cycle [Internet]. 2012 Aug 15 [cited 2019 Aug 22];11(16):3019–35. Available from: http://www.ncbi.nlm.nih.gov/pubmed/22874531

106. Bruce JI. Plasma membrane calcium pump regulation by metabolic stress. World J Biol Chem. 2010;1(7):221.

107. Bruce JIE, Yule DI, Shuttleworth TJ. Ca2+-dependent protein kinase-A modulation of the plasma membrane Ca2+-ATPase in parotid acinar cells. J Biol Chem. 2002;277(50):48172–81.

108. Bruce JIE, Elliott AC. Oxidant-impaired intracellular Ca 2+ signaling in pancreatic acinar cells: role of the plasma membrane Ca 2+ -ATPase . Am J Physiol Physiol. 2007;293(3):C938–50.

109. Hay N. Reprogramming glucose metabolism in cancer: can it be exploited for cancer therapy? Nat Rev Cancer [Internet]. 2016 Oct 16;16(10):635–49. Available from: http://www.nature.com/articles/nrc.2016.77

110. Israelsen WJ, Vander Heiden MG. Pyruvate kinase: Function, regulation and role in cancer. Semin Cell Dev Biol [Internet]. 2015 Jul [cited 2019 Aug 22];43:43–51. Available from: http://www.ncbi.nlm.nih.gov/pubmed/26277545

111. Marín-Hernández A, Rodríguez-Enríquez S, Vital-González PA, Flores-Rodríguez FL, Macías-Silva M, Sosa-Garrocho M, et al. Determining and understanding the control of glycolysis in fast-growth tumor cells. FEBS J [Internet]. 2006 Apr 5 [cited 2019 Aug 22];273(9):1975–88. Available from: http://www.ncbi.nlm.nih.gov/pubmed/16640561

112. Sepúlveda MR, Berrocal-Carrillo M, Gasset M, Mata AM. The plasma membrane Ca2+-ATPase isoform 4 is localized in lipid rafts of cerebellum synaptic plasma membranes. J Biol Chem. 2006;281(1):447–53.

113. El-Yazbi AF, Cho WJ, Schulz R, Daniel EE. Calcium extrusion by plasma membrane calcium pump is impaired in caveolin-1 knockout mouse small intestine. Eur J Pharmacol [Internet]. 2008 Sep 4 [cited 2019 Feb 27];591(1–3):80–7. Available from:

http://www.ncbi.nlm.nih.gov/pubmed/18634779

114. James AD. Metabolic regulation of the plasma membrane calcium pump in pancreatic ductal adenocarcinoma. University of Manchester; 2015.

115. Campanella ME, Chu H, Wandersee NJ, Peters LL, Mohandas N, Gilligan DM, et al. Characterization of glycolytic enzyme interactions with murine erythrocyte membranes in wild-type and membrane protein knockout mice. Blood. 2008;112(9):3900–6.

116. Raikar LS, Vallejo J, Lloyd PG, Hardin CD. Overexpression of caveolin-1 results in increased plasma membrane targeting of glycolytic enzymes: The structural basis for a membrane associated metabolic compartment. J Cell Biochem [Internet]. 2006 Jul 1 [cited 2019 Feb 27];98(4):861–71. Available from: http://www.ncbi.nlm.nih.gov/pubmed/16453288

117. Tanase CP, Dima S, Mihai M, Raducan E, Nicolescu MI, Albulescu L, et al. Caveolin-1 overexpression correlates with tumour progression markers in pancreatic ductal adenocarcinoma. J Mol Histol. 2009;40(1):23–9.

118. Nakamura T, Furukawa Y, Nakagawa H, Tsunoda T, Ohigashi H, Murata K, et al. Genome-wide cDNA microarray analysis of gene expression profiles in pancreatic cancers using populations of tumor cells and normal ductal epithelial cells selected for purity by laser microdissection. Oncogene [Internet]. 2004 Mar 9 [cited 2019 Jan 19];23(13):2385–400; Supplemental Table 1. Available from: http://www.nature.com/articles/1207392

119. Zamaraeva M V., Sabirov RZ, Manabe K ichi, Okada Y. Ca2+-dependent glycolysis activation mediates apoptotic ATP elevation in HeLa cells. Biochem Biophys Res Commun. 2007;363(3):687–93.

120. Mbaya E, Oulès B, Caspersen C, Tacine R, Massinet H, Pennuto M, et al. Calcium signalling-dependent mitochondrial dysfunction and bioenergetics regulation in respiratory chain Complex II deficiency. Cell Death Differ. 2010;17(12):1855–66.

121. James AD, Chan A, Erice O, Siriwardena AK, Bruce JIE. Glycolytic ATP fuels the plasma membrane calcium pump critical for pancreatic cancer cell survival. J Biol Chem [Internet]. 2013 Dec 13 [cited 2019 Jan 17];288(50):36007–19. Available from: http://www.ncbi.nlm.nih.gov/pubmed/24158437

122. Epstein T, Xu L, Gillies RJ, Gatenby RA. Separation of metabolic supply and demand: Aerobic glycolysis as a normal physiological response to fluctuating energetic demands in the membrane. Cancer Metab. 2014;2(1):1–9.

123. James AD, Patel W, Butt Z, Adiamah M, Dakhel R, Latif A, et al. The Plasma Membrane Calcium Pump in Pancreatic Cancer Cells Exhibiting the Warburg Effect Relies on Glycolytic ATP. J Biol Chem [Internet]. 2015 Oct 9 [cited 2019 Jan 17];290(41):24760–71. Available from: http://www.jbc.org/cgi/doi/10.1074/jbc.M115.668707

124. Monteith GR, Davis FM, Roberts-Thomson SJ. Calcium channels and pumps in cancer: Changes and consequences. J Biol Chem [Internet]. 2012 Sep 14 [cited 2019 Jan 19];287(38):31666–73. Available from: http://www.ncbi.nlm.nih.gov/pubmed/22822055

125. Clapham DE. Calcium Signaling. Cell [Internet]. 2007 Dec 14 [cited 2019 Jul 19];131(6):1047–58. Available from: http://structbio.vanderbilt.edu/cabp_da-

126. Berridge MJ, Lipp P, Bootman MD. The versatility and universality of calcium signalling. Nat Rev Mol Cell Biol [Internet]. 2000 Oct [cited 2019 Jul 19];1(1):11–21. Available from: http://www.nature.com/articles/35036035

127. Roderick HL, Cook SJ. Ca2+ signalling checkpoints in cancer: remodelling Ca2+ for cancer cell proliferation and survival. Nat Rev Cancer [Internet]. 2008 May 1 [cited 2019 Jul 20];8(5):361–75. Available from: http://www.nature.com/articles/nrc2374

128. Tonelli FMP, Santos AK, Gomes DA, da Silva SL, Gomes KN, Ladeira LO, et al. Stem cells and calcium signaling. Adv Exp Med Biol [Internet]. 2012 [cited 2019 Jul 20];740:891–916. Available from: http://www.ncbi.nlm.nih.gov/pubmed/22453975

129. Tsai F-C, Kuo G-H, Chang S-W, Tsai P-J. Ca2+ signaling in cytoskeletal reorganization, cell migration, and cancer metastasis. Biomed Res Int [Internet]. 2015 Apr 22 [cited 2019 Jan 22];2015:409245. Available from: http://www.ncbi.nlm.nih.gov/pubmed/25977921

130. Draznin B. Intracellular calcium, insulin secretion, and action. Am J Med [Internet]. 1988 Nov 28 [cited 2019 Jul 20];85(5):44–58. Available from: https://linkinghub.elsevier.com/retrieve/pii/000293438890397X

131. Schönekess BO, Brindley PG, Lopaschuk GD. Calcium regulation of glycolysis, glucose oxidation, and fatty acid oxidation in the aerobic and ischemic heart. Can J Physiol Pharmacol [Internet]. 1995 Nov [cited 2019 Jul 20];73(11):1632–40. Available from: http://www.ncbi.nlm.nih.gov/pubmed/8789418

132. Mattson MP, Chan SL. Calcium orchestrates apoptosis. Nat Cell Biol [Internet]. 2003 Dec [cited

2019 Jul 20];5(12):1041–3. Available from: http://www.nature.com/articles/ncb1203-1041

133. Berridge MJ, Bootman MD, Roderick HL. Calcium signalling: Dynamics, homeostasis and remodelling. Nat Rev Mol Cell Biol. 2003;4(7):517–29.

134. Nussinov R, Muratcioglu S, Tsai C-J, Jang H, Gursoy A, Keskin O. The Key Role of Calmodulin in KRAS-Driven Adenocarcinomas. Mol Cancer Res [Internet]. 2015 Sep [cited 2019 Aug 29];13(9):1265–73. Available from: http://www.ncbi.nlm.nih.gov/pubmed/26085527

135. Cullen PJ, Lockyer PJ. Integration of calcium and RAS signalling. Nat Rev Mol Cell Biol [Internet]. 2002 May [cited 2019 Aug 29];3(5):339–48. Available from: http://www.nature.com/articles/nrm808

136. Laude AJ, Simpson AWM. Compartmentalized signalling: Ca2+ compartments, microdomains and the many facets of Ca2+ signalling. FEBS J. 2009;276(7):1800–16.

137. Dolphin AC. Voltage-gated calcium channels: Their discovery, function and importance as drug targets. Brain Neurosci Adv [Internet]. 2018 Jan 2 [cited 2019 Aug 30];2:239821281879480. Available from: http://journals.sagepub.com/doi/10.1177/2398212818794805

138. Beyond ion-conduction: Channel-dependent and -independent roles of TRP channels during development and tissue homeostasis. Biochim Biophys Acta - Mol Cell Res [Internet]. 2016 Jun 1 [cited 2019 Aug 30];1863(6):1436–46. Available from: https://www-sciencedirect-com.manchester.idm.oclc.org/science/article/pii/S0167488915003924

139. Pankratov Y, Lalo U. Calcium permeability of ligand-gated Ca2+ channels. Eur J Pharmacol [Internet]. 2014 Sep 15 [cited 2019 Aug 30];739:60–73. Available from: https://www.sciencedirect.com/science/article/pii/S0014299913008893?via%3Dihub

140. Parekh AB, Putney JW. Store-Operated Calcium Channels. Physiol Rev [Internet]. 2005 Apr;85(2):757–810. Available from: http://www.physiology.org/doi/10.1152/physrev.00057.2003

141. Prakriya M, Feske S, Gwack Y, Srikanth S, Rao A, Hogan PG. Orai1 is an essential pore subunit of the CRAC channel. Nature [Internet]. 2006 Sep 20 [cited 2019 Aug 30];443(7108):230–3. Available from: http://www.nature.com/articles/nature05122

142. Santulli G, Nakashima R, Yuan Q, Marks AR. Intracellular calcium release channels: an update. J Physiol. 2017;595(10):3041–51.

143. Taylor CW, Tovey SC. IP(3) receptors: toward understanding their activation. Cold Spring Harb Perspect Biol [Internet]. 2010 Dec [cited 2019 Aug 30];2(12):a004010. Available from: http://www.ncbi.nlm.nih.gov/pubmed/20980441

144. Wyrsch P, Blenn C, Pesch T, Beneke S, Althaus FR. Cytosolic Ca2+ shifts as early markers of cytotoxicity. Cell Commun Signal [Internet]. 2013 Feb 6 [cited 2019 Aug 31];11(1):11. Available from: http://biosignaling.biomedcentral.com/articles/10.1186/1478-811X-11-11

145. Criddle DN, Gerasimenko J V., Baumgartner HK, Jaffar M, Voronina S, Sutton R, et al. Calcium signalling and pancreatic cell death: Apoptosis or necrosis? Cell Death Differ [Internet]. 2007 Jul 13;14(7):1285–94. Available from: http://www.nature.com/articles/4402150

146. Jeon D, Yang Y-M, Jeong M-J, Philipson KD, Rhim H, Shin H-S. Enhanced Learning and Memory in Mice Lacking Na+/Ca2+ Exchanger 2. Neuron [Internet]. 2003 Jun 19 [cited 2019 Aug 31];38(6):965–76. Available from: https://www.sciencedirect.com/science/article/pii/S0896627303003349

147. Giladi M, Tal I, Khananshvili D. Structural Features of Ion Transport and Allosteric Regulation in Sodium-Calcium Exchanger (NCX) Proteins. Front Physiol [Internet]. 2016 Feb 9 [cited 2019 Aug 31];7:30. Available from: http://journal.frontiersin.org/Article/10.3389/fphys.2016.00030/abstract

148. Khananshvili D. Sodium-calcium exchangers (NCX): molecular hallmarks underlying the tissue-specific and systemic functions. Pflügers Arch - Eur J Physiol [Internet]. 2014 Jan 27 [cited 2019 Aug 31];466(1):43–60. Available from: http://link.springer.com/10.1007/s00424-013-1405-y

149. Lam AKM, Galione A. The endoplasmic reticulum and junctional membrane communication during calcium signaling. Biochim Biophys Acta - Mol Cell Res [Internet]. 2013 Nov 1 [cited 2019 Aug 31];1833(11):2542–59. Available from: https://www.sciencedirect.com/science/article/pii/S0167488913002279#bb0030

150. Macdonald WA, Stephenson DG. Effects of ADP on sarcoplasmic reticulum function in mechanically skinned skeletal muscle fibres of the rat. J Physiol [Internet]. 2001 Apr 15 [cited 2019 Aug 31];532(Pt 2):499–508. Available from: http://www.ncbi.nlm.nih.gov/pubmed/11306667

151. Inesi G, De Meis L. Regulation of steady state filling in sarcoplasmic reticulum. Roles of back-inhibition, leakage, and slippage of the calcium pump. J Biol Chem. 1989;264(10):5929–36.

152. Lamboley CR, Murphy RM, McKenna MJ, Lamb GD. Sarcoplasmic reticulum Ca2+ uptake and

leak properties, and SERCA isoform expression, in type I and type II fibres of human skeletal muscle. J Physiol [Internet]. 2014 Mar 15 [cited 2019 Aug 31];592(6):1381–95. Available from: http://www.ncbi.nlm.nih.gov/pubmed/24469076

153. He W, Hu Z. The Role of the Golgi-Resident SPCA Ca2+/Mn2+ Pump in Ionic Homeostasis and Neural Function. Neurochem Res [Internet]. 2012 Mar 15 [cited 2019 Aug 31];37(3):455–68. Available from: http://link.springer.com/10.1007/s11064-011-0644-6

154. Hu Z, Bonifas JM, Beech J, Bench G, Shigihara T, Ogawa H, et al. Mutations in ATP2C1, encoding a calcium pump, cause Hailey-Hailey disease. Nat Genet [Internet]. 2000 Jan [cited 2019 Aug 31];24(1):61–5. Available from: http://www.ncbi.nlm.nih.gov/pubmed/10615129

155. Dolman NJ, Tepikin A V. Calcium gradients and the Golgi. Cell Calcium [Internet]. 2006 Nov 1 [cited 2019 Aug 31];40(5–6):505–12. Available from: https://www.sciencedirect.com/science/article/pii/S0143416006001771?via%3Dihub

156. Behne MJ, Tu C-L, Aronchik I, Epstein E, Bench G, Bikle DD, et al. Human Keratinocyte ATP2C1 Localizes to the Golgi and Controls Golgi Ca2+ Stores. J Invest Dermatol [Internet]. 2003 Oct [cited 2019 Aug 31];121(4):688–94. Available from: http://www.ncbi.nlm.nih.gov/pubmed/14632183

157. Rizzuto R, Simpson AWM, Brini M, Pozzan T. Rapid changes of mitochondrial Ca2+ revealed by specifically targeted recombinant aequorin. Nature [Internet]. 1992 Jul [cited 2019 Aug 31];358(6384):325–7. Available from: https://www-nature-com.manchester.idm.oclc.org/articles/358325a0.pdf

158. Mishra J, Jhun BS, Hurst S, O-Uchi J, Csordás G, Sheu S-S. The Mitochondrial Ca2+ Uniporter: Structure, Function, and Pharmacology. Handb Exp Pharmacol [Internet]. 2017 [cited 2019 Aug 31];240:129–56. Available from: http://www.ncbi.nlm.nih.gov/pubmed/28194521

159. Rizzuto R, Pozzan T. Microdomains of intracellular Ca2+: molecular determinants and functional consequences. Physiol Rev [Internet]. 2006 Jan [cited 2019 Aug 31];86(1):369–408. Available from: http://www.ncbi.nlm.nih.gov/pubmed/16371601

160. Nassar A, Simpson AW. Elevation of mitochondrial calcium by ryanodine-sensitive calcium-induced calcium release. J Biol Chem [Internet]. 2000 Aug 4 [cited 2019 Aug 31];275(31):23661–5. Available from: http://www.ncbi.nlm.nih.gov/pubmed/10821828

161. Denton RM. Regulation of mitochondrial dehydrogenases by calcium ions. Biochim Biophys Acta - Bioenerg [Internet]. 2009;1787(11):1309–16. Available from: http://dx.doi.org/10.1016/j.bbabio.2009.01.005

162. Jouaville LS, Pinton P, Bastianutto C, Rutter GA, Rizzuto R. Regulation of mitochondrial ATP synthesis by calcium: Evidence for a long-term metabolic priming. Proc Natl Acad Sci [Internet]. 1999 Nov 23 [cited 2019 Aug 31];96(24):13807–12. Available from: www.pnas.org

163. Takuwa N, Zhou W, Kumada M, Takuwa Y. Ca(2+)-dependent stimulation of retinoblastoma gene product phosphorylation and p34cdc2 kinase activation in serum-stimulated human fibroblasts. J Biol Chem [Internet]. 1993 Jan 5;268(1):138–45. Available from: http://www.ncbi.nlm.nih.gov/pubmed/8416921

164. Schneider G, Oswald F, Wahl C, Greten FR, Adler G, Schmid RM. Cyclosporine inhibits growth through the activating transcription factor/cAMP-responsive element-binding protein binding site in the cyclin D1 promoter. J Biol Chem [Internet]. 2002 Nov 15 [cited 2019 Sep 2];277(46):43599–607. Available from: http://www.ncbi.nlm.nih.gov/pubmed/12215435

165. Dolmetsch RE, Xu K, Lewis RS. Calcium oscillations increase the efficiency and specificity of gene expression. Nature [Internet]. 1998 Apr [cited 2019 Sep 2];392(6679):933–6. Available from: http://www.nature.com/articles/31960

166. Kupzig S, Walker SA, Cullen PJ. The frequencies of calcium oscillations are optimized for efficient calcium-mediated activation of Ras and the ERK/MAPK cascade. Proc Natl Acad Sci U S A [Internet]. 2005 May 24 [cited 2019 Sep 2];102(21):7577–82. Available from: http://www.ncbi.nlm.nih.gov/pubmed/15890781

167. Song H, Dong M, Zhou J, Sheng W, Li X, Gao W. Expression and prognostic significance of TRPV6 in the development and progression of pancreatic cancer. Oncol Rep [Internet]. 2018 Jan 15 [cited 2019 Sep 1];39(3):1432–40. Available from: http://www.ncbi.nlm.nih.gov/pubmed/29344675

168. Yee NS, Kazi AA, Li Q, Yang Z, Berg A, Yee RK. Aberrant over-expression of TRPM7 ion channels in pancreatic cancer: required for cancer cell invasion and implicated in tumor growth and metastasis. Biol Open [Internet]. 2015 Apr 15 [cited 2019 Sep 1];4(4):507–14. Available from: http://www.ncbi.nlm.nih.gov/pubmed/25770184

169. Zhang Y, Zhang J, Jiang D, Zhang D, Qian Z, Liu C, et al. Inhibition of T-type Ca$^{2+}$ channels by endostatin attenuates human glioblastoma cell proliferation and migration. Br J Pharmacol

[Internet]. 2012 Jun;166(4):1247–60. Available from:
http://www.ncbi.nlm.nih.gov/pubmed/22233416

170. Roberts-Thomson SJ, Curry MC, Monteith GR. Plasma membrane calcium pumps and their emerging roles in cancer. World J Biol Chem [Internet]. 2010 Aug 26 [cited 2019 Aug 27];1(8):248–53. Available from: http://www.ncbi.nlm.nih.gov/pubmed/21537481

171. Chen Y-F, Chiu W-T, Chen Y-T, Lin P-Y, Huang H-J, Chou C-Y, et al. Calcium store sensor stromal-interaction molecule 1-dependent signaling plays an important role in cervical cancer growth, migration, and angiogenesis. Proc Natl Acad Sci U S A [Internet]. 2011 Sep 13;108(37):15225–30. Available from: http://www.ncbi.nlm.nih.gov/pubmed/21876174

172. Abdul M, Ramlal S, Hoosein N. Ryanodine receptor expression correlates with tumor grade in breast cancer. Pathol Oncol Res [Internet]. 2008 Jun;14(2):157–60. Available from: http://www.ncbi.nlm.nih.gov/pubmed/18431693

173. Legrand G, Humez S, Slomianny C, Dewailly E, Vanden Abeele F, Mariot P, et al. Ca2+ pools and cell growth. Evidence for sarcoendoplasmic Ca2+-ATPases 2B involvement in human prostate cancer cell growth control. J Biol Chem [Internet]. 2001 Dec 14;276(50):47608–14. Available from: http://www.ncbi.nlm.nih.gov/pubmed/11606580

174. Feng M, Grice DM, Faddy HM, Nguyen N, Leitch S, Wang Y, et al. Store-independent activation of Orai1 by SPCA2 in mammary tumors. Cell [Internet]. 2010 Oct 1;143(1):84–98. Available from: http://www.ncbi.nlm.nih.gov/pubmed/20887894

175. Prevarskaya N, Ouadid-Ahidouch H, Skryma R, Shuba Y. Remodelling of Ca2+ transport in cancer: how it contributes to cancer hallmarks? Philos Trans R Soc Lond B Biol Sci [Internet]. 2014 Mar 19 [cited 2019 Jul 20];369(1638):20130097. Available from: http://www.ncbi.nlm.nih.gov/pubmed/24493745

176. Lehen'kyi V, Flourakis M, Skryma R, Prevarskaya N. TRPV6 channel controls prostate cancer cell proliferation via Ca(2+)/NFAT-dependent pathways. Oncogene [Internet]. 2007 Nov 15;26(52):7380–5. Available from: http://www.ncbi.nlm.nih.gov/pubmed/17533368

177. Buchholz M, Schatz A, Wagner M, Michl P, Linhart T, Adler G, et al. Overexpression of c-myc in pancreatic cancer caused by ectopic activation of NFATc1 and the Ca2+/calcineurin signaling pathway. EMBO J [Internet]. 2006 Aug 9 [cited 2019 Sep 2];25(15):3714–24. Available from: http://www.ncbi.nlm.nih.gov/pubmed/16874304

178. Hardwick JM, Soane L. Multiple functions of BCL-2 family proteins. Cold Spring Harb Perspect Biol [Internet]. 2013 Feb 1;5(2). Available from: http://www.ncbi.nlm.nih.gov/pubmed/23378584

179. Wang HG, Pathan N, Ethell IM, Krajewski S, Yamaguchi Y, Shibasaki F, et al. Ca2+-induced apoptosis through calcineurin dephosphorylation of BAD. Science [Internet]. 1999 Apr 9;284(5412):339–43. Available from: http://www.ncbi.nlm.nih.gov/pubmed/10195903

180. Gil-Parrado S, Fernández-Montalván A, Assfalg-Machleidt I, Popp O, Bestvater F, Holloschi A, et al. Ionomycin-activated calpain triggers apoptosis. A probable role for Bcl-2 family members. J Biol Chem [Internet]. 2002 Jul 26 [cited 2019 Sep 2];277(30):27217–26. Available from: http://www.ncbi.nlm.nih.gov/pubmed/12000759

181. Nakagawa T, Yuan J. Cross-talk between two cysteine protease families. Activation of caspase-12 by calpain in apoptosis. J Cell Biol [Internet]. 2000 Aug 21;150(4):887–94. Available from: http://www.ncbi.nlm.nih.gov/pubmed/10953012

182. Smith MA, Schnellmann RG. Calpains, mitochondria, and apoptosis. Cardiovasc Res [Internet]. 2012 Oct 1 [cited 2019 Sep 2];96(1):32–7. Available from: http://www.ncbi.nlm.nih.gov/pubmed/22581845

183. Cohen JJ, Duke RC. Glucocorticoid activation of a calcium-dependent endonuclease in thymocyte nuclei leads to cell death. J Immunol [Internet]. 1984 Jan;132(1):38–42. Available from: http://www.ncbi.nlm.nih.gov/pubmed/6317746

184. Grimm S. The ER–mitochondria interface: The social network of cell death. Biochim Biophys Acta - Mol Cell Res [Internet]. 2012 Feb 1 [cited 2019 Sep 2];1823(2):327–34. Available from: https://www-sciencedirect-com.manchester.idm.oclc.org/science/article/pii/S016748891100320X?via%3Dihub

185. McConkey DJ, Orrenius S. The role of calcium in the regulation of apoptosis. Biochem Biophys Res Commun [Internet]. 1997 Oct 20;239(2):357–66. Available from: http://www.ncbi.nlm.nih.gov/pubmed/9344835

186. Dubois C, Vanden Abeele F, Prevarskaya N. Targeting apoptosis by the remodelling of calcium-transporting proteins in cancerogenesis. FEBS J [Internet]. 2013 Nov 1 [cited 2019 Sep 2];280(21):5500–10. Available from: http://doi.wiley.com/10.1111/febs.12246

187. Flourakis M, Lehen'kyi V, Beck B, Raphaël M, Vandenberghe M, Abeele F V, et al. Orai1 contributes to the establishment of an apoptosis-resistant phenotype in prostate cancer cells.

Cell Death Dis [Internet]. 2010 Sep 16;1(21):e75. Available from: http://www.ncbi.nlm.nih.gov/pubmed/1364678

188. Berry PA, Birnie R, Droop AP, Maitland NJ, Collins AT. The calcium sensor STIM1 is regulated by androgens in prostate stromal cells. Prostate [Internet]. 2011 Nov;71(15):1646–55. Available from: http://www.ncbi.nlm.nih.gov/pubmed/21432868

189. VanHouten J, Sullivan C, Bazinet C, Ryoo T, Camp R, Rimm DL, et al. PMCA2 regulates apoptosis during mammary gland involution and predicts outcome in breast cancer. Proc Natl Acad Sci U S A [Internet]. 2010 Jun 22;107(25):11405–10. Available from: http://www.ncbi.nlm.nih.gov/pubmed/20534448

190. Vanden Abeele F, Skryma R, Shuba Y, Van Coppenolle F, Slomianny C, Roudbaraki M, et al. Bcl-2-dependent modulation of Ca(2+) homeostasis and store-operated channels in prostate cancer cells. Cancer Cell [Internet]. 2002 Mar [cited 2019 Sep 2];1(2):169–79. Available from: http://www.ncbi.nlm.nih.gov/pubmed/12086875

191. Ridley AJ, Schwartz MA, Burridge K, Firtel RA, Ginsberg MH, Borisy G, et al. Cell migration: integrating signals from front to back. Science [Internet]. 2003 Dec 5;302(5651):1704–9. Available from: http://www.sciencemag.org/cgi/doi/10.1126/science.1092053

192. Wei C, Wang X, Chen M, Ouyang K, Song L-S, Cheng H. Calcium flickers steer cell migration. Nature [Internet]. 2009 Feb 12 [cited 2019 Jan 22];457(7231):901–5. Available from: http://www.ncbi.nlm.nih.gov/pubmed/19118385

193. Tsai FC, Seki A, Yang HW, Hayer A, Carrasco S, Malmersjö S, et al. A polarized Ca2+, diacylglycerol and STIM1 signalling system regulates directed cell migration. Nat Cell Biol. 2014;16(2):133–44.

194. Tsai F-C, Meyer T. Ca2+ pulses control local cycles of lamellipodia retraction and adhesion along the front of migrating cells. Curr Biol [Internet]. 2012 May 8 [cited 2019 Sep 1];22(9):837–42. Available from: http://www.ncbi.nlm.nih.gov/pubmed/22521790

195. Van Lierop JE, Wilson DP, Davis JP, Tikunova S, Sutherland C, Walsh MP, et al. Activation of smooth muscle myosin light chain kinase by calmodulin. Role of LYS(30) and GLY(40). J Biol Chem [Internet]. 2002 Feb 22 [cited 2019 Sep 1];277(8):6550–8. Available from: http://www.ncbi.nlm.nih.gov/pubmed/11748245

196. Franco SJ, Huttenlocher A. Regulating cell migration: calpains make the cut. J Cell Sci [Internet]. 2005 Sep 1 [cited 2019 Sep 1];118(Pt 17):3829–38. Available from: http://www.ncbi.nlm.nih.gov/pubmed/16129881

197. Monet M, Lehen'kyi V, Gackiere F, Firlej V, Vandenberghe M, Roudbaraki M, et al. Role of Cationic Channel TRPV2 in Promoting Prostate Cancer Migration and Progression to Androgen Resistance. Cancer Res [Internet]. 2010 Feb 1 [cited 2019 Sep 1];70(3):1225–35. Available from: http://www.ncbi.nlm.nih.gov/pubmed/20103638

198. Dong H, Shim K-N, Li JMJ, Estrema C, Ornelas TA, Nguyen F, et al. Molecular mechanisms underlying Ca2+-mediated motility of human pancreatic duct cells. Am J Physiol Cell Physiol [Internet]. 2010 Dec [cited 2019 Aug 31];299(6):C1493-503. Available from: http://www.ncbi.nlm.nih.gov/pubmed/20861471

199. Rybarczyk P, Gautier M, Hague F, Dhennin-Duthille I, Chatelain D, Kerr-Conte J, et al. Transient receptor potential melastatin-related 7 channel is overexpressed in human pancreatic ductal adenocarcinomas and regulates human pancreatic cancer cell migration. Int J Cancer. 2012;131(6):851–62.

200. Su L-T, Agapito MA, Li M, Simonson WTN, Huttenlocher A, Habas R, et al. TRPM7 regulates cell adhesion by controlling the calcium-dependent protease calpain. J Biol Chem [Internet]. 2006 Apr 21 [cited 2019 Sep 1];281(16):11260–70. Available from: http://www.ncbi.nlm.nih.gov/pubmed/16436382

201. Aarts M, Iihara K, Wei W-L, Xiong Z-G, Arundine M, Cerwinski W, et al. A Key Role for TRPM7 Channels in Anoxic Neuronal Death [Internet]. Vol. 115, Cell. 2003 [cited 2019 Sep 1]. Available from: http://www.cell.com/cgi/content/full/115/7/863/

202. Schaal C, Padmanabhan J, Chellappan S. The Role of nAChR and Calcium Signaling in Pancreatic Cancer Initiation and Progression. Cancers (Basel) [Internet]. 2015 Jul 31 [cited 2019 Jan 19];7(3):1447–71. Available from: http://www.ncbi.nlm.nih.gov/pubmed/26264026

203. Bruce JIE. Metabolic regulation of the PMCA: Role in cell death and survival. Cell Calcium [Internet]. 2018 [cited 2019 Jan 19];69:28–36. Available from: http://www.ncbi.nlm.nih.gov/pubmed/28625348

204. Strehler EE. Plasma membrane calcium ATPases: From generic Ca2+ sump pumps to versatile systems for fine-tuning cellular Ca2+. Biochem Biophys Res Commun [Internet]. 2015 Apr;460(1):26–33. Available from: http://dx.doi.org/10.1016/j.bbrc.2015.01.121

205. Periasamy M, Kalyanasundaram A. SERCA pump isoforms: Their role in calcium transport and disease. Muscle Nerve [Internet]. 2007 Apr 1 [cited 2019 Aug 26];35(4):430–42. Available from: http://doi.wiley.com/10.1002/mus.20745

206. Di Leva F, Domi T, Fedrizzi L, Lim D, Carafoli E. The plasma membrane Ca2+ ATPase of animal cells: structure, function and regulation. Arch Biochem Biophys [Internet]. 2008 Aug 1 [cited 2019 Aug 26];476(1):65–74. Available from: www.elsevier.com/locate/yabbiABBAvailableonlineatwww.sciencedirect.com

207. Niggli V, Sigel E, Carafoli E. The purified Ca2+ pump of human erythrocyte membranes catalyzes an electroneutral Ca2+-H+ exchange in reconstituted liposomal systems. J Biol Chem [Internet]. 1982 Mar 10;257(5):2350–6. Available from: http://www.ncbi.nlm.nih.gov/pubmed/6460758

208. Milanick MA. Proton fluxes associated with the Ca pump in human red blood cells. Am J Physiol [Internet]. 1990 Mar;258(3 Pt 1):C552-62. Available from: http://www.ncbi.nlm.nih.gov/pubmed/2156439

209. Schwiening CJ, Kennedy HJ, Thomas RC. Calcium-hydrogen exchange by the plasma membrane Ca-ATPase of voltage-clamped snail neurons. Proceedings Biol Sci [Internet]. 1993 Sep 22;253(1338):285–9. Available from: http://www.ncbi.nlm.nih.gov/pubmed/19213150

210. Thomas RC. The effects of HCl and CaCl(2) injections on intracellular calcium and pH in voltage-clamped snail (Helix aspersa) neurons. J Gen Physiol [Internet]. 2002 Oct;120(4):567–79. Available from: http://www.ncbi.nlm.nih.gov/pubmed/12356857

211. Falchetto R, Vorherr T, Carafoli E. The calmodulin-binding site of the plasma membrane Ca 2+ pump interacts with the transduction domain of the enzyme. Protein Sci [Internet]. 1992 Dec 1 [cited 2019 Aug 27];1(12):1613–21. Available from: http://doi.wiley.com/10.1002/pro.5560011209

212. Galan C, Jardín I, Dionisio N, Salido G, Rosado JA. Role of Oxidant Scavengers in the Prevention of Ca2+ Homeostasis Disorders. Molecules [Internet]. 2010 Oct 15 [cited 2019 Aug 27];15(10):7167–87. Available from: http://www.mdpi.com/1420-3049/15/10/7167

213. Pedersen PL, Carafoli E. Ion motive ATPases. I. Ubiquity, properties, and significance to cell function. Trends Biochem Sci [Internet]. 1987 Jan [cited 2019 Aug 26];12:146–50. Available from: https://pdf.sciencedirectassets.com/271294/1-s2.0-S0968000400X01223/1-s2.0-0968000487900715/main.pdf?X-Amz-Security-Token=AgoJb3JpZ2luX2VjEJ%2F%2F%2F%2F%2F%2F%2F%2F%2F%2F%2FwEaCXVzLWVhc3QtMSJIMEYCIQCpOtDfLvFewcTZwz7Fk%2FbhjhnED3nm3ruWIRS5d2qnhwIhAMBP3kyWK

214. Stafford N, Wilson C, Oceandy D, Neyses L, Cartwright EJ. The Plasma Membrane Calcium ATP <scp>ases</scp> and Their Role as Major New Players in Human Disease. Physiol Rev [Internet]. 2017 Jul [cited 2019 Jan 19];97(3):1089–125. Available from: http://www.physiology.org/doi/10.1152/physrev.00028.2016

215. Lopreiato R, Giacomello M, Carafoli E. The plasma membrane calcium pump: new ways to look at an old enzyme. J Biol Chem [Internet]. 2014 Apr 11 [cited 2019 May 12];289(15):10261–8. Available from: http://www.ncbi.nlm.nih.gov/pubmed/24570005

216. Linde CI, Di Leva F, Domi T, Tosatto SCE, Brini M, Carafoli E. Inhibitory interaction of the 14-3-3 proteins with ubiquitous (PMCA1) and tissue-specific (PMCA3) isoforms of the plasma membrane Ca2+ pump. Cell Calcium [Internet]. 2008 Jun 1 [cited 2019 Aug 26];43(6):550–61. Available from: https://www-sciencedirect-com.manchester.idm.oclc.org/science/article/pii/S0143416007001686

217. Rimessi A, Coletto L, Pinton P, Rizzuto R, Brini M, Carafoli E. Inhibitory interaction of the 14-3-3ε protein with isoform 4 of the plasma membrane Ca2+-ATPase pump. J Biol Chem. 2005;280(44):37195–203.

218. Zvaritch E, James P, Vorherr T, Falchetto R, Modyanov N, Carafoli E. Mapping of functional domains in the plasma membrane Ca2+ pump using trypsin proteolysis. Biochemistry [Internet]. 1990 Sep 4;29(35):8070–6. Available from: http://www.ncbi.nlm.nih.gov/pubmed/2175646

219. Brini M, Carafoli E. The plasma membrane Ca2+ ATPase and the plasma membrane sodium calcium exchanger cooperate in the regulation of cell calcium. Cold Spring Harb Perspect Biol [Internet]. 2011 Feb 1 [cited 2019 Jan 20];3(2). Available from: http://www.ncbi.nlm.nih.gov/pubmed/21421919

220. Padányi R, Pászty K, Hegedűs L, Varga K, Papp B, Penniston JT, et al. Multifaceted plasma membrane Ca 2+ pumps: From structure to intracellular Ca 2+ handling and cancer. Biochim Biophys Acta - Mol Cell Res [Internet]. 2016 Jun [cited 2019 Jan 20];1863(6):1351–63. Available from: http://dx.doi.org/10.1016/j.bbamcr.2015.12.011

221.	Oceandy D, Cartwright EJ, Emerson M, Prehar S, Baudoin FM, Zi M, et al. Neuronal nitric oxide synthase signaling in the heart is regulated by the sarcolemmal calcium pump 4b. Circulation. 2007;115(4):483–92.

222.	Enyedi A, Flura M, Sarkadi B, Gardos G, Carafoli E. The maximal velocity and the calcium affinity of the red cell calcium pump may be regulated independently. J Biol Chem. 1987;262(13):6425–30.

223.	Cura CI, Corradi GR, Rinaldi DE, Adamo HP. Biochimica et Biophysica Acta High sensibility to reactivation by acidic lipids of the recombinant human plasma membrane Ca 2 + -ATPase isoform 4xb puri fi ed from Saccharomyces cerevisiae ☆. BBA - Biomembr [Internet]. 2008;1778(12):2757–64. Available from: http://dx.doi.org/10.1016/j.bbamem.2008.08.020

224.	Antalffy G, Pászty K, Varga K, Hegedűs L, Enyedi Á, Padányi R. A C-terminal di-leucine motif controls plasma membrane expression of PMCA4b. Biochim Biophys Acta - Mol Cell Res [Internet]. 2013 Dec;1833(12):2561–72. Available from: https://linkinghub.elsevier.com/retrieve/pii/S0167488913002449

225.	Calì T, Brini M, Carafoli E. Regulation of Cell Calcium and Role of Plasma Membrane Calcium ATPases. 2017 [cited 2019 Jan 20]; Available from: http://dx.doi.org/10.1016/bs.ircmb.2017.01.002

226.	Caride AJ, Filoteo AG, Penniston JT, Strehler EE. The plasma membrane Ca2+ pump isoform 4a differs from isoform 4b in the mechanism of calmodulin binding and activation kinetics: implications for Ca2+ signaling. J Biol Chem [Internet]. 2007 Aug 31 [cited 2019 Aug 26];282(35):25640–8. Available from: http://www.ncbi.nlm.nih.gov/pubmed/17595168

227.	Hardin CD. Comparison of endogenous and exogenous sources of ATP in fueling Ca2+ uptake in smooth muscle plasma membrane vesicles. J Gen Physiol [Internet]. 1992 Jan 1 [cited 2019 Aug 26];99(1):21–40. Available from: http://doi.org/10.1085/jgp.99.1.21

228.	Pani B, Singh BB. Lipid rafts/caveolae as microdomains of calcium signaling. Cell Calcium [Internet]. 2009 Jun [cited 2019 May 12];45(6):625–33. Available from: http://www.ncbi.nlm.nih.gov/pubmed/19324409

229.	Baudrand R, Gupta N, Garza AE, Vaidya A, Leopold JA, Hopkins PN, et al. Caveolin 1 Modulates Aldosterone-Mediated Pathways of Glucose and Lipid Homeostasis. J Am Heart Assoc [Internet]. 2016;5(10). Available from: http://www.ncbi.nlm.nih.gov/pubmed/27680666

230.	Bong AHL, Monteith GR. Calcium signaling and the therapeutic targeting of cancer cells. Biochim Biophys Acta - Mol Cell Res [Internet]. 2018 Nov [cited 2019 Jul 20];1865(11):1786–94. Available from: https://doi.org/10.1016/j.bbamcr.2018.05.015

231.	Lee WJ, Roberts-Thomson SJ, Monteith GR. Plasma membrane calcium-ATPase 2 and 4 in human breast cancer cell lines. Biochem Biophys Res Commun [Internet]. 2005 Nov;337(3):779–83. Available from: https://linkinghub.elsevier.com/retrieve/pii/S0006291X05021522

232.	Chaneton B, Hillmann P, Zheng L, Martin ACL, Maddocks ODK, Chokkathukalam A, et al. Serine is a natural ligand and allosteric activator of pyruvate kinase M2. Nature [Internet]. 2012 Nov 14;491(7424):458–62. Available from: http://www.nature.com/articles/nature11540

233.	Aung CS, Ye W, Plowman G, Peters AA, Monteith GR, Roberts-Thomson SJ. Plasma membrane calcium ATPase 4 and the remodeling of calcium homeostasis in human colon cancer cells. Carcinogenesis [Internet]. 2009 Nov 1 [cited 2019 Jan 20];30(11):1962–9. Available from: http://www.ncbi.nlm.nih.gov/pubmed/19755660

234.	Strehler EE. Plasma Membrane Calcium ATPases as Novel Candidates for Therapeutic Agent Development [Internet]. [cited 2019 Jan 20]. Available from: www.tcdb.org

235.	Okunade GW, Miller ML, Pyne GJ, Sutliff RL, O'Connor KT, Neumann JC, et al. Targeted Ablation of Plasma Membrane Ca $^{2+}$ -ATPase (PMCA) 1 and 4 Indicates a Major Housekeeping Function for PMCA1 and a Critical Role in Hyperactivated Sperm Motility and Male Fertility for PMCA4. J Biol Chem [Internet]. 2004 Aug 6 [cited 2019 Feb 2];279(32):33742–50. Available from: http://www.ncbi.nlm.nih.gov/pubmed/15178683

236.	Caride AJ, Filoteo AG, Penniston JT, Strehler EE. The plasma membrane Ca2+ pump isoform 4a differs from isoform 4b in the mechanism of calmodulin binding and activation kinetics: implications for Ca2+ signaling. J Biol Chem [Internet]. 2007 Aug 31 [cited 2019 Jul 28];282(35):25640–8. Available from: http://www.ncbi.nlm.nih.gov/pubmed/17595168

237.	Oceandy D, Cartwright EJ, Emerson M, Prehar S, Baudoin FM, Zi M, et al. Neuronal Nitric Oxide Synthase Signaling in the Heart Is Regulated by the Sarcolemmal Calcium Pump 4b. Circulation [Internet]. 2007 Jan 30;115(4):483–92. Available from: https://www.ahajournals.org/doi/10.1161/CIRCULATIONAHA.106.643791

238.	Schuh K, Uldrijan S, Gambaryan S, Roethlein N, Neyses L. Interaction of the Plasma

Membrane Ca2+ Pump 4b/CI with the Ca2+/Calmodulin-dependent Membrane-associated Kinase CASK. J Biol Chem [Internet]. 2003 Mar 14 [cited 2019 Aug 27];278(11):9778–83. Available from: http://www.jbc.org.manchester.idm.oclc.org/content/278/11/9778.full

239. Armesilla AL, Williams JC, Buch MH, Pickard A, Emerson M, Cartwright EJ, et al. Novel functional interaction between the plasma membrane Ca2+ pump 4b and the proapoptotic tumor suppressor Ras-associated factor 1 (RASSF1). J Biol Chem [Internet]. 2004 Jul 23 [cited 2019 Aug 27];279(30):31318–28. Available from: http://www.ncbi.nlm.nih.gov/pubmed/15145946

240. Buch MH, Pickard A, Rodriguez A, Gillies S, Maass AH, Emerson M, et al. The sarcolemmal calcium pump inhibits the calcineurin/nuclear factor of activated T-cell pathway via interaction with the calcineurin A catalytic subunit. J Biol Chem [Internet]. 2005 Aug 19 [cited 2019 Aug 27];280(33):29479–87. Available from: http://www.ncbi.nlm.nih.gov/pubmed/15955804

241. Wang L, Velazquez H, Chang J, Safirstein R, Desir G V. Identification of a Receptor for Extracellular Renalase. PLoS One [Internet]. 2015 Apr 23 [cited 2019 Jan 26];10(4):e0122932. Available from: https://dx.plos.org/10.1371/journal.pone.0122932

242. Schuh K, Quaschning T, Knauer S, Hu K, Kocak S, Roethlein N, et al. Regulation of vascular tone in animals overexpressing the sarcolemmal calcium pump. J Biol Chem [Internet]. 2003 Oct 17 [cited 2019 Aug 27];278(42):41246–52. Available from: http://www.ncbi.nlm.nih.gov/pubmed/12900399

243. Williams JC, Armesilla AL, Mohamed TMA, Hagarty CL, McIntyre FH, Schomburg S, et al. The sarcolemmal calcium pump, alpha-1 syntrophin, and neuronal nitric-oxide synthase are parts of a macromolecular protein complex. J Biol Chem [Internet]. 2006 Aug 18 [cited 2019 Aug 27];281(33):23341–8. Available from: http://www.ncbi.nlm.nih.gov/pubmed/16735509

244. Afroze T, Yang G, Khoshbin A, Tanwir M, Tabish T, Momen A, et al. Calcium efflux activity of plasma membrane Ca2+ ATPase-4 (PMCA4) mediates cell cycle progression in vascular smooth muscle cells. J Biol Chem [Internet]. 2014 Mar 7 [cited 2019 Jan 22];289(10):7221–31. Available from: http://www.ncbi.nlm.nih.gov/pubmed/24448801

245. Talarico EF. Plasma membrane calcium-ATPase isoform four distribution changes during corneal epithelial wound healing. Mol Vis [Internet]. 2010;16(April):2259–72. Available from: http://www.pubmedcentral.nih.gov/articlerender.fcgi?artid=2994332&tool=pmcentrez&rendertype=abstract

246. Baggott RR, Alfranca A, López-Maderuelo D, Mohamed TMA, Escolano A, Oller J, et al. Plasma membrane calcium ATPase isoform 4 inhibits vascular endothelial growth factor-mediated angiogenesis through interaction with calcineurin. Arterioscler Thromb Vasc Biol. 2014;

247. Lee WJ, Robinson JA, Holman NA, McCall MN, Roberts-Thomson SJ, Monteith GR. Antisense-mediated inhibition of the plasma membrane calcium-ATPase suppresses proliferation of MCF-7 cells. J Biol Chem. 2005;280(29):27076–84.

248. Hegedūs L, Garay T, Molnár E, Varga K, Bilecz Á, Török S, et al. The plasma membrane Ca2+ pump PMCA4b inhibits the migratory and metastatic activity of BRAF mutant melanoma cells. Int J cancer [Internet]. 2017 Jun 15 [cited 2019 Aug 28];140(12):2758–70. Available from: http://www.ncbi.nlm.nih.gov/pubmed/27813079

249. Curry MC, Luk NA, Kenny PA, Roberts-Thomson SJ, Monteith GR. Distinct regulation of cytoplasmic calcium signals and cell death pathways by different plasma membrane calcium ATPase isoforms in MDA-MB-231 breast cancer cells. J Biol Chem [Internet]. 2012 Aug 17 [cited 2019 Jan 19];287(34):28598–608. Available from: http://www.ncbi.nlm.nih.gov/pubmed/22733819

250. Stan R V. Structure of caveolae. Biochim Biophys Acta - Mol Cell Res. 2005;1746(3):334–48.

251. Parton RG. Caveolae: Structure, Function, and Relationship to Disease. Annu Rev Cell Dev Biol. 2018;34(1):111–36.

252. Örtegren U, Aboulaich N, Öst A, Strålfors P. A new role for caveolae as metabolic platforms. Trends Endocrinol Metab. 2007;18(9):344–9.

253. Cheng JPX, Nichols BJ. Caveolae: One Function or Many? Trends Cell Biol [Internet]. 2016 Mar [cited 2019 May 11];26(3):177–89. Available from: http://dx.doi.org/10.1016/j.tcb.2015.10.010

254. Isshiki M, Ando J, Korenaga R, Kogo H, Fujimoto T, Fujita T, et al. Endothelial Ca2+ waves preferentially originate at specific loci in caveolin-rich cell edges. Proc Natl Acad Sci. 1998;95(9):5009–14.

255. Toselli M, Biella G, Taglietti V, Cazzaniga E, Parenti M. Caveolin-1 expression and membrane cholesterol content modulate N-type calcium channel activity in NG108-15 cells. Biophys J.

2005;89(4):2443–57.

256.    Chaudhary N, Gomez GA, Howes MT, Lo HP, McMahon KA, Rae JA, et al. Endocytic Crosstalk: Cavins, Caveolins, and Caveolae Regulate Clathrin-Independent Endocytosis. PLoS Biol. 2014;12(4).

257.    Kuo A, Lee MY, Yang K, Gross RW, Sessa WC, Program T. Caveolin-1 regulates lipid droplet metabolism in endothelial cells via autocrine prostacyclin stimulated cAMP-mediated lipolysis. 2017 [cited 2019 May 15]; Available from: http://www.jbc.org/cgi/doi/10.1074/jbc.RA117.000980

258.    Volonte D, Liu Z, Shiva S, Galbiati F. Caveolin-1 controls mitochondrial function through regulation of m-AAA mitochondrial protease. Aging (Albany NY) [Internet]. 2016 [cited 2019 May 15];8(10):2355–69. Available from: http://www.ncbi.nlm.nih.gov/pubmed/27705926

259.    Yu D-M, Jung SH, An H-T, Lee S, Hong J, Park JS, et al. Caveolin-1 deficiency induces premature senescence with mitochondrial dysfunction. Aging Cell [Internet]. 2017 [cited 2019 May 15];16(4):773–84. Available from: http://www.ncbi.nlm.nih.gov/pubmed/28514055

260.    Navarro A, Anand-Apte B, Parat M-O. A role for caveolae in cell migration. FASEB J [Internet]. 2004 Dec;18(15):1801–11. Available from: http://www.ncbi.nlm.nih.gov/pubmed/15576483

261.    Senju Y, Itoh Y, Takano K, Hamada S, Suetsugu S. Essential role of PACSIN2/syndapin-II in caveolae membrane sculpting. J Cell Sci. 2011;124(12):2032–40.

262.    Yeow I, Howard G, Chadwick J, Mendoza-Topaz C, Hansen CG, Nichols BJ, et al. EHD Proteins Cooperate to Generate Caveolar Clusters and to Maintain Caveolae during Repeated Mechanical Stress. Curr Biol [Internet]. 2017;27(19):2951-2962.e5. Available from: https://doi.org/10.1016/j.cub.2017.07.047

263.    Yamaguchi T, Lu C, Ida L, Yanagisawa K, Usukura J, Cheng J, et al. ROR1 sustains caveolae and survival signalling as a scaffold of cavin-1 and caveolin-1. Nat Commun [Internet]. 2016;7:1–13. Available from: http://dx.doi.org/10.1038/ncomms10060

264.    Cai Q, Guo L, Gao H, Li X-A. Caveolar fatty acids and acylation of caveolin-1. PLoS One [Internet]. 2013;8(4):e60884. Available from: http://www.ncbi.nlm.nih.gov/pubmed/23593340

265.    Brown DA. Lipid Rafts. Encycl Biol Chem Second Ed. 2013;44:741–4.

266.    Stary CM, Tsutsumi YM, Patel PM, Head BP, Patel HH, Roth DM. Caveolins: Targeting pro-survival signaling in the heart and brain. Front Physiol. 2012;3 OCT(October):1–10.

267.    Delmotte P, Jia L, Sieck GC. The Role of Mitochondria in Calcium Regulation in Airway Smooth Muscle. In: Calcium Signaling In Airway Smooth Muscle Cells [Internet]. Cham: Springer International Publishing; 2014. p. 211–34. Available from: http://link.springer.com/10.1007/978-3-319-01312-1_11

268.    Sowa G. Caveolae, caveolins, cavins, and endothelial cell function: New insights. Front Physiol. 2012;2 JAN(January):1–13.

269.    Harvey RD, Calaghan SC. Caveolae create local signalling domains through their distinct protein content, lipid profile and morphology. J Mol Cell Cardiol [Internet]. 2012 Feb [cited 2019 May 11];52(2):366–75. Available from: http://www.ncbi.nlm.nih.gov/pubmed/21782827

270.    Rybin VO, Xu X, Lisanti MP, Steinberg SF. Differential Targeting of β-Adrenergic Receptor Subtypes and Adenylyl Cyclase to Cardiomyocyte Caveolae. J Biol Chem [Internet]. 2000 Dec 29 [cited 2019 Aug 24];275(52):41447–57. Available from: http://www.ncbi.nlm.nih.gov/pubmed/11006286

271.    Agarwal SR, MacDougall DA, Tyser R, Pugh SD, Calaghan SC, Harvey RD. Effects of cholesterol depletion on compartmentalized cAMP responses in adult cardiac myocytes. J Mol Cell Cardiol [Internet]. 2011 Mar [cited 2019 Aug 24];50(3):500–9. Available from: http://www.ncbi.nlm.nih.gov/pubmed/21115018

272.    Fagerholm S, Örtegren U, Karlsson M, Ruishalme I, Strålfors P. Rapid Insulin-Dependent Endocytosis of the Insulin Receptor by Caveolae in Primary Adipocytes. Cao Y, editor. PLoS One [Internet]. 2009 Jun 19 [cited 2019 Aug 24];4(6):e5985. Available from: https://dx.plos.org/10.1371/journal.pone.0005985

273.    Cohen AW, Razani B, Wang XB, Combs TP, Williams TM, Scherer PE, et al. Caveolin-1-deficient mice show insulin resistance and defective insulin receptor protein expression in adipose tissue. Am J Physiol Physiol [Internet]. 2003 Jul [cited 2019 Aug 24];285(1):C222–35. Available from: http://www.ncbi.nlm.nih.gov/pubmed/12660144

274.    Kirkham M, Fujita A, Chadda R, Nixon SJ, Kurzchalia T V., Sharma DK, et al. Ultrastructural identification of uncoated caveolin-independent early endocytic vehicles. J Cell Biol. 2005;168(3):465–76.

275.    Kiss AL, Botos E. Endocytosis via caveolae: alternative pathway with distinct cellular compartments to avoid lysosomal degradation? J Cell Mol Med [Internet]. 2009 Jul [cited 2019 Aug 24];13(7):1228–37. Available from: http://www.ncbi.nlm.nih.gov/pubmed/19382909

276. Chatterjee M, Ben-Josef E, Robb R, Vedaie M, Seum S, Thirumoorthy K, et al. Caveolae-Mediated Endocytosis Is Critical for Albumin Cellular Uptake and Response to Albumin-Bound Chemotherapy. Cancer Res [Internet]. 2017 [cited 2019 Aug 24];77(21):5925–37. Available from: http://www.ncbi.nlm.nih.gov/pubmed/28923854

277. Commisso C, Davidson SM, Soydaner-Azeloglu RG, Parker SJ, Kamphorst JJ, Hackett S, et al. Macropinocytosis of protein is an amino acid supply route in Ras-transformed cells. Nature [Internet]. 2013 May 30 [cited 2019 Aug 24];497(7451):633. Available from: http://www.ncbi.nlm.nih.gov/pubmed/23665962

278. Liu L, Brown D, McKee M, Lebrasseur NK, Yang D, Albrecht KH, et al. Deletion of Cavin/PTRF causes global loss of caveolae, dyslipidemia, and glucose intolerance. Cell Metab [Internet]. 2008 Oct;8(4):310–7. Available from: http://www.ncbi.nlm.nih.gov/pubmed/18840361

279. Pilch PF, Liu L. Fat caves: Caveolae, lipid trafficking and lipid metabolism in adipocytes. Trends Endocrinol Metab. 2011;22(8):318–24.

280. Fielding CJ, Fielding PE. Relationship between cholesterol trafficking and signaling in rafts and caveolae. Biochim Biophys Acta [Internet]. 2003 Mar 10 [cited 2019 Aug 24];1610(2):219–28. Available from: https://www-sciencedirect-com.manchester.idm.oclc.org/science/article/pii/S0005273603000208#BIB18

281. Raggi C, Diociaiuti M, Caracciolo G, Fratini F, Fantozzi L, Piccaro G, et al. Caveolin-1 Endows Order in Cholesterol-Rich Detergent Resistant Membranes. Biomolecules [Internet]. 2019 Jul 17 [cited 2019 Aug 24];9(7):287. Available from: https://www.mdpi.com/2218-273X/9/7/287

282. Cohen AW, Combs TP, Scherer PE, Lisanti MP. Role of caveolin and caveolae in insulin signaling and diabetes. Am J Physiol Metab [Internet]. 2003 Dec [cited 2019 Aug 24];285(6):E1151–60. Available from: http://www.physiology.org/doi/10.1152/ajpendo.00324.2003

283. Lloyd PG, Hardin CD. Caveolae and the organization of carbohydrate metabolism in vascular smooth muscle. J Cell Biochem. 2001;82(3):399–408.

284. Lockwich TP, Liu X, Singh BB, Jadlowiec J, Weiland S, Ambudkar IS. Assembly of Trp1 in a signaling complex associated with caveolin- scaffolding lipid raft domains. J Biol Chem. 2000;275(16):11934–42.

285. Brazer S-CW, Singh BB, Liu X, Swaim W, Ambudkar IS. Caveolin-1 contributes to assembly of store-operated Ca2+ influx channels by regulating plasma membrane localization of TRPC1. J Biol Chem [Internet]. 2003 Jul 18 [cited 2019 Aug 25];278(29):27208–15. Available from: http://www.ncbi.nlm.nih.gov/pubmed/12732636

286. Tanaka S, Fujio Y, Nakayama H. Caveolae-Specific CaMKII Signaling in the Regulation of Voltage-Dependent Calcium Channel and Cardiac Hypertrophy. Front Physiol [Internet]. 2018 [cited 2019 Aug 25];9:1081. Available from: http://www.ncbi.nlm.nih.gov/pubmed/30131723

287. Ariotti N, Rae J, Leneva N, Ferguson C, Loo D, Okano S, et al. Molecular characterization of caveolin-induced membrane curvature. J Biol Chem. 2015;290(41):24875–90.

288. Tonn Eisinger KR, Woolfrey KM, Swanson SP, Schnell SA, Meitzen J, Dell'Acqua M, et al. Palmitoylation of caveolin-1 is regulated by the same DHHC acyltransferases that modify steroid hormone receptors. J Biol Chem. 2018;293(41):15901–11.

289. Byrne DP, Dart C, Rigden DJ. Evaluating Caveolin Interactions: Do Proteins Interact with the Caveolin Scaffolding Domain through a Widespread Aromatic Residue-Rich Motif? PLoS One. 2012;7(9).

290. Collins BM, Davis MJ, Hancock JF, Parton RG. Structure-Based Reassessment of the Caveolin Signaling Model: Do Caveolae Regulate Signaling through Caveolin-Protein Interactions? Dev Cell. 2012;23(1):11–20.

291. Wang H, Wang AX, Barrett EJ. Caveolin-1 is required for vascular endothelial insulin uptake. Am J Physiol Endocrinol Metab [Internet]. 2011 Jan;300(1):E134-44. Available from: http://www.ncbi.nlm.nih.gov/pubmed/20959538

292. Rybin VO, Xu X, Steinberg SF. Activated Protein Kinase C Isoforms Target to Cardiomyocyte Caveolae. Circ Res [Internet]. 1999 May 14;84(9):980–8. Available from: https://www.ahajournals.org/doi/10.1161/01.RES.84.9.980

293. Trane AE, Pavlov D, Sharma A, Saqib U, Lau K, Van Petegem F, et al. Deciphering the binding of Caveolin-1 to client protein endothelial nitric-oxide synthase (eNOS): Scaffolding subdomain identification, interaction modeling, and biological significance. J Biol Chem. 2014;289(19):13273–83.

294. Yu D-M, Jung SH, An H-T, Lee S, Hong J, Park JS, et al. Caveolin-1 deficiency induces premature senescence with mitochondrial dysfunction. Aging Cell [Internet]. 2017 Aug 1 [cited 2019 Aug 25];16(4):773–84. Available from: http://doi.wiley.com/10.1111/acel.12606

295. Ha T-K, Her N-G, Lee M-G, Ryu B-K, Lee J-H, Han J, et al. Caveolin-1 increases aerobic glycolysis in colorectal cancers by stimulating HMGA1-mediated GLUT3 transcription. Cancer Res [Internet]. 2012 Aug 15 [cited 2019 May 15];72(16):4097–109. Available from: http://cancerres.aacrjournals.org/

296. Puchulu-Campanella E, Chu H, Anstee DJ, Galan JA, Tao WA, Low PS. Identification of the components of a glycolytic enzyme metabolon on the human red blood cell membrane. J Biol Chem [Internet]. 2013 Jan 11;288(2):848–58. Available from: http://www.ncbi.nlm.nih.gov/pubmed/23150667

297. Chu H, Puchulu-Campanella E, Galan JA, Tao WA, Low PS, Hoffman JF. Identification of cytoskeletal elements enclosing the ATP pools that fuel human red blood cell membrane cation pumps. Proc Natl Acad Sci U S A [Internet]. 2012 Jul 31 [cited 2019 Jul 9];109(31):12794–9. Available from: http://www.ncbi.nlm.nih.gov/pubmed/22745158

298. Campanella ME, Chu H, Low PS. Assembly and regulation of a glycolytic enzyme complex on the human erythrocyte membrane. Proc Natl Acad Sci [Internet]. 2005 Feb 15 [cited 2019 Feb 3];102(7):2402–7. Available from: http://www.ncbi.nlm.nih.gov/pubmed/15701694

299. Jenkins CM, Yang J, Sims HF, Gross RW. Reversible High Affinity Inhibition of Phosphofructokinase-1 by Acyl-CoA. J Biol Chem. 2011;286(14):11937–50.

300. Vallejo J, Hardin CD. Caveolin-1 Functions as a Scaffolding Protein for Phosphofructokinase in the Metabolic Organization of Vascular Smooth Muscle †. Biochemistry [Internet]. 2004 Dec [cited 2019 May 14];43(51):16224–32. Available from: https://pubs-acs-org.manchester.idm.oclc.org/doi/10.1021/bi0490035

301. Chatterjee M, Ben-Josef E, Thomas DG, Morgan MA, Zalupski MM, Khan G, et al. Caveolin-1 is Associated with Tumor Progression and Confers a Multi-Modality Resistance Phenotype in Pancreatic Cancer OPEN. Nat Publ Gr [Internet]. 2015 [cited 2019 May 5]; Available from: www.nature.com/scientificreports/

302. Blum R, Kloog Y. Metabolism addiction in pancreatic cancer. Cell Death Dis [Internet]. 2014;5(2):e1065-13. Available from: http://dx.doi.org/10.1038/cddis.2014.38

303. Permert J, Ihse I, Jorfeldt L, von Schenck H, Arnqvist HJ, Larsson J. Pancreatic cancer is associated with impaired glucose metabolism. Eur J Surg [Internet]. 1993 Feb;159(2):101–7. Available from: http://www.ncbi.nlm.nih.gov/pubmed/8098623

304. Tian S, Li P, Sheng S, Jin X. Upregulation of pyruvate kinase M2 expression by fatty acid synthase contributes to gemcitabine resistance in pancreatic cancer. Oncol Lett [Internet]. 2018 Feb;15(2):2211–7. Available from: http://www.ncbi.nlm.nih.gov/pubmed/29434927

305. Ashizawa K, Willingham MC, Liang CM, Cheng SY. In vivo regulation of monomer-tetramer conversion of pyruvate kinase subtype M2 by glucose is mediated via fructose 1,6-bisphosphate. J Biol Chem [Internet]. 1991 Sep 5;266(25):16842–6. Available from: http://www.ncbi.nlm.nih.gov/pubmed/1885610

306. Prakasam G, Iqbal MA, Bamezai RNK, Mazurek S. Posttranslational Modifications of Pyruvate Kinase M2: Tweaks that Benefit Cancer. Front Oncol. 2018;8(February):1–12.

307. Wang H-J, Hsieh Y-J, Cheng W-C, Lin C-P, Lin Y, Yang S-F, et al. JMJD5 regulates PKM2 nuclear translocation and reprograms HIF-1α-mediated glucose metabolism. Proc Natl Acad Sci U S A [Internet]. 2014 Jan 7;111(1):279–84. Available from: http://www.ncbi.nlm.nih.gov/pubmed/24344305

308. Zwerschke W, Mazurek S, Massimi P, Banks L, Eigenbrodt E, Jansen-Dürr P. Modulation of type M2 pyruvate kinase activity by the human papillomavirus type 16 E7 oncoprotein. Proc Natl Acad Sci U S A [Internet]. 1999 Feb 16;96(4):1291–6. Available from: http://www.ncbi.nlm.nih.gov/pubmed/9990017

309. Wörmann SM, Song L, Ai J, Diakopoulos KN, Kurkowski MU, Görgülü K, et al. Loss of P53 Function Activates JAK2-STAT3 Signaling to Promote Pancreatic Tumor Growth, Stroma Modification, and Gemcitabine Resistance in Mice and Is Associated With Patient Survival. Gastroenterology [Internet]. 2016;151(1):180-193.e12. Available from: http://www.ncbi.nlm.nih.gov/pubmed/27003603

310. Haq F, Sung YN, Park I, Kayani MA, Yousuf F, Hong SM, et al. FGFR1 expression defines clinically distinct subtypes in pancreatic cancer. J Transl Med [Internet]. 2018;16(1):1–7. Available from: https://doi.org/10.1186/s12967-018-1743-9

311. Hitosugi T, Kang S, Vander Heiden MG, Chung T-W, Elf S, Lythgoe K, et al. Tyrosine Phosphorylation Inhibits PKM2 to Promote the Warburg Effect and Tumor Growth. Bönig H, editor. Sci Signal [Internet]. 2009 Nov 17;2(97):ra73–ra73. Available from: https://dx.plos.org/10.1371/journal.pone.0178059

312. Huang W, Wang Z, Lei Q-Y. Acetylation control of metabolic enzymes in cancer: an updated

version. Acta Biochim Biophys Sin (Shanghai) [Internet]. 2014 Mar 1;46(3):204–13. Available from: https://academic.oup.com/abbs/article-lookup/doi/10.1093/abbs/gmt154

313. Wang Y, Liu J, Jin X, Zhang D, Li D, Hao F, et al. O-GlcNAcylation destabilizes the active tetrameric PKM2 to promote the Warburg effect. Proc Natl Acad Sci U S A [Internet]. 2017 [cited 2019 Jul 27];114(52):13732–7. Available from: http://www.ncbi.nlm.nih.gov/pubmed/29229835

314. Anastasiou D, Poulogiannis G, Asara JM, Boxer MB, Jiang J, Shen M, et al. Inhibition of pyruvate kinase M2 by reactive oxygen species contributes to cellular antioxidant responses. Science [Internet]. 2011 Dec 2 [cited 2019 Jul 27];334(6060):1278–83. Available from: http://www.ncbi.nlm.nih.gov/pubmed/22052977

315. Snaebjornsson MT, Schulze A. Non-canonical functions of enzymes facilitate cross-talk between cell metabolic and regulatory pathways. Exp Mol Med [Internet]. 2018 Apr 16 [cited 2019 Jun 9];50(4):34. Available from: http://www.nature.com/articles/s12276-018-0065-6

316. Gao X, Wang H, Yang JJ, Liu X, Liu ZR. Pyruvate Kinase M2 Regulates Gene Transcription by Acting as a Protein Kinase. Mol Cell [Internet]. 2012;45(5):598–609. Available from: http://dx.doi.org/10.1016/j.molcel.2012.01.001

317. Yang W, Lu Z. Nuclear PKM2 regulates the Warburg effect. Cell Cycle. 2013;12(19):3154–8.

318. Song KS, Li Shengwen S, Okamoto T, Quilliam LA, Sargiacomo M, Lisanti MP. Co-purification and direct interaction of Ras with caveolin, an integral membrane protein of caveolae microdomains. Detergent-free purification of caveolae microdomains. J Biol Chem [Internet]. 1996 Apr 19 [cited 2019 Sep 10];271(16):9690–7. Available from: http://www.ncbi.nlm.nih.gov/pubmed/8621645

319. Vichai V, Kirtikara K. Sulforhodamine B colorimetric assay for cytotoxicity screening. Nat Protoc [Internet]. 2006 Aug 17 [cited 2019 Sep 10];1(3):1112–6. Available from: http://www.nature.com/articles/nprot.2006.179

320. Grynkiewicz G, Poenie M, Tsien RY. A new generation of Ca2+ indicators with greatly improved fluorescence properties. J Biol Chem [Internet]. 1985 Mar 25;260(6):3440–50. Available from: http://www.ncbi.nlm.nih.gov/pubmed/3838314

321. Huang Y, Putney JW. Relationship between intracellular calcium store depletion and calcium release-activated calcium current in a mast cell line (RBL-1). J Biol Chem [Internet]. 1998 Jul 31 [cited 2019 Sep 10];273(31):19554–9. Available from: http://www.ncbi.nlm.nih.gov/pubmed/9677379

322. Tran NN, Leroy P, Bellucci L, Robert A, Nicolas A, Atkinson J, et al. Intracellular concentrations of fura-2 and fura-2/am in vascular smooth muscle cells following perfusion loading of fura-2/am in arterial segments. Cell Calcium [Internet]. 1995 Nov;18(5):420–8. Available from: http://www.ncbi.nlm.nih.gov/pubmed/8581970

323. Johnson I, Spence M (eds. . Indicators for Ca2+, Mg2+, Zn2+ and Other Metal Ions [Internet]. 11th ed. Johnson I, Spence MTZ, editors. The Molecular Probes ® Handbook. Life Technologies; 2010. Available from: https://www.thermofisher.com/content/dam/LifeTech/global/technical-reference-library/Molecular Probes Handbook/chapter-pdfs/Ch-19-Ca-Mg-Zn-Ion-Indicators.pdf?icid=WE216841

324. Neher E. The use of fura-2 for estimating Ca buffers and Ca fluxes. Neuropharmacology [Internet]. 1995 Nov;34(11):1423–42. Available from: http://www.ncbi.nlm.nih.gov/pubmed/8606791

325. Mankad P, James A, Siriwardena AK, Elliott AC, Bruce JIE. Insulin protects pancreatic acinar cells from cytosolic calcium overload and inhibition of plasma membrane calcium pump. J Biol Chem [Internet]. 2012 Jan 13 [cited 2019 Sep 10];287(3):1823–36. Available from: http://www.ncbi.nlm.nih.gov/pubmed/22128146

326. Barr R, Troxel KS, Crane FL. EGTA, a calcium chelator, inhibits electron transport in photosystem II of spinach chloroplasts at two different sites. Biochem Biophys Res Commun [Internet]. 1980 Jan;92(1):206–12. Available from: https://linkinghub.elsevier.com/retrieve/pii/0006291X80915405

327. Moncoq K, Trieber CA, Young HS. The molecular basis for cyclopiazonic acid inhibition of the sarcoplasmic reticulum calcium pump. J Biol Chem [Internet]. 2007 Mar 30 [cited 2019 Sep 11];282(13):9748–57. Available from: http://www.ncbi.nlm.nih.gov/pubmed/17259168

328. Nakano M, Imamura H, Nagai T, Noji H. Ca$^{2+}$ regulation of mitochondrial ATP synthesis visualized at the single cell level. ACS Chem Biol [Internet]. 2011 Jul 15;6(7):709–15. Available from: http://www.ncbi.nlm.nih.gov/pubmed/21488691

329. Ukeda H, Kawana D, Maeda S, Sawamura M. Spectrophotometric Assay for Superoxide

Dismutase Based on the Reduction of Highly Water-soluble Tetrazolium Salts by Xanthine-Xanthine Oxidase. Biosci Biotechnol Biochem [Internet]. 1999;63(3):485–8. Available from: http://www.ncbi.nlm.nih.gov/pubmed/27393255

330. Ihrlund LS, Hernlund E, Khan O, Shoshan MC. 3-Bromopyruvate as inhibitor of tumour cell energy metabolism and chemopotentiator of platinum drugs. Mol Oncol [Internet]. 2008 Jun;2(1):94–101. Available from: http://www.ncbi.nlm.nih.gov/pubmed/19383331

331. Bertina RM, Steenstra JA, Slater EC. The mechanism of inhibition by oligomycin of oxidative phosphorylation in mitochondria. Biochim Biophys Acta - Bioenerg [Internet]. 1974 Dec 19 [cited 2019 Sep 11];368(3):279–97. Available from: https://www-sciencedirect-com.manchester.idm.oclc.org/science/article/pii/0005272874901753

332. Chen J, Xie J, Jiang Z, Wang B, Wang Y, Hu X. Shikonin and its analogs inhibit cancer cell glycolysis by targeting tumor pyruvate kinase-M2. Oncogene. 2011;30(42):4297–306.

333. Mohamed TMA, Abou-Leisa R, Baudoin F, Stafford N, Neyses L, Cartwright EJ, et al. Development and characterization of a novel fluorescent indicator protein PMCA4-GCaMP2 in cardiomyocytes. J Mol Cell Cardiol [Internet]. 2013 Oct;63:57–68. Available from: http://www.ncbi.nlm.nih.gov/pubmed/23880607

334. Lou PH, Hansen BS, Olsen PH, Tullin S, Murphy MP, Brand MD. Mitochondrial uncouplers with an extraordinary dynamic range. Biochem J. 2007;407(1):129–40.

335. Pande J, Szewczyk MM, Kuszczak I, Grover S, Escher E, Grover AK. Functional effects of caloxin 1c2, a novel engineered selective inhibitor of plasma membrane Ca2+-pump isoform 4, on coronary artery. J Cell Mol Med. 2008;12(3):1049–60.

336. Bartlett DW, Davis ME. Insights into the kinetics of siRNA-mediated gene silencing from live-cell and live-animal bioluminescent imaging. Nucleic Acids Res [Internet]. 2006 [cited 2019 Sep 11];34(1):322–33. Available from: http://www.ncbi.nlm.nih.gov/pubmed/16410612

337. Wittrup A, Lieberman J. Knocking down disease: a progress report on siRNA therapeutics. Nat Rev Genet [Internet]. 2015 Sep 18 [cited 2019 Sep 11];16(9):543–52. Available from: http://www.nature.com/articles/nrg3978

338. Agilent Technologies. Agilent Seahorse XF Real-Time ATP Rate Assay Kit [Internet]. 2018. Available from: https://www.agilent.com/cs/library/usermanuals/public/Report_Generator_User_Guide_Seahorse_XF_Real_Time_ATP_Rate_Assay.pdf

339. Agilent Technologies. Agilent Seahorse XF Real-Time ATP Rate Assay Report Generator User Guide [Internet]. 2018. Available from: https://www.agilent.com/cs/library/usermanuals/public/Report_Generator_User_Guide_Seahorse_XF_Real_Time_ATP_Rate_Assay.pdf

340. Agilent Technologies. Agilent Seahorse XF CO2 Contribution Factor Protocol User Guide [Internet]. 2017. Available from: https://www.agilent.com/en/products/cell-analysis/xf-glycolytic-rate-assay-report-generator

341. Cui C, Merritt R, Fu L, Pan Z. Targeting calcium signaling in cancer therapy. Acta Pharm Sin B [Internet]. 2017;7(1):3–17. Available from: http://dx.doi.org/10.1016/j.apsb.2016.11.001

342. Hillis AL, Lau AN, Devoe CX, Dayton TL, Danai L V, Di Vizio D, et al. PKM2 is not required for pancreatic ductal adenocarcinoma. Cancer Metab [Internet]. 2018 Dec 23;6(1):17. Available from: https://cancerandmetabolism.biomedcentral.com/articles/10.1186/s40170-018-0188-1

343. Rhodes DR, Yu J, Shanker K, Deshpande N, Varambally R, Ghosh D, et al. ONCOMINE: A Cancer Microarray Database and Integrated Data-Mining Platform. Neoplasia [Internet]. 2004;6(1):1–6. Available from: http://linkinghub.elsevier.com/retrieve/pii/S1476558604800472

344. Oncomine [Internet]. [cited 2019 Jan 17]. Available from: www.oncomine.org

345. Badea L, Herlea V, Dima SO, Dumitrascu T, Popescu I. Combined gene expression analysis of whole-tissue and microdissected pancreatic ductal adenocarcinoma identifies genes specifically overexpressed in tumor epithelia. Hepatogastroenterology [Internet]. [cited 2019 Jan 17];55(88):2016–27. Available from: http://www.ncbi.nlm.nih.gov/pubmed/19260470

346. Salem AF, Bonuccelli G, Bevilacqua G, Arafat H, Pestell RG, Sotgia F, et al. Caveolin-1 promotes pancreatic cancer cell differentiation and restores membranous E-cadherin via suppression of the epithelial-mesenchymal transition. Cell Cycle. 2011;10(21):3692–700.

347. Olli KE, Li K, Galileo DS, Martin-DeLeon PA. Plasma membrane calcium ATPase 4 (PMCA4) co-ordinates calcium and nitric oxide signaling in regulating murine sperm functional activity. J Cell Physiol [Internet]. 2018 Jan [cited 2019 Jan 20];233(1):11–22. Available from: https://www.ncbi.nlm.nih.gov/pmc/articles/PMC5581300/pdf/nihms857563.pdf

348. Frank PG, Pavlides S, Cheung MW-C, Daumer K, Lisanti MP. Role of caveolin-1 in the regulation of lipoprotein metabolism. Am J Physiol Cell Physiol [Internet]. 2008 Jul [cited 2019

211

May 15];295(1):C242-8. Available from: http://www.ncbi.nlm.nih.gov/pubmed/18508910

349. Hirama T, Das R, Yang Y, Ferguson C, Won A, Yip CM, et al. Phosphatidylserine dictates the assembly and dynamics of caveolae in the plasma membrane. J Biol Chem [Internet]. 2017 Aug 25 [cited 2019 Apr 2];292(34):14292–307. Available from: http://www.ncbi.nlm.nih.gov/pubmed/28698382

350. Filomatori C V., Rega AF. On the mechanism of activation of the plasma membrane Ca2+-ATPase by ATP and acidic phospholipids. J Biol Chem. 2003;278(25):22265–71.

351. Carafoli E. Calcium Pump of the Plasma Membrane [Internet]. Vol. 71, PHYSIOLOGICAL REVIEWS. 1991 [cited 2019 May 12]. Available from: www.physiology.org/journal/physrev

352. Zhang J, Xiao P, Zhang X. Phosphatidylserine externalization in caveolae inhibits Ca2+ efflux through plasma membrane Ca2+-ATPase in ECV304. Cell Calcium [Internet]. 2009 Feb;45(2):177–84. Available from: http://www.ncbi.nlm.nih.gov/pubmed/18929409

353. Gooptu M, Whitaker-Menezes D, Sprandio J, Domingo-Vidal M, Lin Z, Uppal G, et al. Mitochondrial and glycolytic metabolic compartmentalization in diffuse large B-cell lymphoma. Semin Oncol [Internet]. 2017 Jun 1 [cited 2019 Jul 9];44(3):204–17. Available from: http://www.ncbi.nlm.nih.gov/pubmed/29248132

354. Wei Y, Wang D, Jin F, Bian Z, Li L, Liang H, et al. Pyruvate kinase type M2 promotes tumour cell exosome release via phosphorylating synaptosome-associated protein 23. Nat Commun [Internet]. 2017 Apr 9 [cited 2019 Jul 9];8(1):14041. Available from: http://www.nature.com/articles/ncomms14041